**IST-4-027756 WINNER II****D1.1.2 V1.0*****WINNER II Channel Models*****Part II*****Radio Channel Measurement and Analysis Results*****Contractual Date of Delivery to the CEC:** 30/09/2007**Actual Date of Delivery to the CEC:** 30/09/2007

Author(s):	Pekka Kyösti, Juha Meinilä, Lassi Hentilä, Xiongwen Zhao, Tommi Jämsä, Milan Narandžić, Marko Milojević, Christian Schneider, Aihua Hong, Juha Ylitalo, Veli-Matti Holappa, Mikko Alatossava, Robert Bultitude, Yvo de Jong, Terhi Rautiainen
Participant(s):	<i>EBITG, TUI, UOULU, CU/CRC, NOKIA</i>
Workpackage:	<i>WP1 Channel Model</i>
Security:	PU
Nature:	R
Version:	1.0
Total number of pages:	206

Abstract:

This document contains the results of WINNER measurement campaigns and analysis work relevant to the WINNER II radio channel models. The actual channel models are described in the deliverable D1.1.2 “WINNER II Channel Models”.

Keyword list: Channel modelling, propagation scenario, wideband, channel sounder, cluster, delay domain, angle domain, polarisation, measurements, delay spread, angle spread, arrival, departure, MIMO

Disclaimer:

Executive Summary

This document is Part II of the deliverable D1.1.2. Measurement and analysis results from the duration of Phase I and Phase II of the project are described in this document to give background to parameters and models of D1.1.2.

Authors

Partner	Name	Phone / Fax / e-mail
EBITG	Pekka Kyösti	Phone: +358 40 344 2000 Fax: +358 8 551 4344 e-mail: firstname.lastname@elektrobit.com
EBITG	Juha Meinilä	Phone: +358 40 344 2000 Fax: + e-mail: firstname.lastname@elektrobit.com
EBITG	Lassi Hentilä	Phone: +358 40 344 2000 Fax: +358 8 551 4344 e-mail: firstname.lastname@elektrobit.com
EBITG	Xiongwen Zhao	Phone: +358 40 344 2000 Fax: +358 9 2561014 e-mail: firstname.lastname@elektrobit.com
EBITG	Tommi Jämsä	Phone: +358 40 344 2000 Fax: +358 8 551 4344 e-mail: firstname.lastname@elektrobit.com
OUULU	Mikko Alatossava	Phone: +358 8 814 7638 Fax: +358 8 553 2845 e-mail: mikko.alatossava@ee.oulu.fi
OUULU	Veli-Matti Holappa	Phone: +358 8 814 2890 Fax: +358 8 553 2845 e-mail: crimson@ee.oulu.fi

TUI	Milan Narandžić	Phone: + 49 3677 69 3722 Fax: + 49 3677 69 1113 e-mail: milan.narandzic@tu-ilmenau.de
-----	-----------------	---

TUI	Aihua Hong	Phone: + 49 3677 69 1157 Fax: + 49 3677 69 1113 e-mail: aihua.hong@tu-ilmenau.de
-----	------------	--

TUI	Marko Milojević	Phone: + 49 3677 69 2673 Fax: + 49 3677 69 1195 e-mail: marko.milojevic@tu-ilmenau.de
-----	-----------------	---

TUI	Christian Schneider	Phone: + 49 3677 69 1157 Fax: + 49 3677 69 1113 e-mail: christian.schneider@tu-ilmenau.de
-----	---------------------	---

TUI	Gerd Sommerkorn	Phone: + 49 3677 69 1115 Fax: + 49 3677 69 1113 e-mail: gerd.sommerkorn@tu-ilmenau.de
-----	-----------------	---

CRC	Robert Bultitude	Phone: 1-613-98-2775 Fax: 1-613-990-7987 e-mail: robert.bultitude@crc.ca
-----	------------------	--

CRC	Yvo de Jong	Phone: 1-603-990-9235 Fax: 1-613-990-6339 e-mail: yvo.dejong@crc.ca
-----	-------------	---

NOK	Terhi Rautiainen	Phone: +358 50 4837218 Fax: + 358 7180 36857 e-mail: terhi.rautiainen@nokia.com
-----	------------------	---

Table of Contents

1. Introduction	9
2. Definitions	10
2.1 Terminology	10
2.2 List of Symbols	13
2.3 Propagation Scenarios	15
3. Determination of model parameters.....	16
3.1 A1 – Indoor office	16
3.1.1 A1 – Scenario definition	16
3.1.2 Path-loss update	17
3.1.3 Measurements	17
3.1.4 A1 Path-loss and shadow fading	18
3.1.5 A1 Angle Spread.....	22
3.1.6 A1 LOS probability (D5.4)	24
3.1.7 A1 Delay Spread and maximum excess-delay distribution (D5.4)	24
3.1.8 A1 Distribution of the azimuth angles of the multipath components (D5.4)	26
3.1.9 A1 Angle proportionality factor (D5.4)	26
3.1.10 A1 K-factor	26
3.1.11 A1 Cross Correlations	28
3.1.12 A1 Modelling of PDP (D5.4)	29
3.1.13 A1 Number of Clusters (D5.4).....	30
3.1.14 A1 Distribution of ZDSC delays (D5.4)	30
3.1.15 A1 Delay proportionality factor (D5.4).....	31
3.1.16 A1 Cross-polarization ratio (D5.4).....	32
3.1.17 A1 Literature review	32
3.1.18 Interpretation of A1 results	37
3.2 A2 - Indoor to outdoor.....	37
3.2.1 A2 – Scenario definition	37
3.2.2 A2 Measurements	38
3.2.3 A2 Path-loss and shadow fading (D1.1.1).....	39
3.2.4 A2 Delay spread and maximum excess delay distribution (D1.1.1)	44
3.2.5 A2 Azimuth angle spread at BS and MS (D1.1.1)	45
3.2.6 A2 Cross-polarisation ratio (D1.1.1).....	46
3.2.7 A2 Power Delay Profile (D1.1.1).....	48
3.2.8 A2 Proportionality factor of the delay (D1.1.1)	48
3.2.9 A2 Power Angular Spectrum and main DoA offset (D1.1.1)	48
3.2.10 A2 Number of clusters (D1.1.1).....	49
3.2.11 A2 Time evolution of clusters (D1.1.1)	49
3.2.12 A2 Per cluster shadowing (D1.1.1)	50
3.2.13 A2 Ricean K-factor (D1.1.1).....	50
3.2.14 A2 Literature research.....	51
3.3 B1 – Urban micro-cell	55
3.3.1 B1 – Scenario definition.....	55
3.3.2 Measurements	55
3.3.3 B1 - Path-loss and shadow fading	55

3.3.4	B1 - K-factor distributions	58
3.3.5	B1 - Auto- and cross correlations.....	58
3.3.6	B1 LOS probability.....	59
3.3.7	B1 DS and maximum excess-delay distribution	60
3.3.8	B1 Azimuth AS at BS and MS (D5.4)	63
3.3.9	B1 Distribution of azimuth angles (D5.4).....	64
3.3.10	B1 Modelling of PDP (D5.4)	65
3.3.11	B1 Number of clusters (D5.4).....	66
3.3.12	B1 Distribution of path delays (D5.4).....	66
3.3.13	B1 Delay proportionality factor (D5.4).....	67
3.3.14	B1 Cross-polarisation ratio (D5.4).....	67
3.4	B2 – Bad urban micro-cell.....	68
3.4.1	B2 – Scenario definition.....	68
3.5	B3 – Indoor hotspot.....	69
3.5.1	B3 – Scenario definition.....	69
3.5.2	B3 – Measurements.....	69
3.5.3	B3 – Model parameters	70
3.6	B4 – Outdoor to indoor.....	88
3.6.1	B4 – Scenario definition.....	88
3.6.2	B4 - Measurements	89
3.6.3	B4 Path-loss and shadow fading	90
3.6.4	B4 RMS and maximum excess delay distribution	93
3.6.5	B4 Azimuth AS at BS and MS.....	96
3.6.6	B4 Elevation AS at BS.....	98
3.6.7	B4 Cross-polarisation ratio	98
3.6.8	B4 Power Delay Profile	99
3.6.9	B4 Proportionality factors, delay and angular.....	100
3.6.10	B4 Main DoA and DoD offset	101
3.6.11	B4 Ricean K-factor	103
3.6.12	B4 Cross-Correlations.....	105
3.6.13	B4 Distributions	106
3.6.14	B4 – Validation	107
3.7	B5 – Stationary feeder	108
3.7.1	B5 – Scenario definition.....	108
3.7.2	B5 – Path loss (D5.4)	110
3.7.3	B5 - Power-delay profile (D5.4)	110
3.7.4	B5 - Delay spread (D5.4)	111
3.7.5	B5 - K-factor (D5.4).....	111
3.7.6	B5 - Cross-polarization ratio (D5.4)	111
3.7.7	B5 – Doppler (D5.4)	111
3.7.8	B5 - Angle-spread (D5.4).....	112
3.7.9	B5 - Antenna gain (D5.4).....	112
3.7.10	B5 – Literature review (D5.4).....	112
3.8	C1 – Suburban macro-cell	115
3.8.2	Measurements	115
3.8.3	C1 Path-loss and shadow fading	116
3.8.4	C1 Delay Spread and Maximum Excess Delay Distribution	118
3.8.5	C1 Azimuth AS at BS and MS (D1.1.1)	119
3.8.6	C1 Modelling of PDP (D5.4)	120

3.8.7 C1 Number of ZDSC (D5.4)	120
3.8.8 C1 Distribution of ZDSC delays (D5.4)	120
3.8.9 C1 Delay proportionality factor (D5.4)	121
3.8.10 C1 K-factor	121
3.8.11 C1 Cross Correlations	122
3.8.12 C1 Cross-polarization ratio (D5.4)	123
3.9 C2 – Urban macro-cell	123
3.9.1 C2 – Scenario definition.....	123
3.9.2 Measurements	123
3.9.3 C2 Path-loss and shadow fading	124
3.9.4 C2 LOS probability	127
3.9.5 C2 Rms delay spread and maximum excess delay distributions	128
3.9.6 C2 Azimuth AS at BS and MS.....	133
3.9.7 C2 Ricean K-factor	135
3.9.8 C2 Number of Taps.....	136
3.9.9 C2 Cross Correlation.....	136
3.10 C3 – Bad urban macro-cell.....	138
3.10.1 C3 – Scenario definition.....	138
3.10.2 C3 – Measurements.....	138
3.11 C4 – Urban macro outdoor to indoor.....	139
3.11.1 C4 – Scenario definition.....	139
3.11.2 C4 Path-loss model	140
3.11.3 C4 Channel parameters	141
3.12 D1 – Rural macro-cell	141
3.12.1 D1 – Scenario definition	141
3.12.2 D1 - Measurements	141
3.12.3 D1 Path-loss and shadow fading	142
3.12.4 D1 - Probability of LOS model.....	150
3.12.5 D1 Delay spread and maximum excess delay distribution (D5.4)	151
3.12.6 D1 Azimuth AS at BS and MS (D5.4)	152
3.12.7 D1 K-factor (New)	153
3.12.8 D1 Cross Correlations (New)	153
3.12.9 D1 Modelling of PDP (D5.4)	154
3.12.10 D1 Number of cluster (D5.4)	155
3.12.11 D1 Distribution of cluster delays (D5.4).....	155
3.12.12 D1 Delay proportionality factor (D5.4)	156
3.12.13 D1 Ricean K-factor (D5.4)	156
3.12.14 D1 Cross-polarisation ratio (D5.4).....	157
3.13 D2 – Moving networks	158
3.13.1 D2 - Scenario definition	158
3.13.2 D2a - Measurements	159
3.13.3 D2a - Model parameters.....	161
3.13.4 D2 - Literature research	168
3.13.5 D2 - Interpretation of the results	169
3.14 Path Loss frequency dependency	169

4. Analysis items..... **172**

4.1.1 Delay domain	173
4.1.2 Both domains (Delay-Angular).....	183

4.1.3	Angular domain.....	184
4.1.4	Cluster level	187
4.1.5	Polarization analysis	192
4.2	Common processing methods.....	193
4.2.1	Probability density Function (experimental).....	193
4.2.2	Cumulative probability density function (experimental)	195
4.2.3	Distribution Modelling.....	195
4.2.4	Function Modelling.....	197
4.2.5	Correlation/Covariance	198
5.	References.....	200

1. Introduction

The purpose of this document is to be a compact reference to the models and the parameters of deliverable D1.1.2 “WINNER II Channel Models”. All the results measured and analysed in the project that are relevant to WINNER II channel models are collected in this report. The sources are mainly Part II of D5.4, Part II of D1.1.1 and the new results analysed after November 2006. As a principle, the more recent results either complement or substitute the old results.

Section 2 defines the propagation scenarios. Section 3 gives the measurement and literature review results of the scenario parameters. The grouping is scenario based, except in the case of path loss frequency dependency, which covers all the scenarios. Section 4 describes the analysis items to give more exact definition of the analysed parameters. The analysis items are originally introduced in the WINNER internal report [WIN2IR112]. The reference list is in Section 5.

2. Definitions

2.1 Terminology

3GPP	3rd Generation Partnership Project
3GPP2	3rd Generation Partnership Project 2
ACF	Auto-Correlation Function
ADC	Analog-to-Digital Converter
AN	Antenna Array
AoA	Angle of Arrival
AoD	Angle of Departure
AP	Access Point (BS)
APP	A Posteriori Probability
APS	Angle Power Spectrum
AS	Azimuth Spread
ASA	Azimuth Spread at Arrival
ASD	Azimuth Spread at Departure
AWGN	Additive White Gaussian Noise
B3G	Beyond 3G
BER	Bit Error Rate
BRAN	Broadband Radio Access Networks
BS	Base Station
C/I	Carrier to Interference ratio
CDF	Cumulative Distribution Function
CDL	Clustered Delay Line
CG	Concept Group
CIR	Channel Impulse Response
CRC	Communications Research Centre Canada
CW	Continuous Wave
DoA	Direction of Arrival
DoD	Direction of Departure
DS/DES	Delay Spread
EBITG	Elektrobit
ECDF	Experimentally determined cumulative probability distribution function
ESA	Elevation Spread at Arrival
ESD	Elevation Spread at Departure
ESPRIT	Estimation of Signal Parameters via Rotational Invariance Techniques
ETHZ	Eidgenössische Technische Hochschule Zürich (Swiss Federal Institute of Technology Zurich)
ETSI	European Telecommunications Standards Institute
FDD	Frequency Division Duplex
FIR	Finite Impulse Response
FRS	Fixed Relay Station
FS	Fixed Station
GPS	Global Positioning System
HIPERLAN	High Performance Local Area Network
HUT	Helsinki University of Technology (TKK)
IR	Impulse Response

ISIS	Initialization and Search Improved SAGE
KTH	Kungliga Tekniska Högskolan (Royal Institute of Technology in Stockholm)
LA	Local Area
LNS	Log-Normal Shadowing
LOS	Line-of-Sight
LS	Large Scale
MA	Metropolitan Area
MCSSS	Multi-Carrier Spread Spectrum Signal
METRA	Multi-Element Transmit and Receive Antennas (European IST project)
MIMO	Multiple-Input Multiple-Output
MPC	Multi-Path Component
MRS	Mobile Relay Station
MS	Mobile Station
MUSIC	Multiple Signal Classification
NLOS	Non Line-of-Sight
NOK	Nokia
OFDM	Orthogonal Frequency-Division Multiplexing
OLOS	Obstructed Line-of-Sight
PAS	Power Azimuth Spectrum
PDF	Probability Distribution Function
PDP	Power-Delay Profile
PL	Path Loss
PLO	Phase-locked oscillator
PN	Pseudo Noise
RIMAX	Maximum likelihood parameter estimation framework for joint superresolution estimation of both specular and dense multipath components
RF	Radio Frequency
RMS	Root Mean Square
RT	Roof-top
RX	Receiver
SAGE	Space-Alternating Generalized Expectation-maximization
SCM	Spatial Channel Model
SCME	Spatial Channel Model Extended
SF/SHF	Shadow Fading
SIMO	Single-Input Multiple-Output
SISO	Single-Input Single-Output
SoS	Sum of Sinusoids
std	Standard deviation
SW	Software
TDD	Time Division Duplex
TDL	Tapped Delay-Line
TUI	Technische Universität Ilmenau
TX	Transmitter
UE	User Equipment (MS)
UOULU	University of Oulu
UT	User Terminal (MS)
WA	Wide Area
WINNER	Wireless World Initiative New Radio
WPx	Work Package x of WINNER project

XPR Cross-Polarisation power Ratio
XPRH Horizontal Polarisation XPR
XPRV Vertical Polarisation XPR

2.2 List of Symbols

$\Delta(\bullet)$	Change in parameter value
$(\bullet)^T$	Transpose
$(\bullet)^H$	Hermitian transpose
$(\bullet)^*$	Complex conjugate
$\log_{10}(\bullet)$	base 10 logarithm
$\cos(\bullet)$	Cosine of the argument
$\sin(\bullet)$	Sine of the argument
A	Pairing matrix
C	Correlation matrix
F_{tx}	Tx antenna array response matrix
F_{rx}	Rx antenna array response matrix
H	MIMO channel transfer matrix
N	Normal distribution
U	Uniform Distribution
ϕ	AoA
ψ	AoD
τ	Delay
σ_t	RMS delay spread
σ_ϕ	RMS angle spread of AoA
σ_ψ	RMS angle spread of AoD
c_{AoA}	cluster-wise RMS angle spread of AoA
c_{AoD}	cluster-wise RMS angle spread of AoD
σ_{SF}	Shadow fading standard deviation
σ^2	Variance
ζ	Per cluster shadowing standard deviation
λ	Wavelength
λ_0	Wave number
κ^{vh}	Vertical-to-horizontal XPR
κ^{hv}	Horizontal-to-vertical XPR
v	Doppler frequency
α	Complex gain of a propagation path
c	Speed of light
f_c	Central frequency
h_{bs}	BS antenna height
$h_{bs}^{'}$	Effective BS antenna height
h_{ms}	MS antenna height
$h_{ms}^{'}$	Effective MS antenna height
K_R	Ricean K-factor
n	Index to cluster
P	Power
r_ϕ	AoA distribution proportionality factor
r_ψ	AoD distribution proportionality factor
r_b	Break point distance

r_t	Delay distribution proportionality factor
s	Index to Tx antenna element
t	Time
u	Index to Rx antenna element

2.3 Propagation Scenarios

The propagation scenarios modelled in WINNER are shown in Table 2-1. The propagation scenarios are explained in more detail in the paragraphs of the model parameters. Mapping of the scenarios to the Concept Groups is shown in the Table 2-1 in column “CG”.

Table 2-1. Propagation scenarios specified in WINNER. Scenarios modelled in Phase II are emphasized with bold font.

Scenario	Definition	LOS/ NLOS	Mob. km/h	Frequ ency (GHz)	CG	Note
A1 In building	Indoor office / residential	LOS/ NLOS	0–5	2 - 6	LA	
A2	Indoor to outdoor	NLOS	0–5	2 - 6	LA	AP inside UT outside. Outdoor environment urban
B1 Hotspot	Typical urban micro-cell	LOS NLOS	0–70	2 - 6	LA, MA	
B2	Bad Urban micro-cell	LOS/ NLOS	0–70	2 - 6	MA	Same as B1 + long delays
B3 Hotspot	Large indoor hall	LOS/ NLOS	0–5	2 - 6	LA	
B4	Outdoor to indoor. micro-cell	NLOS	0–5	2 - 6	MA	-Outdoor typical urban B1. -Indoor A1
B5a Hotspot Metropol	LOS stat. feeder, rooftop to rooftop	LOS	0	2 - 6	MA	Same channel model for hot spot and metropol.
B5b Hotspot Metropol	LOS stat. feeder, street-level to street-level	LOS	0	2 - 6	MA	
B5c Hotspot Metropol	LOS stat. feeder, below- rooftop to street-level	LOS	0	2 - 6	MA	Extended B1
B5d Hotspot Metropol	NLOS stat. feeder, above rooftop to street-level	NLOS	0	2 - 6	MA	Extended C2
B5f	Feeder link BS -> FRS. Approximately RT to RT level.	LOS/ OLOS/ NLOS	0	2 - 6	WA	Desired link: LOS or OLOS, Interfering links: LOS/(OLOS) /NLOS FRS -> MS = B1*

Table 2-1 (continued).

Scenario	Definition	LOS/ NLOS	Mob. km/h	Frequ ency (GHz)	CG	Note
C1 Metropol	Suburban	LOS/ NLOS	0–120	2 - 6	WA	
C2 Metropol	Typical urban macro-cell	LOS/NLO S	0–120	2 - 6	MA WA	
C3	Bad Urban macro- cell	LOS/ NLOS	0–70	2 - 6	-	Same as C2 + long delays
C4	Outdoor to indoor macro-cell	NLOS				-Outdoor typical urban C2. -Indoor A1
D1 Rural	Rural macro-cell	LOS/ NLOS	0–200	2 - 6	WA	
D2	a) Moving networks: BS – MRS, rural	LOS	0 – 350	2 - 6	WA	Very large Doppler variability.
	b) Moving networks: MRS – MS, rural	LOS / OLOS/ NLOS	0 – 5	2 - 6	LA	Same as A1 NLOS

3. Determination of model parameters

This section describes the *measurement and analysis results* of the WINNER measurement campaigns as well as the parameters reported in the *open literature*.

3.1 A1 – Indoor office

3.1.1 A1 – Scenario definition

The scenario A1, has been modelled in D5.4. The layout of the scenario is shown in Figure 3-2.

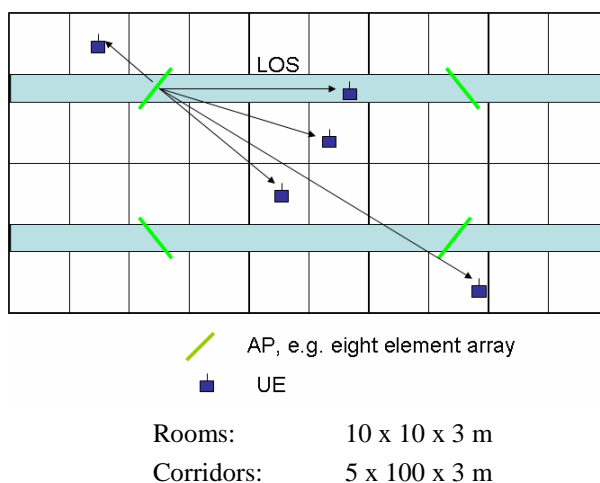


Figure 3-2. Layout of the A1 indoor scenario.

3.1.2 Path-loss update

Path-loss for A1 indoor scenario has been determined in [WIN1D54] and updated in [WIN2D111]. Recently it has turned out that the path-loss model should cover also the through-floor propagation. In literature we have found two models that describe trough-wall penetration, references [ITU] and [COST231]. The former gives a rather straightforward formula and parameter value for the through-floor loss, but the frequencies used are slightly lower than desired in WINNER, i.e. 900 and 1800 MHz. The latter covers also the desired frequency ranges giving results for 2 and 5 GHz. It also gives the value for through-wall loss. However, its formula is more complicated for more than one floor penetrated. Therefore we take into use a model that is a combination of the models. As well we use the average values for the parameters. We have to consider two cases: First is corridor-to-corridor (C-C) case, that is LOS case if the AP and UE are in the same floor, but is a NLOS case, if the AP and UE are in different floors. The other is corridor-to-room (C-R) case. The model proposed is:

$$\begin{aligned} PL &= 18.7 \log_{10}(d) + 46.8 + 20 \log_{10}\left(\frac{f_c}{5.0}\right) + u(n_f)(17 + 4(n_f - 1)), \quad \text{for C-C case} \\ PL &= 36.8 \log_{10}(d[m]) + 43.8 + 20 \log_{10}\left(\frac{f_c[\text{GHz}]}{5.0}\right) + u(n_f)(17 + 4(n_f - 1)), \quad \text{for R-C case} \end{aligned}$$

where d is distance [m], f_c is the carrier frequency [GHz] and n_f is the number of floors between BS and MS, and $u(x)$ is a unit step function, $u(x) = 0$, $x < 0$, and 1 otherwise. Distance is in [m] and frequency in [GHz].

There is still another need to update the model. The earlier A1 indoor NLOS path-loss model has been applicable only for the rooms next to the corridor containing the AP:s. To be able to be used in more general environments, the penetration to next rows of rooms has to be modelled. Unfortunately, the measurement data do not cover all possible cases. This fact has obliged us to find an approximation that is accurate near the AP, but gives probably too small path-loss values at the higher distances from the AP. This should probably not be so harmful, because at these distances the propagation to a room next to the other corridor in the layout (see the Figure 3-2 above) is most likely interference. This model gives then the worst case situation. We simply add now the through-wall attenuation specified in [WIN2D111] to the NLOS path-loss model multiplied with a coefficient that is one less than the number of walls between the corridor with the AP and the room, where the UE is situated. The reason is that the original path-loss is given for the room behind one wall seen from the corridor. The formula for is now for the R-C case:

$$PL = 36.8 \log_{10}(d[m]) + 43.8 + 20 \log_{10}\left(\frac{f_c[\text{GHz}]}{5.0}\right) + u(n_f)(17 + 4(n_f - 1)) + 5(n_w - 1)$$

where d is distance[m], f_c is the carrier frequency [GHz], n_f is the number of floors between BS and MS and n_w is the number of walls between BS and MS. $u(x)$ is a unit step function specified afore.

For heavy walls in the office rooms, 12 (dB) instead of 5 (dB) is proposed for the last term in the equation.

3.1.3 Measurements

3.1.3.1 EBITG campaign (D5.4)

Measurements conducted during 2004 for A1 were performed at two centre-frequencies, 2.45 and 5.25 GHz at Elektrobit premises in Oulu, Finland. The measurement results were included in the deliverable D5.3 [WIN1D53].

In 2005 a new series of measurements was performed at two locations, Oulu University main building and Oulu University wing building Tietotalo. Two different buildings were measured at 5.25 GHz with 100 MHz bandwidth. In the two buildings, more than 8 BSs were chosen with many different routes. Tietotalo is a typical office environment, the corridors of which are narrow with widths around 1.8 meters. In the university main building, the corridors have different width; the widest is around 3.5 meters. In the room measurements at the university main building, the room size is very close to 10 m by 10 m, as in the definition of the scenario A1. In Tietotalo the sizes of the measured rooms were comparable to 10 m by 10 m. The largest combined sets of IRs for deriving channel models and parameters are over 55000.

The indoor environments here are divided into the following 4 cases:

- (1) Corridor-corridor LOS (c-c LOS): both BS and MS were placed at the corridors.
- (2) Room-corridor and corridor-room NLOS (r-c NLOS): BS in a room, MS in an adjacent corridor vice versa.
- (3) Room-room LOS/OLOS (r-r LOS/OLOS): both BS and MS in the rooms.
- (4) Corridor-corridor NLOS (c-c NLOS)

In the analysis, 100 IRs for a drop are used (about 1.4 meters), if no window length is mentioned.

The following definitions are used: paths = peaks = ZDSC, Noise cut levels used in the analysis: For LOS: 28 ~ 35 dB. For NLOS: 15 dB ~ 30 dB.

3.1.3.2 EBITG campaign (D1.1.1)

3.1.3.2.1 Indoor peer-to-peer measurements

Indoor MIMO measurements were performed in the University of Oulu building Tietotalo. Indoor measurements were performed inside the wing containing the BS1 in the figure below.

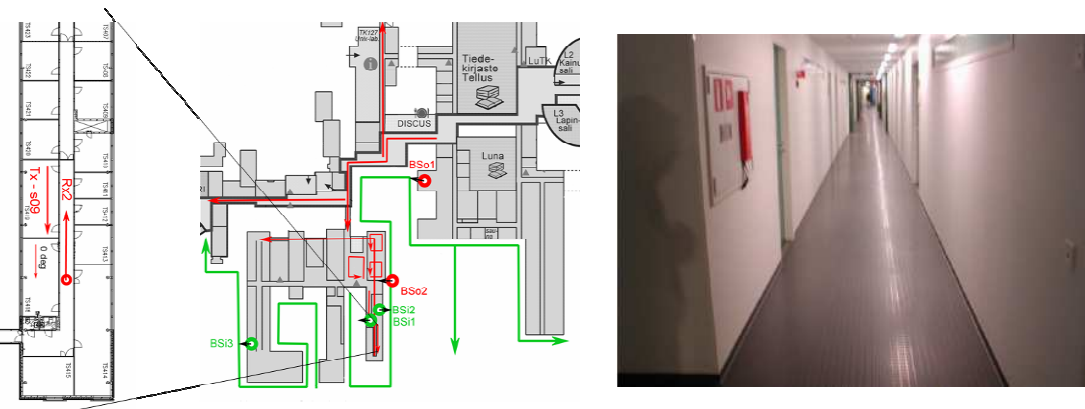


Figure 3-1. The indoor measurement environment.

3.1.4 A1 Path-loss and shadow fading

3.1.4.1 A1 Path-loss and shadow fading (D1.1.1)

In [WIN1D54] various results showed that 2 GHz path-loss models can be obtained from 5 GHz models by using the free-space loss frequency dependence: $PL \sim f^2$. In what follows we extend the measured 5.25 GHz pathloss models to carrier frequencies frequencies 2 – 6 GHz. In addition we will introduce a model for path-loss through one or more walls. Based on layout of [WIN1D54], the number of walls is determined as a function of distance. There is assumed one wall per 10 meters distance, i.e. number of walls is $n_w = \lfloor d/10m \rfloor$, where d is the distance between BS and MS and $\lfloor \cdot \rfloor$ is rounding towards zero.

Penetration between floors will not be modelled, because the models are used only in one floor. The model describing the wall penetration is taken from literature. Other models are based on our own measurements and literature. One correction to the original model is introduced: The Room to Corridor path- loss has been increased by 5 dB.

Generally it is also important to introduce the path-loss dependence on the antenna heights. In A1 indoor case it is assumed insignificant due to the closed environment.

Shadowing is assumed log-normal. The values of the standard deviation are based on our measurements, except for the through-wall case, where it is taken from the literature. The standard deviations are given in the paragraphs above and the correlation distances in [WIN1D54].

3.1.4.1.1 A1 LOS path-loss

The path-loss measured at 5.25 GHz is [WIN1D54]:

$$PL(d) = 46.4 + 18.7 \log_{10}(d[m]), \quad (3.1)$$

the shadow fading standard deviation being $\sigma = 3.1$ dB in the distance range $3m < d < 100m$.

Extended A1 LOS (Corridor-Corridor) path-loss is given below for the frequency range 2 – 6 GHz:

$$\begin{aligned} PL(d) &= 46.4 + 18.7 \log_{10}(d[m]) + 20 \log_{10}(f[\text{GHz}]/5.0), \\ \sigma &= 3.1 \text{ dB}, \quad 3m < d < 100m \end{aligned} \quad (3.2)$$

Here we take the upper bound of shadow fading standard deviation (3.1 dB for 5.25 GHz), and extend the frequency range from 2 to 6 GHz. The model corresponds to the Corridor – Corridor LOS case, but it can be used also in Room to Room cases with negligible error.

3.1.4.1.2 A1 NLOS (Room to Corridor) path-loss

At 5.25 GHz the NLOS path-loss is

$$PL(d) = 43.8 + 36.8 \log_{10}(d[m]) \quad (3.3)$$

Note that we have increased the basic loss 5 dB from 38.8 to 43.8 compared to [WIN1D54] after reviewing our results and literature.

Adding the frequency dependence and taking 5 GHz as the reference, we get for the frequency range 2 – 6 GHz:

$$PL(d, f) = 43.4 + 36.8 \log_{10}(d[m]) + 20 \log_{10}(f[\text{GHz}]/5.0), \quad (3.4)$$

It is assumed that the shadow fading standard deviation is constant over the specified frequency range, $\sigma = 3.5$ dB.

3.1.4.1.3 A1 NLOS (through-wall) path-loss

A1 through wall path-loss could not be determined accurately due to too few measurements. The model has been created using the available literature.

The path-loss (dB) for the NLOS (through-wall) case can be expressed as [KeM90]

$$PL(d, f) = 20 \log_{10}(4\pi df/c) + n_w L_w, \quad (3.5)$$

where L_w = attenuation per wall

n_w = number of traversed walls

The constant n_w is different for different types of wall materials. For light wall constructions attenuation per wall of approximately 5 dB has been reported. For more heavy materials a value of 15 dB can be

found. Both values are taken from [DRX98] but rounded to integer value. As the default value we propose to use 5 dB, which describes a modern construction with light walls. For cases with heavy walls inside the building 12 dB is recommended.

The floor attenuation of 15.5 dB has been reported [ITU]. However, the floor attenuation will be neglected in WINNER2 simulations, because the propagation in only one floor is assumed [WIN1D72].

3.1.4.1.4 Path-loss curves for the indoor (A1) scenario

Path-loss curves for all the different A1 sub-scenarios are shown in the Figure 3-1. For the through-wall case there are two types of wall materials considered: Light and heavy wall material with wall attenuations 5 and 12 dB respectively. It is assumed that either of the attenuations to be used depending of the building type assumed in the simulation, probably corresponding to the worst case.

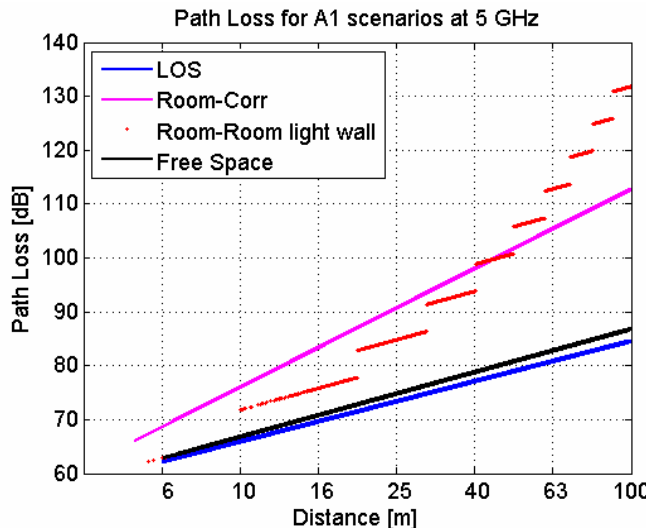


Figure 3-2. Path-loss curves at 5 GHz for the LOS (corridor-corridor) and NLOS (room-corridor, light through wall and heavy through wall) cases.

3.1.4.2 A1 Path-loss and shadow fading (D5.4)

Path-loss (PL) and shadow fading (SF) are considered to be parameters of the highest priority in channel modeling. Path-loss is loss of signal power between transmitter and receiver end. SF is the variance of the PL.

The noise threshold was selected to be -20 dB from the impulse response (IR) peak, and the IR samples below that are removed. Data within a small area is averaged in order to remove the effect of fast fading. The averaging window depended on the environment and the centre-frequency. Spatial averaging is done by combining the wideband MIMO matrices in power.

PL at a certain snapshot is calculated from the calibrated IRs as a wideband path loss

$$PL = -10 \log_{10} \left(\sum_{\tau_i} |h(\tau_i)|^2 \right) + G_T + G_R \quad (3.6)$$

where G_T and G_R are antenna gains at the transmitter and at the receiver, respectively.

The path-loss model is derived using linear regression (LMSE) of the scatter plot of the PL vs. distance between the transmitter and the receiver: $PL(d) = A \log_{10}(d) + B = 10 n \log_{10}(d) + B$, where B is PL intercept, and n is the PL exponent.

3.1.4.2.1 Measurements in corridor - corridor LOS conditions

The measurements were conducted in corridors, the width of which was ranging from 1.5 m to 3.5 m, and so that the BS and MS were in the same corridor with a LOS between them. The path-loss curve for the 5.25 GHz centre-frequency in corridor-corridor LOS propagation condition can be seen in the Figure 3-3.

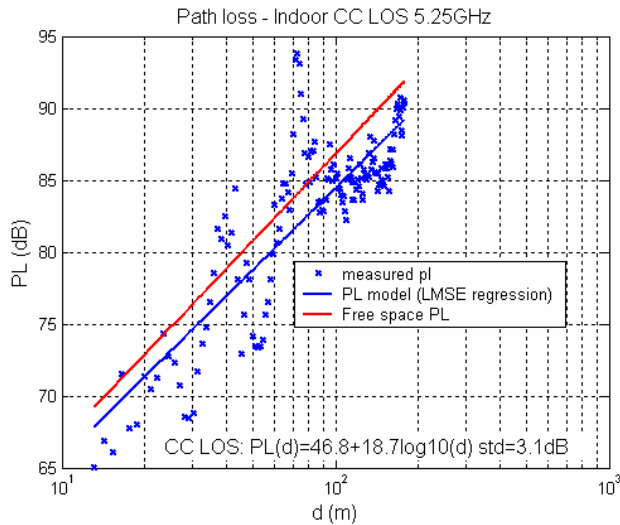


Figure 3-3. Indoor path loss in corridor – corridor LOS conditions.

The equation for the path loss can now be expressed as

$$PL(d) = 46.8 + 18.7 \log_{10}(d), \sigma = 3.1 \text{ dB} \quad (3.7)$$

where d is the distance and σ is the standard deviation of the shadow fading. The equation is valid from 1 m to 200 m.

Very similar results were obtained in the previous measurement campaign [WIN1D53] for LOS conditions, but for limited range. Other similar results, with the path-loss exponent less than 2, have been discussed in several references cited in Section 3.1.17.

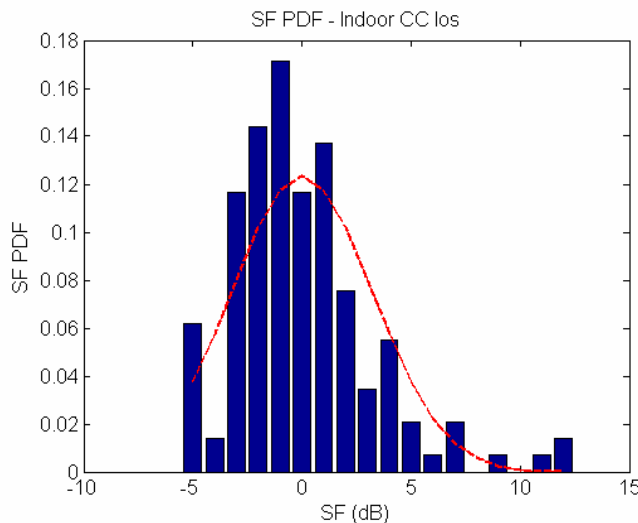


Figure 3-4. Shadow fading distribution in an indoor corridor – corridor LOS environment.

3.1.4.2.2 Measurements in room - corridor NLOS conditions

The path-loss curve for the 5.25 GHz centre-frequency in room – corridor (corridor – room) LOS propagation conditions can be seen in Figure 3-5. The measurements were performed so that either the BS was in the corridor and the MS in the room along the corridor or vice versa. The wooden doors from the corridor to the rooms were closed. It was measured that the attenuation of the door was 4 dB.

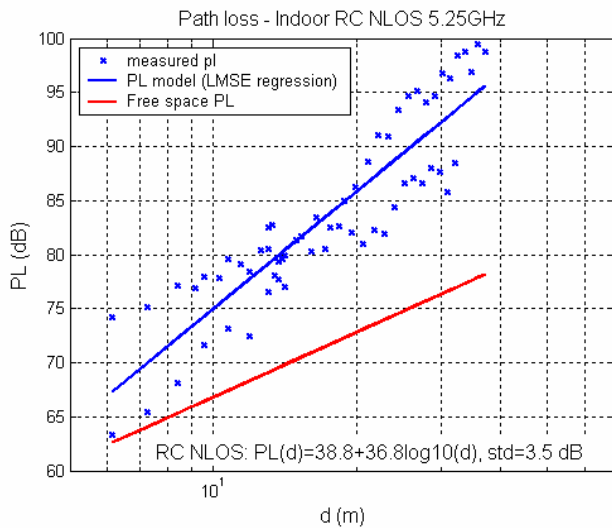


Figure 3-5. Indoor path loss in room – corridor LOS conditions.

The equation for the path loss can now be expressed as:

$$\text{PL}(d) = 38.8 + 36.8 \log_{10}(d), \sigma = 3.5 \text{ dB} \quad (3.8)$$

where d is the distance and σ is the standard deviation of the shadow fading.

The equation is valid from 3 m to 50 m. It is assumed that it can be used until 100 m, although this has not been verified by measurements. From 1 m to 3 m free-space loss formula should be used.

Quite natural assumption is that most part of the path between the MS and BS the signal propagates in the corridor. Therefore it is slightly surprising that the path loss is much steeper in this case than in the corridor – corridor propagation. The reason must be in the mechanism by which the wave couples from the corridor to the room, or vice versa.

LOS probability is the probability that the LOS propagation between the transmitter and the receiver exists.

3.1.5 A1 Angle Spread

3.1.5.1 A1 Angular Spreads at BS and MS (D1.1.1)

The percentiles of azimuth and elevation spreads for the A1 LOS and NLOS are shown in Table 7-1. Note that the results have been obtained from the results of [WIN1D54] by replacing the azimuth figures with the figures obtained for the new campaign. The reason is the fact that the results were originally obtained by using planar directive antennas in BS. In Phase 2 we have concluded that omnidirectional antennas give better models for the A1 scenario. It is assumed that changes in other channel parameters are negligible and can be omitted.

Table 3-1: Percentiles of the RMS azimuth and elevation spreads.

A1 angular spread		LOS		NLOS	
		Azim.	Elev.	Azim.	Elev.
BS, σ_ϕ	10%	32	5	42	6
	50%	44	8	53	11
	90%	59	14	66	22
	mean	45	8	53	13
MS, σ_ϕ	10%	26	4	34	8
	50%	45	10	49	12
	90%	70	15	66	22
	mean	48	10	49	14

The subscenarios A1 room to room NLOS (through wall) are assumed to have the same characteristics as the subscenario corridor to room NLOS in Table 7-1.

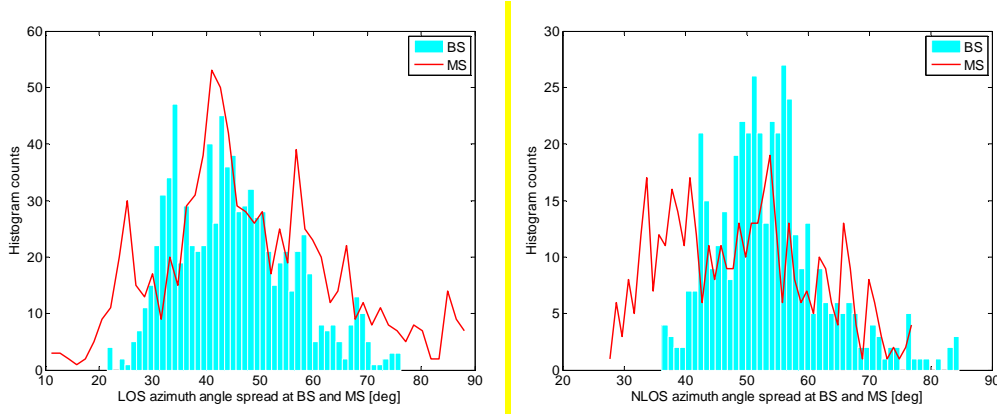


Figure 3-6 Azimuth spread of the indoor LOS (left) and NLOS (right).

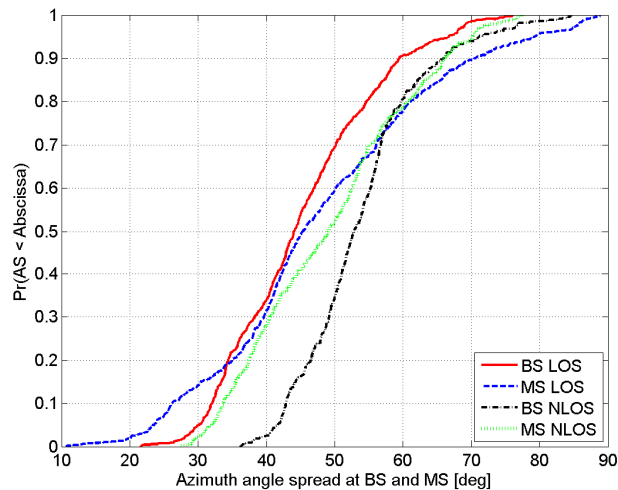


Figure 3-7 All indoor azimuth spreads combined.

3.1.5.2 A1 Angular Spreads at BS and MS (D5.4)

Azimuth angle-spread is calculated like described in [3GPPSCM] from DoA and path power values. It is known as circular angle-spread. Here it is calculated at both BS and MS link end.

The probability density functions and cumulative distribution functions of the azimuth spreads at 5.25 GHz are shown in Figure 3-6 and Figure 3-7 for LOS and NLOS propagation conditions. The percentiles for the CDF functions for the angle-spreads are shown in the Table 3-2 below.

Table 3-2: Percentiles of the RMS azimuth spread.

Combined Tietotalo & Main building		Corri.-Corri. LOS		Corri.-Room NLOS	
		Azim.	Elev.	Azim.	Elev.
BS, σ_ϕ	10%	2.7	4.5	10.2	6.3
	50%	4.8	7.6	21.5	10.9
	90%	16.2	13.6	39.5	21.7

	mean	7.0	8.4	23.0	12.9
MS, σ_ϕ	10%	14.5	4.1	24.6	7.5
	50%	36.6	10.1	37.4	12.1
	90%	67.0	15.4	56.2	21.9
	mean	38.8	9.9	39.3	13.5

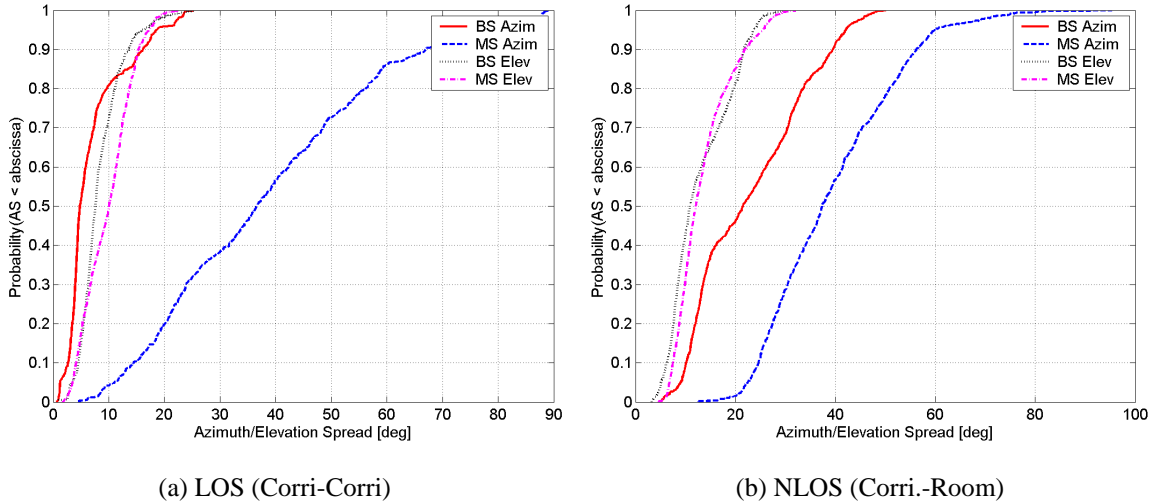


Figure 3-8: Example CDFs of Azimuth spreads at BS and MS.

3.1.6 A1 LOS probability (D5.4)

The probability of line-of-sight (LOS) propagation vs. distance is a function we denote the p_{LOS} function. For scenario A1, this characteristic can be derived analytically because the geometry of the scenario is known exactly.

A simple ad-hoc fit of the derived p_{LOS} function is given as:

$$p_{\text{LOS}}(d) = 1 - (1 - x^3)^{1/3} * (1 - 5 / 50), \quad (3.9)$$

where $x = 1 - \log_{10}(d / 2.5) / \log_{10}(100 / 2.5)$.

3.1.7 A1 Delay Spread and maximum excess-delay distribution (D5.4)

Definition

RMS delay spread is the square root of the second central moment of the PDP normalized to the total power. Max excess delay is the maximum delay after the first peak in PDP.

The measured distributions have been tested against the following theoretic distributions to find out the best fit:

- 1) Log-normal distribution

$$f(x) = \frac{1}{2\pi\sigma} e^{-\frac{(x-\mu)^2}{2\sigma^2}}, \quad F(x) = 1 - Q\left(\frac{x-\mu}{\sigma}\right) \quad (3.10)$$

- 2) Logistic PDF and CDF

$$f(x) = \frac{e^{\frac{x-\nu}{\zeta}}}{\zeta \left(1 + e^{\frac{x-\nu}{\zeta}}\right)^2}, \quad F(x) = 1 - \frac{1}{1 + e^{\frac{x-\nu}{\zeta}}} \quad (3.11)$$

where ν is the location parameter and scale parameter $\zeta > 0$.

- 3) Gumbel (log of Weibull distribution) PDF and CDF

$$f(x) = \frac{1}{\zeta} \exp\left[-\frac{x-\nu}{\zeta} - \exp\left(\frac{x-\nu}{\zeta}\right)\right], \quad F(x) = \exp\left(-\exp\left(-\frac{x-\nu}{\zeta}\right)\right) \quad (3.12)$$

where ν is the location parameter and scale parameter $\zeta > 0$.

3.1.7.1 Scenario A1

The distribution of the RMS-delay spread was investigated. The 10, 50 and 90 % values for the Cumulative Distribution Functions of RMS-delay spread are given below for the 5.25 GHz centre-frequency and different LOS and NLOS propagation conditions.

Table 3-3: RMS delay spreads for A1 indoor scenario.

RMS-DS (ns)		Corri.-Corri.		Corri.-Room	Room-Room
		LOS	NLOS	NLOS	LOS(OLOS)
Percentile	10%	15.0	13.4	13.5	9.4
	50%	38.0	25.2	25.1	14.2
	90%	75.7	48.6	40.6	18.9
	mean	43.0	28.5	26.5	14.2

The distributions of the maximum excess delay were also calculated for the different environments. The 10, 50 and 90 % values for the Cumulative Distribution Functions of the maximum excess delay are given below for the 5.25 GHz centre-frequency and different LOS and NLOS propagation conditions.

Table 3-4: Maximum excess delays for the A1 indoor scenario.

Maximum excess delay range (ns)		Corri.-Corri.		Corri.-Room	Room-Room
		LOS	NLOS	NLOS	LOS(OLOS)
UO main building widest corridor 3.5 m room size (10*10m)	10%	247.1	54.1	97.3	72.5
	50%	265.0	107.5	185.0	95.0
	90%	624.4	249.7	255.0	130.0
	mean	349.0	135.0	181.8	98.1

Cumulative Distribution Functions of the RMS-delay spread are given in the Figure 3-9 a and b below for the 5.25 GHz centre-frequency and c-c LOS and r-c NLOS propagation conditions. Best fit is achieved with the log-normal distribution.

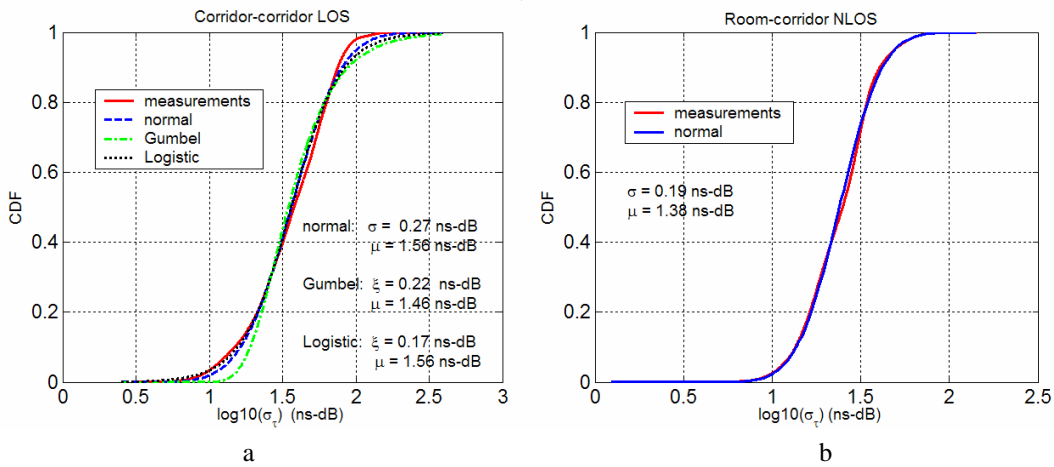


Figure 3-9: a) CDF of the A1 indoor (corridor – corridor) LOS environment, fitting to normal, Gumbel and logistic distributions shown. b) CDF of the A1 indoor (room – corridor) NLOS environment, fitting to normal distribution shown.

3.1.8 A1 Distribution of the azimuth angles of the multipath components (D5.4)

The distribution of the azimuth angle of arrivals and angle of departure for both LOS and NLOS propagation conditions are calculated. Those results are based on superresolution path parameter estimations or the beamform method. CDFs are presented as well as characteristic parameters as 10%, 50%, 90% and mean of the distribution are extracted.

3.1.9 A1 Angle proportionality factor (D5.4)

The angle proportionality factor (r_{AS}) is defined as the ratio between the standard deviation of the azimuth angles of the multipath components and the RMS azimuth spread. This parameter is needed in channel model. The angle proportionality factor is shown in the Table 3-5 below for an indoor (A1) environment for the different LOS and NLOS propagation conditions.

Table 3-5: The percentiles for the CDF of the angle proportionality factor.

Combined Tietotalo & Main building		Corri.-Corri.		Corri.-Room	Room-Room
		LOS	NLOS	NLOS	LOS (OLOS)
BS, r_ϕ	10%	0.98	0.00	0.93	1.38
	50%	1.40	0.78	1.11	1.72
	90%	1.99	1.72	1.63	2.58
	mean	1.45	0.99	1.22	1.90
MS, r_ϕ	10%	1.04	0.00	1.01	0.85
	50%	1.44	0.81	1.31	1.26
	90%	1.74	2.13	1.70	1.59
	mean	1.41	1.64	1.33	1.25

3.1.10 A1 K-factor

3.1.10.1 A1 K-factor (New)

In [WIN1D54] and [WIN2D111] K-factor was given as a function of distance. Now we have increased the level of randomness in the model and will draw the K-factor randomly from the Lognormal distribution: See the results in Figure 3-10.

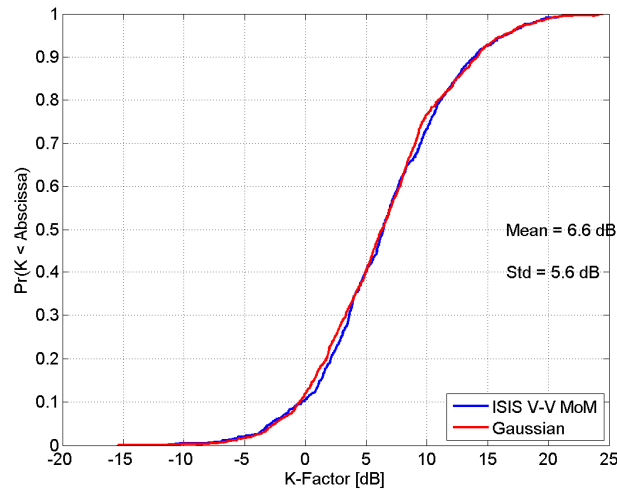


Figure 3-10 A1 K-factor in dB. ISIS V-V MoM means the data is the superresolution data from vertical polarisation and the method of K-factor calculation is the Greenstein's Moments Method.

3.1.10.2 A1 K-factor (D5.4)

Narrowband Ricean K factor in the LOS regions has been analysed. Ricean K-factor is the ratio of power of the direct LOS component to the total power of the diffused non-line-of-sight components.

The narrow-band Ricean K-factor as a function of distance at 100 MHz bandwidth and 5.25 GHz centre-frequency in an indoor environment is considered in the corridor-corridor LOS propagation conditions. CDF of the K-factor is shown in the Figure 3-11. The fitting of the CDF with normal distribution is shown.

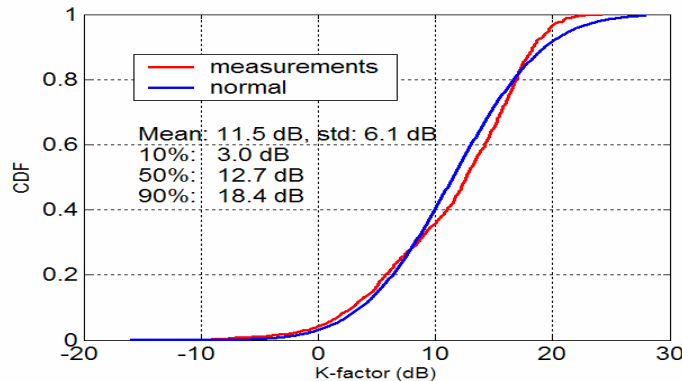


Figure 3-11: a) Distribution of the K-factor in A1 indoor scenario at 5.25 GHz centre-frequency.

K-factor in the A1 indoor scenario and LOS corridor to corridor propagation conditions at 5.25 GHz centre-frequency is shown in the figure Figure 3-12 as function of the BS – MS distance.

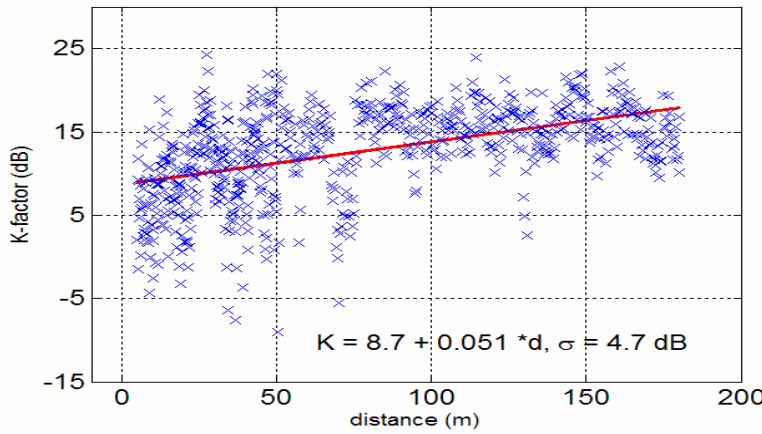


Figure 3-12: K-factor as function of distance in an A1 indoor scenario at 5.25 GHz centre-frequency.

It can be seen that in this measurement the K-factor increases from 9 to 17 dB, when the distance increases from 0 to 150 m. Formula for the K-factor is

$$K = 8.7 + 0.051 \cdot d, \quad (3.13)$$

where d is the distance between the BS and the MS.

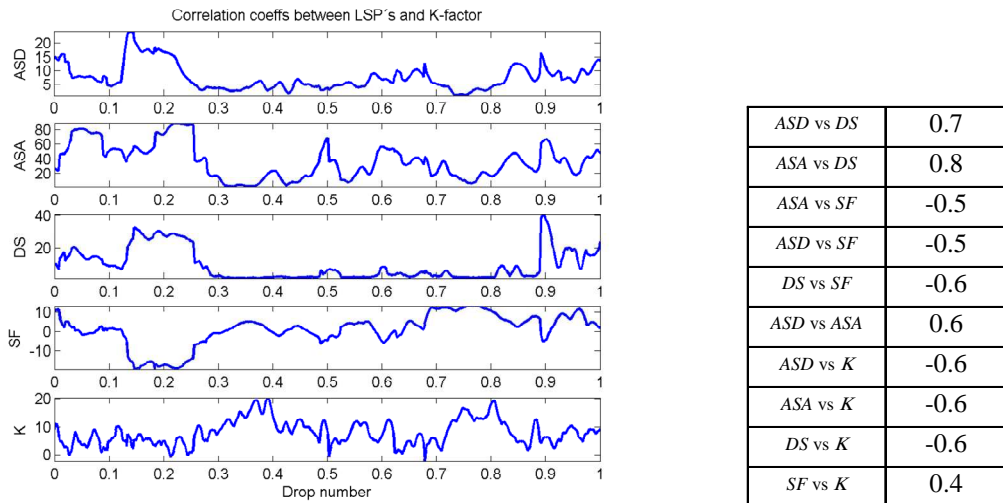
Table 3-6: The 10, 50 and 90 % percentiles for the cumulative distribution function of the narrowband K-factor (dB) for an indoor LOS environment at 5.25 GHz.

Narrowband Ricean K-factor		Corri.-Corri.
LOS		
Percentile	10%	3.0
	50%	12.7
	90%	18.4
	mean	11.5

3.1.11 A1 Cross Correlations

3.1.11.1 A1 Cross Correlations (New)

In [WIN1D54] and [WIN2D111] cross-correlation was analysed between the large scale parameters (LSP's) except the K-factor. However, since we have one K-factor value for each stationarity interval we can calculate the cross-correlation between the K-factor and e.g. delay spread also. Figure 3-13 depicts the correlation as a function of drop number.

**Figure 3-13 Correlation between the LSP's.**

3.1.12 A1 Modelling of PDP (D5.4)

Power Delay Profile (PDP) is the distribution of the power of the multipath components versus delay time. Power delay profiles for LOS and NLOS propagation conditions have been fitted to the exponential function

$$P(\tau) = e^{-b\tau} \quad (3.14)$$

where τ is the excess delay and b is a time constant. Excess delay is difference between delays of the multipath components and the delay of the first multipath component.

Power delay profile at 100 MHz bandwidth and 5.25 GHz centre-frequency in an indoor environment is shown in the figure Figure 3-14 for LOS and NLOS propagation conditions. Power delay profiles for LOS and NLOS propagation conditions have been fitted to the exponential function

$$P(\tau) = e^{-b\tau} \quad (3.15)$$

where τ is the excess delay and b is a time constant.

The results are grouped in the following way: corridor to corridor (c-c) LOS, corridor to room/room to corridor (r-c) NLOS, room to room (r-r) LOS and corridor to corridor (c-c) NLOS. This grouping adapts the results more precisely to the defined A1 scenario. The results for them are shown in the table below.

Table 3-7: Time constants for PDPs (MHz).

c-c LOS	c-r NLOS	r-r LOS	c-c NLOS
50	30	69	32

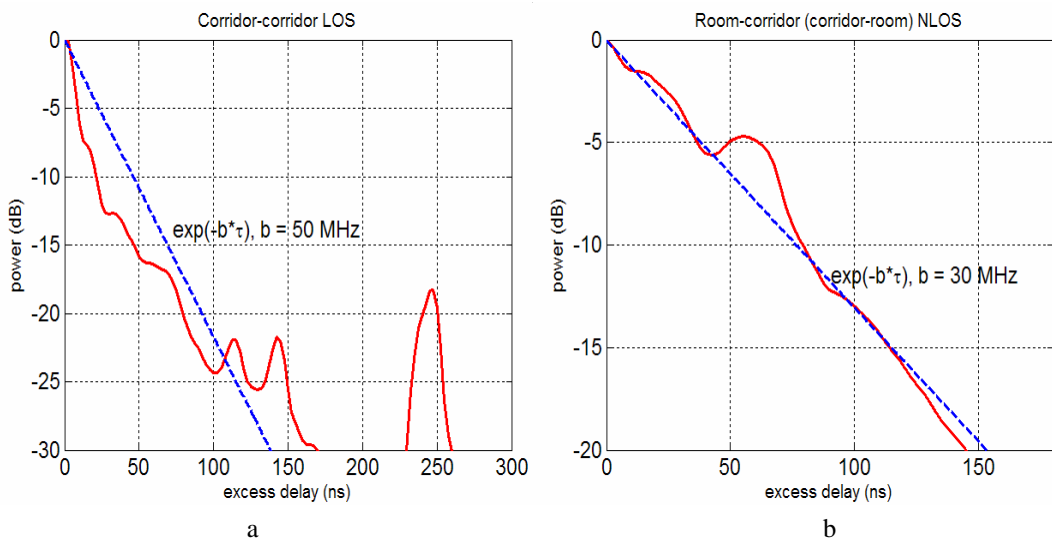


Figure 3-14: Power delay profile at 100 MHz bandwidth and 5.25 GHz centre-frequency in an A1 indoor environment for corridor – corridor LOS and room – corridor NLOS propagation conditions.

The peak at 250 ns delay in the Figure 3-14 a represents a reflection from the corridor end. If desired, it could be introduced in the model depending on the position of the BS. In our model we will neglect it, because of the low level of it.

3.1.13 A1 Number of Clusters (D5.4)

This sub-section presents number of clusters that has been extracted from measurements. The extracted clusters are based on definition that used in the channel model as clusters with zero delay spread. In other words, the considered clustering is in angle domain. These clusters are called zero-delay-spread clusters (ZDSC). Detailed discussion about ZDSC is given in Chapter 4. The distribution of the number of clusters was investigated in an A1 indoor environment. The results are shown below as the 10, 50 and 90 % percentiles of the distribution.

Table 3-8: Percentiles for the number of paths in A1 indoor scenario and different propagation conditions.

Number of paths	Corri.-Corri.		Corri.-Room	Room-Room
	LOS	NLOS	NLOS	LOS(OLOS)
10%	8.0	5.0	4.0	5.0
50%	13.0	8.0	8.0	7.0
90%	19.0	15.0	14.0	9.0
mean	13.0	9.0	9.0	7.0

3.1.14 A1 Distribution of ZDSC delays (D5.4)

Each ZDSC has a number of multipath components that differs in angle of arrivals or angle of departures but they have very close delays, i.e., multipath components that have differential delays within a chip duration are considered as one ZDSC. Since the measurements system does not provide absolute delay, the differential delay of the ZDSCs are extracted from measurements and for both LOS and NLOS conditions.

The percentiles of the distribution of the path delays are shown in the Table 3-9 below. The distribution can be fitted to an exponential distribution, see Figure 3-15.

Table 3-9: The 10, 50 and 90 % percentiles for the cumulative distribution function of the path delays for an indoor environment at 5.25 GHz, and different propagation conditions.

Path delays		Corri.-Corri.		Corri.-Room	Room-Room
		LOS	NLOS	NLOS	LOS(OLOS)
Percentile	10%	11.5	0.0	0.0	0.0
	50%	132.5	72.5	82.5	57.5
	90%	376.3	217.0	220.0	122.5
	mean	174.5	102.8	100.6	61.7

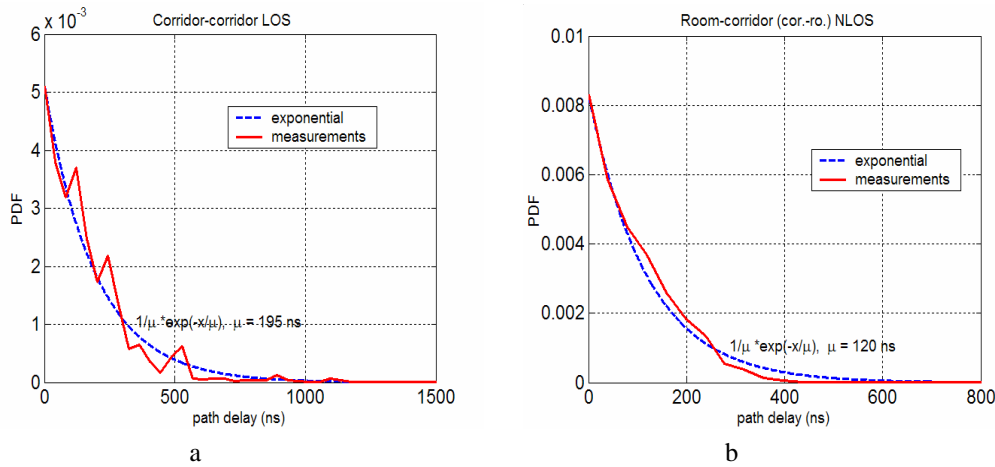


Figure 3-15: a) Distributions of the path delays for the different sub-scenarios.

3.1.15 A1 Delay proportionality factor (D5.4)

The delay proportionality factor (r_{DS}) is defined as the ratio between the standard deviation of the delays of the multipath components and RMS delay spread.

The delay proportionality factor in an A1 indoor environment was calculated. The percentiles for the CDF of the delay proportionality factor are shown in the Table 3-10 below.

Table 3-10: The 10, 50 and 90 % percentiles for the cumulative distribution function of the delay proportionality factor in an indoor environment.

Delay proportionality factor: r_τ		Corri.-Corri.		Corri.-Room	Room-Room
		LOS	NLOS	NLOS	LOS(OLOS)
Percentile	10%	1.9	1.5	1.7	2.4
	50%	3.0	2.2	2.4	3.2
	90%	7.5	3.9	3.2	4.2
	mean	3.9	2.5	2.4	3.2

3.1.16 A1 Cross-polarization ratio (D5.4)

The cross-polarization ratio XPR_V is defined as the ratio of power received from vertical to vertical polarization to the power received from vertical to horizontal polarization as

$$XPR_V = \frac{P_{VV}}{P_{VH}} \quad \text{and} \quad XPR_H = \frac{P_{HH}}{P_{HV}} \quad (3.16)$$

Respectively, XPR_H is defined as the power ratio between HH and HV components. The XPR values are extracted from the estimated propagation paths using the strongest path (LOS) and the reflected paths (scattering). The CDF percentile values of the XPR at 100 MHz bandwidth and 5.25 GHz centre-frequency in an indoor environment is shown in the Table 3-11.

Table 3-11: Percentiles of the cross-polarization ratio.

A1 indoor		direct path (LOS)	scattered paths (NLOS)
XPR_V	10%	13.4	7.1
	50%	23.2	11.2
	90%	31.3	15.8
	mean / std	22.6 / 7.7	11.4 / 3.4
XPR_H	10%	12.3	6.2
	50%	18.3	10.2
	90%	25.3	15.1
	mean / std	18.7 / 5.8	10.4 / 3.4

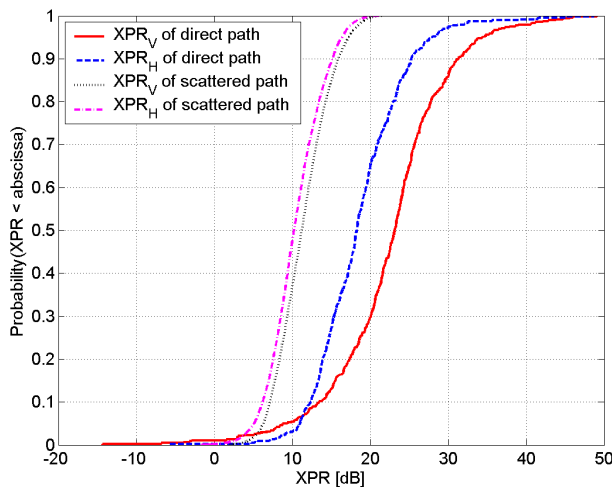


Figure 3-16: CDFs of the XPR_V and XPR_H in an A1 indoor environment.

3.1.17 A1 Literature review

3.1.17.1 A1 Path-loss

In [WHL94], the indoor measurements were performed using network analyzer at 2 and 5 and 17 GHz, the RF bandwidth was 500 MHz. The environment of the measurement locations was composed of a corridor of length 21.7 m, width 2 m and height 3 m and a room with dimensions 7 x 8 x 2.8 m. Both antennas were mounted on stands at a height of 1.8 m.

It was found that in LOS cases, the path-loss exponents are 1.5, 1.7, and 1.6 respectively at the three frequency bands. There is almost no difference and one cannot find how the path-loss exponents change with frequencies. However, for OLOS cases, the path-loss exponents were increased with the centre-frequencies.

In [SG00], the measurements were performed at 5.2 GHz (RF BW was not clear) and mainly investigated the path-loss models for indoor environments including the same floor corridor-corridor (LOS), corridor-room (NLOS), and room-room (NLOS) measurements and also different floor path-loss measurements. Antenna type: two patch antennas or two dipole antennas were applied.

1. Same floor measurement results:

	office		school		
	corr-corr. (LOS)	corr.-room (NLOS)	room-room (NLOS)	corr.-room (NLOS)	room-room (NLOS)
n	1.3	3.1	4.1	5.0	7.0
PL_0 (dB)	47.4	46.1	47.9	30.6	11.3
σ (dB)	2.2	2.9	2.7	2.1	3.9

2. Cross floor measurement results:

Horizontally polarized antennas:

Case 1: The transmitter Tx was located at the 6th floor, then the receiver Rx was moving in a corridor at 5th floor.

Case 2: The Tx was at 6th floor, and the Rx was moving in vertical line between floors 0 and 5.

	Case 1	Case 2
n	2.4	5.6
PL_0 (dB)	76.4	69.5
σ (dB)	1.8	0.69

The transmission loss due to one floor is about 30 dB in the office building. The floor losses are not increased linearly as in Keenan-Motley model. One experiment was performed at both 5 GHz and 900 MHz to determine the dependence of loss on frequencies. However, no significant difference was seen, except for the expected difference in free-space loss.

In reference [KZV01], different kind of path-loss models were obtained based on measurements performed at 5.3 GHz with RF BW 30 MHz. They can be found in the following table.

TABLE I
PATHLOSS MODELS

Category	Environment	Config.	d [m]	n	STD [dB]	σ_{slow} [dB]	antennas TX - RX
LOS	HUT1	corridor	8-60	1.3	4.7	4.0	omni-omni
	HUT1	corridor	8-60	1.3	5.3	4.2	horn-patch
	HUT2	corridor	10-70	1.5	4.8	4.0	horn-omni
	VTT	corridor	3-25	1.4	3.4	2.5	omni-omni
	Airport	hall	8 - 100	1.3	2.0	1.3	omni-omni
NLOS	part. type						
		HUT1 C	corridor-room	5-30	4.8	5.5	omni-omni
	HUT2 A	corridor-room	10-72	2.9	3.1	1.7	horn-omni
	HUT2 A	corridor-corridor	13-38	2.6	5.6	5.1	omni-omni
	VTT B	corridor-corridor	6-25	3.5	2.7	1.1	omni-omni
	Airport	hall	35- 200	1.9	2.7	1.7	omni-omni
Different floors	HUT1 [16]	corridor-room	5-30	6.5	6.0		omni-horn*
	VTT	corridor-corridor	5-25	5.7	5.8		omni-omni

*rotating horn, value for maximum signal level

3.1.17.2 A1 Rms delay spread

In [NAH93] the mean RMS delay spread decreases with centre-frequencies as shown in the table below.

Location	Frequency						
	2-2.5 GHz		5-5.5 GHz		17-17.5 GHz		
	mean	s.d.	mean	s.d.	mean	s.d.	
T1	LOS	34.5	13.2	14.4	3.0	11.0	2.2
	OBS	39.6	10.5	22.0	4.5	15.3	8.4
T2	LOS	37.5	11.8	14.8	3.0	11.6	1.6
	OBS	37.7	12.0	21.2	9.4	19.2	10.5
T3	LOS	49.0	5.4	15.7	11.7	26.9	17.7
	OBS	37.6	17.0	22.1	5.5	27.6	10.6

The difference between frequency ranges 2-2.5 GHz and 5-5.5 GHz in the table above is quite big, the ratio is 1/3 ... ½. From 5-5.5 GHz to 17-17.5 GHz the difference is much smaller, if anything.

In [NAH93] and [KZV01] the indoor RMS delay spread statistic values were summarized in the table

Class	F [GHz]	Distance (m)	σ_t [ns]	Value given	Method	Ref
LOS	5.3	3-100	20-120	CDF 90%	WCS	[KZV01]
	2.25	1-15	34.5-49.0	mean	VNA	[NAH93]
	5.25	1-15	14.4-15.7	mean	VNA	[NAH93]
NLOS	5.3	5-200	30-180	CDF90%	WCS	[KZV01]
	2.25	1-15	34.5-49	mean	VNA	[NAH93]
	5.25	1-15	14-15.7	mean	VNA	[NAH93]

WCS: wideband channel sounder.

3.1.17.3 A1 Angle-spreads

Reference [DRX98] was considering the tap and cluster angle-spreads of indoor WLAN channels by using frequency domain measurements. The measured data with 400 MHz BW (5.0-5.4 GHz) were employed. FD (freq. domain)-SAGE was applied.

1. Cluster and cluster AS: a cluster was based on the observation that multipath components (MPCs) arrive in groups. AS means RMS angle-spread.
2. Average tap AS: To find a tap AS for the channel with a specific delay resolution $1/f_c$, all the MPCs were collected for every $1/f_c$ and put them in the same delay bin. For each individual tap, the instantaneous tap AS was calculated.

Average tap AS and cluster AS

	Number of clusters	Average Tap AS (mean)	Cluster AS (mean)
Data set 69	4	19.1°	20.2°
Data set 71	5	11.6°	12.4°
Data set 73	5	12.1°	13.3°
Data set 75	4	18.5°	21.2°
Data set 78	5	12.2°	13.2°
Data set 81	5	12.0°	13.0°
Data set 84	5	12.4°	13.3°
total	33	13.7°	14.9°

Average tap AS with different bandwidths

	10 MHz	20 MHz	50 MHz	100 MHz
Data set 69	19.9°	19.8°	19.3°	19.1°
Data set 71	12.3°	12.2°	11.7°	11.6°
Data set 73	13.1°	12.7°	12.6°	12.1°
Data set 75	20.4°	19.8°	19.0°	18.5°
Data set 78	13.1°	13.0°	12.7°	12.2°
Data set 81	12.9°	12.7°	12.5°	12.0°
Data set 84	13.0°	12.9°	12.7°	12.4°

It is interesting to notice that the mean tap AS and cluster AS have some difference, but small. The tap AS changes with RF bandwidth, but the difference is quite small.

In [Xia96] mean azimuth spread on MS side at 5 GHz is 60.67° and standard deviation is 14.26°. In the measurement setup BS antenna height was 3 m and MS antenna height 1.2 m.

Measurement results from the COST 273 action for indoor office environment are collected in [BBK+02]. The following table contains information about azimuth, elevation and delay spreads as well as about the number of identified clusters:

Doc.	Azimuth Spread [Rms deg]				Elevation Spread [Rms deg]				Delay Spread [ns]		No of Clus	Carrier/BW [GHz/MHz]	Environment
	Total		Cluster		Total		Cluster		Total	Cluster			
	BS	MS	BS	MS	BS	MS	BS	MS					
TD-02-105									10-20		1-2	6.0/10000	Corr-room
TD-03-060									5-30		1	5.2/2000	Corr-room
TD-04-080									5-10			6.0/10000	Sing. room
TD-04-166/167			2-3	2-5							2-13	5.2/120	Corr/room
TD-04-192			0-15	0-15			0-3	0-3	27-57		15	6.85/7500	Empty room
TD-04-193	40*	37			6	7						5.3/60	Corr-room
Kiv1999a		20-100							10-120			5.3/50	Room-room
Poo2003				5-30*						20	2.5	5/6000	Typical office
Sib2000									10-40			5.1/120-200	Corr-room
Med2001	5-30	30-70			4-9	4-9						5.2/200	Corr-room
Qui1999	25-80	25-80										1.8/200	Room-room
Kiv1997									10-50			5.3/50	Corr-room
Yu2004			13-20								4-5	5.2/400	landscape
Ch02003c	15-40*	15-40*							5-40			5.2/120	Corr NLOS
Ch02003c	7*	7*							5-40			5.2/120	Corr LOS
Cho2003h			9	9						13-38		5.2/120	Large room
Cho2003h			3 LOS	3 LOS						13-38		5.2/120	Large room
Spe2000				22-26					17	5-7	3-5	7/500	Indoor
Cra2002				37					45	2		UWB	Corr-room
This TD			5	5	5	5	5	5	45		4	5.2/200	Corr-corr
This TD		42	5	5	5	5	5	5	54		2		Corr-room
This TD	70	70	5	5	5	5	5	5	74		9		Room-room
Range	5-80	7-100	0-20	0-37	4-9	4-9	0-3	0-3	5-120	2-38	1-15	1.8-7/50-10000	
Typical	25	50	10	15	6	6	1.5	1.5	20	20	1-4		

3.1.17.4 A1 Spatio-temporal correlation properties

Reference [EGT+99] is about the spatio-temporal correlation properties for 5.2 GHz indoor propagation environments. The RF bandwidth is 120 MHz. The definitions of the RMS delay spread and RMS azimuth angle-spread are the same as in D5.3. The heights of both antennas were 1.8, and 2.5 m, respectively.

The measurements were performed in a large room (OFF), and entrance foyer (FOY), and two corridors (corr1 was a new building, and corr2 was an old building). The linear relationship between RMS AS and DS was found in OFF-LOS case,

$$\tau_{RMS} = 0.84 * \phi_{RMS} - 1.6 \text{ (ns)} \quad (3.17)$$

In some other cases, the relationships cannot be fitted into linear. However, the spatio-temporal correlation coefficient can be found in the following table.

TABLE I
AVERAGES VALUES FOR RMS DELAY SPREAD AND RMS AZIMUTH SPREAD
AND THE SPATIO-TEMPORAL CORRELATION COEFFICIENT

Environment	Average τ_{RMS} [ns]	Average ϕ_{RMS} [°]	$\rho_{\tau,\phi}$
LOS in OFF	15.39	12.99	0.73
LOS in FOY	13.91	18.45	0.76
LOS in COR1	10.56	7.96	0.73
NLOS in OFF	23.06	20.52	0.30
NLOS in FOY	39.71	32.52	0.15
NLOS in COR1	12.71	29.38	0.14
NLOS in COR2	15.81	40.94	0.04

It can be seen that in all LOS cases, DS and AS have good correlations, however, in all NLOS cases, the correlation coefficients are quite small.

In reference [MRA93], the cluster AoAs were found to follow Gaussian distribution, and the cluster time-of-arrivals (TOA) were found to be exponentially distributed.

3.1.18 Interpretation of A1 results

3.1.18.1 A1 Path-loss

3.1.18.1.1 Proposed path-loss model

The results for path loss and shadowing have been summarized in Table 3-12.

Table 3-12: Path-loss and shadowing characteristics in the indoor environment.

Indoor	LOS (c-c)	NLOS (r-c)
PL at 5.25 GHz	$46.8 + 18.7 \log_{10}(d)$, $d > 1\text{m}$	$\text{PL}(d) = 38.8 + 36.8 \log_{10}(d)$ $d > 5\text{m}$
SF standard deviation at 5.25 GHz	$\sigma = 3.1 \text{ dB}$	$\sigma = 3.5 \text{ dB}$

3.1.18.1.2 Probability of LOS

The probability of line-of-sight (LOS) propagation vs. distance is a function we denote the pLOS function. For scenario A1, this characteristic can be derived analytically because the geometry of the scenario is known exactly.

A simple ad-hoc fit of the derived pLOS function is given as:

$$\text{pLOS}(d) = 1 - (1 - x^3)^{1/3} * (1 - 5 / 50), \quad (3.18)$$

where $x = 1 - \log_{10}(d / 2.5) / \log_{10}(100 / 2.5)$.

3.1.18.2 A1 Power-delay profile

The PDP at a corridor to corridor environment is modelled as a decaying exponential. The measured PDP has a spike that can be identified coming due to a reflection from the end of the corridor, see Section 3.1.12. In our model we have neglected it, because the delay of the spike depends on the location of the BS in the corridor. The constants of the decay have been determined in the same paragraph. It is relatively easy to extend the model to include the spike, when the location of the BS is fixed. However, it is not included in the current model. This is justified by the model simplicity and also the relative low level of the measured spike. For the corridor to room environment the model fits quite well in the exponential model.

3.2 A2 - Indoor to outdoor

3.2.1 A2 – Scenario definition

In indoor-to-outdoor scenario (Figure 3-9) the MS antenna height is assumed to be at 1 – 2 m, and BS antenna height at 2 – 2.5 m + floor height. The corresponding outdoor and indoor environments are B1 and A1, respectively. It is assumed that the floors 1 to 3 are used in simulations, floor 1 meaning the ground floor.

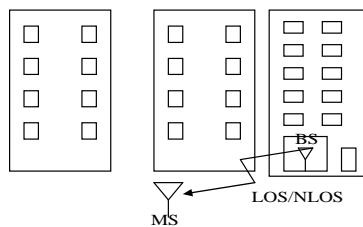


Figure 3-9: Indoor to outdoor scenario.

Based on [AHHM07] and [HACK07] scenarios A2 and B4 are reciprocal and for this reason they are combined in part I of D1.1.2. In here the measurement results for both of the scenarios are shown. **B4 results are discussed in section 3.6.**

The comparison of these scenarios is based on the high-resolution propagation parameters estimated from the measurement data. The measurements took place in the campus area of Oulu University, Finland, which is considered as urban micro cellular environment.

The results in [AHHM07] consider large scale and small scale parameters, and the comparison of Outdoor-to-Indoor and Indoor-to-Outdoor scenarios is shown in Table 3-13 below. The reader should note that in the Outdoor-to-Indoor scenario, a planar array antenna was applied for the transmitter. This leads to a difference in angle spread of the outdoor terminal.

Table 3-13. Large scale parameters comparison

Parameter		Out-to-In	In-to-Out
Delay spread [ns]	median	40	34
	std	23	17
AoD angle spread [°]	median	18	50
	std	12	20
AoA angle spread [°]	median	61	50
	std	20	27
K-factor [dB]	median	6	6
	std	6	6
XPR _V / XPR _H [dB]	median	4 / 12	3 / 9
	std	11 / 11	8 / 11

The Table 3-14below [HACK07] shows the results in cluster level analysis. The cluster parameter estimator presented in [CBH+06] is applied for the high resolution channel data. A cluster represents a collection of multipath components that are collocated in the delay-angular domain. The clustering algorithm [CC05] can be applied after using the ISIS algorithm for the extracted small scale parameters from the measurements. The outputs of the algorithm are the identified and tracked clusters with their parameters over the cluster lifetime periods.

Table 3-14 Cluster level parameter comparison

Parameter	Out-to-In	In-to-Out
Cluster AoD azimuth spread [°]	2.7	6.9
Cluster AoA azimuth spread [°]	6.5	3.5
Cluster delay spread [ns]	6.5	3.5
Per-cluster shadowing [dB]	2.7	2.4
Num of clusters per snapshot	12.0	10.6
Number of paths within cluster	4.2	3.7
Cluster birth rate [clusters/m]	13.1	10.3
Cluster lifetime [m]	0.4	0.5

3.2.2 A2 Measurements

The propagation scenarios were measured in the campus area of OuluUniversity, Finland. The base station was located inside the building on the first and fourth floor. There were three BS measurement positions in each floor, and for every of these positions, the MS moved multiple outdoor routes as shown in Figure 3-17, where the BS positions are marked with green marks and some exemplary routes with a green solid line. The zero angle of the BS antenna is shown with a black solid line. The height of the BS antenna was 2 meters and the height of the MS antenna was 1.5 meters. In Figure 3-17, an example view of the building from the inside is provided.

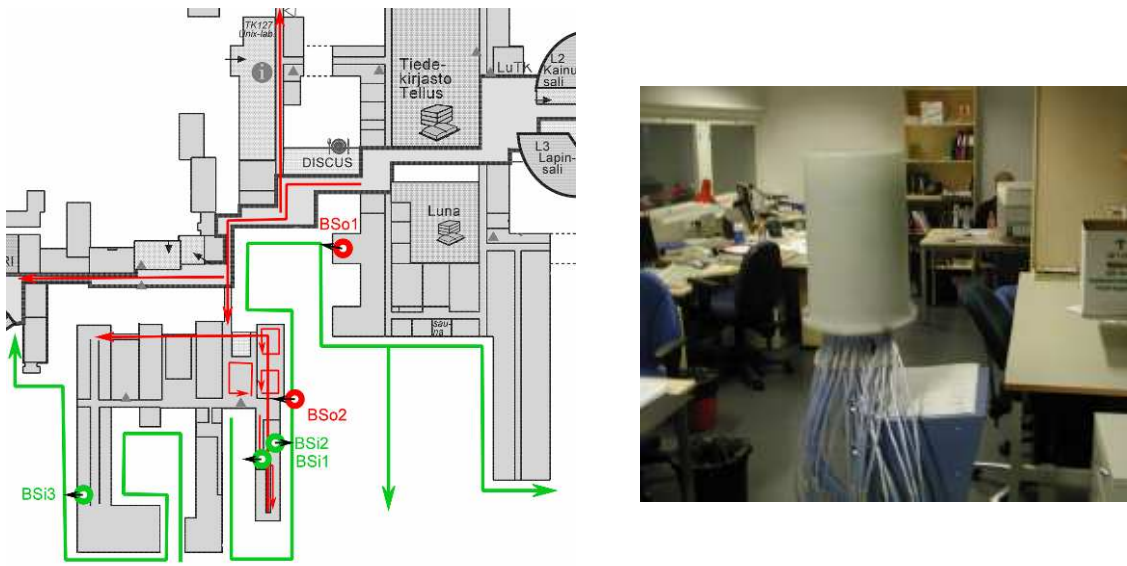


Figure 3-17. Routes measured in in-to-out scenario. The BS positions and routes are marked with a green solid line for the in-to-out case. The red refer for the out-to-in case. Inside view on the right.

3.2.3 A2 Path-loss and shadow fading (D1.1.1)

3.2.3.1 Sub-scenarios

For the propagation in A2 scenario there exist some different sub-scenarios. They are important mainly for the path-loss characteristics. These sub-scenarios are shortly discussed below.

The indoor to outdoor environment A2 is somewhat more complex than the single scenarios. Normally it has been sufficient to model LOS and NLOS conditions. For the A2, we have to define the paths BS – wall (indoors), penetration through the exterior wall and path from the wall to the MS. The BS – wall path can be LOS or NLOS depending on the BS location. The penetration through the wall depends on the wall, windows and the grazing angles both sides the wall. Eventually the wall – MS path can be either LOS or NLOS. In addition, the floor affects also the propagation.

We can recognize the following sub-scenarios for analysing the propagation:

- a) BS near (in the room next to) the exterior wall, MS in WLOS (Wall in LOS towards MS).
- b) BS near exterior wall, MS in WNLOS (Wall in NLOS towards the MS) behind one corner.
- c) BS near the exterior wall, MS in WNLOS on the opposite side of the building (wing).
- d) BS far from the exterior wall, MS in WLOS.

The sub-scenario (c) will be neglected, because the propagation over or through the building is assumed highly lossy. Sub-scenario (d) can be combined with (a) by modelling the indoor path properly. Therefore we will have just the sub-scenarios (a) and (b) left. Actually our measurements cover only the case (a). Case (b) will be covered by the results found from the literature.

3.2.3.2 Results from literature for path-loss

There is a model for penetration of the signal from outdoors to indoors that was created in the COST 231 project [COST231]. The model is based on measurements in the frequency range from 900-1800 MHz and at distances up to 500 m. This means that it can not be applied automatically in the frequency range 2 – 6 GHz, but we believe that the basic approach can be used. For LOS conditions the model is defined in the figure below [COST231].

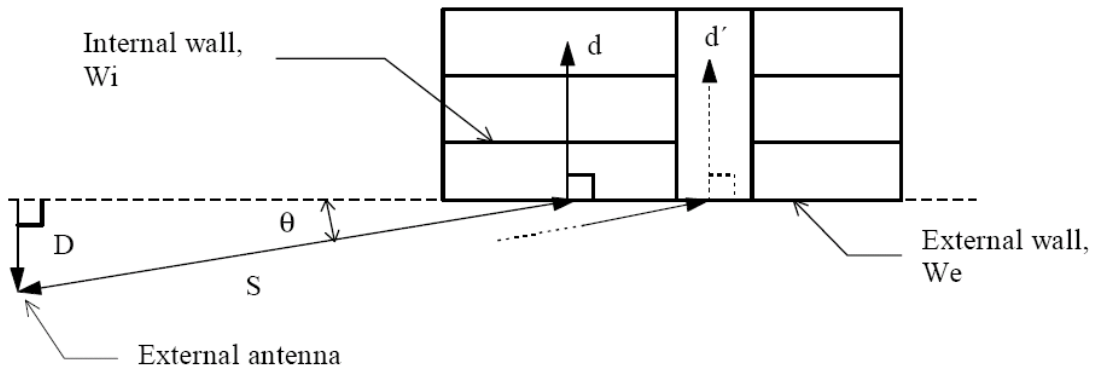


Figure 3-18. Definition of grazing angle θ and distances D , S and d . In the building an example of a possible wall layout at one single floor is shown. The distance d is a path through internal walls and the distance d' is a path through a corridor without internal walls.

Formula for the path-loss is given below:

$$L / \text{dB} = 32.4 + 20 \log(f) + 20 \log(S + d) + W_e + WG_e \left(1 - \frac{D}{S} \right)^2 + \max(\Gamma_1, \Gamma_2) \quad (3.19)$$

where $\Gamma_1 = W_i p$ and $\Gamma_2 = \alpha(d - 2)\left(1 - \frac{D}{S}\right)^2$.

D and d are the perpendicular distances and S is the physical distance between the external antenna and the external wall at the actual floor, see Figure 3-18. All distances are in metres, frequency is in GHz. The angle is determined through the expression $\sin(\theta) = D/S$. W_e is the loss in dB in the externally illuminated wall at perpendicular penetration $\theta = 90$ degrees. WG_e is the additional loss in dB in the external wall when $\theta = 0$ degrees. W_i is the loss in the internal walls in dB and p is the number of penetrated internal walls ($p = 0, 1, 2, \dots$). In the case that there are no internal walls, as along d' shown in Fig. 4.6.1, the existing additional loss is determined with α in dB/m.

The following parameter values are recommended in the model (for 900 – 1800 MHz):

$W_e : 4 - 10$ dB, (concrete with normal window size 7 dB, wood 4 dB)

$W_i : 4 - 10$ dB, (concrete walls 7 dB, wood and plaster 4 dB)

WG_e : about 20 dB

α : about 0.6 dB/m

In the NLOS case the total loss between isotropic antennas relative the outside reference loss, L_{outside} , is determined with the following equation:

$$L / \text{dB} = L_{\text{outside}} + W_e + WG_e + \max(\Gamma_1, \Gamma_3) - G_{FH} \quad (3.20)$$

where $\Gamma_3 = \alpha d$ and $G_{FH} = h G_h$.

W_e , Γ_1 , and d are similar to the corresponding definitions in the section above, line of sight conditions. G_h is the height gain in dB/m. h is the height in metres above the outdoor reference path loss level. For the NLOS case there are several illustrative figures and explanations in [COST 231], but they are not copied here.

There is the following general statement about the calculating of the penetrated power in [COST 231]:
It has been found that the best method in order to estimate the received power at a fixed location within a building, is to consider all the paths through the external walls as shown in Figure 3-19. For each path, the received power is determined according to the methods described above and the sum of these separate power levels will then be the total received power. Those paths that are expected to give rise to loss levels far greater than the remaining paths, can of course be omitted.

The situation is depicted in the Figure 3-19 [COST231].

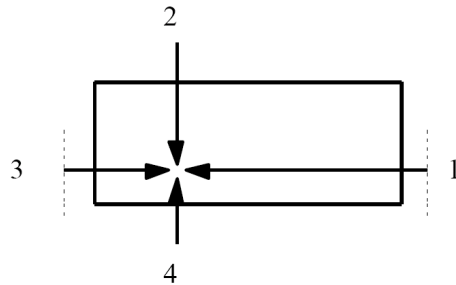


Figure 3-19. Relevant propagation paths into a building.

In [MOT02] the authors discuss the propagation from outdoors to indoors through wall openings like doors and windows. They compare this model to the COST 231 model, where penetration is modelled so that it happens at the nearest point in the wall, i.e. perpendicularly towards the interior. The measurements were performed at 8.45 GHz and the coefficients are given for this frequency. The environment was a big department store with glass doors. Presumably the building forms one big space with shelves and possibly light walls inside the building. The authors claim that their model is more precise in the case, when there exists openings in the wall. The formula for the penetration loss is given below.

$$L_p / \text{dB} = W_e + WG_e (1 - \cos\theta)^2 + WG_i \sin(\phi) \quad (3.21)$$

where W_e is the loss across the wall opening for perpendicular penetration, WG_e is the outdoor angular dependency coefficient and WG_i is the indoor angular dependency coefficient.

The angles ϕ and θ define the direction of the MS indoors and the BS outdoors (or vice versa) seen at the wall opening. The situation can be seen in the Figure 3-20 [MOT02].

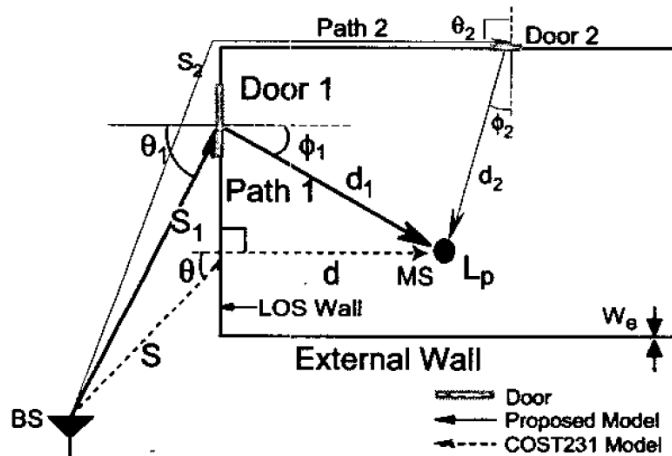


Figure 3-20. Big department store with the BS outdoors and MS indoors. Main propagation path comes through a door.

Loss from the wall opening to the indoor MS (or BS) is calculated slightly differently from that in the COST231 model:

$$L_i = \alpha d \quad (3.22)$$

where α is the attenuation constant and d is the distance between the wall opening and MS (BS).

The outdoor loss is proposed to be calculated with models used in the macro or micro cell as appropriate. The values for the different constants are:

WG _e (dB)	20.0
W _e (dB)	17.2
α (dB/m)	0.348
WG _i (dB)	20.0

The values are different from the [COST231]. Reason can be the higher frequency range and also the special type of the building. [COST231] does not specify the indoor angle dependence at all.

In [SS01] the authors present a theoretical model for the calculation of the path-loss by integrating over the relevant aperture that is in this case the exterior wall. The wall shall be divided in smaller elements and the field strength to be calculated through these elements to the interior of the house. Internal walls and doors can be handled in a simplified manner. Results are presented compared to measurements and the COST 231 model [COST231]. Shown results outperform the COST 231 model. Actually this approach could be useful in this project. The only drawback is that it is more complicated than the models in [COST231] and [MOT02]. For this reason the formulas are not shown here.

3.2.3.3 Path-loss model

Based on our measurements and the literature cited above we propose the following path-loss model:

- Path-loss is composed of three parts: i) indoor BS – wall attenuation, ii) through-wall attenuation and iii) basic BS – MS attenuation, walls neglected.

- Indoor BS – wall attenuation is like in the A1 channel model.
- Through wall attenuation is modelled like in the [COST231].
- Basic BS – MS attenuation is modelled as in the B1 channel model (see path loss table (4-4) in part1 of D1.1.2)..

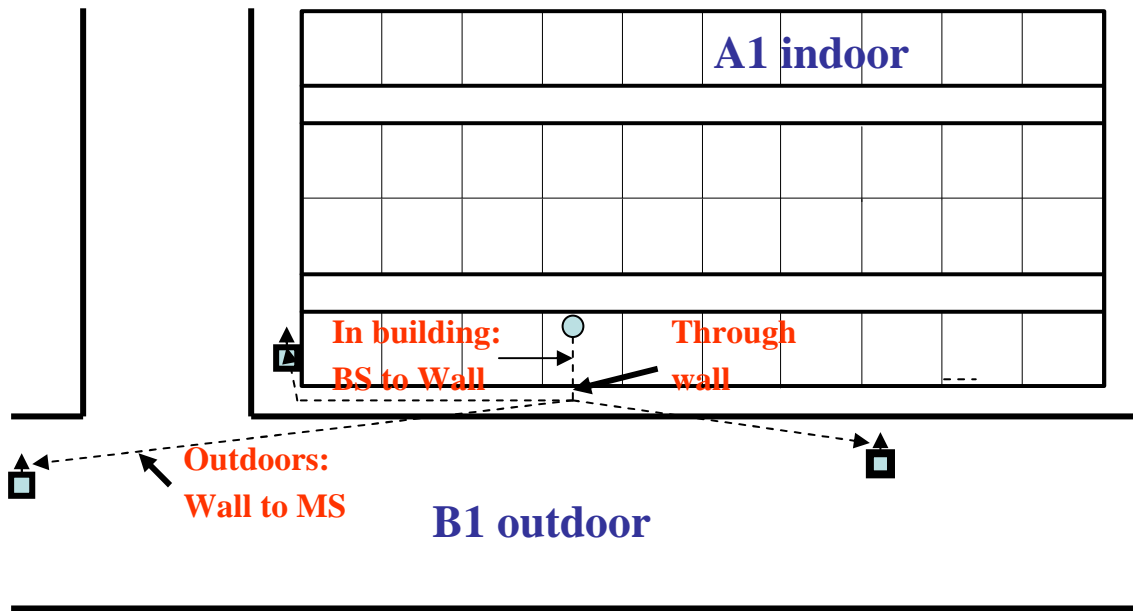


Figure 3-21. A2 Indoor to Outdoor environment. BS indoors and MS outdoors.

Now the path-loss model can be expressed as:

$$\begin{aligned}
 PL &= PL_b + PL_{tw} + PL_{in} \\
 \text{where} \\
 PL_b &= \max(41 + 20 \log(f[\text{GHz}]/5) + 22.7 \log_{10}(d_{out}[\text{m}] + d_{in}[\text{m}]), PL_{free}) \\
 PL_{tw} &= W_e + WG_e \left(1 - \frac{D}{d_{out}}\right)^2 = We + WG_e (1 - \cos(\theta))^2 \\
 PL_{in} &= \alpha d_{in}
 \end{aligned} \tag{3.23}$$

This can be written for the desired A2 scenario, where indoor scenario is A1 and outdoor scenario is B1, as follows:

$$\begin{aligned}
 PL &= PL_b + PL_{tw} + PL_{in} \\
 \text{where} \\
 PL_b &= PL_{B1}(d_{out} + d_{in}) \\
 PL_{tw} &= We + WG_e (1 - \cos(\theta))^2 \\
 PL_{in} &= \alpha d_{in}
 \end{aligned} \tag{3.24}$$

Above PL_{free} is the free space loss, PL_b is the basic loss between the BS and UT along the route $d_{out} - d_{in}$ without wall effects, PL_{in} is the loss inside the building and PL_{tw} is the loss through the outer wall. The parameters in the equation are:

d_{out} = outside distance,
 d_{in} = inside distance,
 D = perpendicular distance from the MS to the building wall,
 α = loss coefficient for the indoor propagation,
 W_e = Loss through wall for the perpendicular penetration ,
 WG_e = Loss through wall for the parallel penetration. and
 θ = angle between the normal of the wall and outgoing (incoming) ray

Fom our measurements the most appropriate values for the model constants have been found and they are:

W_e : 18 dB,
 WG_e : 15 dB
 α : 0.5 dB/m.

Actually the best fit was obtained with the value 0.3 dB/m of α , but to make it compliant with the indoor model through-wall loss 5 dB we selected slightly higher value 0.5 dB/m.

Comparing these values with the [COST231] and [MOT02] coefficients we get the following comparison table:

	WINNER	[COST231]	[MOT03]
W_e :	18 dB,	4 - 10 dB,	17.2
WG_e :	15 dB	20 dB	20.0
α :	0.5 dB/m	0.6 dB/m	0.348

The values from our measurements match quite well with the ones from the [COST231] and [MOT02] models. It should be noted that the match between the measurements and the model is not very exact: The predicted minima for the path-loss may occur in different places than predicted by the model. Model predicts the minimum path-loss at the closest point to the inside BS. In the real world the locations of the minima depend on the locations of the windows, doors or other wall openings. The minima tend also to be sharper than predicted by the model. However, to be able to model these phenomena would need more

precise description of the environment than is practical. In general the model is seen suitable for describing the path-loss behaviour from inside to outside and is adopted for the Indoor to Outdoor scenario.

An alternative form for the path-loss is obtained by replacing the continuous attenuation by stepwise one. Then

$$PL = PL_b + PL_{rw} + PL_{in}$$

where

$$PL_b = \max(41 + 20 \log(f[\text{GHz}]/5) + 22.7 \log_{10}(d_{out}[m] + d_{in}[m]), PL_{free})$$

$$PL_{rw} = W_e + WG_e \left(1 - \frac{D}{d_{out}}\right)^2 = We + WG_e (1 - \cos(\theta))^2$$

$$PL_{in} = n_w L_w$$

where n_w is the number of walls and L_w is the indoor wall loss. The default value for L_w is 5 dB.

Standard deviation of the path-loss is 7 dB and the correlation distance is assumed the same as in B1.

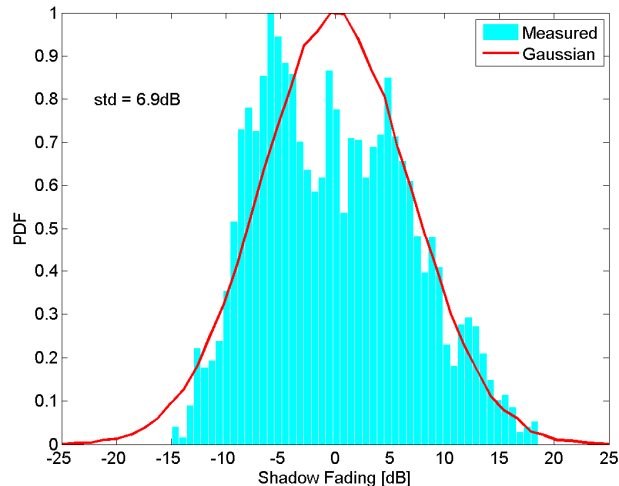


Figure 3-22 PDF of the shadow fading of the A2 indoor-to-outdoor scenario.

3.2.4 A2 Delay spread and maximum excess delay distribution (D1.1.1)

Table 3-15 Percentiles of the rms delay spread

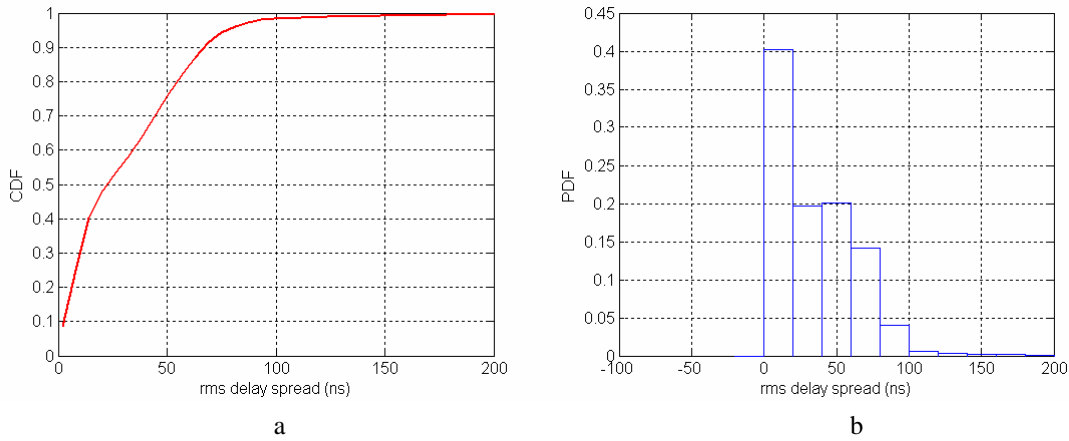


Figure 3-23. RMS delay spread. a) Cumulative density function. b) Probability density function.

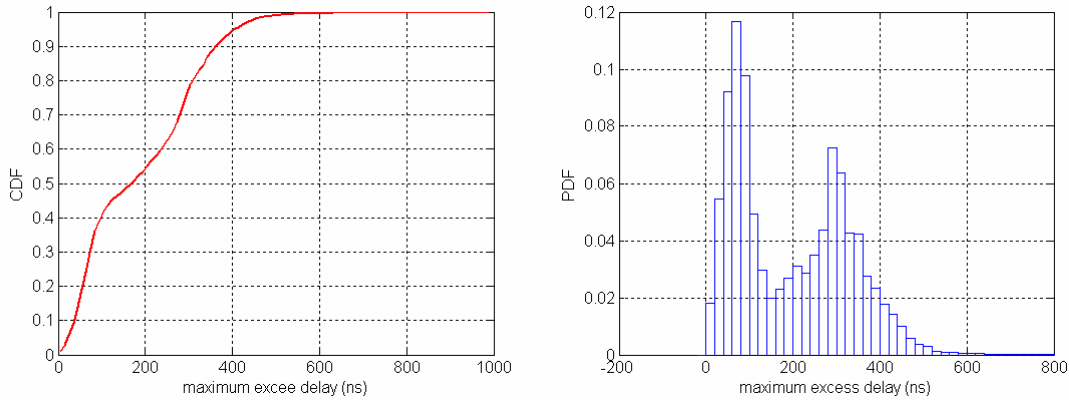


Figure 3-24. Maximum excess delay. a) Cumulative density function. b) Probability density function.

Table 3-16. Percentiles of the rms delay spread

Percentile	Maximum excess delay (ns)
10%	37
50%	175
90%	362
mean	194

3.2.5 A2 Azimuth angle spread at BS and MS (D1.1.1)

The percentiles for the CDF functions of the angle spreads are shown in the table Table 3-17. Histograms of the azimuth spreads of the first and fourth floor are presented in Figure 3-25 a and b, respectively. The cumulative distribution functions of the all data combined are shown in Figure 3-26 for the base station and mobile terminals.

Table 3-17. Percentiles of the RMS azimuth spread.

Azimuth spread	Percentiles	1 st floor	4 th floor	All combined
BS, σ_ϕ	10%	39.4	26.5	32.2
	50%	58.9	42.9	54.8
	90%	74.5	67.6	73.0
	mean / std	57.4 / 14.4	44.9 / 15.5	53.6 / 15.8
MS, σ_ϕ	10%	4.5	2.3	4.1
	50%	24.0	21.3	22.9
	90%	48.4	38.5	46.4
	mean / std	26.0 / 16.9	21.4 / 14.1	24.6 / 16.3

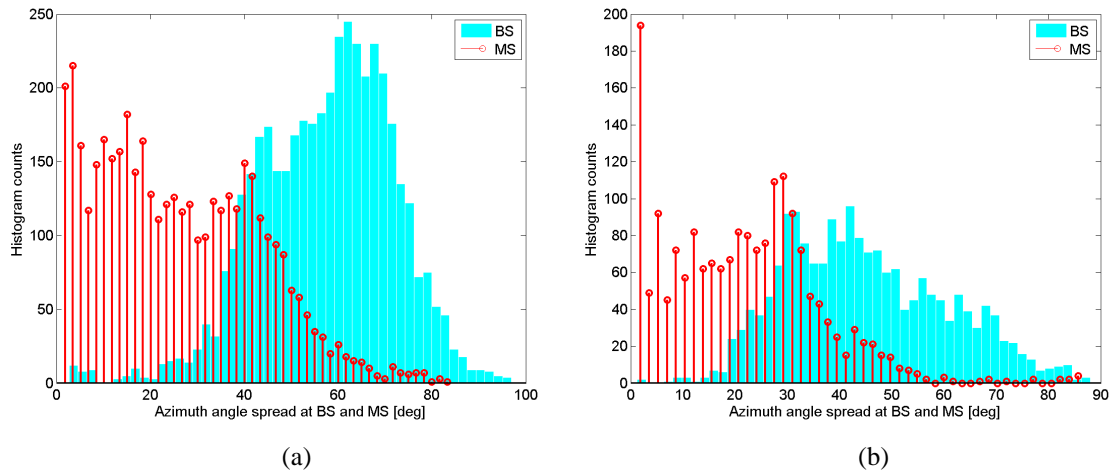


Figure 3-25. Azimuth spread of the indoor-to-outdoor scenario. First floor (a) and fourth floor (b).

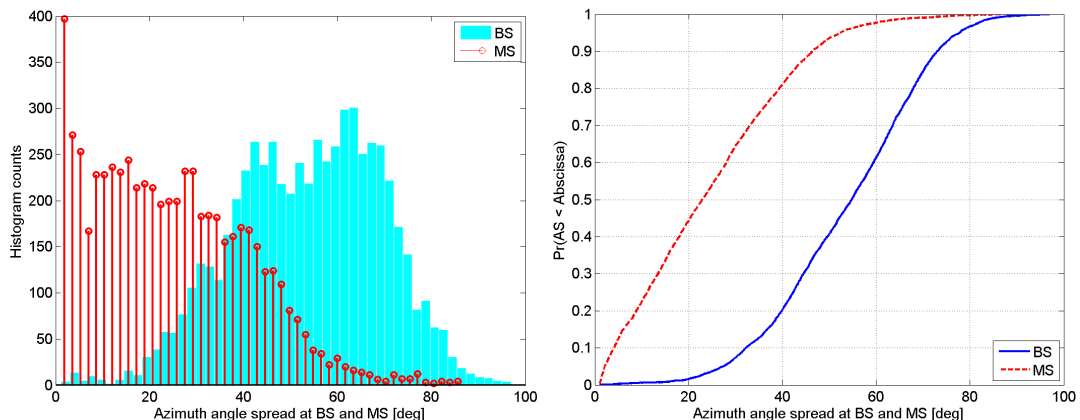


Figure 3-26. RMS azimuth spread of the indoor-to-outdoor scenario. Both floors combined.

3.2.6 A2 Cross-polarisation ratio (D1.1.1)

The CDF percentile values of the XPR at 5.25 GHz centre-frequency in an indoor-to-outdoor environment is shown in the Table 3-18. The direct path is a path with the maximum power. XPR of the scattered paths is calculated by merging all the remaining paths into the same pool. Figure 3-27 shows the histogram of the XPR values and the corresponding CDF is presented in Figure 3-28.

Table 3-18 Percentiles of the cross-polarization ratio.

A2 indoor-to-outdoor		Direct path (OLOS / NLOS)	Scattered paths (NLOS)
XPR _V [dB]	10%	-5.2	-6.8
	50%	8.0	5.5
	90%	21.2	19.8
	mean / std	8.1 / 10.4	6.1 / 10.5
XPR _H [dB]	10%	-5.8	-8.6
	50%	9.0	4.7
	90%	21.8	17.9
	mean / std	8.5 / 10.9	4.6 / 10.5

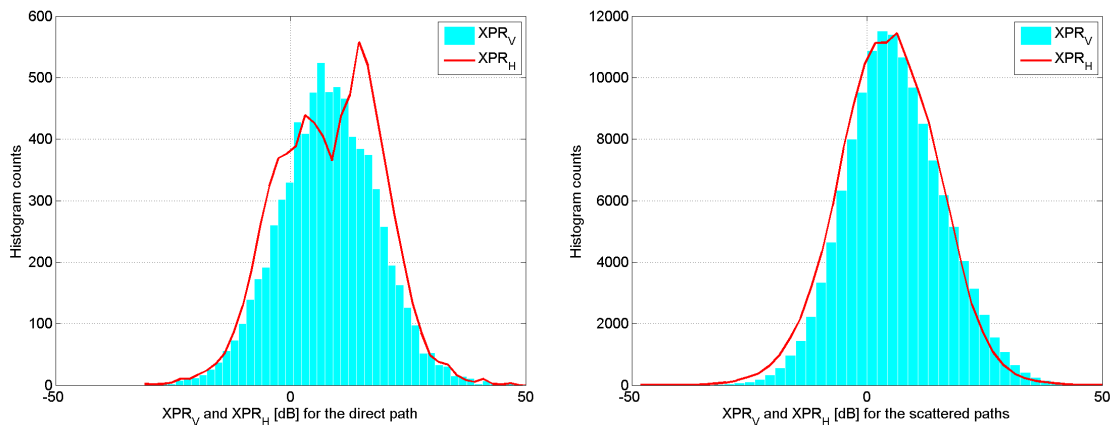


Figure 3-27. Histograms of the cross-polarisation ratios. Direct path (a) and scattered paths (b).

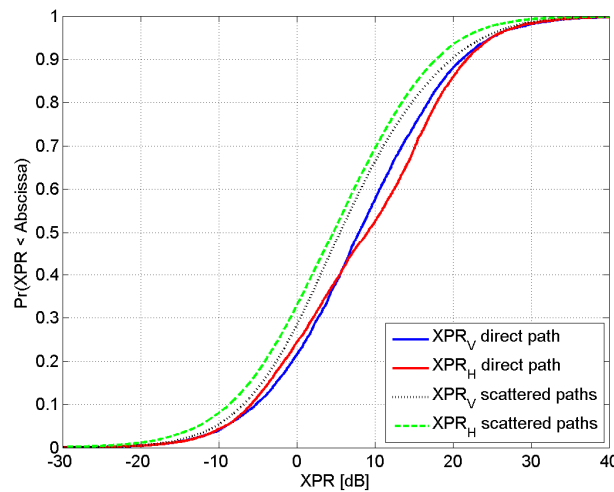


Figure 3-28. CDF of the cross-polarisation ratios for indoor-to-outdoor scenario.

3.2.7 A2 Power Delay Profile (D1.1.1)

Power delay profiles for the A2 Indoor to Outdoor scenario have been shown in Figure 3-29 with two different dynamic ranges. Dual slope model fit is shown in the figure b.

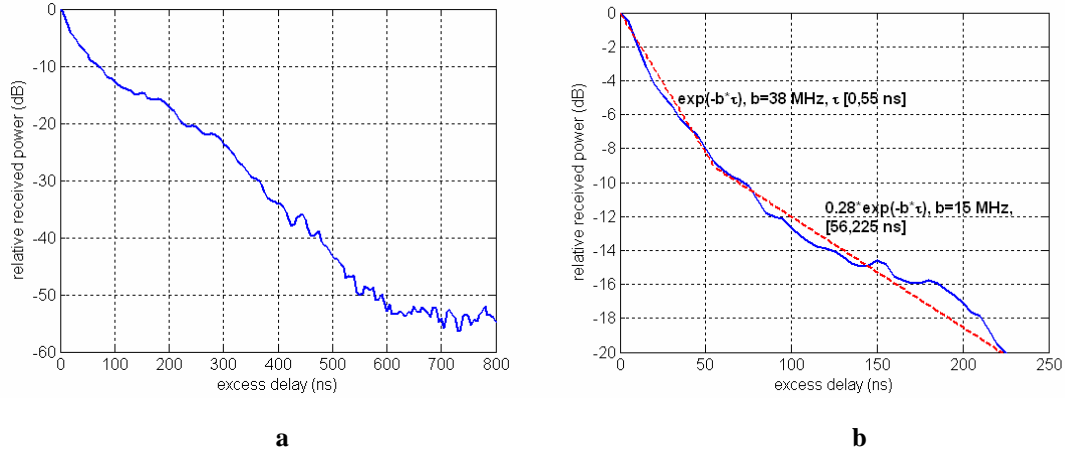


Figure 3-29. Power Delay Profile for A2 Indoor to Outdoor scenario. a) All data. b) Data for dynamic range 20 dB.

The formulas for the different segments are shown in the figure: The time constants are 38 MHz and 15 MHz for the first and second segment, respectively.

3.2.8 A2 Proportionality factor of the delay (D1.1.1)

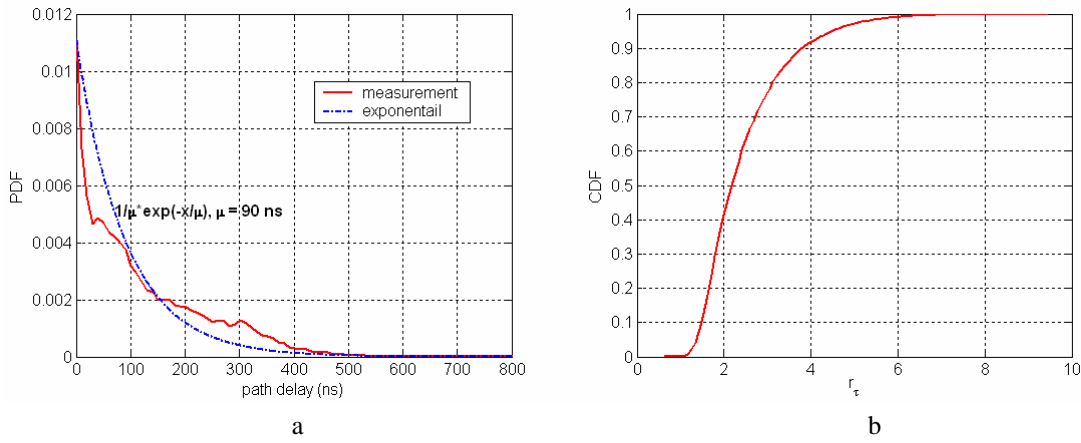


Figure 3-30. a) Distribution of path delays. b) Proportionality factor r_D .

3.2.9 A2 Power Angular Spectrum and main DoA offset (D1.1.1)

Power angular spectrum (PAS) is a distribution of the power over the DoD/DoA angles. It is calculated from the super-resolution data by directing the LOS direction towards the other terminal. The shift is done for the Power-DoD-DoA multi-dimensional matrix for each snapshot. Figure 3-31a shows the PAS for the BS and the MS where MS is outdoors and BS indoors. The main DoA offset is the difference between the mean angle and the LOS direction and is presented in Figure 3-31b.

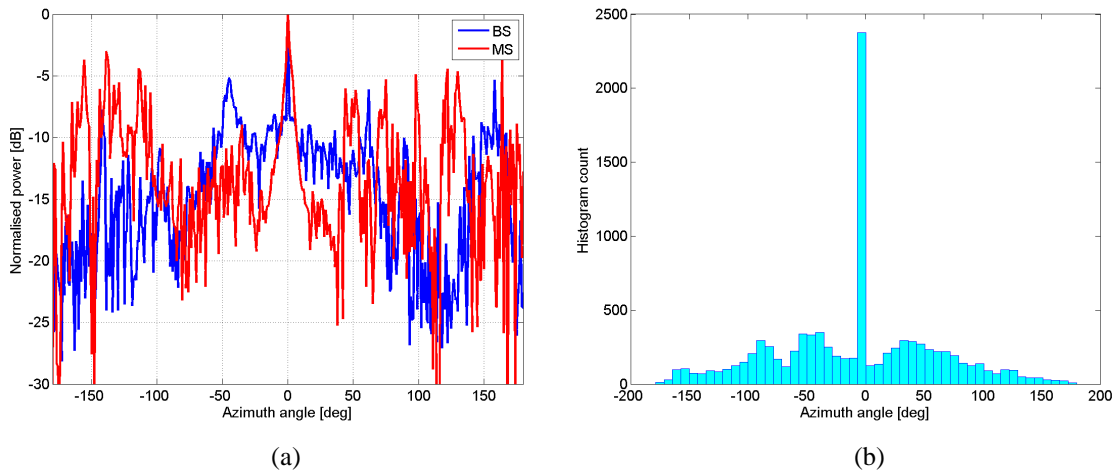


Figure 3-31. Power angular spectrum for the BS and the MS in (a) and the main AoA offset in (b).

3.2.10 A2 Number of clusters (D1.1.1)

The number of clusters is calculated from SISO data by counting the maxima of the PDP. This slightly differs from the number of clusters calculated from the super resolution data. Figure 3-32 shows the CDF and the PDF of the number of clusters. Percentiles of the CDF are shown in the Table 3-19.

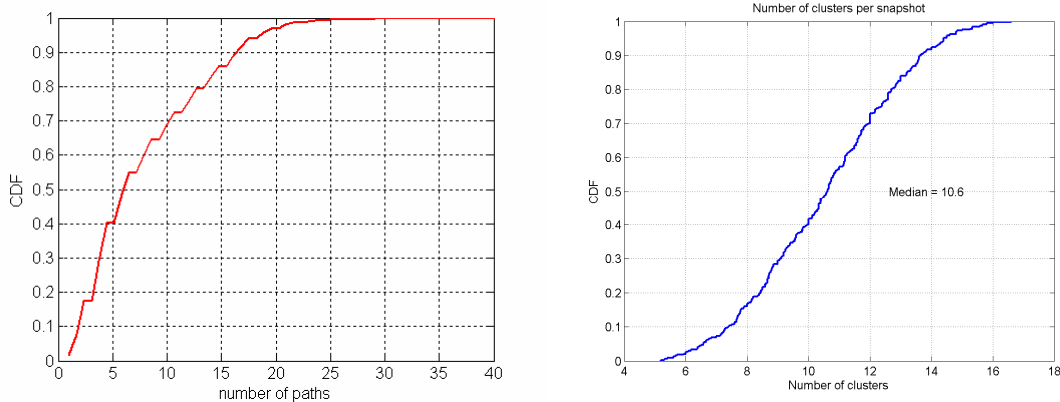


Figure 3-32. Number of clusters extracted from IR (left) and ISIS (right) data.

Table 3-19. Percentiles for the number of clusters extracted from IR / ISIS data

Percentile	# of clusters from IR	# of clusters from ISIS
10%	2.0	7.5
50%	7.0	10.6
90%	16.0	13.5
mean	8.5	11.0

3.2.11 A2 Time evolution of clusters (D1.1.1)

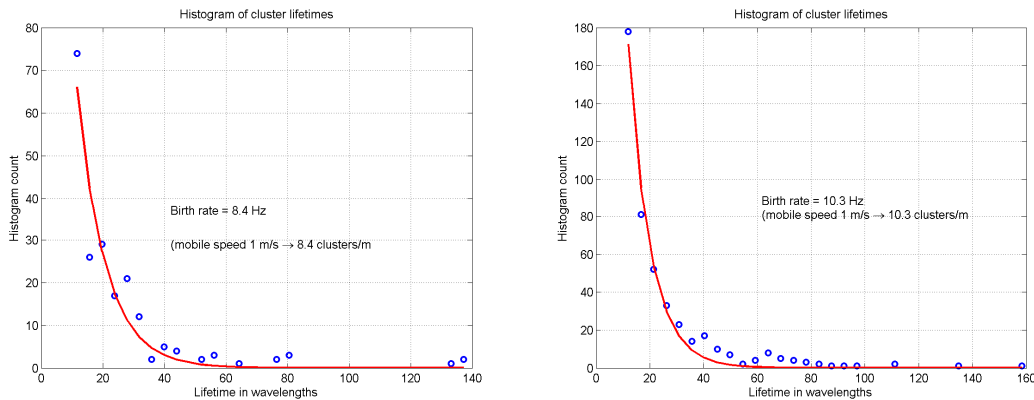


Figure 3-33 Histograms of the cluster lifetime for two different measurement routes.

3.2.12 A2 Per cluster shadowing (D1.1.1)

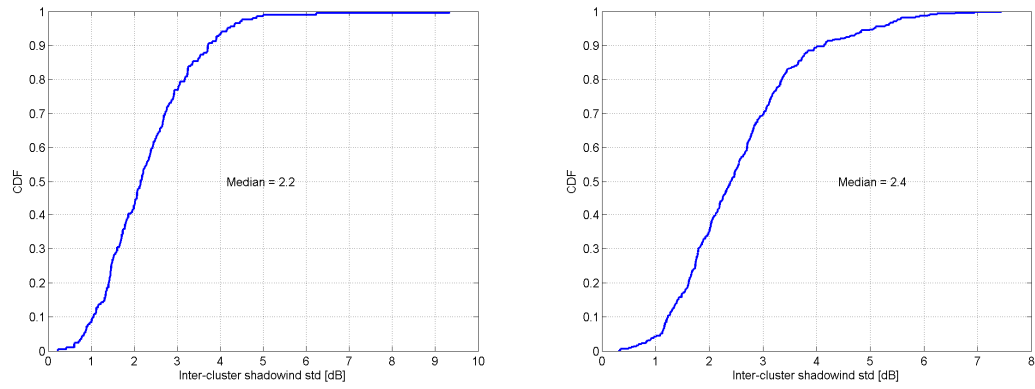


Figure 3-34 Per-cluster shadowing standard deviation for two measurement routes.

3.2.13 A2 Ricean K-factor (D1.1.1)

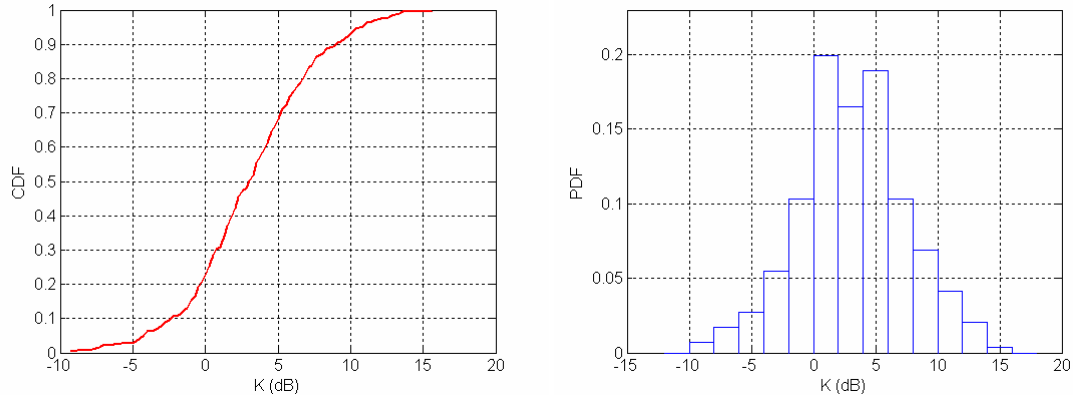


Figure 3-35. Narrowband Ricean K-factor. a) CDF. b) Histogram

Table 3-20. Percentiles of the narrowband Ricean K-factor.

K (in dB)	A2 NLOS
10%	-2.4
50%	3.2
90%	9.0
mean	3.2

3.2.14 A2 Literature research

In [KP02] the authors specify the spherical Outdoor to Indoor power spectrum. They assume it separable for the spherical angle coordinates θ and ϕ . The authors test measurement results at 1890 MHz against different commonly used models, like Laplacian and Gaussian functions, and a model called statistical and specified in [AP02]. It turns out that this statistical model fits best to the measurement results. It is assumed that the statistical model can be written in the form

$$P_\theta(\phi, \theta) = P_\theta(\phi)P_\theta(\theta)$$

and

$$P_\phi(\phi, \theta) = P_\phi(\phi)P_\phi(\theta)$$

The formula of the statistical model for the power distribution in angle coordinates θ or ϕ is:

$$P(\alpha) = \frac{s^2}{s^2 + (\sin \alpha - \overline{\sin \alpha})^2}$$

$$\text{where } s = \sqrt{\sin^2 \alpha - (\overline{\sin \alpha})^2}$$

In the formula α represents either θ or ϕ as required.

The formulas are simplified by assigning $E[\sin \alpha] = 0$. This means that the power distribution is defined relative to the mean direction of arrival. In addition the formula is approximated by a constant far from the main direction. Then we get [AP02]

$$P_\theta(\phi) = \sqrt{A_\theta} \frac{s_{\theta\phi}^2}{s_{\theta\phi}^2 + \sin^2 \phi}$$

$$P_\theta(\theta) = \sqrt{A_\theta} \frac{s_{\theta\theta}^2}{s_{\theta\theta}^2 + \sin^2 \theta}$$

$$P_\phi(\phi) = \sqrt{A_\phi} \frac{s_{\phi\phi}^2}{s_{\phi\phi}^2 + \sin^2 \phi}$$

$$P_\phi(\theta) = \sqrt{A_\phi} \frac{s_{\phi\theta}^2}{s_{\phi\theta}^2 + \sin^2 \theta}$$

$$\text{when } -\frac{\pi}{2} \leq \phi \leq \frac{\pi}{2} \quad \text{and}$$

$$-\frac{\pi}{2} \leq \theta \leq \frac{\pi}{2}$$

$$P_\theta(\phi) = \sqrt{A_\theta} a_{\theta 0}$$

and

$$P_\phi(\phi) = \sqrt{A_\phi} (a_{\phi 0} - b_\phi |\phi|)$$

when $-\pi \leq \phi \leq -\frac{\pi}{2}$ or

$$\frac{\pi}{2} \leq \phi \leq \pi$$

Note that the angle θ has been specified from $-\pi/2$ to $\pi/2$. The definitions above mean that the θ -polarised power reaches maximum in the direction of $\theta = 0$ and $\phi = 0$. The power decreases until the $\phi = \pm 90$ degrees and $\theta = \pm 90$. Same is true for ϕ -polarised power, but it should be noted that the absolute directions of the two maxima may be different. (See [KP02].) These two ranges specify solid angle containing the half space. In the opposite half space θ remains constant over 180 degrees in the opposite side of the maximum. The ϕ -polarised power on the other hand decays linearly in the same region until it reaches the minimum exactly in the opposite direction compared to the maximum (of the ϕ -polarised power).

The measurement results have been shown as figures together with the different modelling functions. Also the parameters for the best fitting statistical model have been expressed, but the values like RMS azimuth or elevation spreads have not been given. From the figures it can be estimated that the spreads are approximately:

	Value	Note
RMS AS of θ -polarisation	25	Original polarisation
RMS ES ¹ of θ -polarisation	17	Original polarisation
RMS AS of ϕ -polarisation	100	Cross-polarisation
RMS ES of ϕ -polarisation	>70	Cross-polarisation

1) ES means elevation spread.

At the same time, XPR was evaluated. Mean XPR was 5.5 dB. This means that the total energy cross-polarized has been quite high. One possible reason is the used horn-antenna. It is also noteworthy that the cross-polarized power is spread in much higher solid angle than the original polarisation.

In [Rudd03] measurements are reported that were performed using BS station installed in a balloon to be able to measure the penetration into typical houses in UK at frequencies 1.3, 2.4 and 5.7 GHz. The arrangement allowed to obtain the losses as function of elevation angle. Also the loss dependence on building floor was examined. The most interesting result is that the curves for 2.4 and 5.7 GHz are almost identical. For elevation angles from 0 to 30 degrees the reported loss was almost constant and 14.5 dB could be used as a common value. The dependence on floor was not very clear and will be omitted here.

The authors of [SCT03] describe signal penetration through window at several carrier frequencies. The case is such that the loss across the window is negligible and through the wall it is much higher, apparently more than 20 dB at 10 GHz. It can be easily seen that in such a case the attenuation of the signal will depend on the area of the window (neglecting the propagation through walls) almost directly. At the same time the transmitted power, assuming propagation from inside to outside the building, is concentrated on a beam determined by the window, see Figure 3-36 and Figure 3-37 [SCT03].

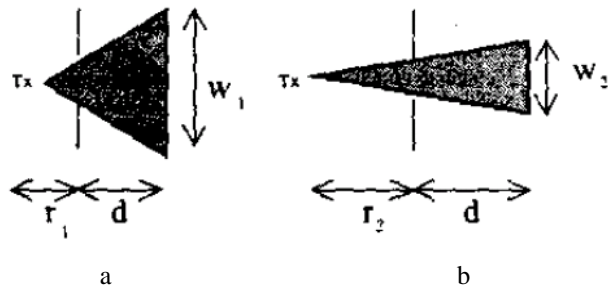


Figure 3-36. Transmitted power concentrated in solid angle determined by Tx near window (a) and Tx far away from one (b).

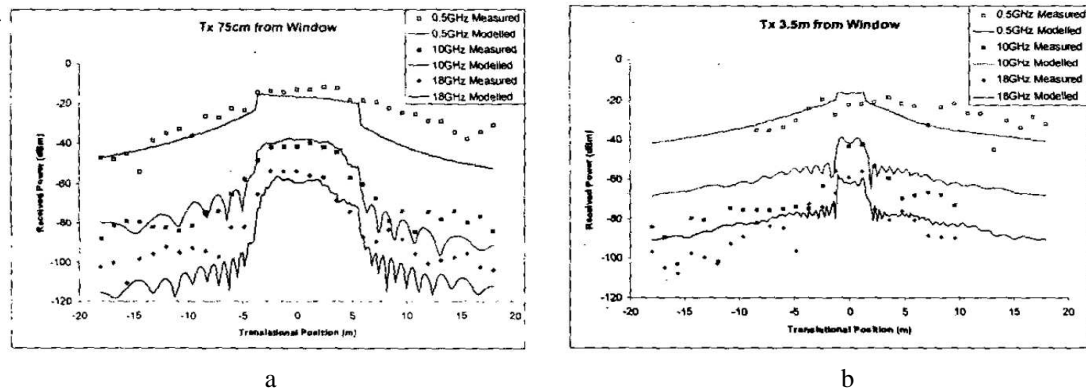


Figure 3-37. Measured and predicted relative beam widths for a) Tx nearby the window and b) Tx far from the window. The carrier frequencies are from top to down: 0.5, 10 and 18 GHz.

The authors of [WOT99] describe and analyse their measurements. Wideband measurements were carried out in Oxford, UK at 2.4 and 5.7 GHz, covering a bandwidth of 80 MHz for static outdoor to indoor scenarios. Mean excess delay, RMS delay spread and RMS azimuth spread for the indoor terminal are given in the table below.

	Urban	Suburban	Rural
Mean excess delay (ns)	34	22	13
RMS delay spread (ns)	37	24	19
RMS azimuth spread	89	81	67

Number of multipaths per cluster and cluster RMS delay spread and RMS azimuth spread are shown below for clusters with more than one path.

	Urban	Suburban	Rural
Nr. of multipaths per cluster (all clusters)	1.7	1.5	1.6
RMS delay spread (ns)	21	12	11
RMS azimuth spread	7.0	8.8	8.4

The RMS azimuth spreads are quite high indicating almost uniform distribution in azimuth of the received power.

In [DDA00] the authors discuss theoretically propagation from outdoors to indoors. They claim that the RMS delay-spread remains about the same when moving from outdoors to indoors. The RMS azimuth spectrum may be greater indoors due to inhomogeneous wall construction, which gives rise to reflections that cause broadening of the azimuth spectrum. Numerical values given are 10 degrees for outdoors and 15 degrees for indoors. We understood that the treatment neglected the reflections inside the building. Probably this has only small effect on the delay spread. On the other hand, for the azimuth spread the effect could be considerable.

In [WAE+04] the Outdoor to Indoor propagation at 5.2 GHz is investigated by measurements. The environment, where the measurements were conducted, is a building of Lund University in Sweden. The transmitters were placed on the roof of a three floor wing of the building. Receiving locations were in another wing in the second floor, 17m apart from the transmitter wing. Three Tx locations were used. The receiving locations were i) in rooms against north wall facing the transmitter locations, ii) in rooms against south wall facing away from the transmitters and iii) in the corridor between the north and south facing rooms.

The mean RMS angular spreads were:

DOA: 39.6 , 42.0 and 44.4 degrees for north, south and corridor locations respectively.

DOD: 9.4 , 8.4 and 10.1 degrees for north, south and corridor locations respectively.

The values of the DOA spreads fell in the range 20 to 58 degrees for the north and south rooms and the corridor. Similarly the DOD spreads fell in the range 2.5 to 26 degrees. The reported mean RMS delay spreads were :8, 13 and 10 ns for north, south and corridor locations respectively. The values ranged from 2.5 to 30 ns.

Also the relative power included in the paths was investigated as a function of the number of paths for part of the locations. Typically 70 % of the total power was obtained with 10 paths, 80 % was obtained with 20 paths and 90 % was not quite obtained with 40 paths. On the other hand, 80 % or more of the received power was included in 40 paths in more 75 % of all locations.

In [WMA+05] same authors discuss some statistical properties of the Outdoor to Indoor channels in the same measurement as in [WAE+04]. They show that the signals are normally Ricean distributed, although some deviations may occur due to shadowing of the antenna elements. They also investigate Ricean K-factor of the channel impulse responses (CIR). The values ranged from 0.3 to 6.3 dB. The authors also show that the joint AOA and DOA angle distributions are not separable. This means that the Kronecker model is not applicable in the Outdoor to Indoor (and thus Indoor to Outdoor) scenario. One interesting detail in these joint distributions is that the rays seem to arrive mostly at 50 degree elevation angle. This would be easily explained, if there would be windows near the ceiling in the receiving rooms.

In [MHA+04] the authors discuss a measurement campaign, where the BS with a directive antenna is in a window at 6th floor, in a position that imitates being out of doors. MS location was varied in five locations per floor at three floors, namely floors 4, 6 and 8. Floor 8 was almost in LOS condition, floors 4 and 6 slightly in NLOS. In the reference there was a detailed capacity discussion. For our purposes we could find the following results:

- Heat protective window coating cause more than 20 dB extra loss in the connection.
- Path-loss ranged from 0 to 30 dB above the free-space loss depending on the existing or missing LOS condition. In the higher storeys the path-loss was smaller.
- RMS angle spread was relatively high at MS, as could be seen in the figures, and correspondingly much lower at BS, which is very understandable due to the geometry.
- Measured correlation length was about 4 wave-lengths at BS and $\frac{1}{4}$... $\frac{1}{3}$ wave-lengths at MS.

Unfortunately the authors do not present more numerical values for these data, but concentrate on capacity.

[Cha03] discusses the outdoor to indoor propagation at 2 GHz. The transmitter was placed outdoors at a low height, 1.5 m below the E floor. (ground ???) Measurements were conducted at first and second floor. The relevant results of this article are the following:

- The additional attenuation in the corridors was about 20 – 25 dB for 5 to 10 peoples moving in the corridor.
- Ricean K-factor was 21.3 dB in first floor and 18.7 dB in the second floor.

In the analysis we start with the following assumptions:

3.3 B1 – Urban micro-cell

3.3.1 B1 – Scenario definition

In urban micro-cell scenarios the height of both the antenna at the BS and that at the MS is assumed to be well below the tops of surrounding buildings. Both antennas are assumed to be outdoors in an area where streets are laid out in a Manhattan-like grid. The streets in the coverage area are classified as “the main street”, where there is LOS from all locations to the BS, with the possible exception of cases in which LOS is temporarily blocked by traffic (e.g. trucks and busses) on the street. Streets that intersect the main street are referred to as perpendicular streets, and those that run parallel to it are referred to as parallel streets. This scenario is defined for both LOS and NLOS cases. Cell shapes are defined by the surrounding buildings, and energy reaches NLOS streets as a result of propagation around corners, through buildings, and between them.

3.3.2 Measurements

Measurements for urban micro-cellular scenario were taken in Helsinki city center at 53. GHz center frequency. The used chip rate was either 60 MHz or 100 MHz.

Micro-cellular measurements were also taken in Ottawa downtown quasi-simultaneously at 2.25 GHz and 5.8 GHz frequencies. The chip rates of 5 and 50 mchps were used in these measurements.

3.3.3 B1 - Path-loss and shadow fading

3.3.3.1 Frequency extension for B1

In D5.4 the PL models for B1 urban microcells in regular street grid environment read as

$$PL_{LOS} = 22.7 \log_{10}(d_1[m]) + 41.0 \quad 10m < d < 650m$$

$$PL_{NLOS} = 0.096 * d_1[m] + 65 + (28 - 0.024 * d_1) \log_{10}(d_2[m]) \quad 10m < d_1 < 550m, w/ 2 < d_2 < 450m \quad (3.25)$$

$$h_{BS} = 8m, h_{MS} = 2m$$

where d_1 and d_2 are shown in Figure 3-38. Results in [KI04][OTT+01][SMI+02] show that path loss shows fairly closely $20\log_{10}(f)$ frequency dependency in range 0.5-15 GHz.

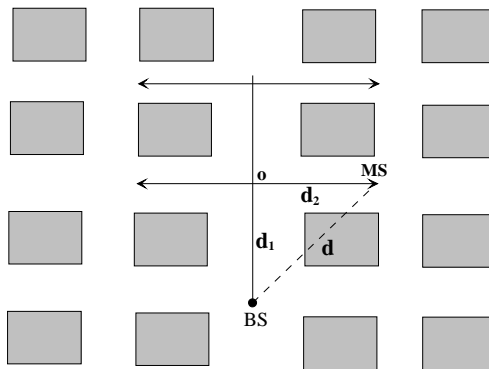


Figure 3-38: Layout of regular street grids.

Corner loss characteristics (transition from LOS to NLOS) as a function of f were examined in range 3-15 GHz in [SMI+02]. With BS height 10 m path loss dependency on f in this case was reported as $26.3\log_{10}(f)$, which is slightly greater than just that due to wavelength difference. However, different frequency scaling for LOS and NLOS models would lead to difficulties in model (dis)continuity. Therefore we prefer to choose for all the cases the same frequency scaling $20\log_{10}(f)$, where f is the target frequency in GHz (between 2...6 GHz).

3.3.3.2 Range extension for B1

In [MKA02] the existence of breakpoint (for two-slope LOS modeling) was examined at frequencies 3, 8 and 16 GHz. It was found that if MS height is close to the average height of pedestrians and cars on the street (~ 1.5 meters) no breakpoint was observed. If the MS height was increased to 2.7 meters, which is clearly above the average height of cars and pedestrians, the breakpoint becomes visible in the PL scatter plot.

If we assume that for WINNER microcellular channel models the typical MS height is ~ 1.5 -2 meters and BS height ~ 7 -10 meters, then breakpoint modeling is not needed in microcellular PL models for MS-BS distances below 1000 meters. For other MS heights and longer ranges, however, it needs to be taken into account. Therefore a two-slope model with effective height breakpoint is proposed [MKA02][OTT+01]:

$$R_{bp} = 4 \frac{(h_{BS} - h_o)(h_{MS} - h_o)}{\lambda} \quad (3.26)$$

After the breakpoint the propagation slope is set to four. According to [MKA02] the effective height varies according to traffic conditions from 0.5 (no or low traffic) to 1.5 (heavy traffic). Here we assume moderate traffic conditions, and set $h_o=1$.

Now the range extension for B1 LOS model is proposed as

$$PL_{LOS} = 22.7\log_{10}(d_1[m]) + 41 + 20\log_{10}(f[GHz]/5), \quad d_1 < R_{bp} \quad (3.27)$$

$$PL_{LOS} = 40\log_{10}(d_1[m]) + 41 - 17.3\log_{10}(R_{bp}) + 20\log_{10}(f[GHz]/5), \quad d_1 \geq R_{bp} \quad (3.28)$$

In above the transition at breakpoint distance is continuous. In addition we should assume BS height clearly above the ground level so that the modeled link is a microcellular connection and not peer-to-peer. Therefore we propose the following ranges: $5 \text{ m} < h_{BS} < 20 \text{ m}$ and $1.5 \text{ m} < h_{MS} < 20 \text{ m}$, where the upper limit is assumed still below rooftop level. This is the best guess range extension to the B1 LOS path loss model without suitable measurement data available. The maximum range is now assumed to be several (“as many as needed”) kilometers. Note that the B1 model is now the same as for B5c fixed stationary feeder below rooftop to street level model. Figure 3-39 illustrates the two-slope model with breakpoint for different BS and MS heights at 5 GHz frequency.

For B1 NLOS model we slightly modify the equation given in [ZRK+06], and propose

$$PL_{NLOS} = PL_{LOS}(d_1[m]) + 20 - 12.5n_j + 10n_j\log_{10}(d_2[m]) \quad (3.29)$$

This is valid for $d_2 > w/2$, where w is the street width. For $d_2 \leq w/2$ LOS model can be used. Minimum allowed street width $w=7$ m, and proposed default $w=15$ m. Minimum street width definition is needed to ensure that NLOS path loss is always greater or equivalent than the LOS path loss for selected d_1 .

Note that the frequency scaling is included in the above NLOS model through the first d_1 dependent term. In the original B1 NLOS model the propagation exponent along the perpendicular street decreases with increasing d_2 distance as [ZRK+06]

$$n_j = 2.8 - 0.0024d_1[m] \quad (3.30)$$

This approach was based on measurements, and found valid for $d_1 < \sim 400$ -500 m. With increasing d_1 the propagation exponent becomes unrealistically small, which has not been confirmed by measurements. Therefore we assume that for values $d_1 < \sim 400$ m the exponent remains the same as with $d_1 = 400$ m, i.e. 1.84:

$$n_j = \max(2.8 - 0.0024d_1[m], 1.84) \quad (3.31)$$

Examples of the extended B1 NLOS models are shown in Figure 3-39.

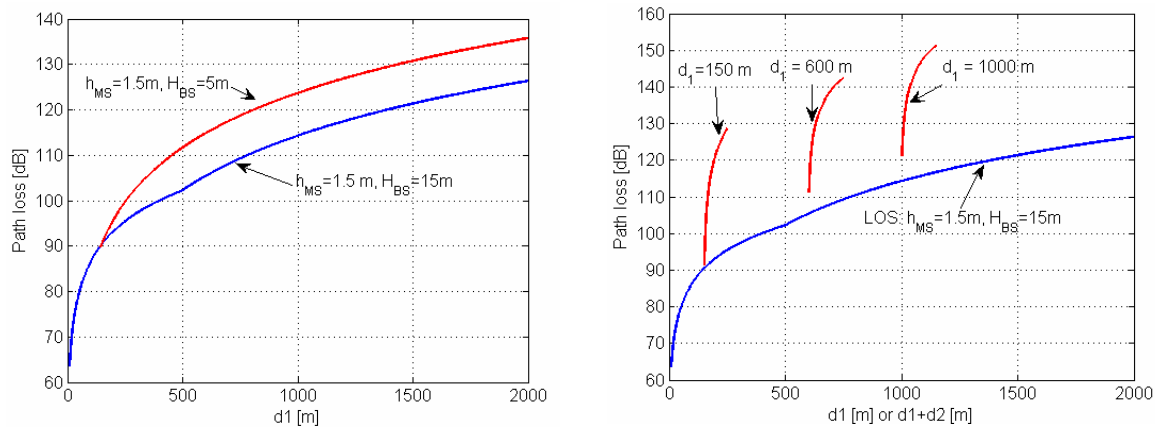


Figure 3-39: Left: Examples of two-slope path loss model for B1 LOS with different BS and MS heights. Right: Examples of B1 NLOS path loss models with different d_1 .

3.3.3.3 B1 Path loss model reciprocity

When transmitter is located at a street crossing, some receiver points can be received through two different routes as shown in Figure 3-40. Now $d_1 = D_2$, and $d_2 = D_1$, and plugging these numbers into NLOS path loss equations yields to different results $PL_{NLOS}(d_1, d_2)$ and $PL_{NLOS}(D_1, D_2) = PL_{NLOS}(D_2, D_1)$. Similar issue of reciprocity may arise at any TX and (NLOS) RX locations (not only street crossing), if TX and RX heights from ground level are equal. In that case swapping TX and RX locations should not change the path loss value.

In order to remove this ambiguity from the model, we simply *choose* to take the NLOS path loss as $PL_{NLOS} = \min(PL_{NLOS}(d_1, d_2), PL_{NLOS}(d_2, d_1))$, if a) TX and RX are located at street crossings, or b) TX and RX heights are equal.

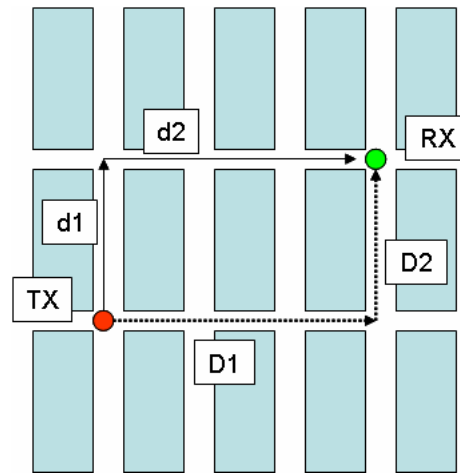


Figure 3-40: When TX is at street crossing, some RX points can be received through two equivalent ways, shown as solid and dashed arrows

3.3.3.4 B1 Path loss model for WINNER II

As a summary, the following set of equations is proposed for path loss models for B1 with BS height and carrier frequency variation between 2-6 GHz.

The path loss model for urban microcellular B1 LOS is

$$PL_{LOS}(d_1) = 22.7 \log_{10}(d_1[m]) + 41 + 20 \log_{10}(f[\text{GHz}] / 5), \quad d_1 < R_{bp}$$

$$PL_{LOS}(d_1) = 40 \log_{10}(d_1[m]) + 41 - 17.3 \log_{10}(R_{bp}) + 20 \log_{10}(f[\text{GHz}] / 5), \quad d_1 \geq R_{bp} \quad (3.32)$$

$$\text{with } R_{bp} = 4 \frac{(h_{BS} - 1)(h_{MS} - 1)}{\lambda}$$

and for NLOS microcells as

$$\begin{aligned} PL_{NLOS}(d_1, d_2) &= PL_{LOS}(d_1[m]) + 20 - 12.5n_j + 10n_j \log_{10}(d_2[m]) \\ \text{with } n_j &= \max(2.8 - 0.0024 * d_1[m], 1.84) \end{aligned} \quad (3.33)$$

In case the transmitter is located at a street crossing, or TX and RX are at equal heights from the ground level, the NLOS model is written as

$$PL_{NLOS}(d_1, d_2) = \min(PL_{NLOS}(d_1, d_2), PL_{NLOS}(d_2, d_1)) \quad (3.34)$$

We also propose the validity ranges as

$$d_1 = 10m \dots 5km \quad d_2 = w/2 \dots 2km \quad (w > 7m) \quad h_{BS} = 5 \dots 20m \quad h_{MS} = 1.5 \dots 20m \quad f_c = 2 \dots 6GHz$$

Please note, however, that the measurements behind the model [ZRK+06] do not fully cover these ranges, and the validity ranges beyond the measured ones are mainly based on educated guessing.

3.3.4 B1 - K-factor distributions

K-factor was analysed for narrowband complex signals using 5.3 GHz measurements taken in Helsinki city center. It was calculated for LOS street sections using the moment method [GME99]. Figure 3-41 shows the K-factor distribution in LOS microcellular environment together with a Gaussian fit.

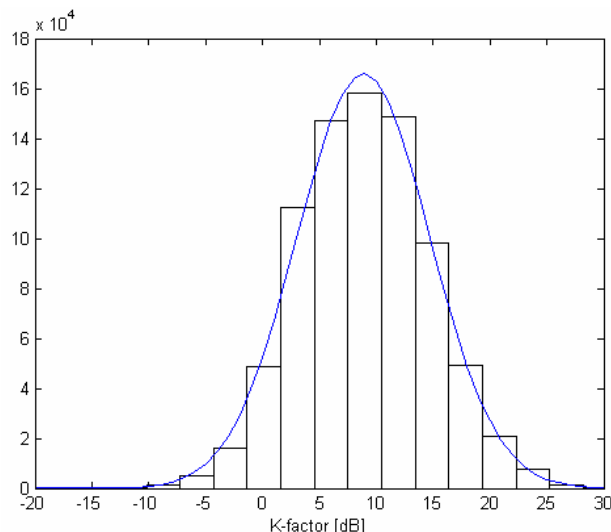


Figure 3-41: K-factor distribution for LOS microcellular environment. The solid line shows a Gaussian fit with mean 8.9 dB and standard deviation 5.8.

3.3.5 B1 - Auto- and cross correlations

Autocorrelation functions obtained from Helsinki 5.3 GHz measurements for B1 LOS scenarios are shown in Figure 3-42, and cross-correlation coefficients between shadow fading, K-factor and log10(DS) are listed in Table 3-21.

a)

b)

c)

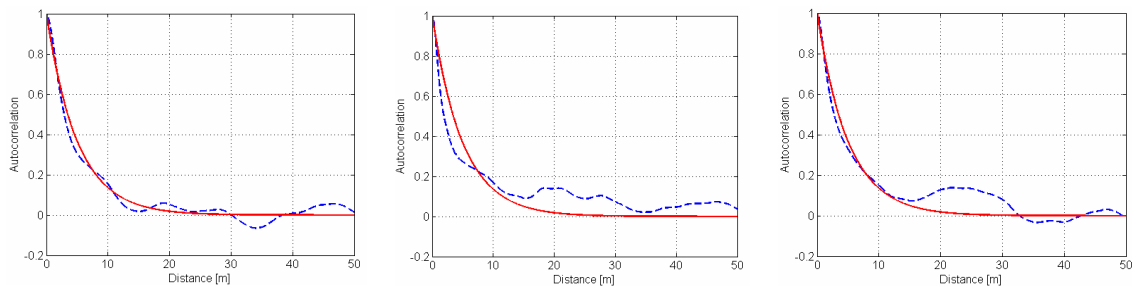


Figure 3-42: Autocorrelation functions for a) shadow fading, b) K-factor, c) logarithm of rms delay spread. Red solid lines show an exponential fit $y = \exp(-x/5)$.

Table 3-21: Cross-correlation coefficients.

$\langle \text{SF}, \log_{10}(\text{DS}) \rangle$	-0.47
$\langle \text{SF}, \text{K-factor} \rangle$	0.54
$\langle \text{K-factor}, \log_{10}(\text{DS}) \rangle$	-0.67

3.3.6 B1 LOS probability

The existence of LOS/NLOS propagation conditions can be determined in two different ways. If the terminal locations are known with respect to a street grid, the propagation condition can be determined deterministically. If, on the other hand, no such knowledge of the environment is available, the model uses the following expression for LOS probability:

$$P_{\text{LOS}}(d) = \min(18/d, 1) \cdot [1 - \exp(-d/36)] + \exp(-d/36)$$

in which d represents the horizontal distance between the BS and MS antennas. A plot of this expression is provided in Figure 3-43.

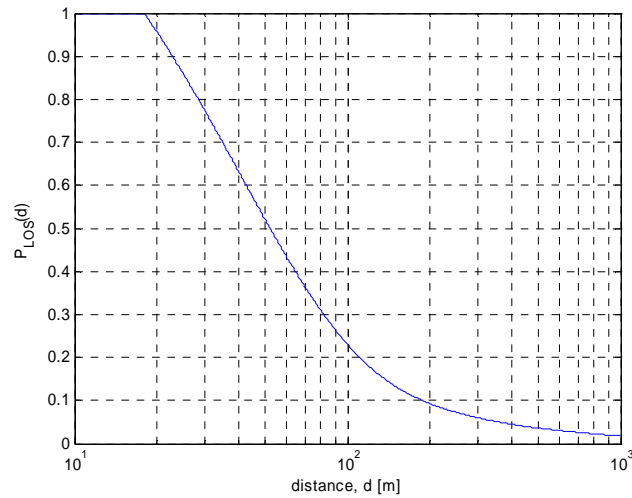


Figure 3-43: B1 LOS probability as a function of distance.

During dynamic simulation, evaluation of the expression for LOS probability determines the percentage of time during which the LOS and NLOS parameter sets are used. During drop-based simulation, the LOS/NLOS conditions for all links are drawn randomly at the beginning of each drop, and kept constant until the next drop.

The above expression for LOS probability is based on a model which is considered valid for a variety of BS and MS heights and rooftop levels in urban environments characterized by a rectangular street grid [Jon07]. Following [Jon07], LOS probability can be modelled as

$$P_{LOS}(d) = P_{LOS,1}(d) \cdot [1 - P_{LOS,2}(d)] + P_{LOS,2}(d)$$

in which

$$P_{LOS,1}(d) = \min\left(\frac{nw}{2\alpha\pi d}, 1\right)$$

is the probability that the MS is on one of n LOS streets leading away from the BS location, and

$$P_{LOS,2}(d) = \exp(-(d - d_0)/L)$$

is the LOS probability associated with areas other than on the LOS streets. In the latter equation,

$$d_0 = \max\left[d \cdot \frac{h_{BS} - h_{RT}}{h_{BS} - h_{MS}}, 0\right]$$

is the distance from the BS location beyond which the LOS path is below the average rooftop level, h_{RT} , and L denotes the mean unobstructed path length associated with propagation paths below the average rooftop level. Further, w denotes the street width, and α , $0 \leq \alpha \leq 1$, is the fraction of the area surrounding the BS that is not occupied by buildings. The validity of the exponential model for $P_{LOS,2}(d)$ has been verified by means of ray-tracing computations for a simulated urban environment modelled on downtown Ottawa, Canada, and the mean unobstructed path length, L , for this area has been estimated as 36 m. The expression for LOS probability associated with the B1 scenario was arrived at by setting h_{BS} and h_{MS} to 10 and 1.5 m, respectively, and h_{RT} to 15 m. The other parameters were chosen as follows: $n = 3$, $w = 20$ m, $\alpha = 0.7$ and $L = 36$ m.

3.3.7 B1 DS and maximum excess-delay distribution

3.3.7.1 B1 Rms delay spread results (D1.1.1)

CRC urban microcell measurements were made in two separate, but similar, experiments. These were conducted on different days in the same measurement area, with the same simulated BS Tx site on Laurier Avenue between Bank St. and Kent St. in downtown Ottawa. During one experiment, 5 mchps, 511 chip PN sequences were used for quasi-simultaneous channel soundings at 2.25 GHz and 5.8 GHz. The snapshot rate was 750 snapshots/sec, and measurements in the 2.25 GHz and 5.8 GHz bands were recorded sequentially, both bands being sampled within a time interval of 205 microseconds. During the other experiment, 50 mchps, 255 chip PN sequences were used for quasi-simultaneous channel soundings at 2.25 GHz and 5.8 GHz. The snapshot rate was 400 snapshots/sec, and 4 PN sequence lengths were recorded in each band for noise averaging. Measurements in the 2.25 GHz and 5.8 GHz were recorded sequentially, and data from both bands were recorded within a time interval of 20 microseconds. Measurement parameters were different for the two experiments to meet requirements for other measurement objectives, not discussed here. Back-to-back calibration tests were conducted prior to all experiments, and these showed equivalent equipment delay spread characteristics in the two bands, for each chip rate.

Using data from each experiment, estimates were made of SISO channel rms delay spreads in both bands from average power delay profiles (APDPs) corresponding to 1-sec-long time series. All APDPs were thresholded at a value of -20 dB with respect to peak power prior to the rms delay spread calculations. Two comparisons were made based on the results.

The first comparison was of rms delay spreads in the two frequency bands, given the same chip rate. Figure 3-44 shows a scatter plot of the results from the 5 mchps soundings, and Figure 3-45 shows a scatter plot of the results from the 50 mchps soundings.

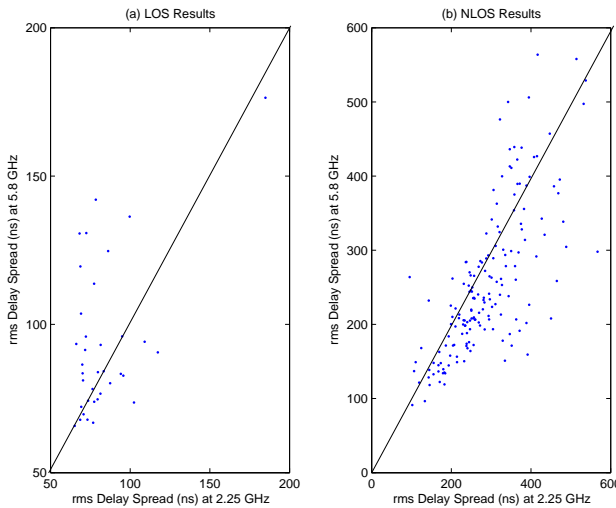


Figure 3-44: Rms delay scatter plots for 5 mchps SISO channel soundings in Ottawa.

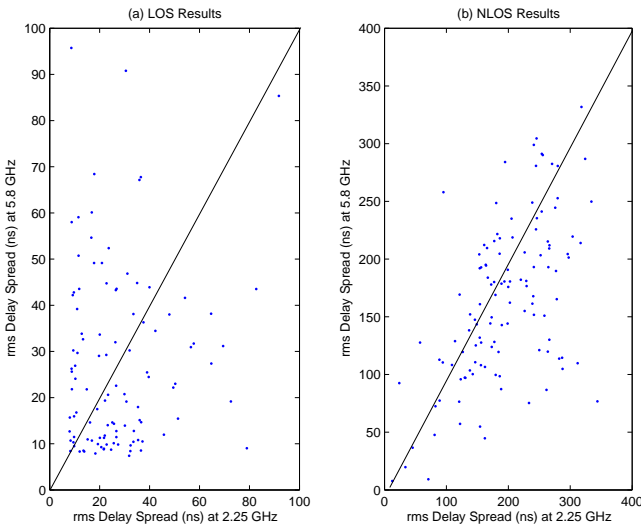


Figure 3-45: Rms delay scatter plots for 50 mchps SISO channel soundings in Ottawa.

It can be seen from both figures, that, except in the LOS/5mchps case, rms delay spreads were greater at 2.25 GHz on most of the measured street sections. Reasons for this are not clear at the time of writing. In the LOS/5mchps case, rms delay spreads were greater at 5.8 GHz on 61% of the 36 street sections for which data were analysed. In the NLOS/5mchps case, rms delay spreads were greater at 2.25 GHz on 72% of 170 street sections. In the LOS/50 mchps and NLOS/50 mchps cases, rms delay spreads were greater at 2.25 GHz on 58% of 110 street sections, and 68% of 120 street sections, respectively.

While the above scatter plots show comparisons between the results for each street section, CDFs are required to show statistics associated with these results, when all locations throughout the measurement area are considered. Figure 3-46 shows experimentally-determined CDFs for all four cases discussed in the foregoing.

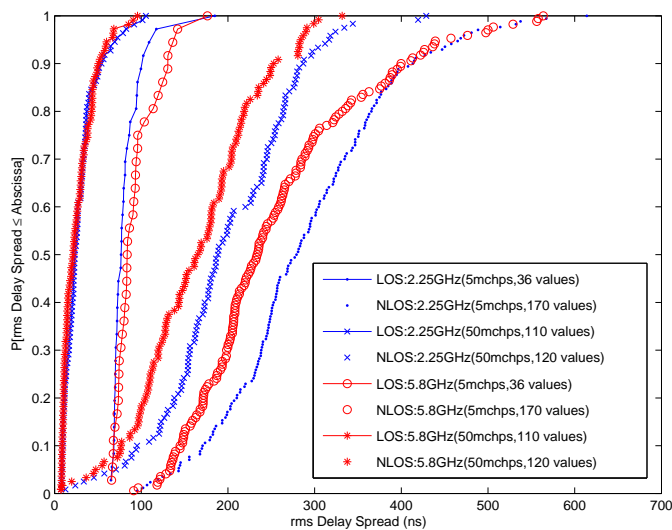


Figure 3-46: Experimentally-determined CDFs for rms delay spreads on LOS and NLOS channels in Ottawa estimated from 5 mchps and 50 mchps soundings.

As one would expect from examination of the scatter plots, it is clear from Figure 3-46 that in all cases, except the LOS/5mchps case, rms delay spreads were slightly greater at 2.25 GHz for all percentiles. The difference between the 5 mchps and 50 mchps sounding results is also clear from this figure. As the sounder chip rate, or system RF bandwidth increases, rms delay spread values decrease. It is to be reported in [GRZ07] that plane wave simulations, using single-interaction geometrical multipath propagation models show that there is nonlinear, but monotonic relationship between rms delay spread and PN sounding system chip rates. As chip rates increase, rms delay spreads decrease, then level off at the chiprate that results in resolution of most multipath components. Simulations tuned to give the experimental values plotted in the foregoing, but extrapolated to 200 mchps show that the initial slope of the decrease is steeper in LOS than in NLOS cases, but in both cases, rms delay spread values level off at a minimum, for chip rates greater than about 40 mchps.

In the LOS cases, the median rms delay spread estimated with the 50 mchps sounder at both 2.25 GHz and 5.8 GHz is about 22 ns. The corresponding 90th percentile is about 50 ns. That in NLOS cases is about 190 ns at 2.25 GHz and 160 ns at 5.8 GHz. The corresponding 90th percentiles are about 282 ns and 296 ns, respectively. Although KS tests would likely show that the differences in these experimental results are not very significant, the scatter plots indicate that 2.25 GHz rms delay spreads are equal to, or slightly greater than 5.8 GHz rms delay spreads in all cases. Careful calibration measurements have led to the conclusion that this is not a result of differences in measurement equipment and antenna characteristics in the two frequency bands.

3.3.7.2 B1 Rms delay spread results (D5.4)

The mean RMS delay spread for LOS and NLOS cases has been calculated for large number of channel segments. The mean value of each channel segment has been calculated for data collected of every 10λ , where about five channel impulse responses has been measured per wavelength. Fitting the log of the measured RMS delay spread with different distributions is shown in Figure 3-47. For NLOS case, the lognormal distribution is not very close to measurement data as well as the log-logistic distributions. For LOS case, the Gumbel distribution follows most of the points of the measurement CDF. The closest distribution is the Gumbel distribution, which is a special case of the Fisher-Tippett Distribution. It is particularly convenient for extreme values data. It may be used as an alternative to the normal distribution in the case of skewed empirical data.

To simplify the model also B1 DS distribution is modelled as log-Normal in WINNER II model.

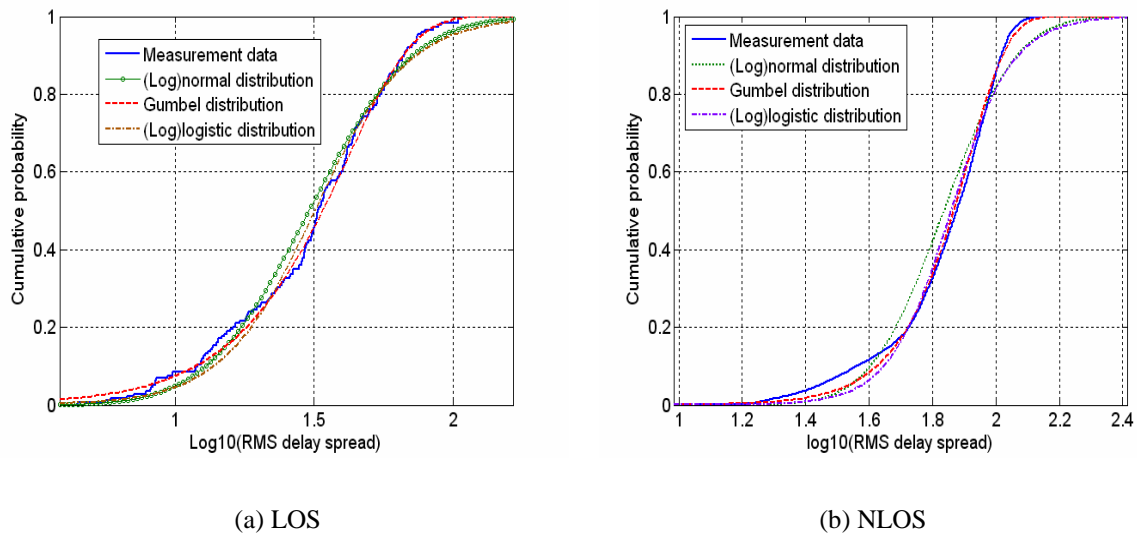
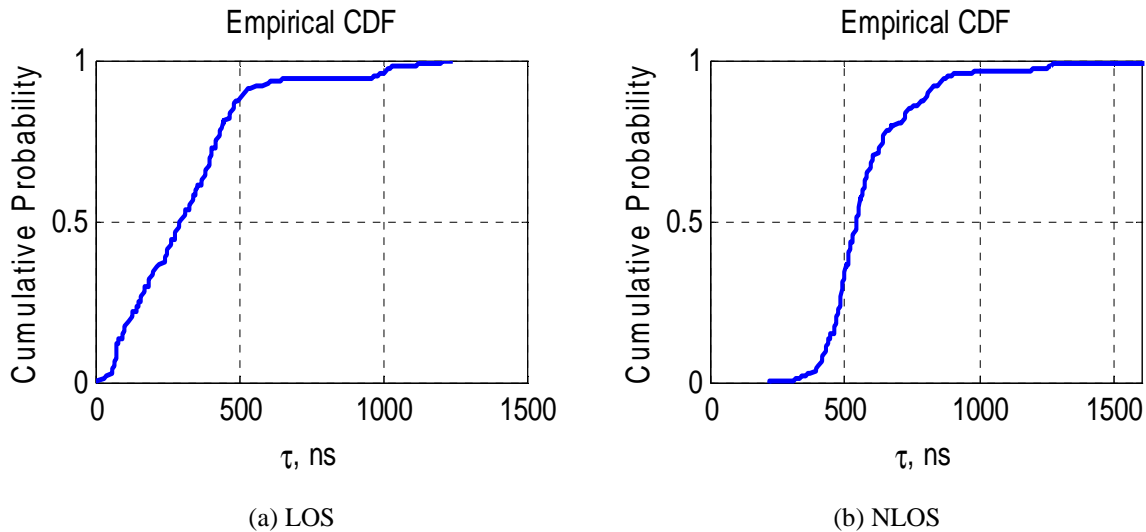
**Figure 3-47: RMS delay spread in Scenario B1.**

Figure 3-48 shows the maximum excess delay for both LOS and NLOS propagation conditions. Table 3.22 presents mean and standard deviations of both RMS delay spread and the ZDSC excess delays for both LOS and NLOS cases.

**Figure 3-48: ZDSC excess delay.****Table 3.22: Mean and standard deviation of the RMS delay spread and maximum excess delay.**

Propagation condition		LOS	NLOS
Centre frequencies (GHz)		5.25	5.25
RMS delay spread	Mean (ns)	37	74
	Std (ns)	25	25
Max excess delay	Mean (ns)	327	567
	Std (ns)	234	130

3.3.8 B1 Azimuth AS at BS and MS (D5.4)

Figure 3-49 shows RMS azimuth angle-spread at the MS and for LOS and NLOS propagation conditions. Figure 3-50 presents RMS azimuth angle-spread at the BS for both LOS and NLOS propagation conditions. We have not made any statistical fitting comparison based on some well known techniques like KS test. However, based on Figure 3-49 the lognormal distribution assumption is not as good as the log-logistic distribution in fitting the RMS azimuth angle-spread at the MS for the case of LOS, while Gumbel distribution has better fitting for the NLOS case. Distributions fitting to the RMS azimuth spread at the BS can be seen in Figure 3-50. Again for the LOS case, the log-logistic distribution has better fitting to measurements than the lognormal distribution. And again for NLOS case, the Gumbel distribution has better fitting for the NLOS case.

To simplify the model also B1 AS distributions are modelled as log-Normal in WINNER II model.

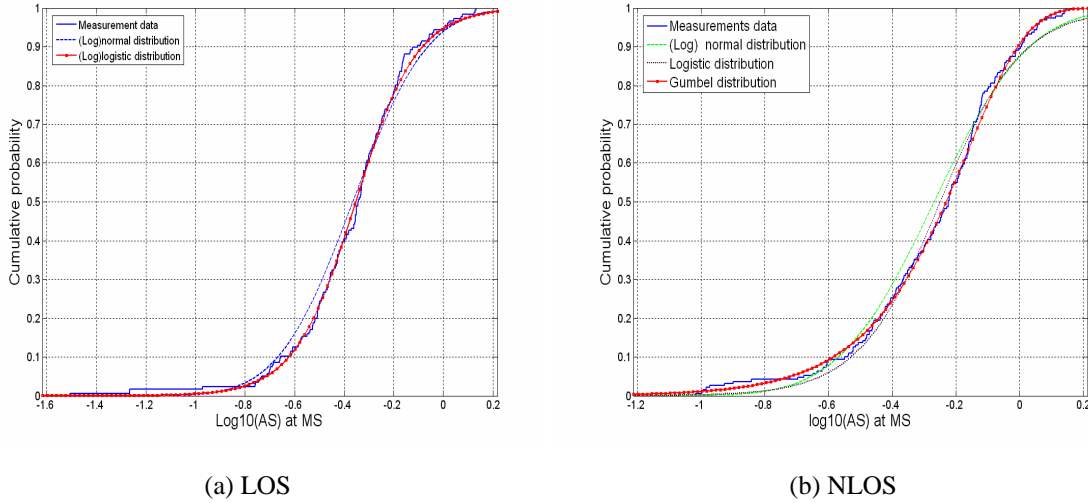


Figure 3-49: RMS azimuth angle-spread at the MS.

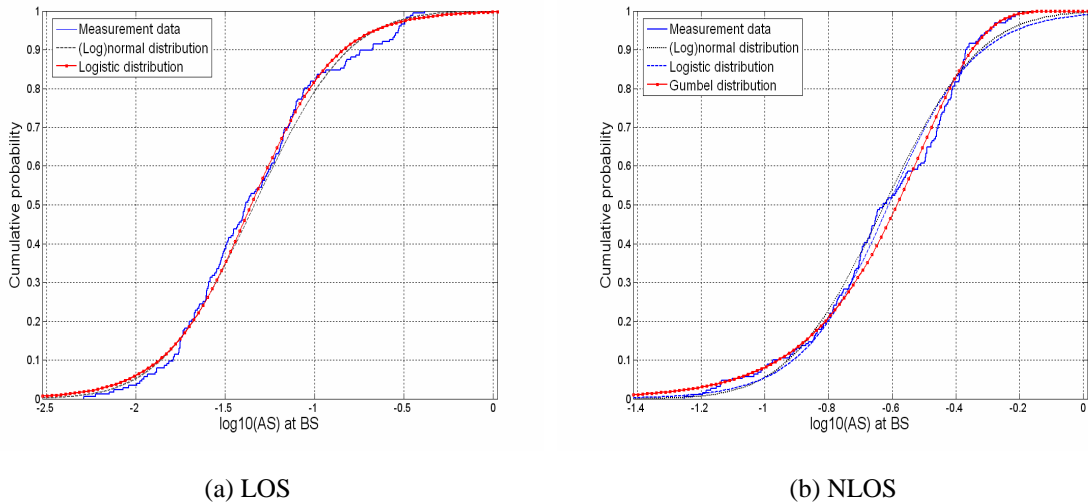
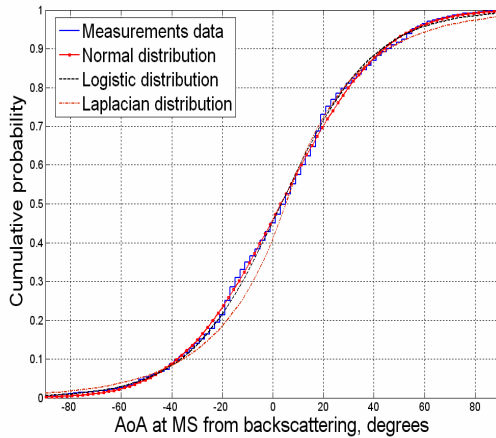


Figure 3-50: RMS azimuth angle-spread at the BS.

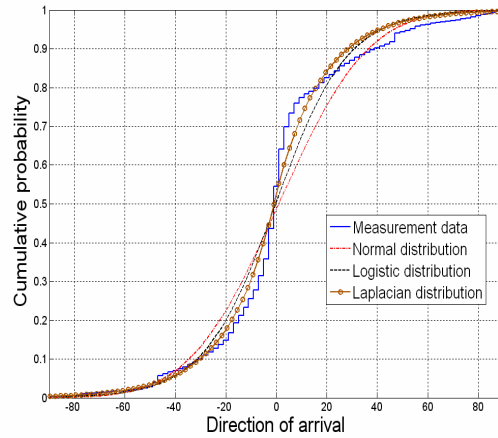
3.3.9 B1 Distribution of azimuth angles (D5.4)

The azimuth angle of arrivals at the MS (receive) and angle of departure from the BS (transmitter) for both LOS and NLOS propagation conditions has been extracted from measurement data using beamforming techniques. It was noted that for LOS conditions there are two propagation mechanisms that take place for signals arrive the MS. The forward propagation, i.e., direct propagation direction from BS to the MS, and the backscattering for signals that travel beyond the MS and scatter back to the MS from

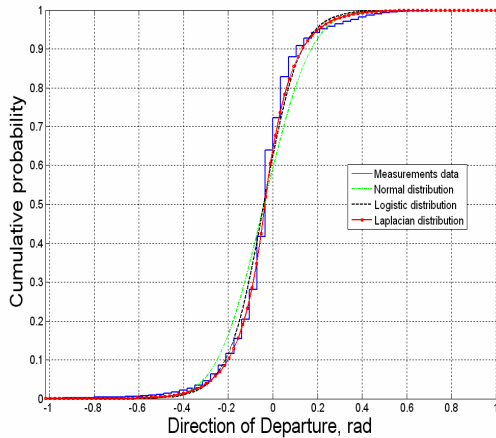
the opposite direction. These two sources of arriving signals at the MS make the modelling of the azimuth arrivals to be different. Figure 3-51 shows the cumulative probability distribution function of arrival angles at the MS from both directions. The logistic and normal distributions are closer in fitting with measurement data from that with Laplacian distribution for signals that arrive due to backscattering. In the forward propagation case, the normal distribution is not in good fit with measurements data. Laplacian distribution is not in an excellent fitting with measurements but closer. For angle of departure from the BS to both LOS and NLOS cases the logistic and Laplacian are in better agreement with measurement data compared to normal distribution as can be seen in Figure 3-52.



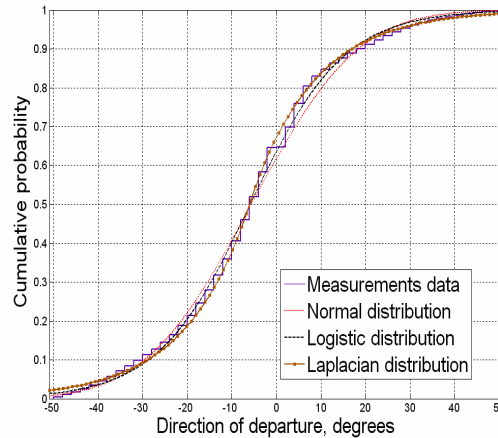
(a) DoA due to Backscattering propagation



(b) DoA from forward propagation.

Figure 3-51: Azimuth direction of arrivals of multipath components in LOS cases.

(a) DoD LOS case



(b) DoD NLOS case.

Figure 3-52: Azimuth direction of departure of multipath components in LOS and NLOS cases.

3.3.10 B1 Modelling of PDP (D5.4)

Mean measured power delay profiles (PDP) of LOS and NLOS averaged over all corresponding routes are shown in Figure 3-53. They are modelled and shown to be exponential decaying function.

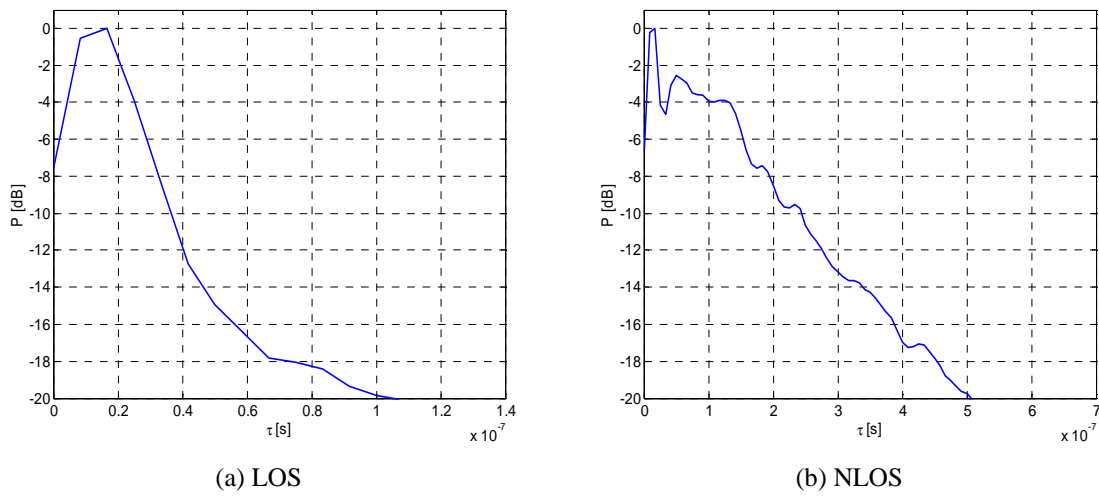


Figure 3-53: PDP of LOS and NLOS conditions.

3.3.11 B1 Number of clusters (D5.4)

Figure 3-54 shows the cumulative probability of the clusters in both LOS and NLOS conditions. Table 3.23 lists the 10, 50, 90 percentiles of the empirical cumulative probability of the extracted number of ZDSCs.

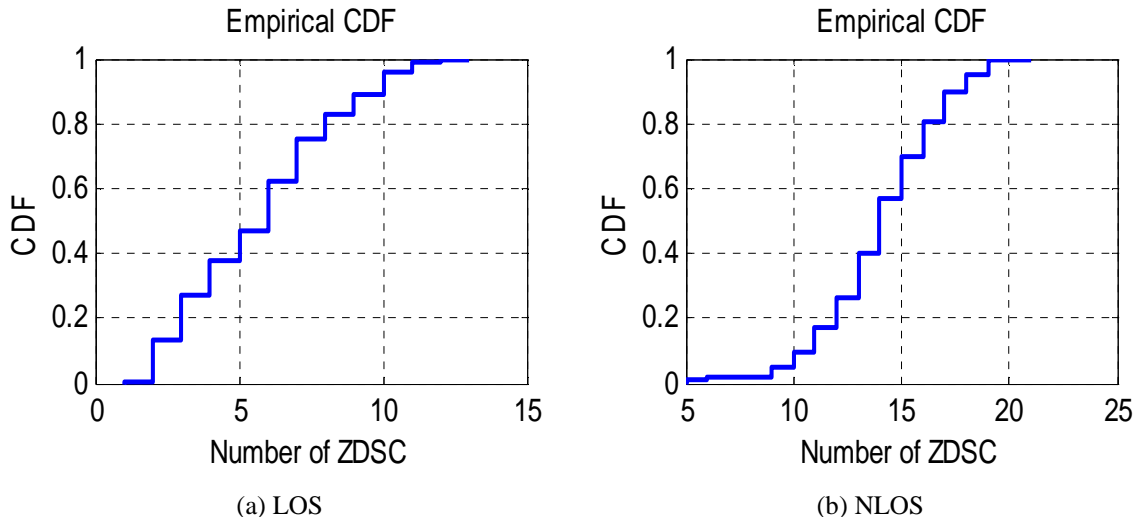


Figure 3-54: Number of clusters (Zero Delay Spread Clusters).

Table 3.23: Number of extracted clusters.

Percentile	10	50	90
LOS	2	6	10
NLOS	11	14	17

3.3.12 B1 Distribution of path delays (D5.4)

Figure 3-55 shows the empirical probability density function of the differential delays of the clusters in LOS and NLOS cases. It can be seen that the distribution of cluster delays follows exponential shape for

LOS case and follows uniform distribution shape in NLOS up to about 400 ns and after 400 ns it has exponential shape.

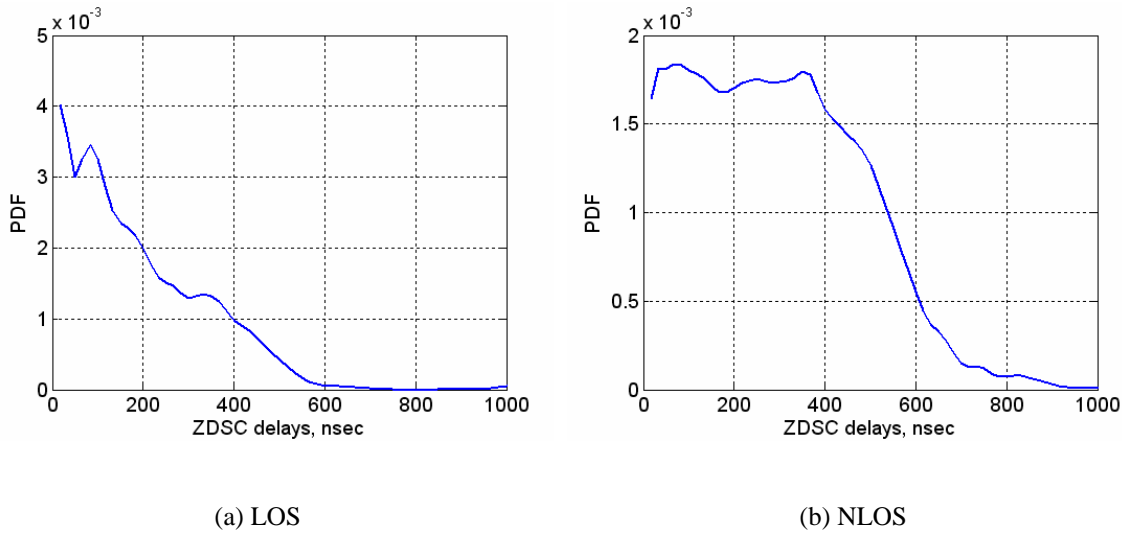


Figure 3-55: Empirical probability density functions of the cluster delays.

3.3.13 B1 Delay proportionality factor (D5.4)

Figure 3-56 shows the empirical cumulative distribution function of the proportionality factor both in LOS and NLOS. The median values are used as a fixed parameter in channel modelling part.

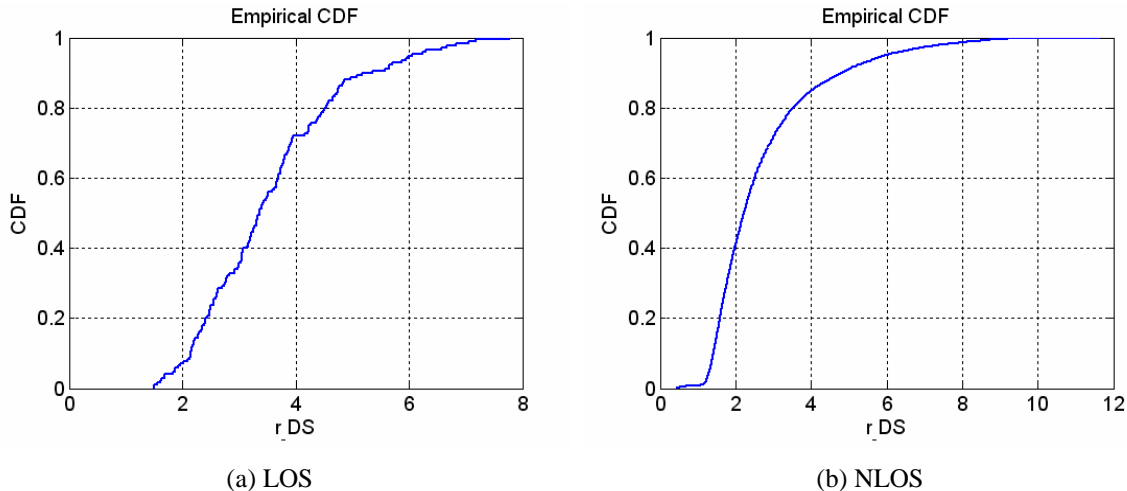


Figure 3-56: Delay proportionality factor r_{DS} .

3.3.14 B1 Cross-polarisation ratio (D5.4)

The CDF of the cross-polarization ratio (XPR) at 100 MHz bandwidth and 5.25 GHz centre-frequency in a rural environment is shown in the Figure 3-57 and Figure 3-58 for LOS and NLOS environments, respectively. Also 10, 50 and 90% percentiles are shown in Table 3.24 and Table 3.25.

Table 3.24: Cross-polarization ratio in LOS.

	P _{V/H} [dB]	XPR _V [dB]	XPR _H [dB]
Mean	-1.0	8.6	9.5
Median	-1.2	8.7	9.8
STD	2.1	1.8	2.3

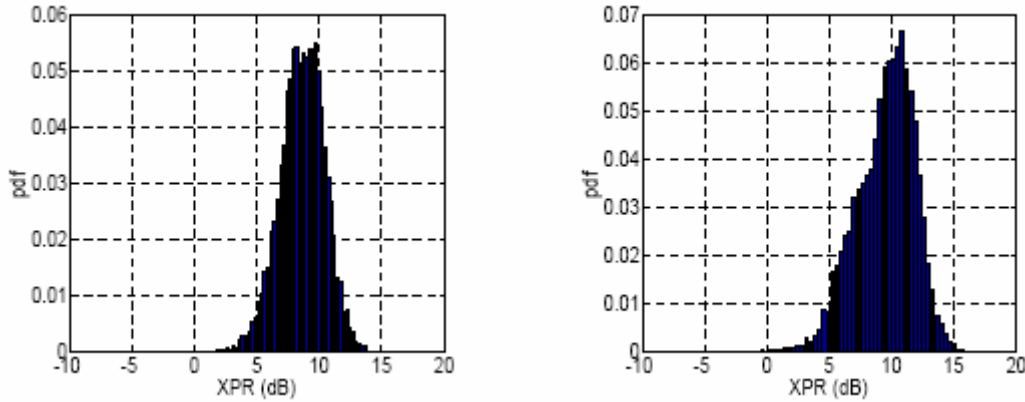


Figure 3-57: Distribution of XPR in LOS microcell: left VP and right HP.

Table 3.25: Cross-polarization ratio in NLOS.

	P _{V/H} [dB]	XPR _V [dB]	XPR _H [dB]
Mean	0.4	8.0	6.9
Median	0.5	7.9	6.8
STD	2.5	1.8	2.8

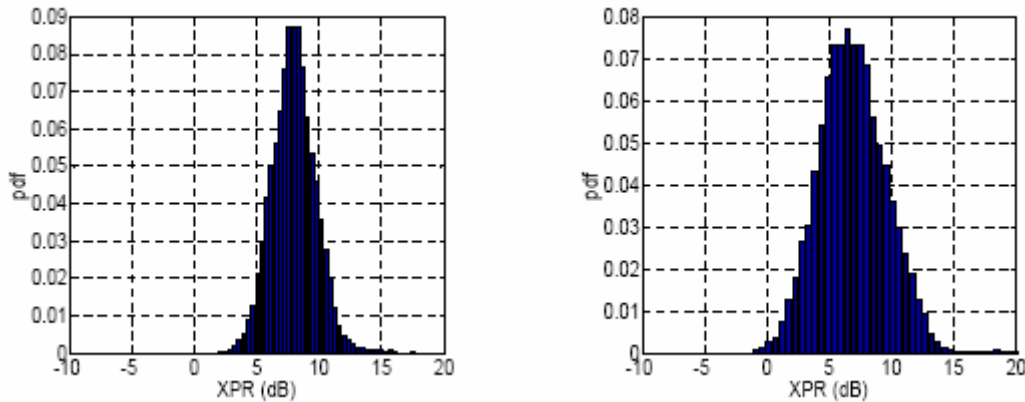


Figure 3-58: Distribution of XPR in NLOS microcell: left VP and right HP.

3.4 B2 – Bad urban micro-cell

3.4.1 B2 – Scenario definition

Bad urban micro-cell scenarios are identical in layout to Urban Micro-cell scenarios, as described above. However, propagation characteristics are such that multipath energy from distant objects can be received at some locations. This energy can be clustered or distinct, has significant power (up to within a few dB of the earliest received energy), and exhibits long excess delays. Such situations typically occur when there are clear radio paths across open areas, such as large squares, parks or bodies of water.

Open literature provides very little results on bad urban microcells.

In WINNER channel models bad urban channels are an option, which can be switched on for urban micro- and macrocellular users. The procedure is described in detail in section 4 in Part I.

3.5 B3 – Indoor hotspot

3.5.1 B3 – Scenario definition

Scenario B3 represents the propagation conditions pertinent to operation in a typical indoor hotspot, with wide, but non-uniform coverage and low mobility (0-5 km/h). Traffic of high density would be expected in such scenarios, as for example, in conference halls, factories, train stations and airports, where the indoor environment is characterised by larger open spaces, where ranges between a BS and a MS or between two MS can be significant. Typical dimensions of such areas could range from 20 m × 20 m up to more than 100m in length and width and up to 20 m in height. Both LOS and NLOS propagation conditions could exist.

3.5.2 B3 – Measurements

WINNER B3 scenario is parameterized based on two measurement environments: university lecture hall /foyer and industrial hall for rapid prototyping and testing. Measurements are performed in Humboldt (2004) and Newton (2006) buildings located in TU Ilmenau campus, Germany. Both buildings have steel construction and many glass walls/surfaces. The centre-frequency for both measurements was 5.2 GHz and the bandwidth was 120 MHz.

3.5.2.1 B3 – Lecture hall measurement

Humboldt building measurements are taken inside the lecture hall (conference hall) and the entrance area (foyer) next to it (Figure 3-59). The foyer is characterized by a 2 floor open environment, with dimension of 15m x 30m x 8m. The conference hall is a typical lecture hall environment with slowly elevated sitting rows; the dimensions are 30m x 35m x 15m.

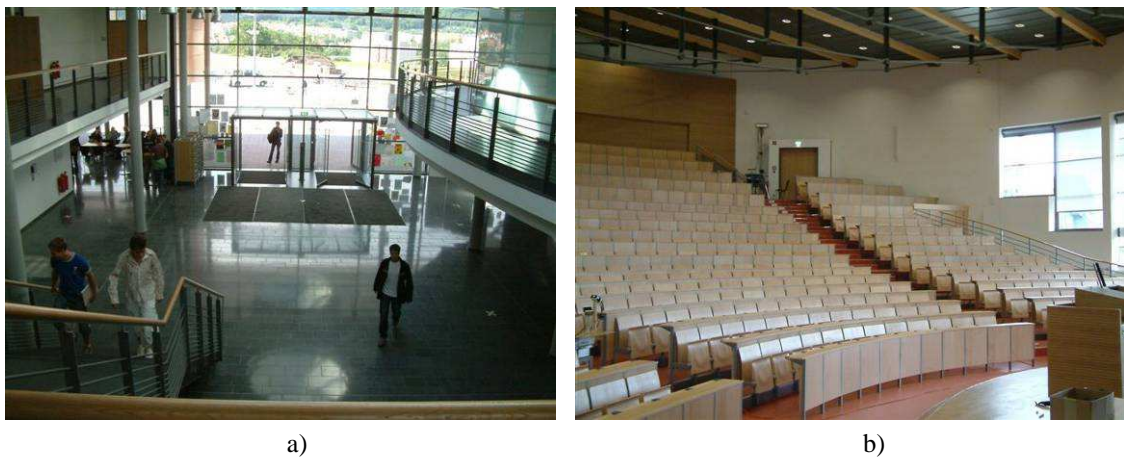


Figure 3-59: Interior of Humboldt building: a) foyer, b) lecture hall.

Measurements with moving transmitter are repeated for several stationary receiver positions. Additionally, for NLOS/OLOS measurements in the lecture hall, LOS was artificially obstructed by absorbing material. These measurements were performed with the RUSK ATM MIMO sounder [Medav], and PULA8 and UCA16 antenna arrays (see Part I, Table 2-6). Since disk-cones of UCA16 are single (vertically) polarized, the results given for this environment correspond to VV combination of Tx-Rx polarization. Model parameters are determined as mean values over data set consisting of ten channel impulse responses what corresponds to modeled channel segment.

3.5.2.2 B3 – Industrial hall measurement

Inside the **Newton building** data is collected in the ground and the first floor (balcony) of the big open hall for rapid prototyping and testing (Figure 3-60) with approximate dimensions 60m x 20m x 8m.



Figure 3-60: Interior of hall rapid prototyping and testing: a) viewpoint from the AP, b) position of the AP.

All measurement routes (Figure 3-61) share common, highly elevated (6 m) transmitter position, marked in Figure 3-60 b) as AP (Access-Point). As a consequence dominant propagation condition observed in measurement data was Line-of-Site (LoS).

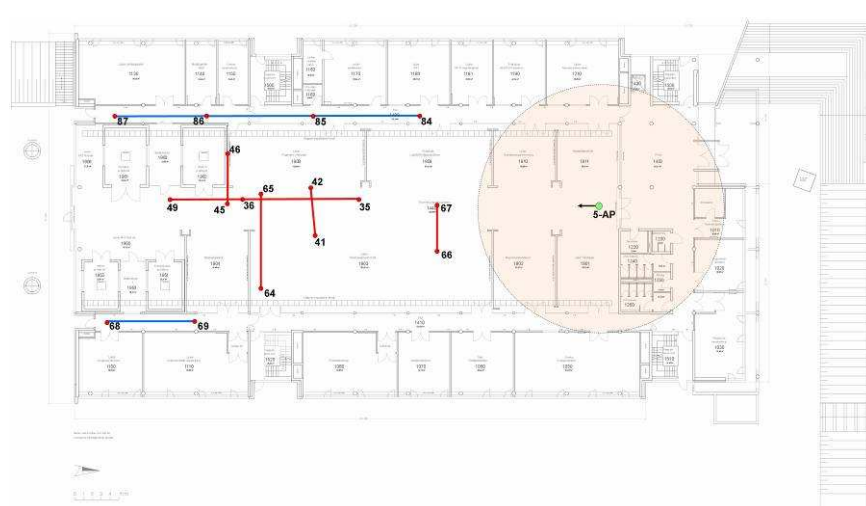


Figure 3-61: Measurements routes: red – ground floor, blue – balcony at the first floor level.

Measurements were performed by RUSK TUI-FAU channel sounder (Part I, Table 2-5) and PULA8 (Tx) and PUCPA24 (Rx) antenna arrays (Part I, Table 2-6). These were full polarimetric measurement and therefore results will be presented for all combinations of Tx and Rx polarizations. However, parameters of the WINNER model given in the part I will correspond to VV case.

All model parameters are determined from the same data set. The majority of the parameters are calculated in delay domain, with exception of angular dependant parameters that are based on angles resolved with high-resolution parameter estimation (RIMAX algorithm). The data in delay domain are calculated by thresholding the average power delay profile 20 dB below the highest peak. The presented data is limited to those snapshots (space-time positions) providing all necessary (relevant to WINNER model) large scale parameters (LSPs). This was necessary to have consistent results between LSP distributions and distance dependant features as e.g. correlation coefficient or path loss.

3.5.3 B3 – Model parameters

3.5.3.1 B3 – Path-loss and shadow fading

Note, in the B3 shdow fading results below, a positive SF is defined as less received power as expected by path loss prediction. Which is opposite to D1.1.2 definition.

3.5.3.1.1 B3 LoS

Due to reflections from the walls, floor and ceiling (wave-guiding effect), indoor propagation environments under LoS condition typically have the path-loss distance exponent in the range from 1.3 to 1.7. ([COST259], Pg. 86).

The measured and modeled path loss for B3 LOS scenario is shown in Figure 3-62.

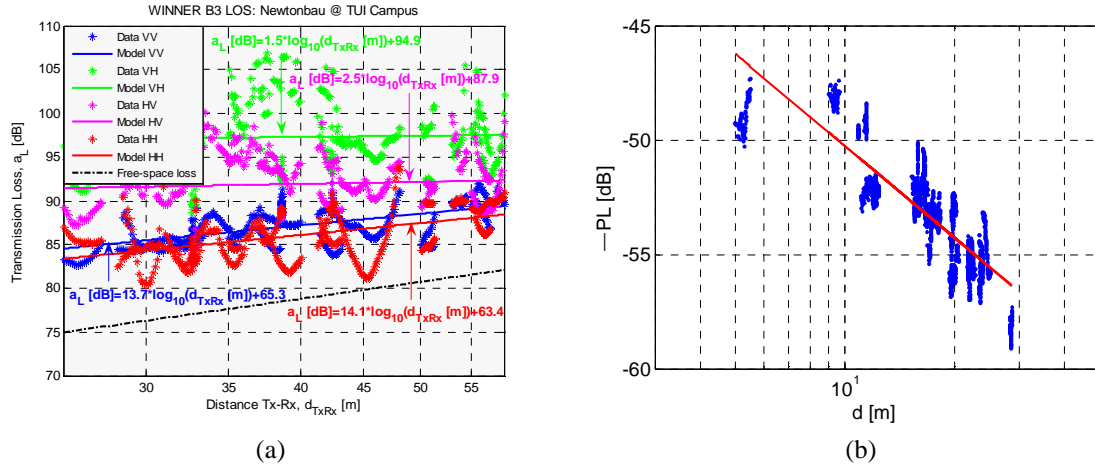


Figure 3-62: Path-loss under LOS propagation condition:
(a) industrial-like environment (Newton building), (b) lecture hall (Humboldt building).

It can be observed that path-loss for VV and HH combination of Tx-Rx polarization is similar in industrial-like environment, giving:

$$PL \text{ [dB]} = 13.7 \log_{10}(d) + 65.3 \text{ for VV case, and}$$

$$PL \text{ [dB]} = 14.1 \log_{10}(d) + 63.5 \text{ for HH case.}$$

Also, similar results for VV polarization are observed in lecture hall/foyer (Figure 3-62 b) where linear regression of path loss (PL) over logarithmic distance, for LoS condition, gives:

$$PL \text{ [dB]} = 13.4 \log_{10}(d) + 36.9 \text{ with } \sigma_{SF} = 1.4 \text{ dB.}$$

It can be noticed that attenuation of the cross-polarized components (Figure 3-62 a) shows insignificant dependence upon analyzed distance ranges.

Probability distributions of the shadow fading corresponding to path-loss models from Figure 3-62 are shown in Figure 3-65.

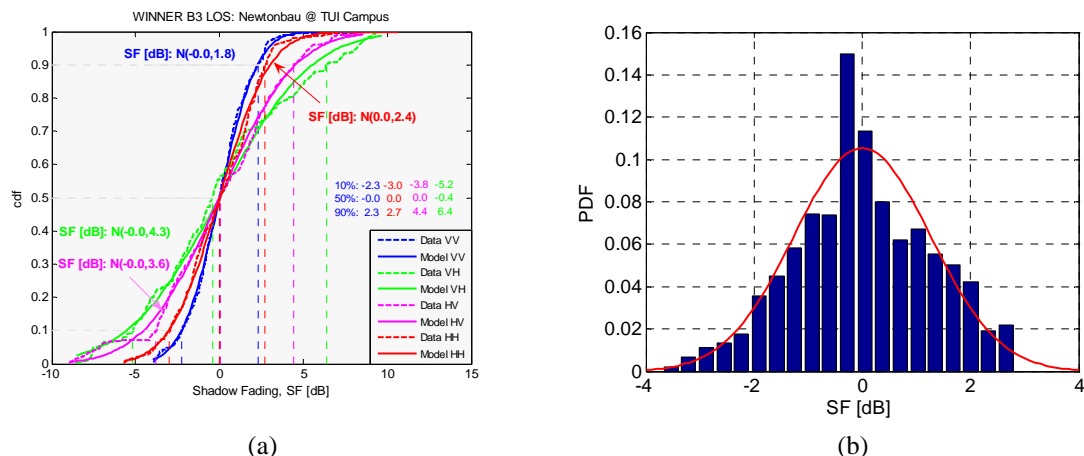


Figure 3-63: Shadow Fading distribution under LoS propagation condition:
(a) industrial-like environment (Newton building), (b) lecture hall (Humboldt building).

For VV polarization observed standard deviation of shadow fading were 1.8 dB in industrial hall and 1.4 dB in lecture hall.

3.5.3.1.2 B3 NLoS/OLoS

Path loss under NLoS conditions is very dependant upon building materials and interior geometry. Results reported here for NLoS and OLoS, are quite specific since they are measured inside huge halls without fully closed areas (e.g. separate rooms). Therefore given data can not be generalized to “generic” NLoS/OLoS path loss that includes wall attenuation.

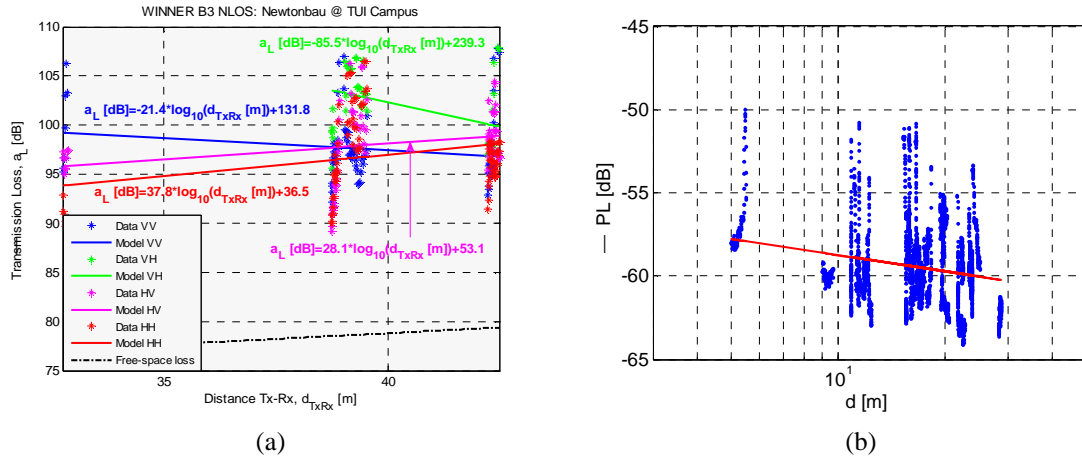


Figure 3-64: Path-loss under NLoS propagation condition:
(a) industrial-like environment (Newton building), (b) lecture hall (Humboldt building).

Results obtained for HH polarization are as expected from other scenarios:

$$PL \text{ [dB]} = 37.8 \log_{10}(d) + 36.5,$$

however the path loss calculated for VV polarization showed negative exponent. In this case distance range covered with data samples is very low and therefore some specificity in measurement environment could create “false” regression parameters.

When artificial blocking of direct component is used to create OLoS condition quite low distance exponent of the path loss is obtained:

$$PL \text{ [dB]} = 3.2 \log_{10}(d) + 55.5 \text{ with } \sigma_{SF} = 2.1 \text{ dB},$$

hardly showing any change in the level of the received power with increased distance (in the same room). This behavior resembles the low distance exponent obtained for path-loss of cross-polarized components given in previous subsection.

In Figure 3-65, probability distributions of the shadow fading are shown.

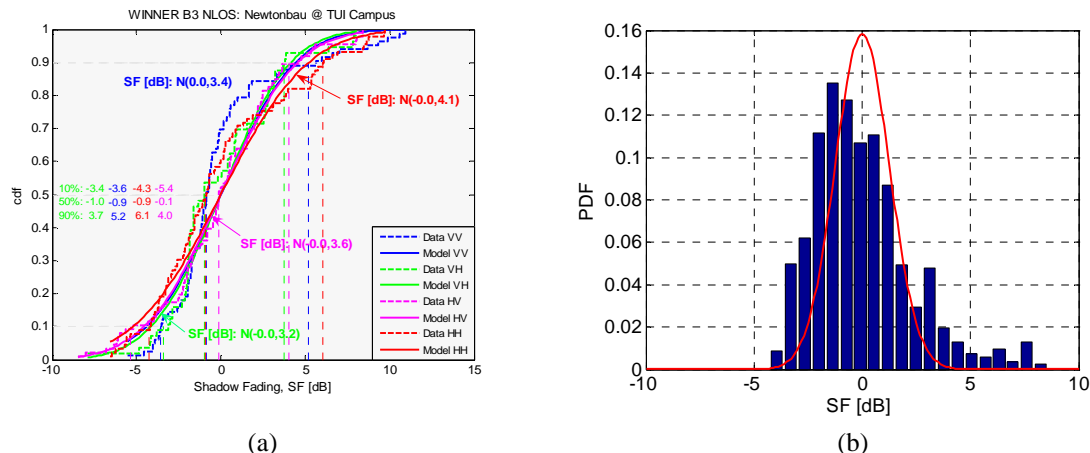


Figure 3-65: Shadow Fading distribution under NLoS propagation condition:
(a) industrial-like environment (Newton building), (b) lecture hall (Humboldt building).

In VV case standard deviation of shadow fading was approx. 1 dB higher than in LoS case: 3.4 dB in industrial hall and 2.1 dB in lecture hall.

3.5.3.2 B3 – Ricean K-factor

The cumulative distribution functions of Ricean K-factor for B3 LoS scenario, as well as their log-normal fit, are shown in Figure 3-66.

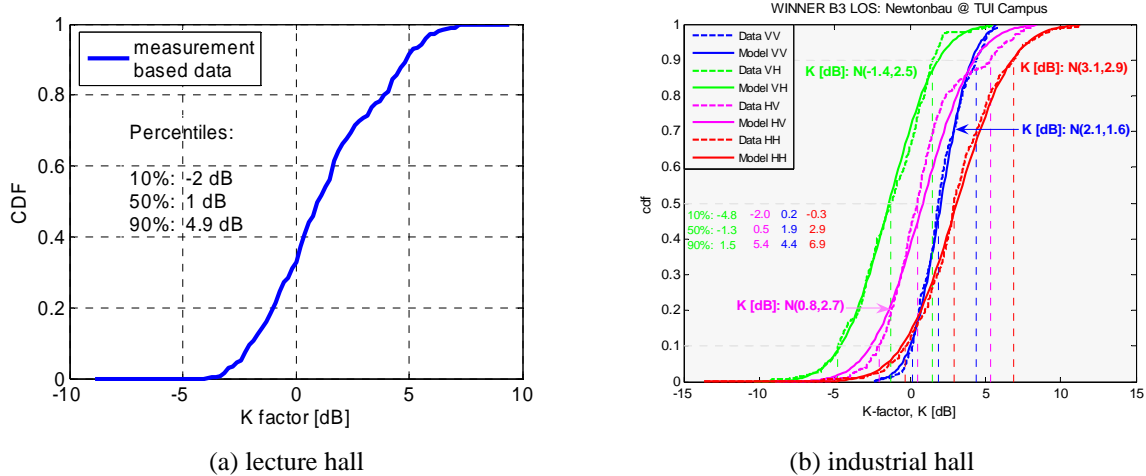


Figure 3-66: CDF of Ricean K factor for B3 LoS scenario.

The values of the K-factor corresponding to 10, 50 and 90 % of the cdf, are given in Table 3-26.

Table 3-26: K-factor [dB] in B3 scenario for VV polarization.

K-factor [dB]		LoS		NLoS
		Lecture	Industrial	Industrial
Percentile	10%	-2	0.2	-3.4
	50%	1	1.9	-2.0
	90%	4.9	4.4	-0.7

The Ricean K factor for scenario B3 LoS as a function of the distance and the CDF of it are shown in Figure 3-67.

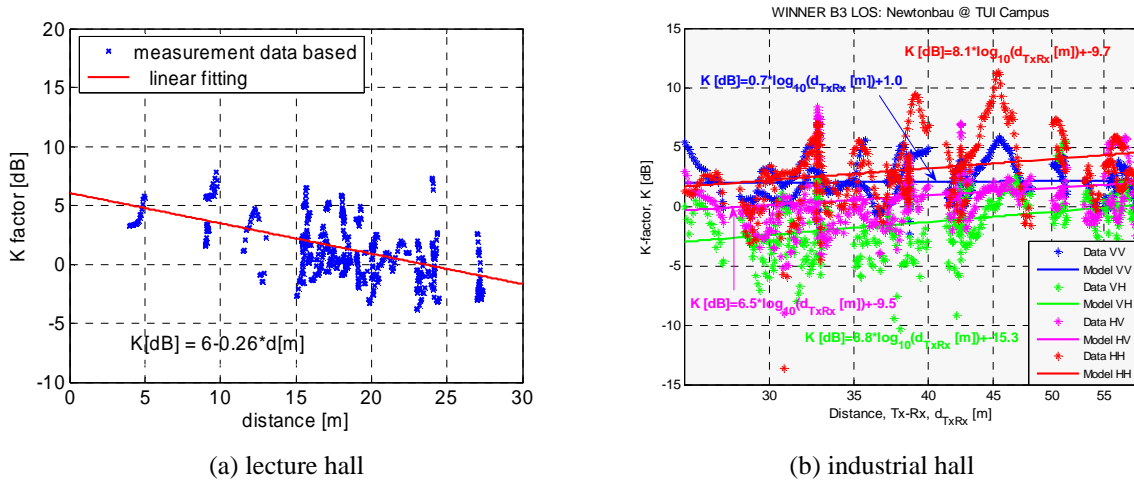
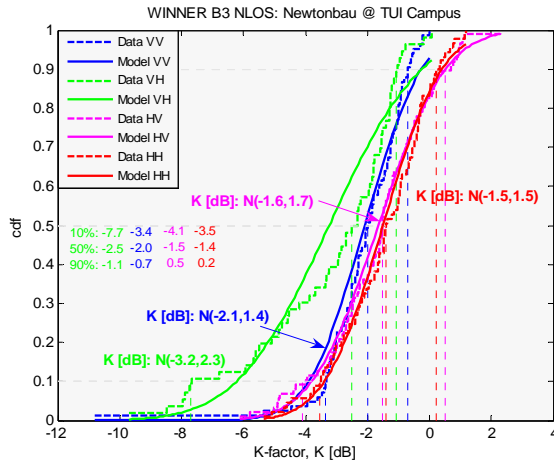


Figure 3-67: Scenario B3 LOS: Ricean K factor as a function of distance.

By comparing the K-factor distance dependence (Figure 3-67) for VV polarization in lecture hall (decreasing) and industrial hall (increasing), it is not possible to determine general behavior for B3 LOS scenario.

The K-factor cdf and its log-normal model are given also for NLoS case in Table 3-26 and in Figure 3-68. Median value of K-factor for VV polarization under NLoS conditions is approx. 4 dB lower than for LoS.

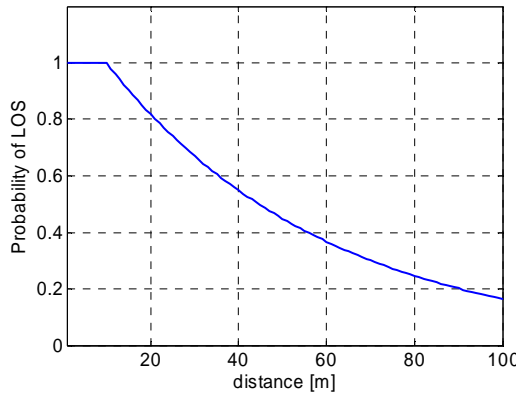
**Figure 3-68: CDF of Ricean K factor for B3 NLoS scenario.**

3.5.3.3 B3 – LOS probability

In [COST259] measurement results for the big factory hall environment are presented. Length, width and height are 90, 30 and 10 m respectively. BS height was 8 m and MS height was 1.5 m. Average probability of LOS was 0.5. Up to 10 m distance in such a big halls there is almost always LOS (if Rx is placed right). Therefore, we propose for the big factory halls, airport and train stations:

$$P_{LOS} = \begin{cases} 1, & d < 10m \\ \exp(-(d - 10) / 45), & \text{otherwise} \end{cases} \quad (3.35)$$

where d is in meters. The figure below shows this function of the distance.

**Figure 3-69: Probability of LOS in factory halls, airports, and train stations.**

If Rx is placed at the ceiling (or some other appropriate place) LOS will be almost guaranteed. The strongest reason not to have LoS would be a person between Tx and Rx. Since the measurements inside

big lecture hall were performed when the hall was empty, probability of LoS condition was 100%. For the NLOS measurements obstructions were artificially made. We propose:

$$P_{LOS} = \begin{cases} 1, & d < 5m \\ 1 - \frac{d-5}{150}, & 5m < d < 40m \end{cases} \quad (3.36)$$

where d is in meters. This function is presented in the figure below.

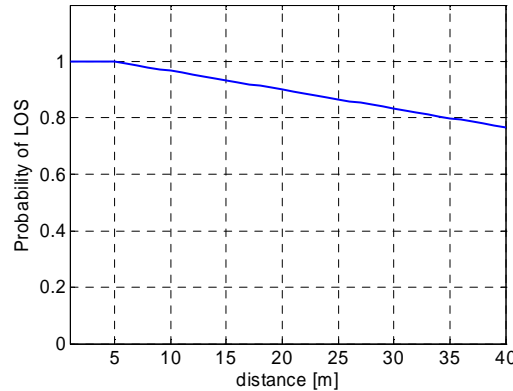
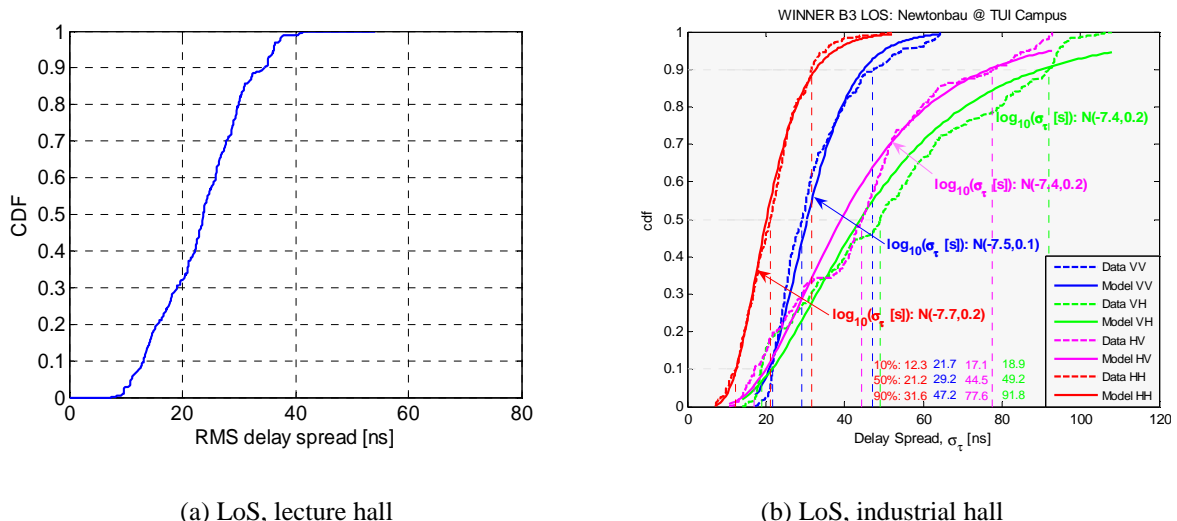


Figure 3-70: Probability of LOS in lecture or conference halls.

3.5.3.4 B3 – Delay spread and maximum excess delay distribution

Delay spread (DS) cumulative distribution functions (cdfs) are shown in Figure 3-71 for different propagation conditions (rows) and measurement environments (columns). DS values corresponding to 10, 50 and 90 % of the cdf, are given in Figure 3-71 and Table 3-27. Appropriate log-normal model minimizing mean square error is also given in Figure 3-71 for each Tx-Rx polarization measured in industrial hall environment.



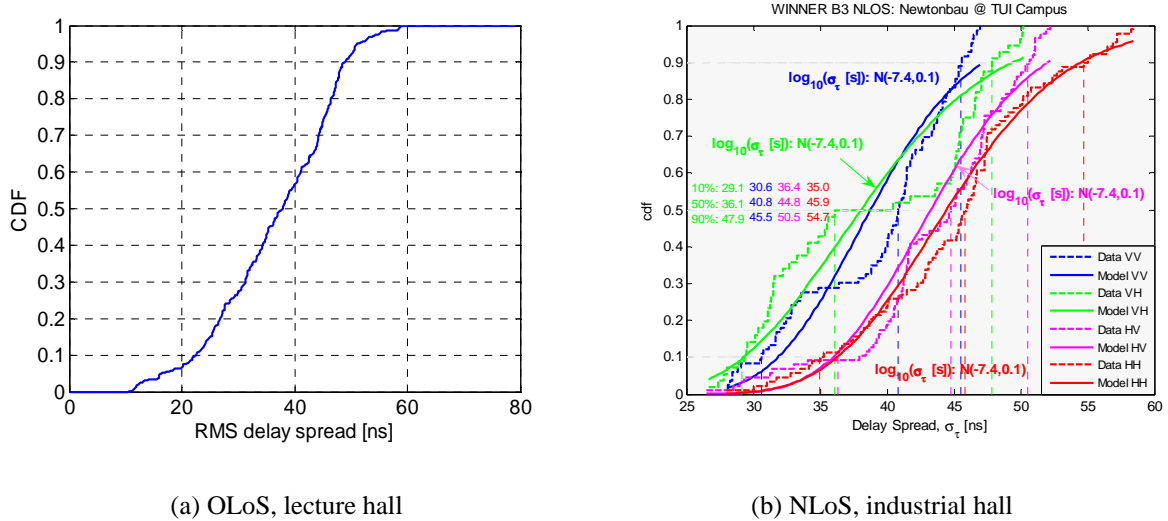


Figure 3-71: RMS delay spread, scenario B3.

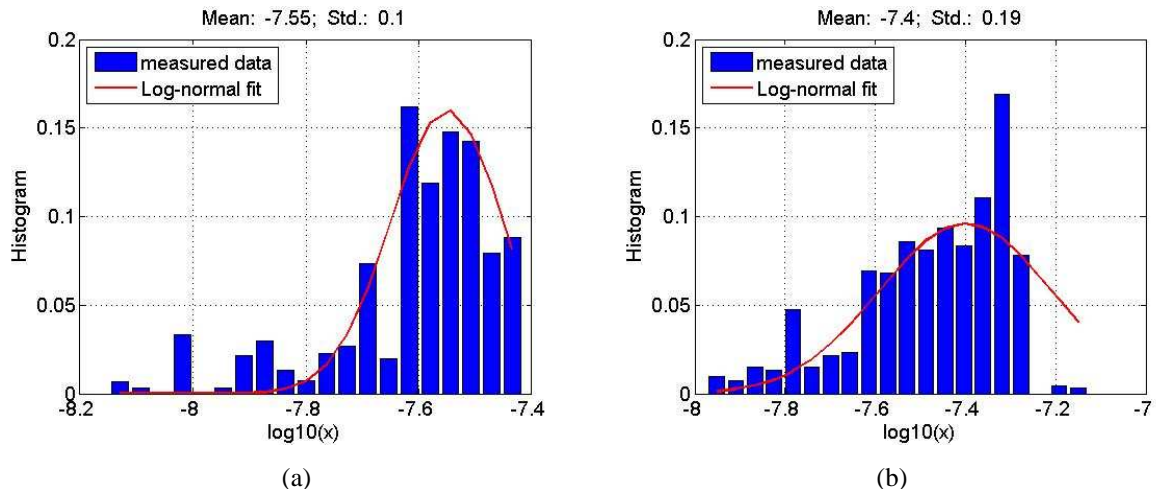


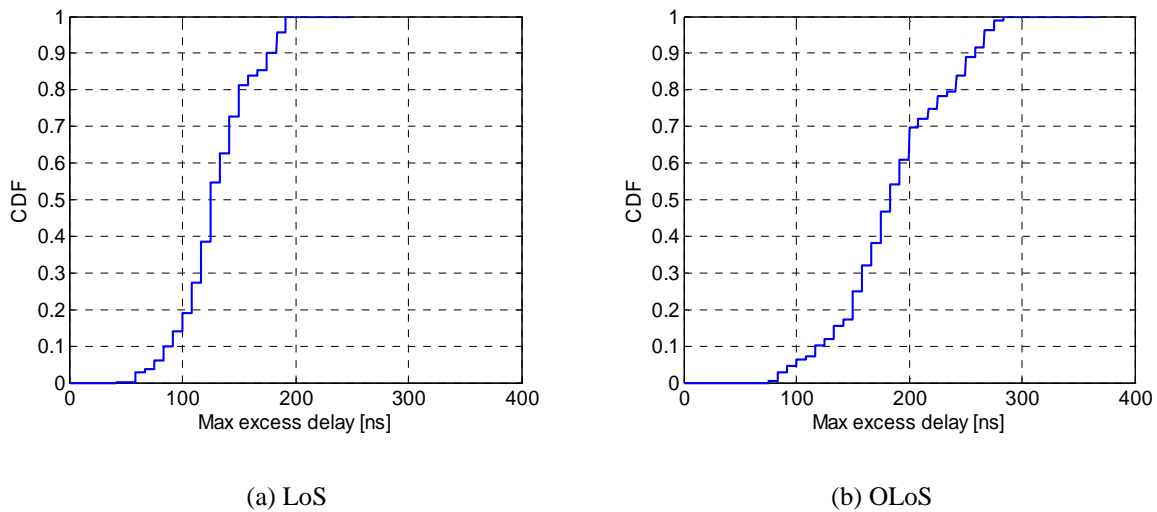
Figure 3-72: Log-normal fitting of the delay spread pdf in lecture hall: (a) LoS (b) OLoS. X denotes delay.

Table 3-27: RMS delay spread [ns] for B3 scenario and VV polarization.

RMS delay spread [ns]		LoS		NLoS	
		Lecture	Industrial	Lecture	Industrial
Percentile	10%	13.2	21.7	22.3	30.6
	50%	23.7	29.2	37.7	40.8
	90%	34.6	47.2	48.9	45.5

From Figure 3-71, Figure 3-72 and Table 3-27 it can be seen that both measured environments for VV polarization show similar distribution of DS values.

Although maximum excess delay is not used as a WINNER model parameter, it is convenient to have insight into maximum measured values. It is important to note that observed values of DS and maximum excess delay may show strong dependence on receiver noise and/or noise thresholding/estimation method.

**Figure 3-73: Maximum excess delay, scenario B3.****Table 3-28: Maximum excess delay [ns] for B3 scenario and VV polarization.**

Maximum excess delay [ns]		LoS	NLoS
Percentile	10%	83.4	116.7
	50%	125.0	175.1
	90%	175.0	249.9
	mean	129.3	186.1

3.5.3.5 B3 – Angular spread

Departure and arrival angles that are necessary for double-directional channel characterization are estimated using high resolution parameter estimation algorithm RIMAX. The RMS angle-spread is calculated using the circular angle-spread formula [3GPPSCM]. Parameters of assumed log-normal model are obtained by minimizing mean square error. An evaluation of the statistical fitting based on some well known techniques like KS test is not applied.

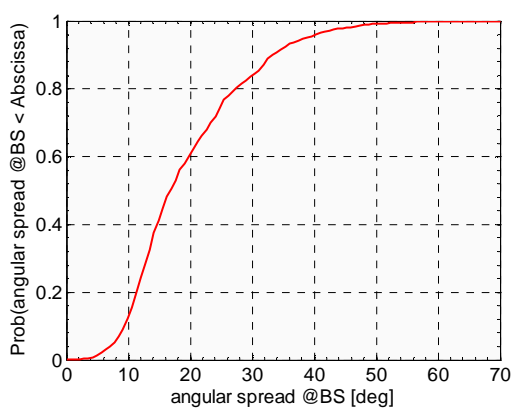
3.5.3.5.1 B3 - Azimuth angle spread at BS and MS

The values of azimuth spread (AS) corresponding to 10, 50 and 90 % of the cdf, are given in Table 3-29 for both link ends, both propagation conditions and both measured environments. Going from LoS to NLoS it can be noticed that AS is slightly decreasing for highly elevated BS (energy that reaches receiver), while AS at MS is increasing.

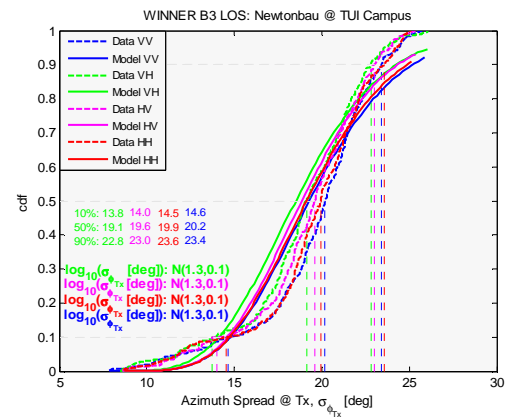
The cumulative distribution functions of the RMS azimuth spreads of the B3 scenario for LOS and NLOS propagation conditions are shown respectively in Figure 3-74 and Figure 3-75.

Table 3-29: RMS azimuth spread [deg] for the B3 scenario under LoS condition (VV pol.).

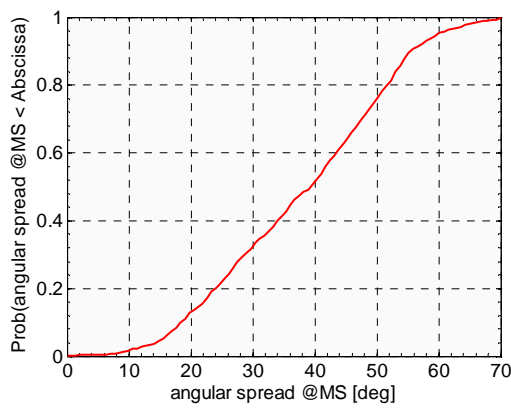
Link end		BS				MS			
Prop. condition		LOS		NLOS		LOS		NLOS	
Environment		Lect.	Indust.	Lect.	Indust.	Lect.	Indust.	Lect.	Indust.
Percentile	10	9	14.6	5	6.4	7	18.8	25	48.5
	50	17.5	20.2	14.5	8.5	41.5	62.8	39.5	68.2
	90	33	23.4	28	19.6	55	87.3	52	73.4



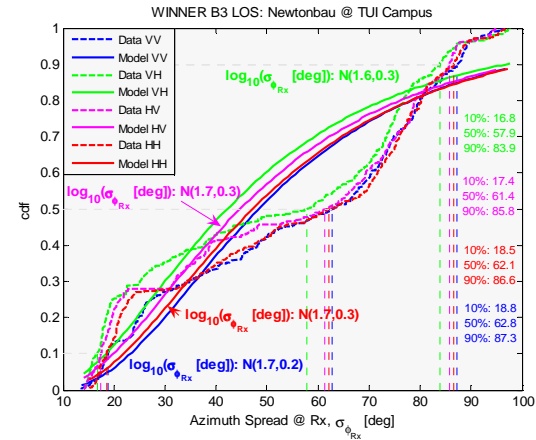
(a) BS (AoA), lecture hall



(b) BS (AoD), industrial hall

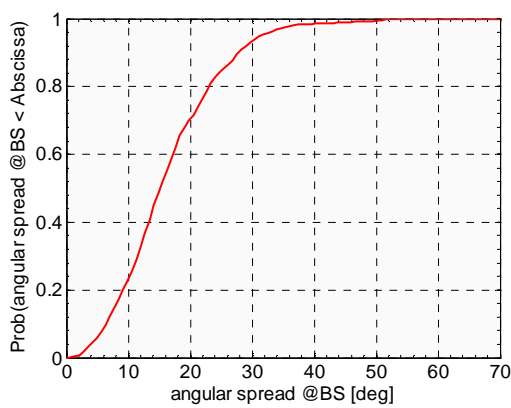


(c) MS (AoD), lecture hall

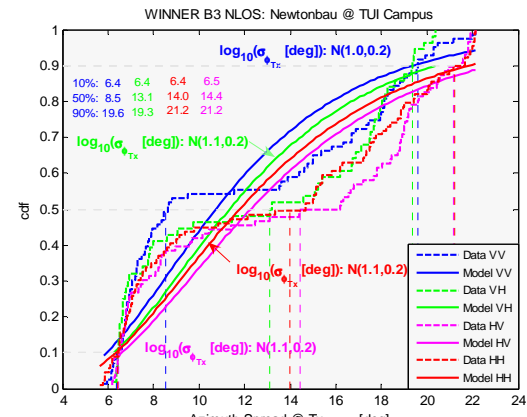


(d) MS (AoA), industrial hall

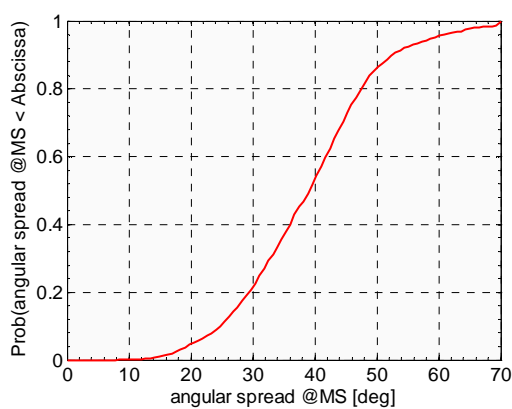
Figure 3-74: RMS azimuth spreads for the B3 scenario under LOS propagation condition.



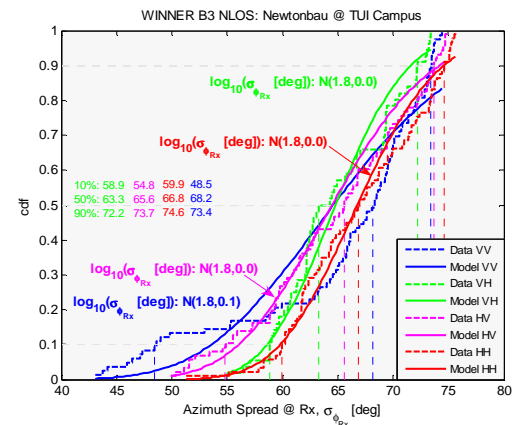
(a) BS (AoA), lecture hall



(b) BS (AoD), industrial hall



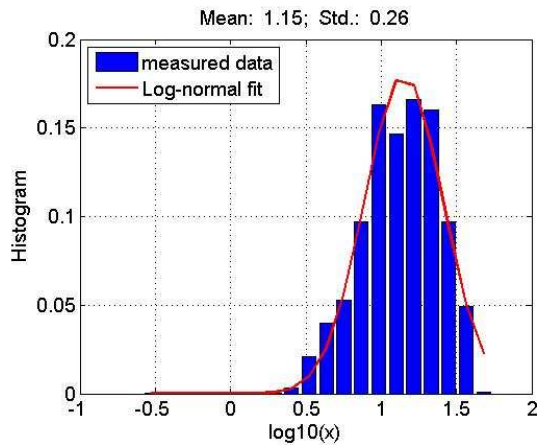
(c) MS (AoD), lecture hall



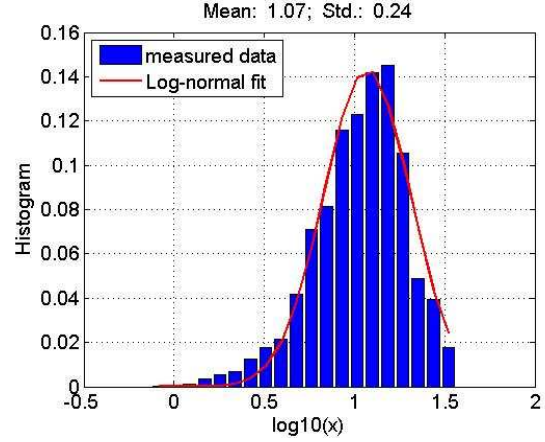
(d) MS (AoA), industrial hall

Figure 3-75: RMS azimuth spreads for the B3 scenario under NLOS propagation condition.

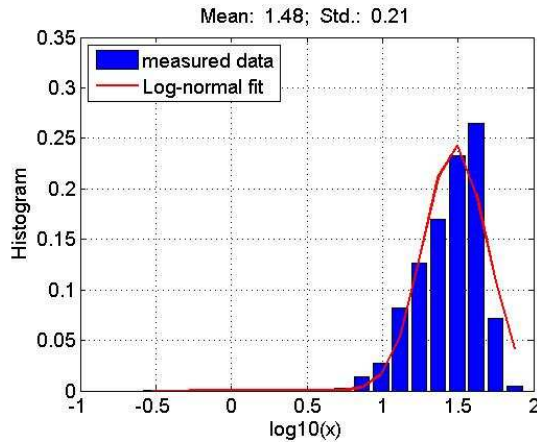
Log-normal fitting of AS distribution for industrial hall is shown in Figure 3-74 (LoS) and Figure 3-75 (NLoS). Additionally, Figure 3-76 is showing pdf fitting of data from the lecture hall.



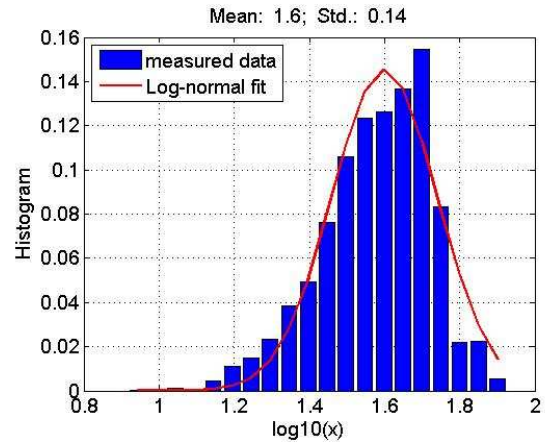
(a) BS (AoA), LoS



(b) BS (AoA), NLoS



(c) MS (AoD), LoS



(d) MS (AoD), NLoS

Figure 3-76: Log-normal fitting of the azimuth spread PDF for the lecture hall. X denotes azimuth spread.

3.5.3.5.2 B3 – Elevation angle spread at MS

The cumulative distribution functions of the RMS elevation spread of the B3 scenario in LOS and NLoS propagation conditions is shown in Figure 3-77. Log-normal fitting of AS cdf is shown in the same figure.

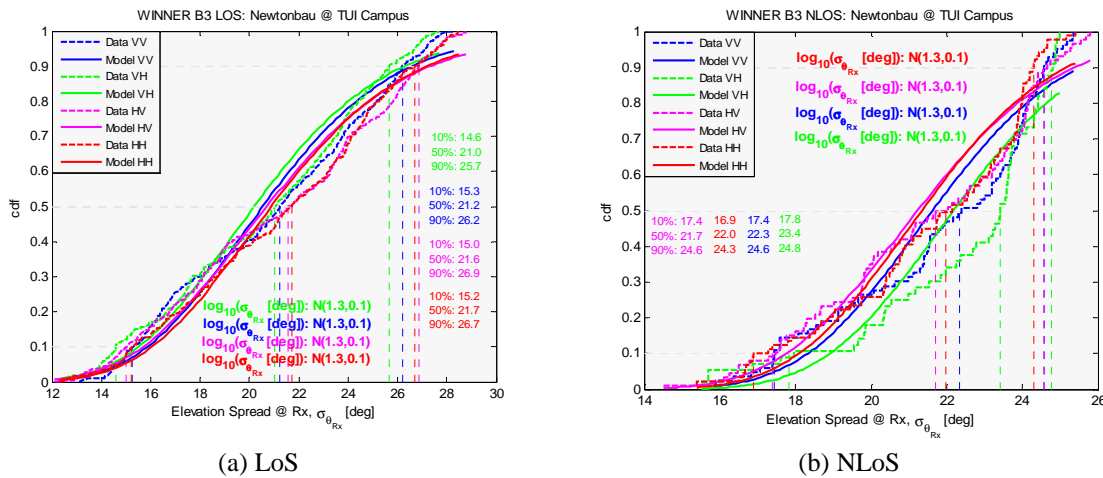


Figure 3-77: RMS AoA elevation spreads (@MS) for the B3 (industrial) scenario.

The values of elevation spread (ES) corresponding to 10, 50 and 90 % of the cdf, are given in Table 3-30 for LoS and NLoS propagation conditions.

Table 3-30: RMS AoA elevation spreads (@MS) for the B3 (industrial) scenario and VV polarization.

AoA spreads (@MS) [deg]		LoS	NLoS
Percentile	10%	15.3	17.4
	50%	21.2	22.3
	90%	26.2	24.6

From Figure 3-77 and Table 3-30 it can be seen that distribution of elevation spread for B3 scenario is similar under both LoS and NLoS conditions.

3.5.3.6 B3 – LSP correlation coefficients

The correlated Large-Scale-Parameters in WINNER channel model are Delay Spread, Angular (Azimuth, Elevation) Spreads, Shadow fading and K-factor. The correlations are reproduced in model based on:

- a) distance dependence of the auto-correlation coefficient that is determined for all LSPs,
- b) cross-correlation coefficient between LSPs at zero distance.

Autocorrelation function (ACF) is modeled as exponentially decaying function with single parameter called decorrelation distance (distance at which ACF becomes lower than 1/e). In this subsection ACFs calculated from measured data and their exponential models will be given for LoS and NLoS cases.

3.5.3.6.1 B3 – Distance dependent auto-correlations

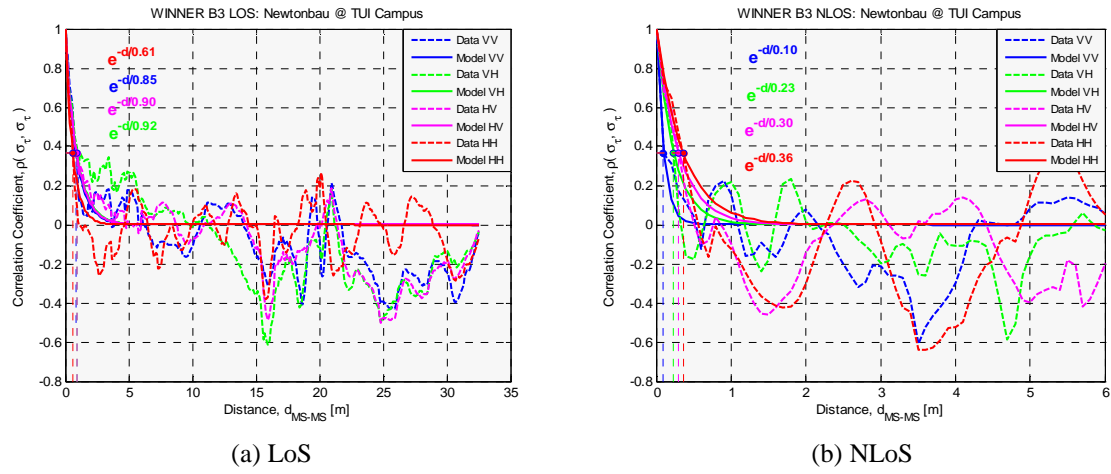


Figure 3-78: Distance dependence of the delay-spread autocorrelation in B3 scenario.

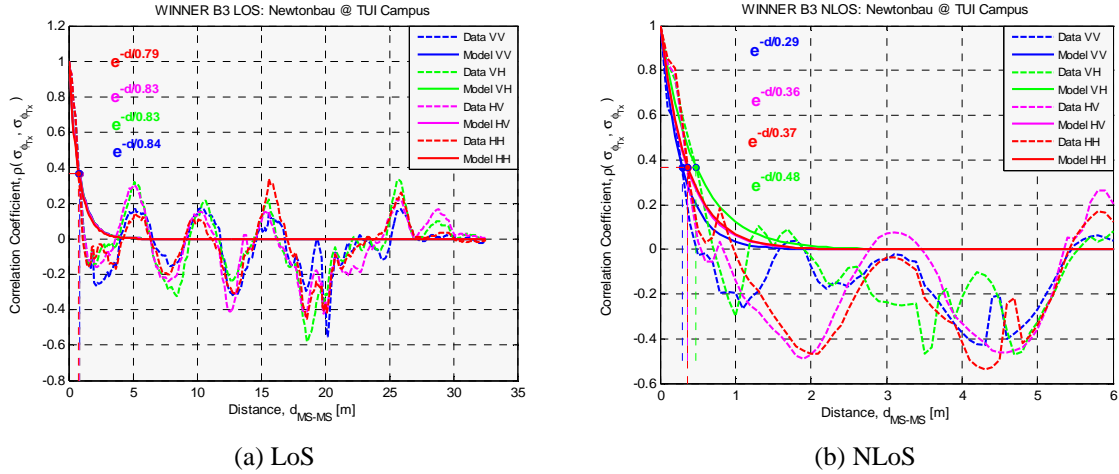


Figure 3-79: Distance dependence of the BS (AoD) azimuth-spread autocorrelation in B3 scenario.

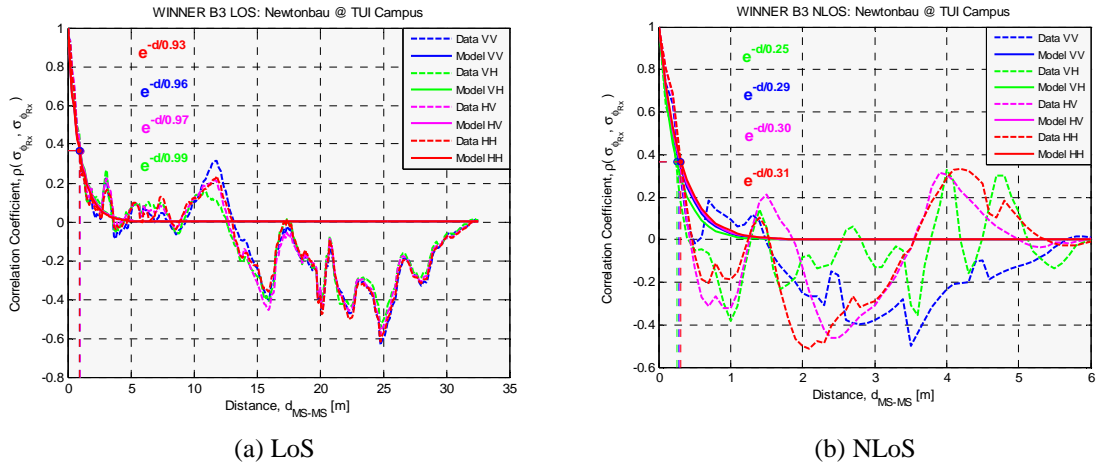


Figure 3-80: Distance dependence of the MS (AoA) azimuth-spread autocorrelation in B3 scenario.

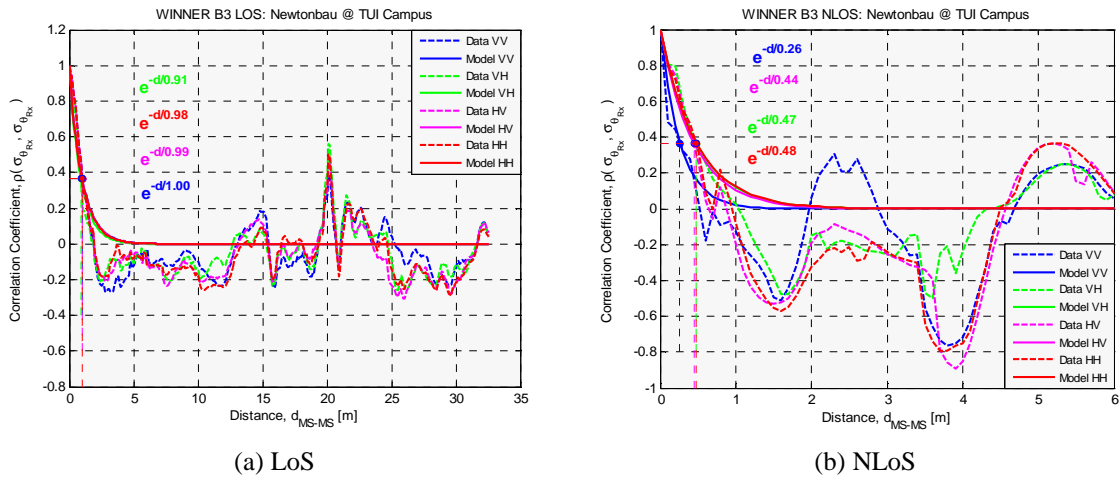


Figure 3-81: Distance dependence of the MS (AoA) elevation-spread autocorrelation in B3 scenario.

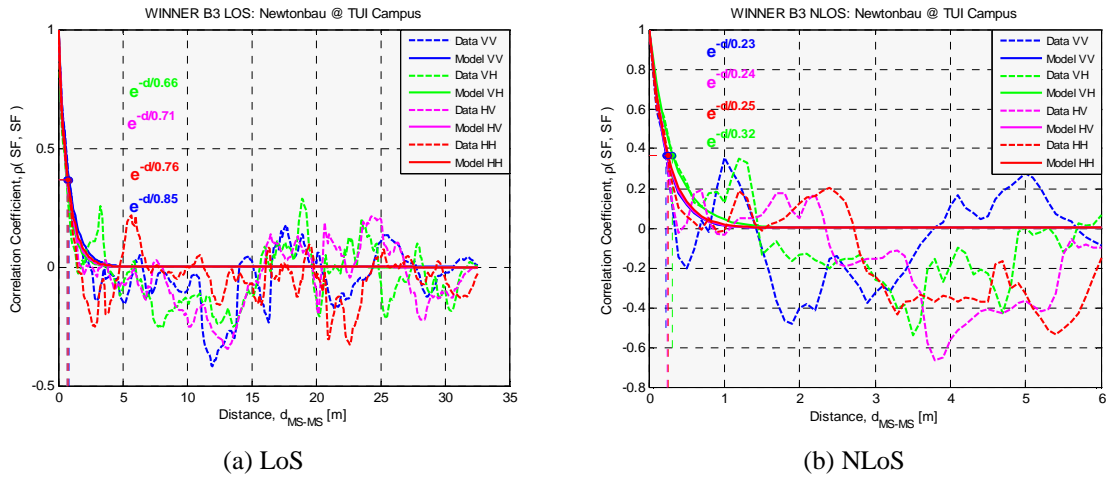


Figure 3-82: Distance dependence of the shadow fading autocorrelation in B3 scenario.

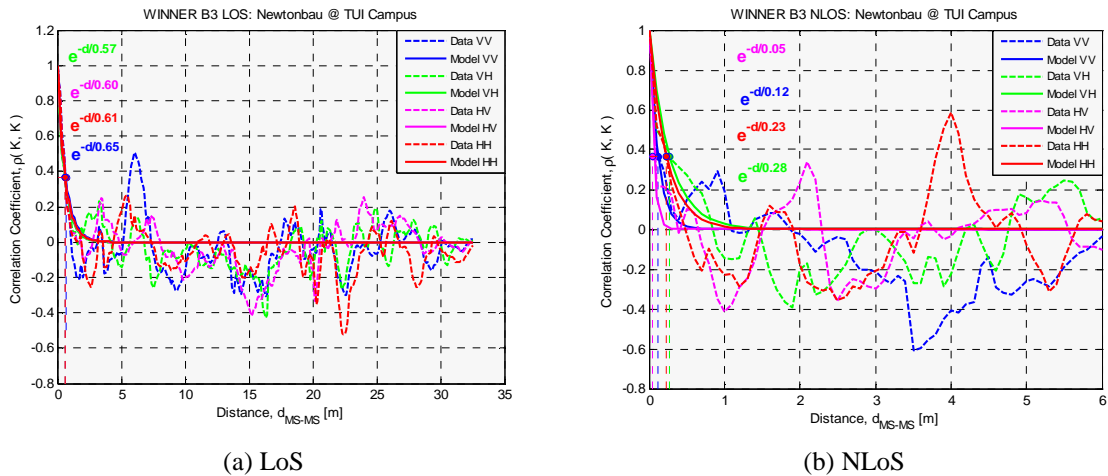


Figure 3-83: Distance dependence of the MS AoA azimuth-spread autocorrelation in B3 scenario.

It can be noticed that all LSPs in industrial environment have rather short decorrelation distance. Under LoS condition and for VV polarization its value is in the range from 0.7- 1 m, and decorrelation distance is even 3-4 times lower for NLoS condition. Since higher decorrelation distances are observed in lecture hall [WIN1D54], B3 model parameters will be chosen as average between these two measured environments.

3.5.3.6.2 B3 – Cross-correlations

Cross correlations of LSPs that are calculated at zero distance under LoS condition are given in matrix below. The following labeling is used: DS denotes Delay-Spread, DAS denotes Departure-Azimuth-Spread, AAS is Arrival-Azimuth-Spread, AES is Arrival-Elevation-Spread, SF denotes Shadow-Fading, and K is K-factor.

$$\rho_{LoS}(0) = \begin{bmatrix} DS & DAS & AAS & AES & SF & K \\ 1 & -0.3 & -0.4 & -0.2 & 0.1 & -0.3 \\ & 1 & 0.3 & 0.3 & -0.3 & 0.2 \\ & & 1 & 0.2 & 0.2 & -0.1 \\ & & & 1 & 0.1 & -0.1 \\ & & & & 1 & -0.6 \\ & & & & & 1 \end{bmatrix} \quad (3.37)$$

For VV polarization significant negative correlation is observed between DS and AAS (-0.4) and SF and K-factor (-0.6). It is interesting to note that given cross-correlation coefficients are slightly different for HH polarization. In that case high correlation levels are observed between DS and SF (0.62) and DS and K-factor (-0.5).

Under NLoS condition cross-correlations for VV polarization are as follows:

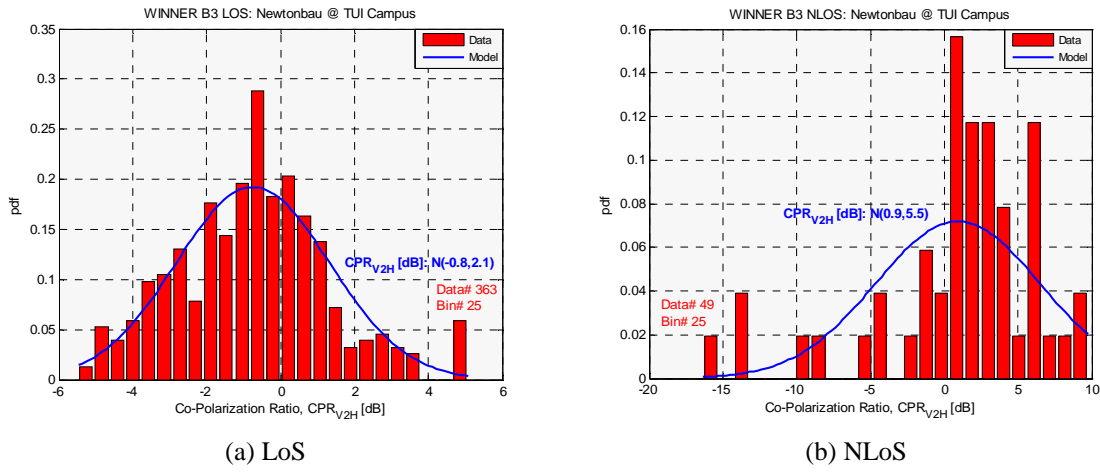
$$\rho_{NLoS}(0) = \begin{bmatrix} DS & DAS & AAS & AES & SF & K \\ 1 & -0.1 & 0.0 & -0.3 & 0.1 & -0.2 \\ & 1 & -0.4 & 0.2 & 0.3 & -0.3 \\ & & 1 & -0.3 & -0.2 & 0.0 \\ & & & 1 & -0.2 & 0.4 \\ & & & & 1 & 0.0 \\ & & & & & 1 \end{bmatrix} \quad (3.38)$$

Although, in general correlation decreases, there are some opposite cases, e.g. correlation coefficient between AES and K-factor becomes 0.4 (was -0.1). These results may be related to significantly lower NLoS measurement data set.

3.5.3.7 B3 – Polarisation ratios

3.5.3.7.1 B3 – Co-polarisation ratio (CPR)

Co-polarization ratio is expressing ratio of the vertically transmitted-vertically received (VV) and horizontally transmitted- horizontally received powers (Figure 3-84). It can be noticed that HH polarization is providing more power (~1dB) in LoS, while it is opposite for NLoS. In respect to LoS, the CPR variance is increased under NLoS condition.

**Figure 3-84: B3 co-polarization ratio.**

3.5.3.7.2 B3 – Cross-polarisation ratio (XPR)

The probability density functions of V->H and H->V XPRs are shown in Figure 3-85 and Figure 3-86, respectively. In analyzed measurement data V->H XPR is approx. 4 dB higher than H->V XPR. XPR under LoS condition is 3 dB (H->V) to 4 dB (V->H) bigger then for NLoS.

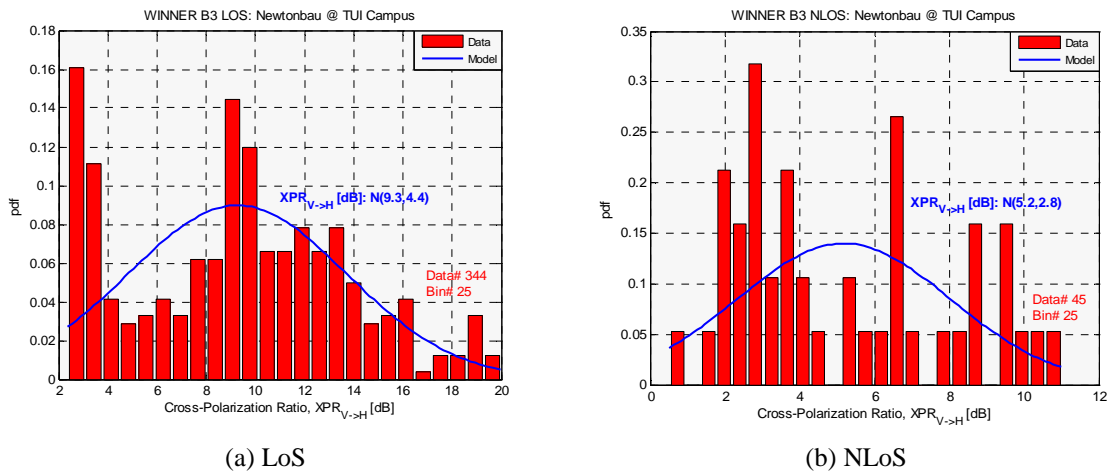
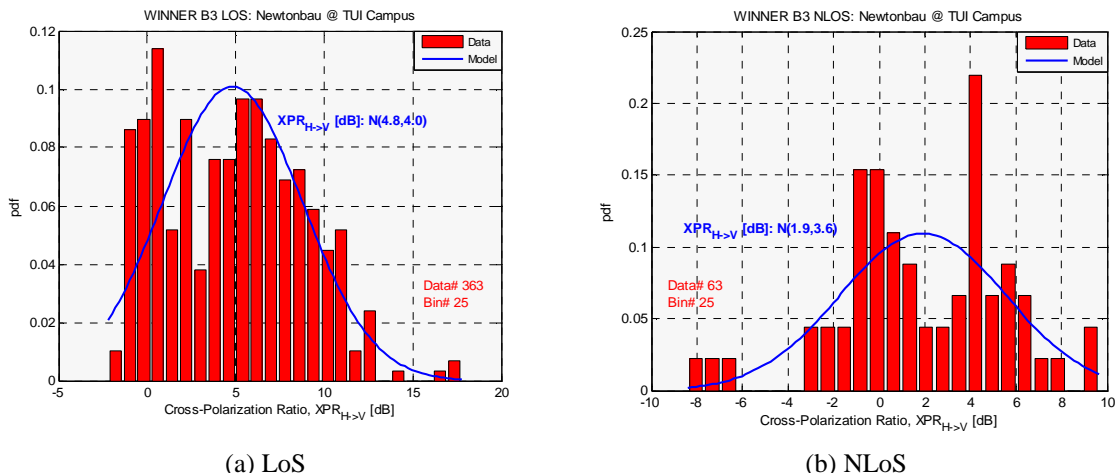
**Figure 3-85: B3 XPR V->H.****Figure 3-86: B3 XPR H->V.**

Table 3-31: Percentiles of the cross-polarization ratio.

Propagation condition		LOS		NLOS	
XPR type		V->H	H->V	V->H	H->V
Percentile	10	3.0	-0.3	2.0	-2.2
	50	9.4	4.9	4.2	1.5
	90	15.1	10.1	9.4	6.4

Since reference polarization for model parameterization is chosen to be VV, reference XPR will be V->H. The standard deviation for the V->H XPR under LoS was found to be 4.6 dB, and 2.8 dB for NLOS.

3.5.3.8 B3 – Power Delay Profile

Power delay profiles measured in lecture hall are shown in the figure below for LoS and OLoS propagation conditions.

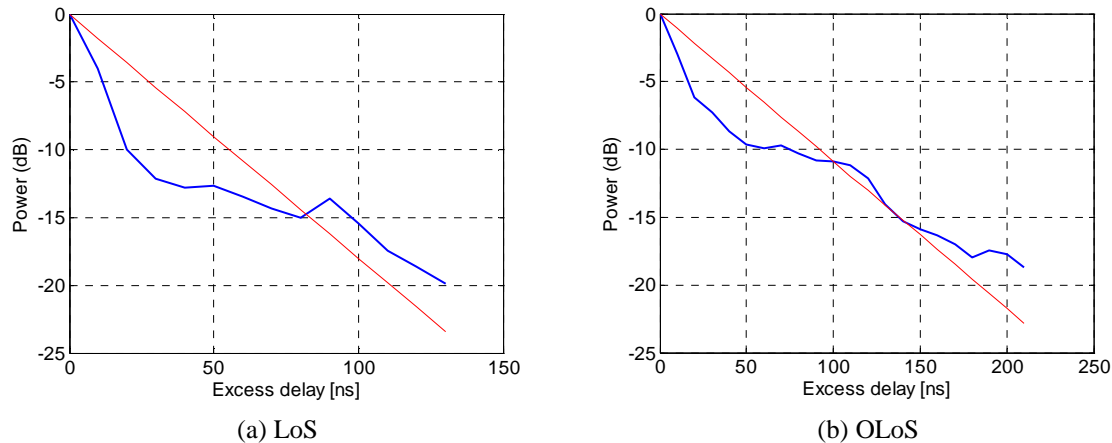
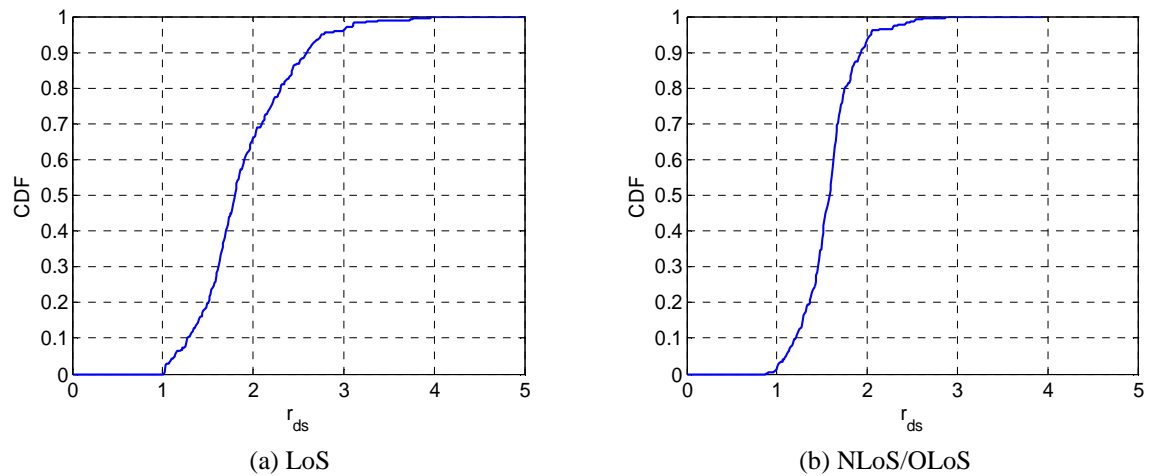


Figure 3-87: Modeling of power delay profile (PDP) in indoor environment.

It is found that the PDP exp. decay is 28.01 ns for LoS and 45.66 ns for NLoS conditions.

3.5.3.9 B3 – Delay proportionality factor

Figure 3-88 shows the empirical cumulative distribution function of the delay proportionality factor in scenario B3 for both LOS and NLOS case. Percentiles of delay proportionality factor are given in the Table 3-32.

**Figure 3-88: Delay proportionality factor r_{DS} .****Table 3-32: Percentiles of delay proportionality factor.**

Delay proportionality factor		LOS	NLOS
Percentile	10%	1.27	1.19
	50%	1.80	1.58
	90%	2.59	1.93
	mean	1.90	1.58

3.5.3.10 B3 – Distribution of the azimuth angles of the multipath components

The cumulative distribution functions of the AoAs and AoDs for the multipath components are shown in Figure 3-89 and Figure 3-90 for LOS and NLOS propagation conditions. These results are based on the high-resolution algorithm RIMAX [RIMAX].

The percentiles for the CDF functions for the AoAs and AoDs are shown in Table 3-33.

Table 3-33: Percentiles of the distribution of azimuth angles.

Link end		BS		MS	
Propagation condition		LOS	NLOS	LOS	NLOS
Percentile (degrees)	10	-49.1	-41.8	-107.3	-125.5
	50	-1.8	-1.8	-5.5	-5.5
	90	38.2	38.2	110.9	114.5
	mean	-1.3	-0.4	-0.1	-3.5

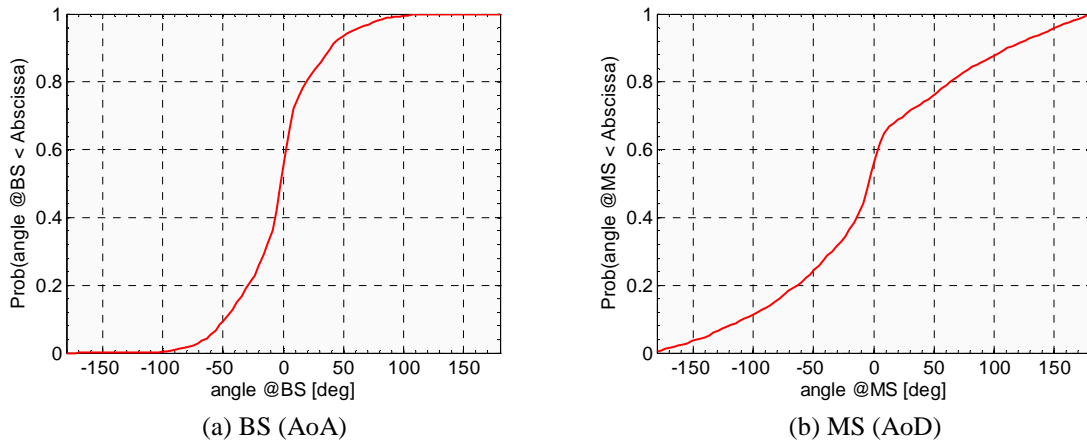


Figure 3-89: CDFs of azimuth angles for the B3 scenario under LOS propagation condition.

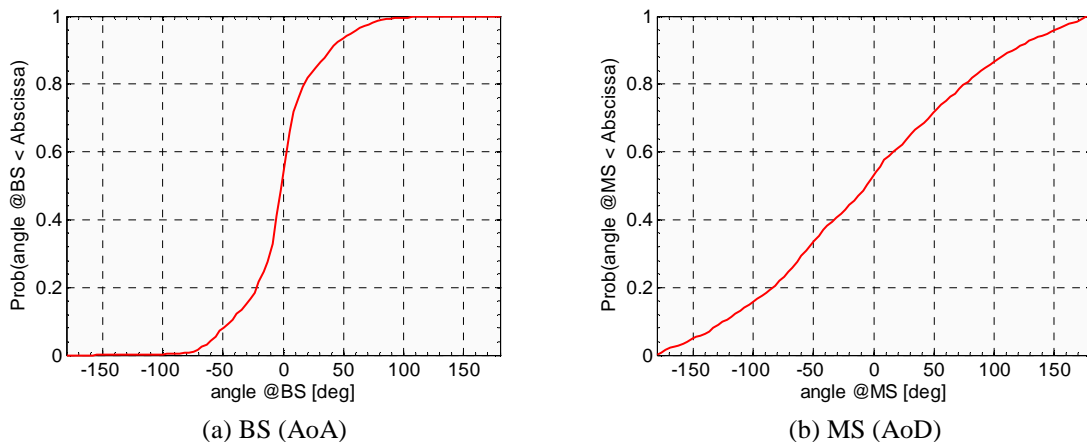


Figure 3-90: CDFs of azimuth angles for the B3 scenario under NLOS propagation condition.

3.5.3.11 B3 – Number of clusters

The number of the clusters is calculated after resampling the data to 100 MHz. Table 3-34 presents the 10, 50 and 90 percentiles of the cumulative distribution of the number of clusters.

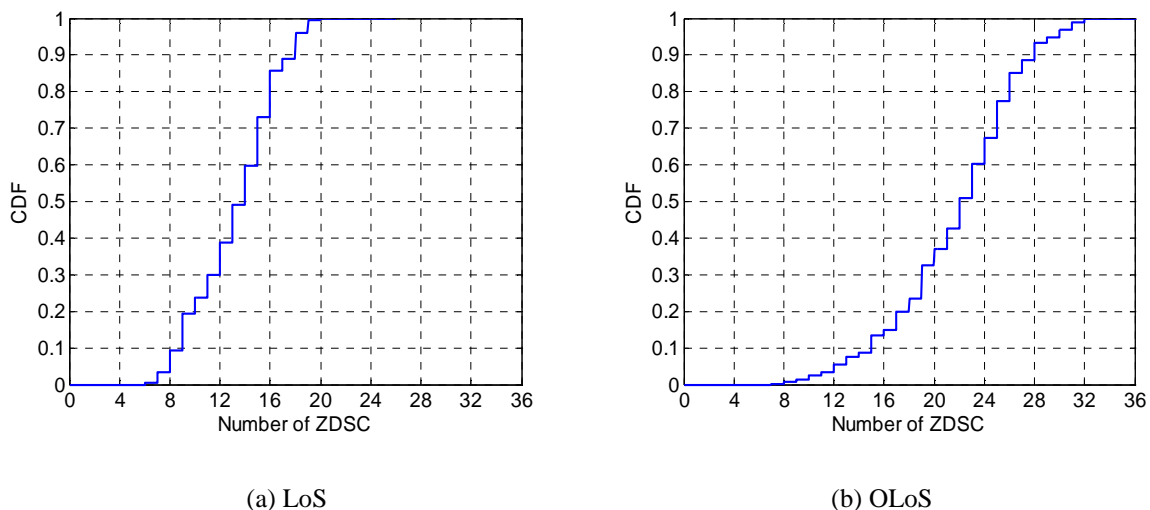
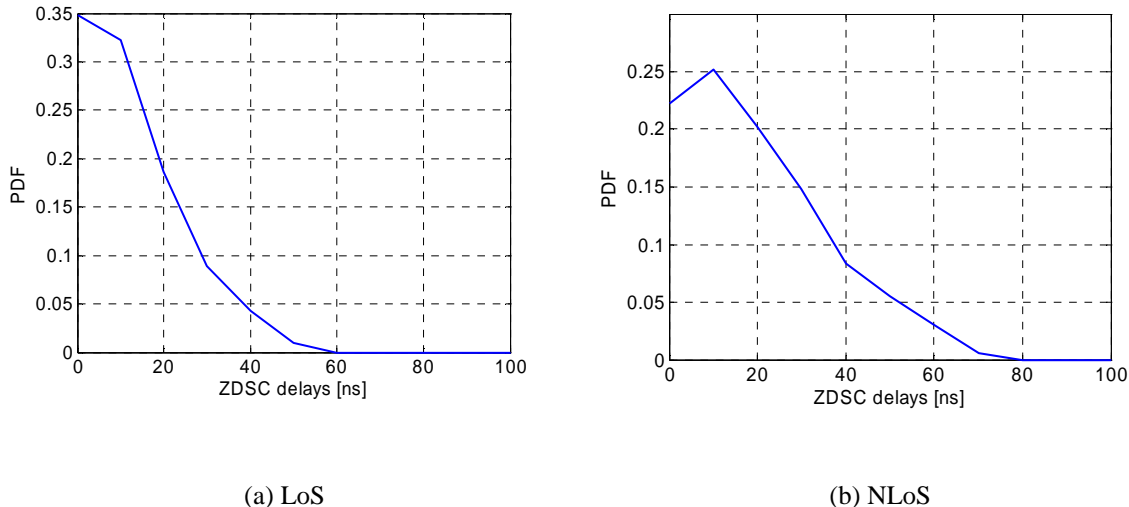


Figure 3-91: Number of clusters.**Table 3-34: Number of clusters.**

Number of clusters		LoS	OLoS
Percentile	10%	8	14
	50%	13	22
	90%	17	27
	mean	13	22

3.5.3.12 B3 – Distribution of cluster delays

In Figure 3-92 distributions of the cluster delays for the scenario B3 for LOS and NLOS conditions are presented. As expected, in NLOS case probability of cluster with higher delays is higher as in the LOS case.

**Figure 3-92: Distributions of the cluster delays for the different sub-scenarios.**

3.6 B4 – Outdoor to indoor

3.6.1 B4 – Scenario definition

Outdoor-to-indoor in urban macrocell (C4) is identical with B4 because the antenna heights are irrelevant as explained in Chapter 7.6. In outdoor-to-indoor scenario the MS antenna height is assumed to be at 1 – 2 m (plus the floor height), and the BS antenna height below roof-top, at 5 - 15 m depending on the height of surrounding buildings (typically over four floors high). Outdoor environment is metropolitan area B1, typical urban microcell where the user density is typically high, and thus the requirements for system throughput and spectral efficiency are high. The corresponding indoor environment is A1, typical indoor small office. It is assumed that the floors 1 to 3 are used in simulations, floor 1 meaning the ground floor.

Based on [AHHM07] and [HACK07] scenarios A2 and B4 are reciprocal and for this reason they are combined in part I of D1.1.2. *See more details of the merging process on the section 3.2 where A2 results are discussed.*

Measurements for this (B4) scenario were performed in University of Oulu (OUULU) and in Canadian Research Center (CRC). CRC conducted outdoor-to-indoor measurements in a 100 MHz bandwidth centred at 4.95 GHz. The transmitter was housed in a large van, parked in front of a 4-story brick building, on the broad (windowed) side of the building. Measurements conducted in the university of Oulu consisted of several routes and BS locations. BS was in a height of 6 meters and the height of the indoor Rx antenna was 1.5 meters.

Results reported by OUULU and CRC are different for several reasons. The main reason is the differences in building characteristics. Due to the fact that OUULU is located in Europe and CRC in North-America, the building materials and dimensions deviate from each other significantly. This is bound to result in different analysis conclusions. Other minor reasons for deviations could include the sounder characteristics and applied settings, the antenna characteristics, the methods used to move the receive antenna during the measurements, as well as the distances over which it was moved corresponding to individual results. Although attempts were made to make analysis procedures the same, there were peculiarities of the recorded data that made some data preprocessing differences necessary.

Since the OUULU data set is more complete, with corresponding AoA information, and the analysis procedures section of this report is more closely aligned with analyses conducted at OUULU, the OUULU results were chosen for reporting in the generic channel model table, Table 4-5. The CRC results are left, however, for examination in this section, as comparison of these with the OUULU results is a good example of how results reported in the literature can vary, and, as discussed in the opening sentence of this paragraph, why such variations can occur.

3.6.2 B4 - Measurements

OUULU measurements were conducted on a sunny summer day in the campus area of University of Oulu. 5.25 GHz center frequency together with 100 MHz bandwidth was applied using Propsound Channel Sounder (see Part I, 2.4.1). ODA_5G25 and PLA_5G25 antennas (see Part I, Table 2-4) were employed in Rx and Tx ends, respectively. From the campus area it is easy to find urban-like outdoor environment with different indoor environments. Several measurement routes were investigated with the receiver moving indoors while the transmitter was fixed on a rooftop or a lifter. These routes were chosen to demonstrate different indoor environments e.g. having big glass windows as in newer buildings or thick concrete walls as in older buildings. Also smaller and bigger rooms and different kind of corridors were measured. Measurement routes covered mainly the first floor but few routes were also measured in second, third and fourth floor. First floor routes and pictures of outdoor and indoor environments are depicted below.

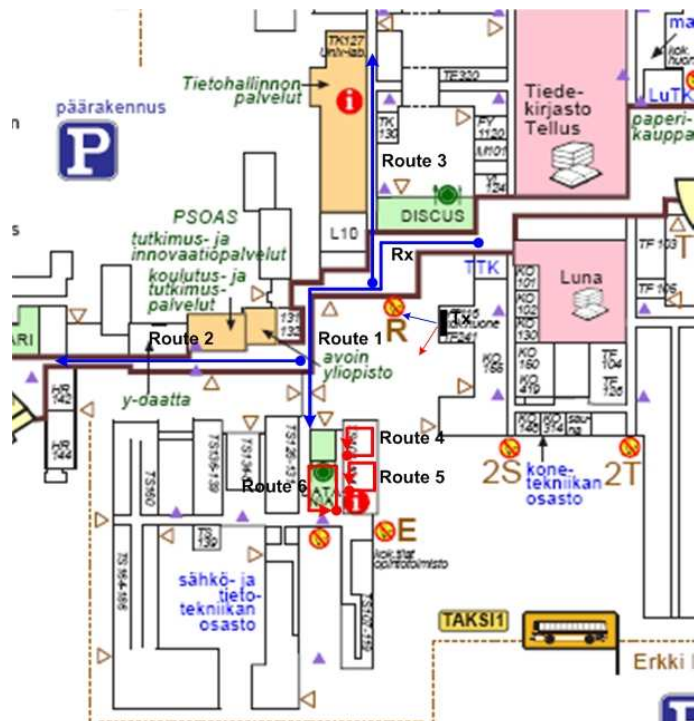


Figure 3-93: Measurement routes.

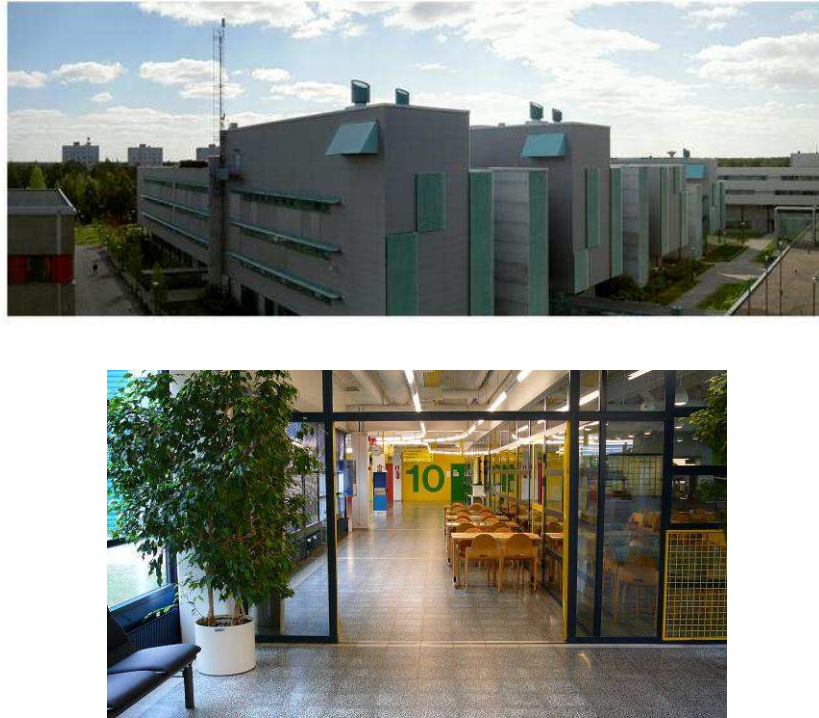


Figure 3-94: Picture from BS (top) and MS (bottom).

3.6.3 B4 Path-loss and shadow fading

3.6.3.1 B4 Measurement results

Path loss and shadow fading are considered as the most important parameters in channel modelling. Path loss (PL) denotes the loss of signal power between the transmitter (Tx) and the receiver (Rx) and shadowing or slow fading is the variation of PL.

The threshold for an effective path in impulse response (to be taken into account in snap shot's power calculation) was set to 20 dB below the power of the maximum peak in the power delay profile (PDP). All the paths in IR that were below this limit, were removed. Furthermore, the dynamic range of the snap shot's peak path's power was checked. The limit for it was set to 23 dB above the noise level. If this limit was not met, then the snap shot in question was discarded. The effect of fast fading was removed by averaging over a small distance. Due to the indoor environment in the receiving end and the applied frequency of 5.25 GHz, this distance was not bigger than 1 meter which corresponds to 13 wavelengths. The measured PL is calculated as wideband path loss as

$$PL = -10 * \log_{10} \left(\sum_{t=1}^N |h_t|^2 \right) + G_T + G_R,$$

where N is the number of effective paths, h_t is the channel coefficient for t delayed path and G_T and G_R are the antenna gains at Tx and Rx, respectively.

Since scenario A2 is reciprocal to the outdoor-to-indoor B4 scenario, the pathloss formula is assumed to be the same. That is, the path loss model presented for scenario A2, is applied in here as well. Hence, the path loss can be expressed as:

$$PL = PL_b + PL_{tw} + PL_{in}$$

where

$$PL_b = PL_{B1}(d_{out} + d_{in})$$

$$PL_{tw} = We + WG_e (1 - \cos(\theta))^2$$

$$PL_{in} = \alpha d_{in}$$

From A2 and B4 measurements the most appropriate values for the model constants have been found and they are:

$$\begin{aligned} W_e &: 14 \text{ dB} \\ WG_e &: 15 \text{ dB} \\ \alpha &: 0.5 \text{ dB/m.} \end{aligned}$$

The measurements conducted at the University of Oulu, which consists of 3-5 floor office type buildings in a narrow street-like grid with some citypark-like openings. The width of the corridors is ~3.5 meters. The building walls are mainly concrete and are approximately 30 cm thick. However, occasionally glass walls are encountered. The transmitter was located outside in a height of 6 meters and Rx moved along corridors in four floors.

The measured PL and the path loss model can be seen in Figure 3-95. The measured PL is shown as black dots, and the model is shown as red solid line. The x-axis is the number of the measured radio channel snap shots (SS) applied in the path loss model validation. In B4 scenario, this number was approximately 130 000 SS. The figure shows that the model overestimates the path loss in rooms where large windows exists (SSs of 1 to 30 000). However, for rooms and corridors with windows of typical size, the model is quite precise. The model is valid for ranges of 3-1000 meters. Shadow fading is the variation of the PL and it is found to be 7 dB. The correlation distance for shadow fading is 5.9 meters.

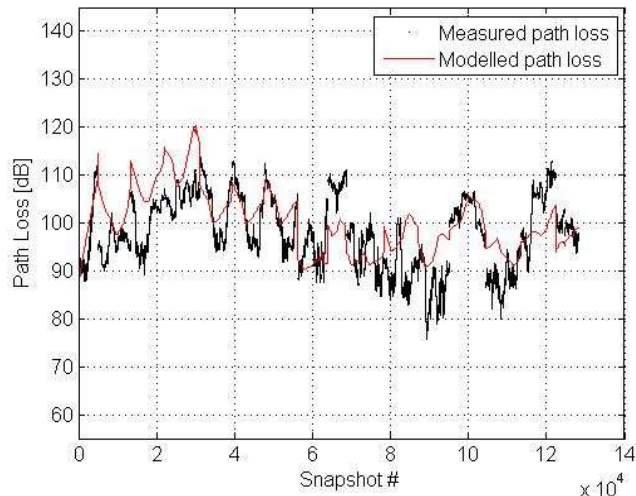


Figure 3-95: Measured and modelled path loss.

In Table 3-35, the path loss values in dB are given for four cases where the number of concrete walls between Tx and Rx varies.

Table 3-35: Path loss dependence on the number of walls between Tx and Rx.

# of walls / distance (m)	1 wall / 3.7	2 walls / 7.3	3 walls / 11.5	4 walls / 15.6
Path loss (dB)	69.9	79.4	87.1	92.8
Free space loss (dB)	58.2	64.1	68.1	70.7

In CRC measurements the excess transmission losses were estimated in a similar manner to work reported in [deJKH02] by evaluating the sum of the squares of the values in Average Power Delay Profiles (APDPs) for each measurement run, comparison against a calibration reference, and appropriately accounting for free space loss and measurement system gains and losses. Excess loss varied from floor-to-floor and depending on whether the Rx was on the illuminated or back side of the building or in the hallway. In summary, such losses varied from 20-50 dB in the basement, 10-30 dB on the ground floor, 7-27 dB on the second floor, and from 7-32 dB on the third (top) floor.

3.6.3.2 B4 Literature review

There are some outdoor to indoor measurement campaigns reported in literature but very few of them discuss path loss or shadow fading.

In [SS01] a propagation loss model for LOS outdoor to indoor scenario is proposed. Measurements to test the validity of this model were carried out at 2.385 and 5.184 GHz in three different U.K. cities and the proposed model is said to be in agreement with the measurements.

In [MHA+04] the measurements were performed in Kista, a part of city of Stockholm with mostly office buildings at 1947 MHz. The base station was placed at a window at the 6th floor of an office building and the mobile at 6 different locations on three different floors of another office building. The distance between them was 300 m. The average path loss measurement results are pictured in Figure 3-96. Path loss of more than 20 dB in excess of free space loss was measured even in LOS condition. This was due to heat protective window coating.

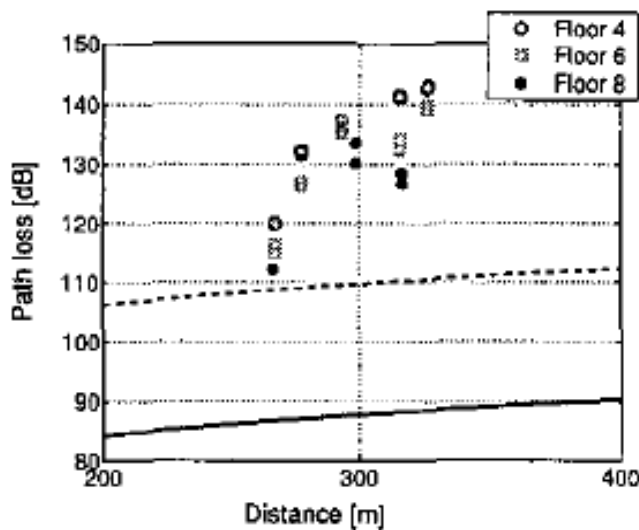


Figure 3-96: Average path loss measured at each location and array orientation. The solid line corresponds to free space loss and the dashed line to free space loss + 22dB.

In reference [CKC03] the transmitter was placed outside a building where the receiver was moving in the corridors on the first and second floors and the measurements were conducted at 2 GHz. The maximum distance between the transmitter and the receiver was 15 meters and the maximum RF output was +13 dBm. The path loss exponent was observed to be of the order -1.0 for both floors. Path loss for second floor is presented in the figure below.

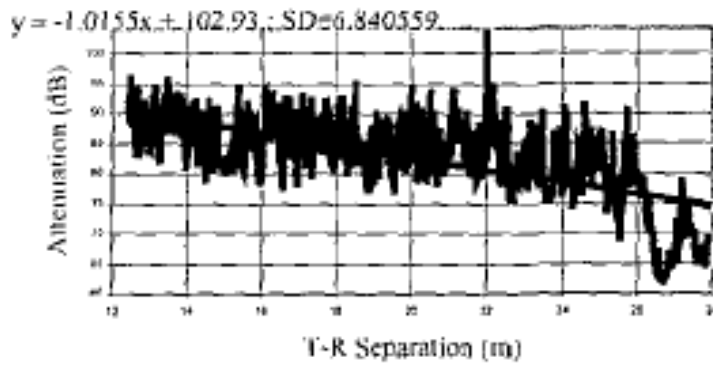


Figure 3-97: Signal attenuation on the second floor at 2 GHz.

[MOT02] proposes an outdoor-to-indoor path loss model that considers the paths through wall openings. The measurements were conducted at a department store at 8.45 GHz and the transmitting antenna was at a height of 14 meters. The path loss model assumes that the loss is a sum of outdoor propagation loss, wall opening penetration loss, and indoor propagation loss. The measurements show that the penetration loss of wall openings ranges from 5 to 28 dB with a mean value of 17.2 dB. The indoor attenuation coefficient was measured to be 0.348 dB/m.

3.6.3.3 Interpretation of B4 results

The results show that a concrete wall attenuates the signal approximately 9dB. This is in the range of values reported in [MOT02]. The measured path loss exponent of 2.12 is also very understandable and in line with the values reported in [WIN1D54].

3.6.4 B4 RMS and maximum excess delay distribution

3.6.4.1 B4 Measurement results

The measurements conducted at the University of Oulu. The Tx was located in a lifter in a height of 6 meters, which corresponds to approximately 2nd-3rd floor in the building. The results are analyzed over several routes in different floors of the building.

In Figure 3-98, the cumulative distribution function (cdf) of the measured RMS delay spread and its normal distribution are shown. The normal distribution applied values 55.7 ns and 37.7 ns as mean and standard deviation, respectively. The correlation distance of RMS delay spread was found to be 9.8 meters.

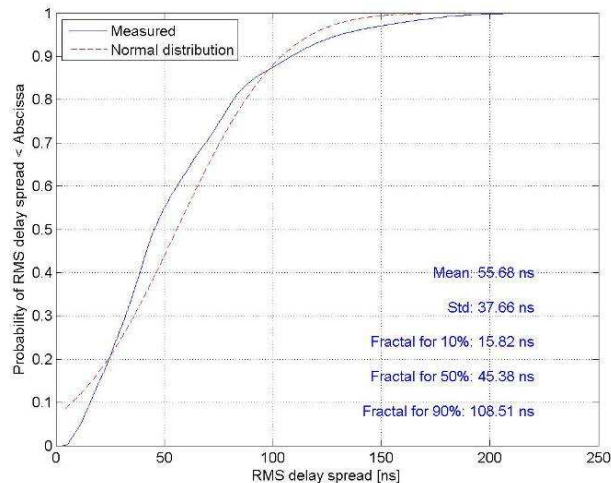


Figure 3-98: Cdf of RMS delay spread.

In Figure 3-99 the cdf for maximum excess delay spread is shown together with normally distributed cdf model. The correlation distance of the maximum excess delay spread was found to be 12 meters.

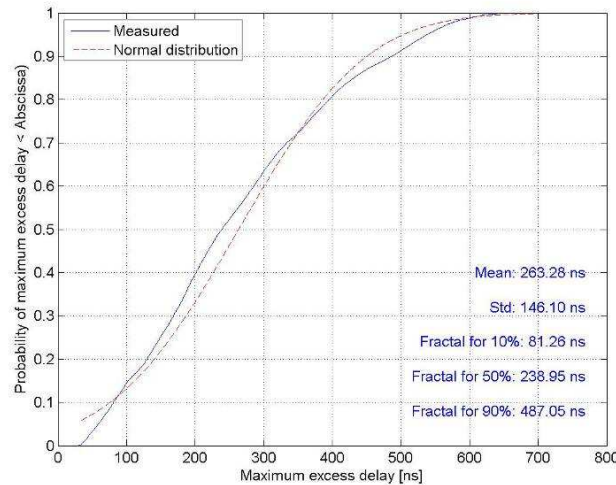


Figure 3-99: Cdf of Maximum excess delay spread.

In CRC measurements the values for rms delay spread varied with measurement location, but their minimum and maximum values were about the same on all floors, being 9 ns and 30 ns, respectively. The median values were about 16 ns, except on the second floor, where the median was 21 ns. The reason for the higher values on the second floor is not clear at the time of writing. Figure 3-100, shows an experimentally determined cumulative probability distribution function (ECDF) for rms delay spreads from all measurement locations in the building. For values estimated using a 20 dB threshold, the figure shows a median of 19 ns, with maximum and minimum values of 8 and 29 ns, respectively.

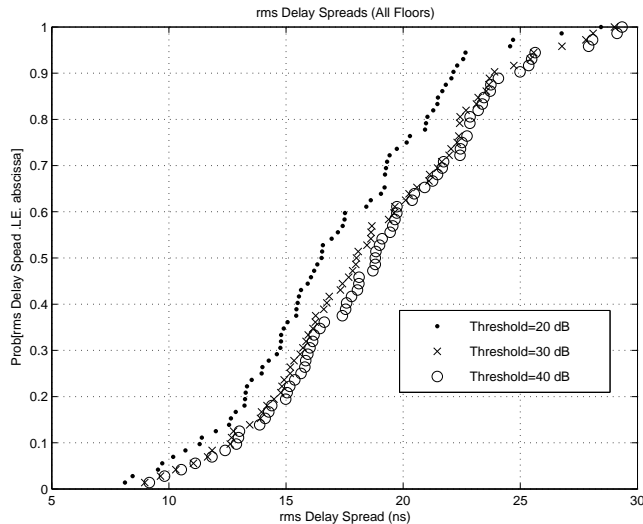


Figure 3-100: ECDF of rms delay spreads computed from data recorded in all measurement locations, on all floors.

3.6.4.2 B4 Literature review

In [WAE+04] radio channel measurements were performed at 5.2 GHz and a signal bandwidth of 120 MHz in outdoor-to-indoor office propagation scenario in Lund University, Sweden. In the measurements the transmitter was placed on three different locations on a roof top and the receiver was in an office

building southwards from the transmitter. The receiver was either in the northern rooms which were nearest to the transmitter, in the southern rooms or in the corridor between the northern and southern rooms as pictured in Figure 3-101 [WAE+04].

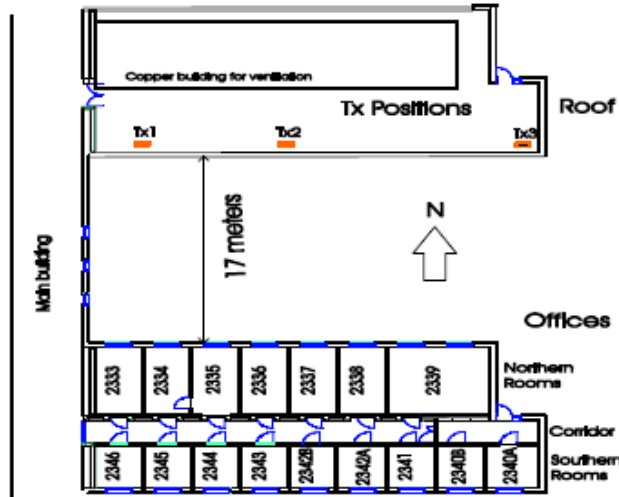


Figure 3-101: Measurement location in reference [WAE+04].

The rms delay spread was about 7-10 ns for half of the cases when the receiver was located in the northern rooms. The rms delay was 12-15 ns for 50 percent of the cases when the receiver was located in the southern rooms and for the corridor about 8 to 11 ns depending on the transmitter location on the roof top. The delay spread was observed to be in the range of 5-25 ns.

In [AHY06] the rms delay spread of the channel is observed to be approximately 40 ns for half of the channel samples. The measurements were conducted at 5.25 GHz and 100 MHz bandwidth in the campus area of the university of Oulu, Finland. The transmitter was located outside a building at a height of 12 m and receiver was moving in a laboratory room on the first floor of the building at a height of 1.3 m.

In [WOT99] wideband measurements were carried out at 2.44 and 5.74 GHz in Oxford, UK for static outdoor-to-indoor scenario using dual channel vector network analyzer. The measurement bandwidth was 80 MHz. Measurement environments were categorized into urban, suburban and rural. The RMS delay spread for multipath arrivals was measured to be 37 ± 8 , 24 ± 20 and 19 ± 8 ns for urban, suburban and rural environments respectively. The mean excess delay was 34 ± 10 , 22 ± 30 and 13 ± 8 ns for urban, suburban and rural environments respectively. When moving from urban to suburban and rural environments, the RMS and mean delay spread decreases. After grouping multipath arrivals into clusters the RMS delay spread was 21 ± 3 , 12 ± 6 and 11 ± 3 ns for urban, suburban and rural environments respectively.

[C02] reports measurements at 3.6-4.2 GHz band in Ministry of the Communications building, in Rome, Italy. The building is 8 floors, 25 meters high and U-shaped. The transmitter was placed on the top of the other wing of the building and the receiver was placed at seven sites inside the opposite wing. The distance between the transmitter and the receiver was 40-60 meters. Example of the obtained mean excess delay and RMS delay spread are pictured in Figure 3-102 and Figure 3-103 [C02] respectively.

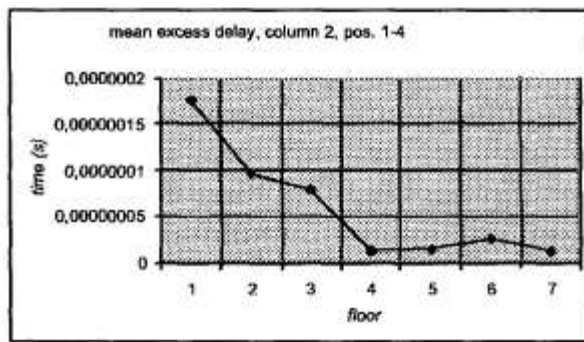


Figure 3-102: Mean delay spread.

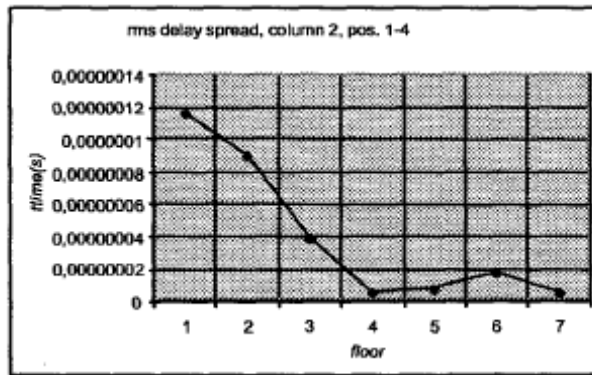


Figure 3-103: RMS delay spread.

3.6.4.3 Interpretation of B4 results

Measured delay spread values are relatively large compared to literature. However, delay spread calculations are highly dependant on the way the threshold level is chosen, i.e., the way we choose which delay taps are taken into account and which are not.

In our measurement analysis, the threshold was set in such a way that all the taps that are less than 20 dB below the level of the peak power, were accounted for. Furthermore, the dynamic range of a snap shot was required to be at least 23 dB in order to be accounted for in the analysis. Another option is to select those taps that are more than, for example, 3 dB above the noise level as effective taps. If this method had been applied the delay spread results would have been higher, approximately 1.3 times the values presented in Section 2.6.2.1.

3.6.5 B4 Azimuth AS at BS and MS

3.6.5.1 B4 Measurement results

Azimuth angle spread is calculated as described in [3GPPSCM] from DoA, DoD and path powers. It is known as circular angle spread. In the analysis results Tx is considered as the outdoor base station (BS) and Rx as the indoor mobile station (MS).

Corresponding values for both terminals averaged over all routes are shown in Table 3-36. The cdf curves, based on the values in Table 3-36, are shown in Figure 3-104.

Table 3-36: RMS azimuth angle spread averaged over all routes.

Stat (degrees) \ Terminal	Tx (outdoor)	Rx (indoor)
Mean	16.5	59.7

Std	12.4	18.3
10%	2.0	35.6
50%	12.7	60.9
90%	27.3	82.6
CorrDist (m)	10.6	6

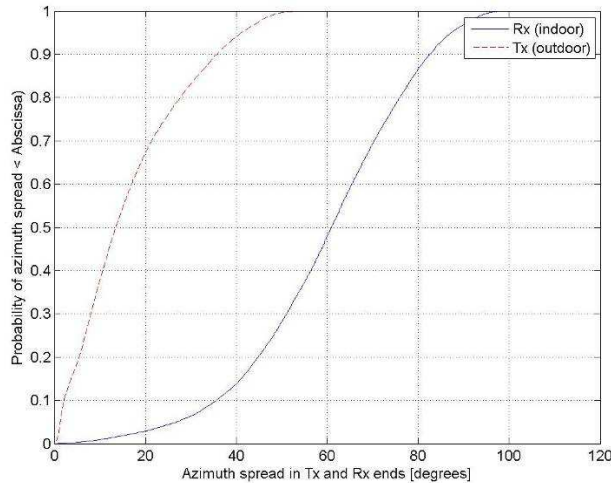


Figure 3-104: Cdf for RMS azimuth spread for both terminals.

3.6.5.2 B4 Literature review

In [WAE+04] angular spread and rms angular spread were reported. The measurements were performed at 5.2 GHz and bandwidth of 120 MHz in Lund University, Sweden. The transmitter was placed on a roof top [WAE+04]. The receiver was placed in the northern rooms, in the corridor and in the southern rooms. The angular spread at the indoor link was measured to be 30-55 degrees and at the outdoor link 4-20 degrees. When comparing the rms angular spreads at the receiver end (DOA), the transmitter position does not affect the rms spread or the mean angular spread. At the transmitter end (DOD) the transmitter position causes large differences in the rms spread.

[MHA+04] reports narrowband MIMO radio channel measurements in an urban macrocellular outdoor-to-indoor propagation scenario at 1947 MHz. The location of the measurements was Kista, a part of the city of Stockholm mostly containing office buildings with 5-8 storeys. The base station was placed at a large window at the 6th floor of an office building and the mobile was placed at different locations on different floors of another office building at 300 m distance of the base station. The angular spread was observed to be small due to lack of scattering (2-12 degrees).

In [WOT99] wideband measurements were carried out at 2.44 and 5.74 GHz in Oxford, UK for static outdoor-to-indoor scenario using dual channel vector network analyzer. The measurement bandwidth was 80 MHz. Measurement environments were categorized into urban, suburban and rural. The RMS azimuth spread for multipath arrivals was measured to be 89±21, 81±15 and 67±16 degrees for urban, suburban and rural environments respectively. After grouping the multipath arrivals into clusters, the RMS azimuth spread was 7.0±1.0, 8.8±1.9 and 8.4±1.5 for urban, suburban and rural environments respectively.

3.6.5.3 Intherpretation of B4 results

The measured RMS azimuth spread results are well in line with the existing literature results.

3.6.6 B4 Elevation AS at BS

Azimuth angle spread is calculated as described in [3GPPSCM] from DoA, DoD and path powers. In Figure 3-105, the cdf for elevation angle spread is shown.

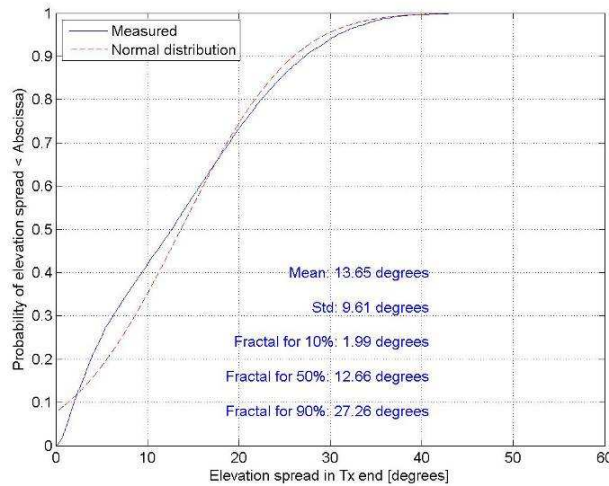


Figure 3-105: Cdf for elevation angle spread at Tx

3.6.7 B4 Cross-polarisation ratio

3.6.7.1 B4 Measurement results

The cross-polarization ratio (XPR) vertical (\downarrow) is defined as the ratio of power received from vertical to vertical polarization to the power received from vertical to horizontal polarization. Respectively, XPR_h is defined as the ratio between the powers of horizontal to horizontal and horizontal to vertical polarizations. In Table 3-37, XPR values averaged over all the routes are given in dB. PeakXPR denotes the peak path's XPR values, whereas scatXPR is the XPR values for the scattered multipaths (all except the peak path). The cdfs are plotted in Figure 3-106.

Table 3-37: Cross-polarization ratios averaged over all the routes.

Stat (dB) \ Terminal	Peak XPR_v	Peak XPR_h	Scat XPR_v	Scat XPR_h
Mean	3.99	9.54	-1.11	5.64
Std	11.21	11.31	8.87	8.76
10%	-10.73	-6.04	-11.84	-5.18
50%	4.14	11.23	-1.43	5.71
90%	17.96	22.38	10.11	16.24

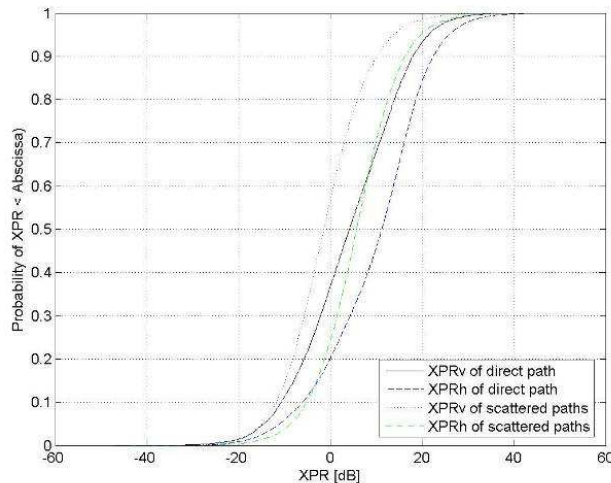


Figure 3-106: Cdfs for cross-polarizations ratios (XPR).

3.6.7.2 Interpretation of B4 results

The results are well in line with the results in [WIN1D54]. Furthermore, the results show that polarization change from horizontal to vertical involves more power loss than a change from vertical to horizontal.

3.6.8 B4 Power Delay Profile

3.6.8.1 B4 Measurement results

Power delay profile (PDP) is the distribution of the powers of the multipath components versus the delay. Typical PDP in an outdoor to indoor environment is shown in Figure 3-107. The PDPs are fitted to exponential function

$$PDP(t) = e^{-bt},$$

where t is the multipath delay and b is the time constant.

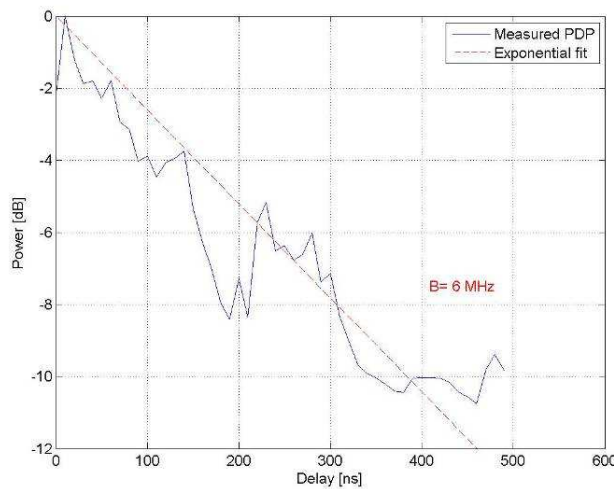


Figure 3-107: Typical power delay profile.

3.6.8.2 Interpretation of B4 results

Typical PDP curve is very reasonable. In indoor environment, the receiver is likely to receive multiple relatively strong multipaths.

3.6.9 B4 Proportionality factors, delay and angular

3.6.9.1 B4 Measurement results

The delay proportionality factor is defined as the ratio between the standard deviation of the delays of the multipath components and RMS delay spread. In Figure 3-108, the cdf of the measured delay proportionality factor averaged over all the routes is given. The mean value is 1.58 and the standard deviation (std) is 0.26. The red dashed line is the fitted normally distributed cdf with above mentioned mean and std values.

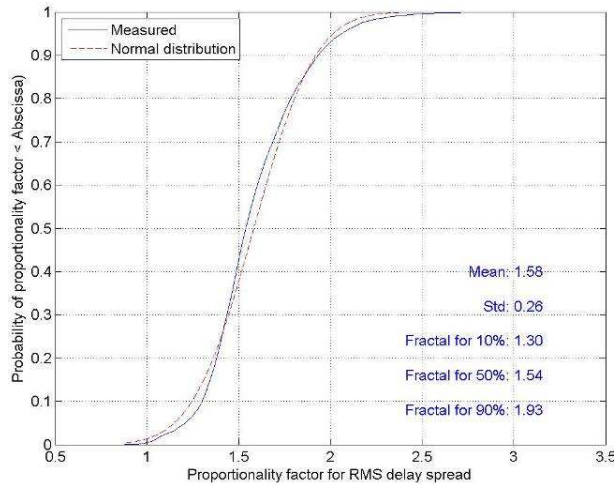


Figure 3-108: Cdf for RMS delay spread proportionality factor.

The angular proportionality factor is defined as the ratio between the standard deviation of the azimuth angles of the multipath components and the RMS angular spread. In Figure 3-109, the cdf of the measured azimuth angular proportionality factor averaged over all the routes is given for both terminals. The mean and the standard deviation (std) values are given in Table 3-38.

Table 3-38: Angular proportionality factor statistics for both terminals.

Stat \ Terminal	Tx (outdoor)	Rx (indoor)
Mean	1.20	1.73
Std	0.39	1.13
10%	0.78	1.09
50%	1.15	1.46
90%	1.67	2.57

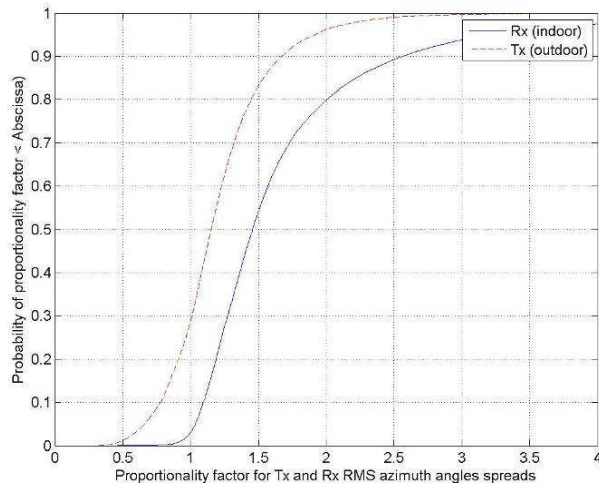


Figure 3-109: Cdf for RMS angular spread proportionality factor at Tx and Rx ends.

In Figure 3-110, the proportionality factor for elevation angle spread is shown for Tx end. The mean and std values are 1.16 and 0.4, respectively.

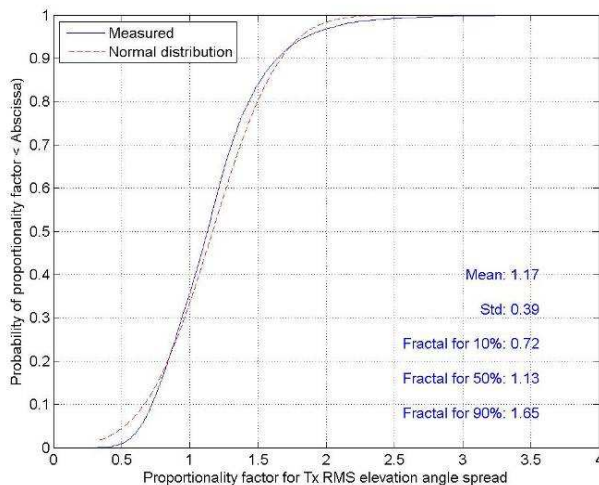


Figure 3-110: Proportionality factor for elevation angle spread at Tx.

3.6.9.2 Interpretation of B4 results

The measured delay proportionality values were well inline with the values presented for similar scenarios such as A1 in [WIN1D54].

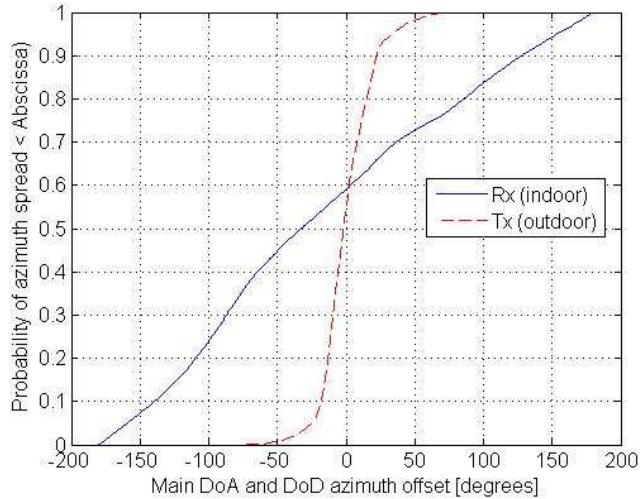
3.6.10 B4 Main DoA and DoD offset

3.6.10.1 B4 Measurement results

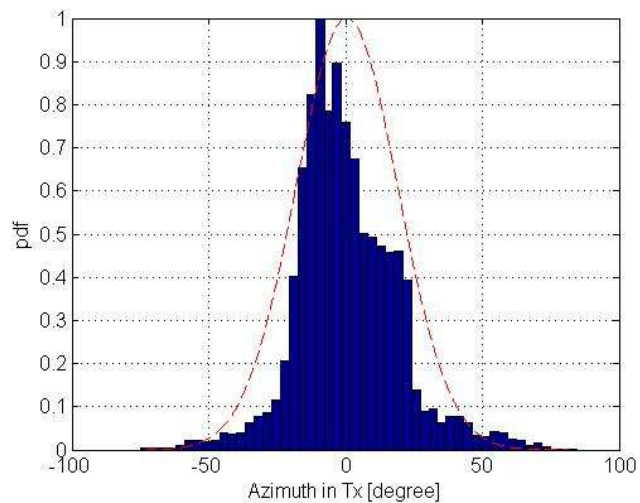
Main DoA and DoD angles are defined as the difference between the LoS direction and the mean angle of the angles of the effective multipaths. In outdoor case this difference is relatively small. However in indoor terminal, the values can vary significantly as shown in Table 3-39. The cdfs of main azimuth angle offset for both terminals are presented in Figure 3-111.

Table 3-39: Main azimuth angle direction offset compared to LoS path averaged over all routes.

Stat (degrees) \ Terminal	Tx (outdoor)	Rx (indoor)
Mean	0.5	-17.6
Std	18.7	97.9
10%	-18.2	-139.4
50%	-1.9	-32.5
90%	22.2	128.4

**Figure 3-111: Cdf for main DoA and DoD azimuth offset.**

In Figure 3-112, the pdf for the azimuth angles at Tx (outdoor) terminal is shown. The red dashed line is the normally distributed pdf fitted to the data. The corresponding figure for elevation angles is presented in Figure 3-113.

**Figure 3-112: Pdf for DoDs in azimuth domain for BS (outdoor).**

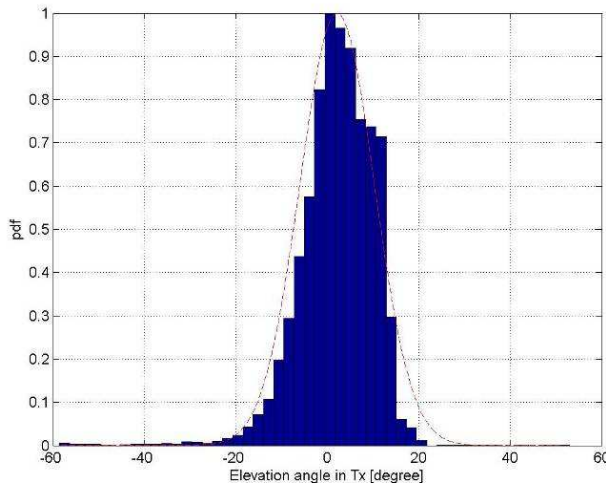


Figure 3-113: Pdf for DoDs in elevation domain for BS (outdoor)

3.6.10.2 Interpretation of B4 results

The fact that outdoor transmitter (BS) has significantly lower main angular offsets than the indoor MS is very reasonable. In indoor environment, the receiver is close to several walls and equipments that are likely to produce some reflections.

3.6.11 B4 Ricean K-factor

3.6.11.1 B4 Measurement results

Ricean K-factor is calculated as the narrowband K-factor. It can be used to describe the stability of the narrowband power as the Rx moves along the route. The observation interval was chosen to be 0.75 meter which corresponds to approximately 13 wavelengths. In Figure 3-114, the cdf for the averaged K-factor over all the analysis routes in the university of Oulu is shown together with its statistics and normally distributed cdf model. In addition, the K-factor (KF) formula was calculated to be $KF = 1.31 - 0.03 * d$, where d is the distance.

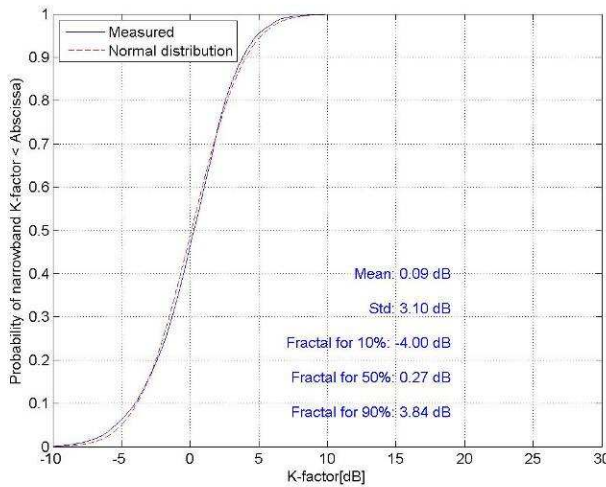


Figure 3-114: Cdf of K-factor.

In CRC measurements the equivalent CW envelope fading distributions were estimated, as outlined in [RJB89], from the variations in single spectral lines in measured channel transfer function time series from all measurement locations in the building. Figure below is an ECDF of the results.

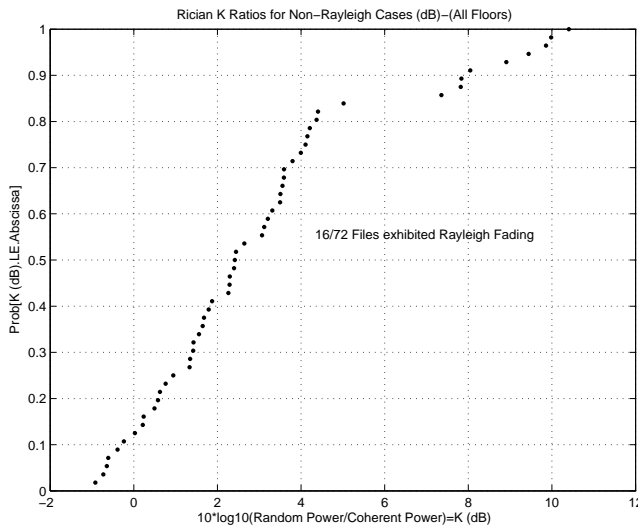


Figure 3-115: ECDFs for K ratios on Rician channels on all floors in the building.

The text in the figure explains that Rayleigh fading was exhibited in only 16 of the 72 measurement locations. Fading in the other locations exhibited Rician Characteristics, with K ratios that ranged from –1 dB to +11 dB. In the Rayleigh cases, coherence bandwidths would be approximately equal to the reciprocal of rms delay spreads. The minimum would therefore be about $1/(30 \text{ ns})$ or 33 MHz. Such bandwidths are already extremely large, but would be greater on the Rician channels [RJB02], where the reciprocal rms delay spread-coherence bandwidth relationship does not apply.

3.6.11.2 B4 Literature review

In [AHY06] the outdoor-to-indoor radio channel measurements were done at 5.25 GHz and 100 MHz bandwidth in the campus area of the university of Oulu, Finland. The transmitter was located outside a building at a height of 12 m and receiver was moving in a laboratory room on the first floor of the building at a height of 1.3 m. There were windows on the measurement route, which affected the results. The measurements showed that the distribution of the signal envelope follows Rayleigh distribution. The Ricean K-factor was not extracted, instead Nakagami distribution was used. The Nakagami m-factor was measured to be 2-3 for the strongest tap and 1-2 for the weaker paths in half of the cases.

In [WMA+05] radio channel measurements were done at 5.2 GHz and 120 MHz bandwidth in Lund University, Sweden. The transmitter was placed at three different locations on a roof top of a building. The receiver was placed in an office building 17 meters southwards from the transmitter either in rooms or in a corridor. The Ricean K factor and the LOS power factor measured in different locations are presented in following table [WMA+05].

Table 3-40: Comparison of LoS power factor and Ricean K-factor

Comparison of LOS power factor and Ricean K-factor.

Position	Rx elements	K_{LOS}	K_{rice}
Tx1 Rx2334ME	8-11	0.93	1.08
Tx1 Rx2334MM	8-11	2.47	4.28
Tx2 Rx2336NM	7-10	2.23	2.10
Tx2 Rx2336MW	8-11	5.74	4.16
Tx2 Rx2337ME	9-12	2.83	3.03

[NAP05] does not report values for Ricean K factor, but the magnitude distribution follows the Rayleigh distribution. The measurements were performed at 2140 MHz with chip rate 7.665 MHz. The receiver was placed in an office building and the transmitter outside the building at two different locations at height of 5.7 m for outdoor-to-indoor scenario.

In [CKC03] the transmitter was placed outside a building where the receiver was moving in the corridors on the first and second floors and the measurements were conducted at 2 GHz with the maximum RF output being +13 dBm. The maximum distance between the transmitter and the receiver was 15 meters. The Ricean K-factor was observed to be 21.3 and 18.7 for the first and second floors respectively.

Reference [SMJ+99] presents measurements at 2.44 GHz and 80 MHz span with 3 different transmitter sites and the receiver located in a room. The transmit power was 20 dBm and the measurements were conducted with dual channel VNA-based wideband channel measurement system. The Ricean K-factor was observed to have a very large variability on both channels.

3.6.11.3 Interpretation of B4 results

The measured K-factor values are well in range with the values encountered in literature review. However, in [AHY06] and in [WMA+05] the observed values are smaller. In our measurements, a transmit power of 26 dBm was applied, the height of the Tx was 6 meters and the distance between Tx and Rx was relatively short. In this light, the increase of the Ricean K-factor values compared to [AHY06] and in [WMA+05] is understandable.

3.6.12 B4 Cross-Correlations

3.6.12.1 B4 Measurement results

In Table 3-41, the cross-correlation coefficients for different parameters are given. Logarithmic RMS (LogRMS) delay spread versus shadow fading is shown in Figure 3-116.

Table 3-41: Cross-correlation coefficients between parameters

Parameters	Cross-correlation coefficient
AoD vs. SF	-0.35
AoA vs. SF	-0.22
AoD vs. RMS DS	0.31
AoA vs. RMS DS	0.06
AoA vs. AoD	-0.03
SF vs. logDS	0.34

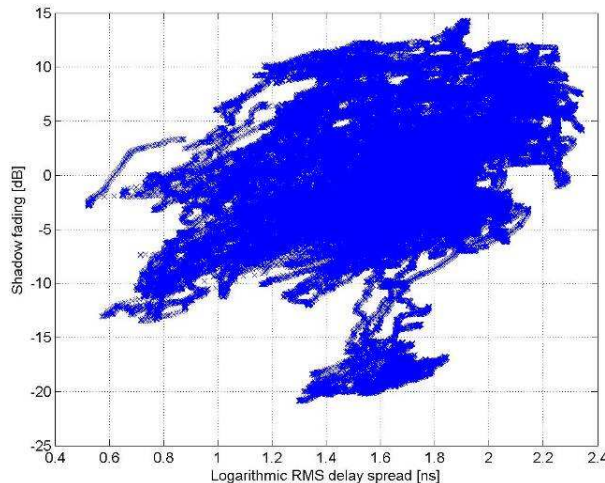


Figure 3-116: Correlation between logarithmic RMS delay spread and shadow fading.

3.6.12.2 Interpretation of B4 results

RMS delay spread is shown to increase as the shadow fading (SF) increases. Indoor MS correlations with delay spread (DS) or SF are low whereas outdoor (BS) correlations with DS and SF are higher. This can easily be explained with different environments.

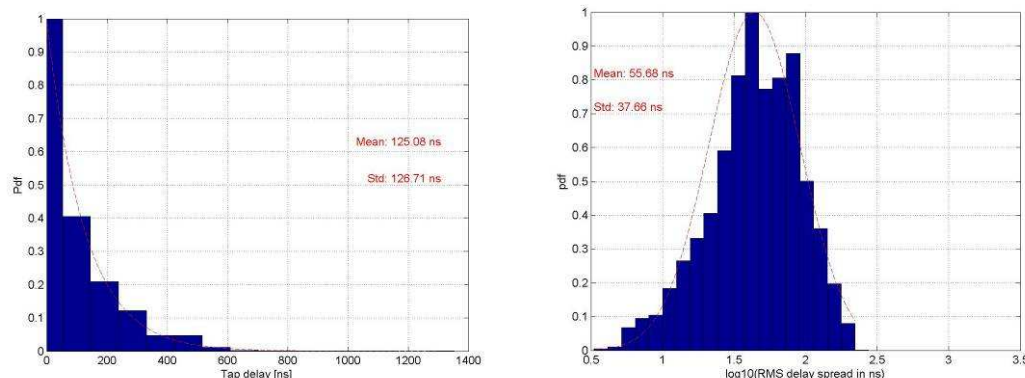
3.6.13 B4 Distributions

In Table 3-42, the distributions for the following parameters are given: maximum excess delay spread (delays), RMS delay spread (DS), angle of departure (AoD outdoor), angle of arrival (AoA indoor), azimuth spread at Tx (Tx AS), azimuth spread at Rx (Rx AS), shadow fading (SF) and K-factor (K).

The tested distributions were normal (N), log-normal (LN), 10*log-normal (10LN), exponential (Exp) and uniform (U) distribution. Probability density functions to verify these distributions are given in Figure 3-117. Some of these figures are shown already before but they are shown again here to make all the distributions easily available.

Table 3-42: Distributions among parameters

Parameter	Delays	DS	AoD (outdoor)	AoA (indoor)	Tx (outdoor) AS	Rx (indoor) AS	SF	K
Distribution	Exp	LN	N	U(-180,180)	LN	N	10 LN	10 LN



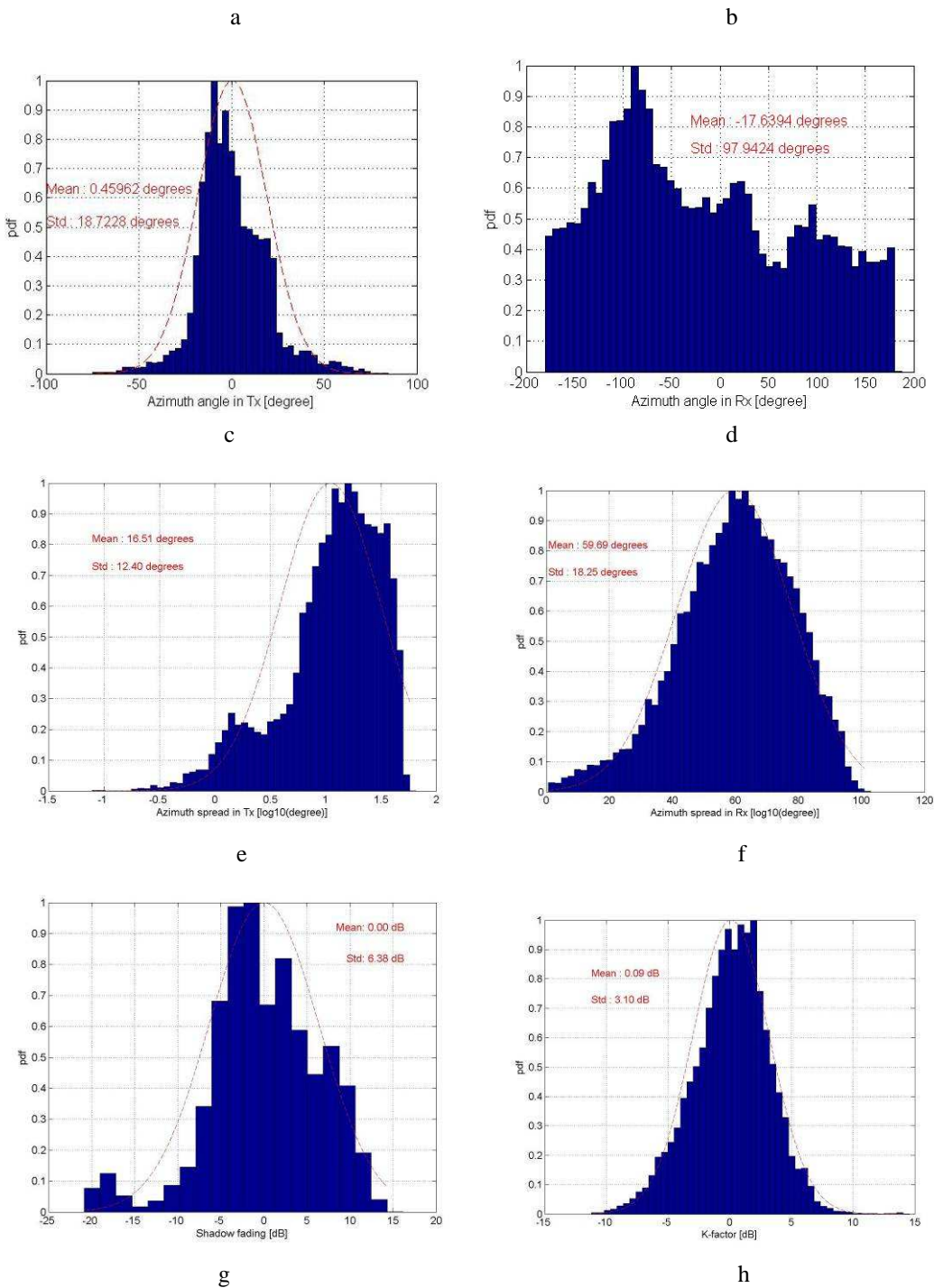


Figure 3-117: Distributions among the following parameters: a) maximum excess delay spread, b) RMS delay spread, c) AoD, d) AoA, e) Tx azimuth spread, f) Rx azimuth spread, g) shadow fading and h) Ricean K-factor.

3.6.14 B4 – Validation

3.6.14.1 Measurements at 3.7 GHz in Outdoor-to-Indoor B4 scenario

Measurements conducted at 3.7 GHz center frequency at the University of Oulu during summer 2007 were done partly in order to validate the results presented in this deliverable. The measurements were performed with dipole antennas and, hence, the results are limited to shadow fading and temporal domains. The measured routes were along the routes measured with 5.25 GHz. However, for the validation measurements only some of the routes were applied.

In Table Table 3-43, the parameters are compared in 5.25 and 3.7 GHz. The results show that the values obtained with both frequencies are quite similar. The largest difference is in shadow fading value where a 2 dB difference is obtained with 5.25 GHz. This is however, understandable since in larger frequencies, the scattering of the signal occurs more frequently and from smaller objects than in lower frequencies.

Table 3-43: Comparison of measured parameters with 3.7 and 5.25 GHz.

Parameter / Frequency [GHz]	3.7	5.25
Shadow fading [dB]	5	7
RMS delay spread [ns]	50	49
Number of clusters	16	16

3.7 B5 – Stationary feeder

3.7.1 B5 – Scenario definition

Fixed feeder links scenario is described in [WIN1D54] and defined as propagation scenario B5. This scenario has also been partly modelled in [WIN1D54]. In B5, both terminals are fixed. Based on this, the scenario was divided in four categories or sub-scenarios in [WIN1D54]. These are B5a (LOS stationary feeder: rooftop to rooftop), B5b (LOS stationary feeder: street level to street level), B5c (LOS stationary feeder: below rooftop to street level) and B5d (NLOS stationary feeder: rooftop to street level). Height of street level terminal antenna is assumed to be 3-5 meters. To cover the needs of CG WA one modified sub-scenario is needed in phase 2, scenario B5f: LOS/NLOS stationary feeder: rooftop-to-below/above rooftop. All the sub-scenarios will be described below.

In stationary scenarios, the Doppler shifts of the rays are not a function of the AoAs. Instead, they are obtained from the movement of the scatterers. In B5 we let one scatterer per cluster be in motion while the others are stationary. In [TPE02] a theoretical model is built where the change of phase of scattered waves between time t and $t+\Delta t$ is given by

$$4\pi \frac{f_c}{c} \Delta t \cos(\gamma_p) \cos(\alpha_p) \quad (3.39)$$

where α_p is the angle between the direction of scatterer movement and γ_p the direction orthogonal to the reflecting surface and γ the reflection angle. By proper selection of these angles different Doppler spectrums may be achieved. For B5d also an additional term in the path-loss model has to be included.

The feeder scenarios are specified here in connection of the micro-cellular environment. Actually the feeders can be used also in the macro-cellular cases. In this document it is assumed that the useful macro-cellular feeder link, C5, is identical with the feeder model B5c.

3.7.1.1 B5a

The signal in B5a can be assumed to consist of a strong LOS signal and single bounce reflection. Also far away reflections can occur. The connection is almost like in free space, so that the path-loss does not depend noticeably on the antenna heights. For this scenario fixed angle spread, delay spread and XPR values are applied. Directive antennas are very effective in reducing the delay spread and other multi-path impacts as explained in [PT00]. However, the model is applicable for omni-directional antennas for up to 300 meters in distance. By using directive antennas the range can be extended approximately to 8 km.

A static (non-fading) channel component is added to the impulse response. We select this parameter to be 10 dB. The power-delay profile (of all paths except the direct) is set as exponential, based on the results in [OBL+02] and [SCK05]. The shadow fading is Gaussian with mean zero and standard deviation of 3.4 dB based on [PT00]. B5a sub-scenario was specified and modelled in [WIN1D54]. The same channel model is used also in Phase II.

3.7.1.2 B5b

In B5b it is assumed that both the transmitter and receiver have many scatterers in their close vicinity similar as theorized in [Sva02]. In addition there can also be long echoes from the ends of the street. There is a LoS ray between the transmitter and receiver and when this path is strong, the contribution from all the scatters is small. However, beyond the breakpoint distance the scatterers start to play an important role.

In papers e.g. [Bul02], [SBA+02] the results for different carrier frequencies are very similar. Therefore, in B5b model the frequency is disregarded. The principle adopted for the WINNER phase 1 model allows for various correlations between different parameters such as angle-spread, shadow-fading and delay-spread. In this case, dependency between path loss and delay-spread [MKA02] is applied. This dependence is handled by selecting one of three different CDL models given in [WIN1D54]. Based on the delay-spread formula in [MAS02] we select the delay spread to be 30 ns when the path loss is less than 85 dB, 110 ns when the path loss is between 85 dB and 110 dB, and finally 380 ns when the path loss is greater than 110 dB. With these settings the delay-spread used here is a factor 40%-156% of the delay-spread formula of [MAS02] for path losses up to 137 dB. We call these path-loss intervals range1, range2 and range3 and different clustered-delay line models will be provided for the three cases.

In terms of path loss, the break point distance calculated as

$$r_b = 4 \frac{(h_b - h_0)(h_b - h_0)}{\lambda} \quad (3.40)$$

becomes important leading to so called two slope -model. The power delay profile (of all paths except the direct) is set as exponential, based on the results in [SMI+00]. A per-path shadow fading of 3 dB is used to obtain some variation in the impulse responses. A static (non-fading) channel component is added to the impulse response. Based on [FDS+94] we select this parameter to be 10 in range1, 2 in range2, and 1 in range3. Also K-factor changes according to range. B5b sub-scenario was specified and modelled in [WIN1D54]. The same channel model is used also in Phase II.

3.7.1.3 B5c and B5d

B5c and B5d can be considered as LOS of B1 and NLOS of C2 respectively. Only support for Doppler spectrum of stationary cases has to be introduced. B5c is probably the most important Feeder link scenario, because it will be used in urban micro-cell relay scenario. B5c is almost identical to the B1 micro-cellular LOS scenario. The only difference in environment is the assumed antenna height of the mobile/relay. Same channel model will cover both of the cases, except the difference in Doppler spectrum (mobility). Feeder link ends are stationary and the Doppler frequency results from motion of the environment. In B5c some clusters represent vehicles with speed of ~50 km/h and the rest of the clusters represent stationary objects like walls and building corners.

Actually B5d seems less useful for a Feeder link scenario. Therefore it is not discussed here further.

3.7.1.4 B5f

The sub-scenario is shown in the figure below.

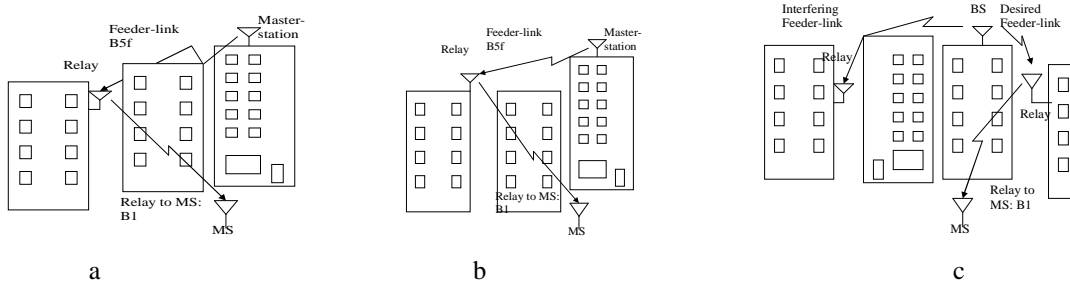


Figure 3-118 B5f scenario for three cases: a) NLOS (OLOS) b) LOS c) Combined interference case.

B5f scenario consists of the cases with relay antennas some meters over the roof-top or some meters below the roof-top. Key point is, if the link is LOS or NLOS: It is possible to create LOS links with the antennas below roof-tops. As well it is possible to implement NLOS links with antennas above the average roof-top level. Our approach is that the desired BS to FRS links can be planned to be LOS or

OLoS, or at least “good” links. It is assumed that the interfering links from undesired BS to FRS can be LOS or NLOS. (Although in practice this can be also affected by careful planning.) It should be pointed out that the link FRS to MS is covered by the model B1. Interference to undesired feeder link may occur.

In B5f it is assumed that the relay station is shadowed due to some obstacle. The proposed model is based on literature and formed from the B5a LOS fixed relay model by attenuating artificially its direct component by 15 dB in average and summing to it a normally distributed random decibel number with standard deviation 8 dB. The path loss formula is based on the references [ZEA99] and [GEA03]. The other model parameters are the same as in B5a. The model B5f can also be understood as NLOS part of the model B5a.

3.7.2 B5 – Path loss (D5.4)

3.7.2.1 Scenario B5a

We use the path-loss model of [PT00] as given below. We assume that it is applicable from 30 meters to 2km distance with a correction term for frequency, i.e.

$$\text{Loss} = 36.5 + 20\log_{10}(f_c / 2.5\text{GHz}) + 23.5\log_{10}(d) + \delta_{\text{slow}}, \quad 300 \text{ m} < d < 8 \text{ km} \quad (3.41)$$

We note that for the 30m to 300m range (for which [PT00] presents no measurements), the path-loss model almost coincides with cases in [Dug99] with the smallest path-loss. These cases are probably the ones with the least obstructed LOS. The model of [PT00] is for 2.5GHz. For other centre-frequencies, f_c , it seems reasonable to translate by using the free-space frequency dependence as the propagation scenario (e.g. path-loss exponent) is close to free-space propagation.

The shadow fading is Gaussian with mean zero and standard deviation $\sigma_{SF} = 3.4$ dB based on [PT00].

3.7.2.2 Scenario B5b

Based on the observation of numerous papers that the path loss follows approximately a free-space law before the breakpoint distance we will assume that loss is given by

$$\text{Loss}(r) = -20\log(\lambda/(4\pi r)) + \sigma_{\text{free}} + \delta_{\text{free}}, \quad r \leq r_b, \quad d < 1 \text{ km} \quad (3.42)$$

where the first part is recognized as the free-space path-loss, δ_{free} is a Gaussian distributed random variable (shadow fading), with standard deviation $\sigma_{\text{free}} = 3$ dB. This path-loss model (i.e., (4.10)) can be used for a maximum distance of 1 km. Many measurements seem to show path loss lower than the free-space before the breakpoint and indeed it can happen due to constructive multi-path. However, to avoid producing overly optimistic results the extra loss σ_{free} has been introduced such that the probability of a lower than free-space loss is only some 14%. The breakpoint distance is calculated as

$$r_b = 4 \frac{(h_b - h_0)(h_b - h_0)}{\lambda} \quad (3.43)$$

where we, somewhat pessimistically, set the effective ground level h_0 to 1.6 meter. For distances larger than r_b we set the path loss to

$$\text{Loss}(r) = \sigma_{\text{free}} - 20\log_{10}(\lambda/(4\pi r_b)) + 40\log(r/r_b) + \delta_{\text{beyond}}, \quad r > r_b, \quad (3.44)$$

where the first two terms correspond to the (mean) path-loss at r_b and δ_{beyond} is a Gaussian shadow-fading term with mean zero and standard deviation 7 dB.

3.7.3 B5 - Power-delay profile (D5.4)

3.7.3.1 Scenario B5a

The power-delay profile (of all paths except the direct) is set as exponential, based on the results in [OBL+02] and [SCK05].

3.7.3.2 Scenario B5b

The power-delay profile (of all paths except the direct) is set as exponential, based on the results in [SMI+00]. A per-path shadow fading of 3 dB is used to obtain some variation in the impulse responses.

3.7.4 B5 - Delay spread (D5.4)

3.7.4.1 Scenario B5a

The RMS-delay-spread is set to 40 ns, based on [PT00]. In order to have a valid model, it requires beamwidths comparable to those employed in [PT00].

3.7.4.2 Scenario B5b

Based on the delay-spread formula in [MAS02] i.e.

$$s[ns] = \exp(\beta PL_{dB}) \quad (3.45)$$

we select the delay spread to be 30 ns when the path loss is less than 85 dB, 110 ns when the path loss is between 85 dB and 110 dB, and finally 380 ns when the path loss is greater than 110 dB. With these settings the delay-spread used here is a factor 40%-156% of the delay-spread formula of [MAS02] for path losses up to 137 dB. We call these path-loss intervals range1, range2 and range3 and different clustered-delay line models will be provided for the three cases.

3.7.5 B5 - K-factor (D5.4)

3.7.5.1 Scenario B5a

A static (non-fading) channel component is added to the impulse response. We select this parameter to be 10 dB. This is based on the worst case (smallest value) in [SCK05]. In [OBL+02] a somewhat smaller average of 2.3 dB is seen but this is probably due to the LOS obstructions by trees.

3.7.5.2 Scenario B5b

A static (non-fading) channel component is added to the impulse response. Based on [FDS+94] we select this parameter to be 10 in range1, 2 in range2, and 1 in range3 (for a definition of the ranges see the section on delay-spread above.)

3.7.6 B5 - Cross-polarization ratio (D5.4)

3.7.6.1 Scenario B5a

The polarization scrambling (i.e. the power transfer between a transmitted vertically polarized to a received horizontally polarized antenna, and vice versa) is highly related to reflection on rough surfaces. This effect should be small in LOS scenarios. A high XPR means that there is little power transfer between the components. This means that we should be able to use the highest XPR values measured in [Dug99]. However, in order to avoid overly optimistic results we chose the mean value of [Dug99] i.e. 30dB.

3.7.6.2 Scenario B5b

Based on the results in [KVV05] we set the XPR to 9 dB.

3.7.7 B5 – Doppler (D5.4)

3.7.7.1 Scenario B5a

The Doppler is modelled by moving the scatterers appropriately. We chose the spectrum of [DGM+03] since it is assumed to be the most similar to the application here.

3.7.7.2 Scenario B5b

We propose the introduction of individual Doppler frequencies similar to the model in [TPE02]. We select the Doppler model [Erc01] which has somewhat larger Doppler spread than [DGM+03] probably due to the influence of traffic.

3.7.8 B5 - Angle-spread (D5.4)

3.7.8.1 Scenario B5a

Based on our visual inspection of the plots in [SCK05] we set the AoD and AoA of the non-direct paths to be Gaussian with composite power weighted angle-spread of 2 degrees. The ZDSC angle-spread is set to 0.5 degree.

3.7.8.2 Scenario B5b

Based on our visual inspection of the plots in [MIS01] we set the AoD of all the paths to be uniformly distributed between 0 and 360 degrees. The direct path is aligned with the geometrical angle between the transmitter and receiver. The intra-cluster angle-spread is set to 2 degrees.

3.7.9 B5 - Antenna gain (D5.4)

3.7.9.1 Scenario B5

The antenna pattern that can be used in the simulation is specified by

$$A(\gamma) = -\min \left[12 \left(\frac{\gamma}{\gamma_{3dB}} \right)^2, A_m \right], \text{ where } 180^\circ < \phi < -180^\circ \quad (3.46)$$

where γ is defined as the angle between the direction of interest and the boresight of the antenna. The γ_{3dB} is the 3 dB beamwidth in degrees (e.g., 35 degrees, and Am is the maximum attenuation (e.g., 23 dB). The gain can be selected as 17 dBi. However, other antenna patterns can also be used, if needed.

3.7.10 B5 – Literature review (D5.4)

Note also that for the feeder scenarios we do not have any data and therefore the modelling is based entirely on the literature study. Section 3.7.10.1 below addresses the Doppler spectrum for fixed applications, while Section 3.7.10.2 and 3.7.10.3 reviews publications on basic parameters for the “rooftop to rooftop” and “street level” to “street-level” scenarios.

3.7.10.1 Doppler for stationary scenarios

In common for the feeder scenarios studied here is the assumption that the position of the transmitter and receiver are fixed. In mobile-communications temporal variations are modelled by using a moving transmitter travel through an environment of fixed scatterers. In fixed applications the temporal variations are induced by the movements of the scatterers. In [TPE02] a theoretical model is built where the change of phase of scatter between time t and t+Δt is given by

$$4\pi \frac{f_c}{c} \Delta t \cos(\gamma_p) \cos(\varphi_p), \quad (3.47)$$

where φ_p is the angle between the direction of scatterer movement and the direction orthogonal to the reflecting surface and γ_p the reflection angle. By proper selection of these angles different Doppler spectrums may be achieved. The results in [DGM+03] show a very narrow spectrum of only some 0.07 Hz. In [Erc01] a much higher bandwidth of 5-6 Hz is proposed. We suspect that the higher bandwidth in [Erc01] is a worst case to account for influence from traffic.

3.7.10.2 Scenario B5a - rooftop-to-rooftop

The references [OBL+02], [PT00], [Dug99], [SDD00], [SCK05] treat scenarios similar to the described scenarios. In paper [OBL+02] a model based on measurements of rooftop-to-rooftop propagation in a residential scenario at 5 GHz is presented. The transmitter antenna is a dipole and the receiver omnidirectional. Distances in the range 30-330 meters have been considered and the LOS is sometimes obstructed by trees. A path-loss model (isotropic in dB) is derived from the measurements

$$\text{Loss} = 46.9 + 28 \log_{10}(d) + \delta_{slow}, \quad 30m < d < 330m \text{ (5GHz)}, \quad (3.48)$$

where d is the distance in meters and δ_{slow} is a shadow fading term with zero mean and standard deviation 7.26 dB. Delay spread figures are also presented in the paper. From a CDF graph presented in the paper the 20%, 50% and 80% levels of the delay-spread is read as 20, 45 and 75 ns, respectively. A tapped delay-line model is fitted to the data. Only the first tap of the tapped delay-line is Ricean (the others are Rayleigh). From the tapped delay-line a narrow-band K-factor of 1.7 can be derived. The tapped delay-line has a shape similar to an exponential decay.

The paper [PT00] presents results from path loss and delay-spread measurements at sub-urban sites at 2.5 GHz. The transmitter is mounted at 43 meter height while the receiver is at 5.2 m, 10.4 m or 16.5 m. The transmitter had a beam-width of 53 degrees and gain 11.5 dBi. Two different receiver antennas were employed one omni-directional with 9 dBi gain and one directional with 21 dBi gain and 10 degree beam-width. From a figure in the document the following path-loss model is obtained

$$Loss = 36.5 + 23.5\log 10(d) + \delta_{slow}, \quad 300m < d < 8km, (2.5GHz) \quad (3.49)$$

where the standard deviation of the shadowing in this case is only 3.4 dB. It is commented that path-loss results with different receiver heights are similar in LOS situations. Delay spread results are also reported. In particular the minimum, mean and maximum delay-spread in LOS cases is found to be 20 and 2390 ns, with the omni-directional antennas while the maximum is effectively reduced to only 40ns when the directional receive antennas is used. In [Dug99] and [SDD00] extensive measurements in urban areas at 5 GHz are presented. The results cover path loss, side-lobe level and cross-polarization isolation. No distinction between LOS and NLOS is made although it is evident from the path-loss results that some locations are in LOS. Three different transmitter sites are used with ninety receiver locations. Based on a viewgraph with path-loss results (with 16 meter receiver antenna height) we have derived the following path-loss model from the measurements in [Dug99]

$$Loss = -12.5 + 46.4\log 10(d) + \delta_{slow}, \quad 400\text{meter} < d < 2\text{km}, (5.2GHz) \quad (3.50)$$

where the standard deviation of δ_{slow} is 11.5 dB. Our interpretation of the steep slope and widely varying signal level is that it is due to a mixture of LOS and severely shadowed cases. Cross-polarization ratio (XPR) results presented in the paper ranges from 15 dB to 45 dB with a mean of 30 dB. In [SDD00], it is reported that for a receiver antenna with (relative) side-lobe level of 25 dB, the effective side-lobe level measured in field was 20dB. Path-loss models from all the papers above are shown in Figure 3-119.

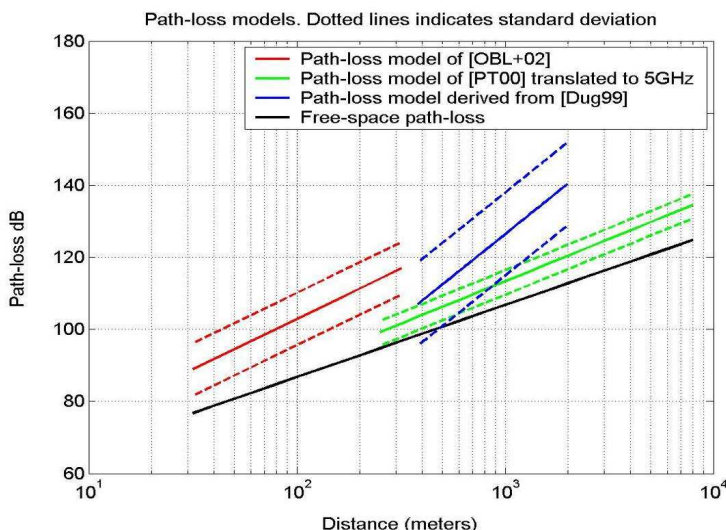


Figure 3-119: Comparison of the path-loss models of [OBL+02], [PT00], free-space and a path-loss model we obtain from the results in [Dug99].

In [SKE05], roof-top to roof-top MIMO measurements at 5.2 GHz are presented. Four different links with distances of 210, 55, 180, 116 meter have been measured all with clear LOS. Measurement results include Doppler, K-factor, delay-spread, power-delay-profile, frequency correlation and plots DoA/DoD super-resolution results from two out of the four links. Doppler spreads of around 1 Hz at the 10 dB level. This spectrum seems to be identical in the measurements for all delay components. The K-factors measured are in the range 9.6 to 17.5 dB. The measured power delay profiles seem to be similar to a direct component plus exponential decay with some randomization. Mean delay-spreads are in the range 6-30

ns. The super-resolution plots show many components but most of them are very weak. A reasonable guess using only the plots is a power-weighted RMS delay-spread of 2 degrees.

3.7.10.3 Scenario B5b - street-level-to-street-level

A classical two ray model with ground reflection results in a so-called breakpoint distance located at a distance r_b given by

$$r_b = 4 \frac{h_b h_m}{\lambda}, \quad (3.51)$$

where h_b and h_m are the heights of the two ends of the link, respectively. When the distance between the two antennas is smaller than r_b almost free-space path-loss is experienced. This has been observed in a number of studies [SBA+02], [OTH00], [SMI+00], [MKA02], [FBR+94] but due to reflections from cars and other objects during traffic the actual breakpoint occurs at

$$4 * (h_b - h_0) * (h_m - h_0) / \lambda \quad (3.52)$$

where h_0 is an effective ground height of typically 1.2-1.6 meters. At 5GHz we thus need 3.5 to 4 meter high antennas to achieve 380 meter free-space propagation.

In [SBA+02] and [Bul02] path loss and delay-spread measurements at 1.9 GHz and 5.8 GHz are performed in a scenario similar to what is considered here. The transmitter antenna is biconical and mounted six meters above ground in two different locations. The receiver antenna is omni-directional mounted on a minivan at 1.7 meters height and is mobile. The fading patterns at 1.9 GHz and 5.8 GHz are said to be "remarkably similar" although the measurements were not carried out simultaneously at the two frequencies. No obvious difference LOS and NLOS streets were found in teRMS of the difference in path loss between the two frequencies. The distribution of the difference between 1.9 GHz and 5.9 GHz path loss (in dB) is said to be modelled well by a Gaussian distribution with standard deviation 4 dB for both transmitter locations. The mean of the difference in one location was 12 dB and for the other 7 dB. In the paper the path-loss model of [SMI+00] is found to fit the 1.9 GHz measurements on LOS streets. This model is given by

$$PL_{LOS} = e^{-sr} \left(\frac{\lambda}{4\pi} \right)^2 \left| \frac{1}{r_t} e^{-jkr_t} + R \frac{1}{r_m} e^{-jkr_m} \right|^2 \quad (3.53)$$

where r_t is the line-of-sight path-length, R is the reflection coefficient of the road surface, and s is the visibility factor. The variable r_m is the distance via reflection which is described as

$$r_m = \sqrt{r^2 + ((h_b - h_0) + (h_m - h_0))^2} \quad (3.54)$$

where h_b and h_m are the base- and mobile-station heights and h_0 is an effective surface height which is different from zero due to reflections from cars and other obstacles. A best fit to the eighteen LOS streets was found to be $h_0 = 1.2m$ and $s = 0.001$. The RMS-error from this model in the eighteen LOS streets is listed in a table. We notice that the breakpoint distance which is based on the clearance of the first Fresnel zone with the parameters of the paper appears at such a short distance as 60 meters. The path-loss curve is similar to a fourth-order slope beyond the breakpoint. We calculate an average the RMS error to be 7.1 dB from this data. The RMS-delay spread is reported to be 15-20% lower at 5.9 GHz than at 1.9 GHz. From inspection of the plots in the paper it appears that for LOS cases the delay-spread is 100-150 ns quite independently of the frequency.

The paper [SMI+00] presents measurements with the transmitter at a height of 4 meters and the receiver at 2.7 meters in a Japanese residential area at 3.5 GHz. The height of the buildings is on average eight meters and is therefore higher than the antennas. If the ground level, h_0 , is set to zero then breakpoint distance appears at 678 meters. The measurements up to 460 meters confirmed that free-space propagation conditions existed. Delay-spreads never exceeded 200 ns for the LOS measurements. The plotted power-delay profiles for LOS case seemed to show approximately the form of an exponential decay plus a direct path.

The paper [MKA02] studies the impact of the traffic intensity in an urban area on the effective ground level. In the paper the base-station height is 4meters and the mobile-station height 1.6 meter or 2.7 meter. Measurements are done at 3.35, 8.45 and 15.75 GHz. The effective ground level is estimated to about 0.5

meter during night-time and 1.4meter during daytime. The paper also presents RMS-delay-spread values versus path loss during night-time. From these figures we deduce that it is less than 200 ns at midnight before the breakpoint distance. Beyond the breakpoint a 3.6 to 4.6 path-loss slope is observed. The standard deviation around the mean value seems to be about ± 5 dB before the breakpoint and ± 10 dB after the breakpoint. A formula for the delay-spread is fitted to the data as

$$s[ns] = \exp(\beta PL_{dB}), \quad (3.55)$$

where β is 0.050 during day-time and 0.049 during night time. The sample-points used for the fitting of this formula contain measurements at 3.35, 8.45 and 15.75 GHz. The paper does not state any variation with frequency.

In [FBR+94] micro-cell measurements at 1900 MHz are analyzed for path loss and delay-spread with an MS height of 1.7meter and base-station heights of 3.7, 8.5, and 13.3. A path-loss model is fitted where a free-space propagation law is used up to the breakpoint and a 3rd or 4th order law is recommended beyond that point, shadow fading estimates are in the range 7-8 dB. No effective street-level modelling is used – maybe measurements were done when there was no traffic? An exponential dependence between the path loss and delay-spread as in previous reference is also found – however this time the model considers the maximum delay-spread. A visual inspection of the viewgraph of the paper seems to confirm that typical delay-spreads obey the formula of [MKA02] given above.

In [FDS+94] measurements were done with the transmitter at 4meter height and the receiver on the top of a Van at 2.5 meters. The measurements were done on Southampton University Campus at 1.8 GHz. The results for LOS show a K-factor between 1 and 30 at range of up to the breakpoint. In contrast for the NLOS measurements the K-factor is between 0 and 2.

In [KVV05] polarization is analyzed in various urban scenarios. The one, most similar to what is considered here, is the urban micro-cell LOS case although the base-station is considerably more elevated than what we are considering here and the mobile-station is less (BS height 10 meters, MS height 1.6 meter in the measurements). For this scenario an XPR of around 9 dB is obtained.

In [MIS01] directional measurements in an urban area with rotating antennas at 8.45 GHz are presented. The base-station height is four or eight meters while the mobile-station height is 3.0 meters. The angle-spread of the main arriving wave is found to be less than 1.5 degrees in all LOS scenarios. The weaker paths in the paper seem to be virtually uniform distributed over the entire azimuth.

3.8 C1 – Suburban macro-cell

3.8.1.1 Scenario definition

In suburban macrocells base stations are located well above the rooftops to allow wide area coverage. Buildings are typically low residential or town houses with one or few floors. Occasional open areas such as parks or playgrounds between the houses make the environment rather open. Streets have random orientations, and no urban-like regular strict grid structure is observed. Vegetation is modest.

3.8.2 Measurements

Measurements for the suburban C1 LOS scenario were conducted at the centre-frequency 5.25 GHz. Measurements were performed in Heinäpää relatively near to Oulu centre in an area, where the houses are lower than in the centre of the town, with some parking lots, parks and trees along the streets in between the houses. The height of the houses varied typically from 3 to 6 stories. The Figure 3-120 shows the measurement environment in Heinäpää, Oulu, Finland. In the following subsection only path-loss for the C1 LOS is considered that is originally discussed in [WIN2D111]. All other channel parameters are discussed in the subsections labelled (D5.4) and come originally from [WIN1D54].

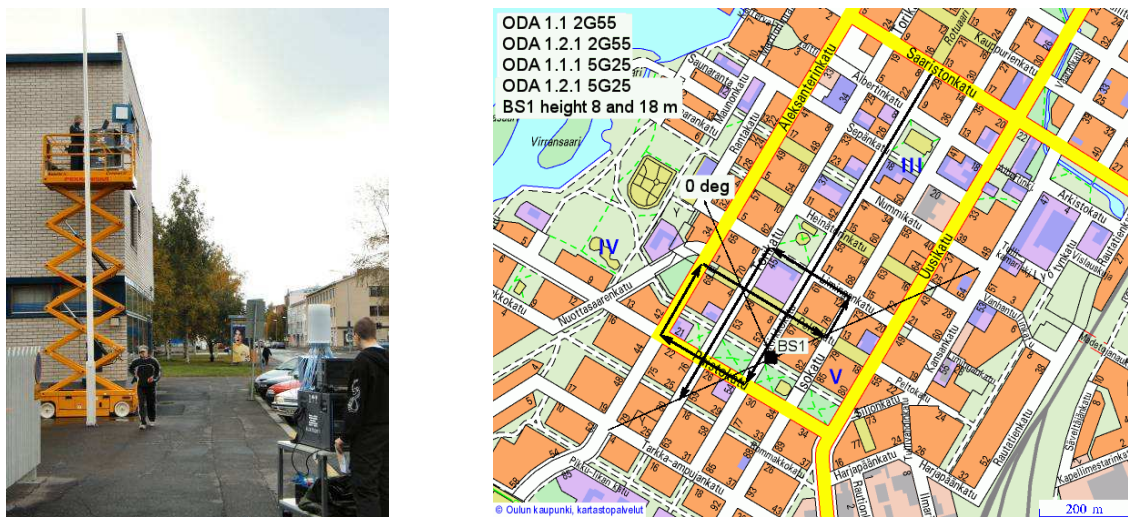


Figure 3-120 Measurement route for the moving MIMO measurement in BS location 1

WINNER measurements for C1 NLOS scenario were made at 5.3 GHz centre frequency and 100 MHz chip rate in a typical Finnish suburban residential area with rather wide streets [RJK05]. Buildings in the area are mainly one- or two-storey single or detached houses. There are open areas between the buildings, such as playgrounds, parks or small forest areas. BS height in the measurements was ~25 meters, which is well above the surrounding buildings, and at or above the height of the highest neighbouring trees. Only close to BS there were clear unobstructed LOS areas, and further away the MS-BS connection was obstructed mainly by trees. Deep NLOS conditions were achieved at long MS-BS distances. Maximum measured MS-BS distances were ~1100 meters.

The parameters proposed for C1 WINNER II model are not solely from those measurements, but also results from literature have been used for model parameter design.

3.8.3 C1 Path-loss and shadow fading

3.8.3.1 C1 Path loss and shadow fading (D1.1.1)

3.8.3.1.1 LOS case

In [WIN1D54] the LOS path-loss was given at 5.25 GHz as

$$PL(d) = 41.6 + 23.8 \log_{10}(d) \quad 20 \text{ m} < d \leq d_{BP} \quad (3.56)$$

$$= 41.6 + 40 \log_{10}(d / d_{BP}) + 23.8 \log_{10}(d_{BP}) \quad d_1 \geq d_{BP} \quad (3.57)$$

$$\sigma = 4.0 \text{ dB}, \quad 20 \text{ m} < d \leq d_{BP}; \quad \sigma = 6.0 \text{ dB}, \quad d > d_{BP}$$

Extended to 2 – 6 GHz the path-loss formula can be presented as follows:

$$PL(d,f) = 41.2 + 23.8 \log_{10}(d) + 20 \log_{10}(f[\text{GHz}]/5), \quad 20 \text{ m} < d \leq d_{BP} \quad (3.58)$$

$$PL(d,f) = 40.0 \log_{10}(d_1 [\text{m}]) + 11.65 - 16.2 \log_{10}(h_{BS} [\text{m}]) - 16.2 \log_{10}(h_{MS} [\text{m}]) + 3.8 \log_{10}(f[\text{GHz}]/5.0), \quad d > d_{BP} \quad (3.59)$$

$$\sigma = 4.0 \text{ dB}, \quad 20 \text{ m} < d \leq d_{BP}; \quad \sigma = 6.0 \text{ dB}, \quad d > d_{BP}$$

where d = distance

$$d_{BP} = 4 \cdot h_{BS} \cdot h_{MS} \cdot f_c / c$$

h_{BS} = the height of the base station

h_{MS} = the height of the mobile station

f = the centre-frequency (Hz)

c = the velocity of light in vacuum

σ = standard deviation.

The height gain factor in (15b) has to be restricted to values giving loss greater than equation (15a). In the formula it has been assumed that the effective antenna height is the real height, because in suburban areas it is assumed that the vehicle density is relatively small.

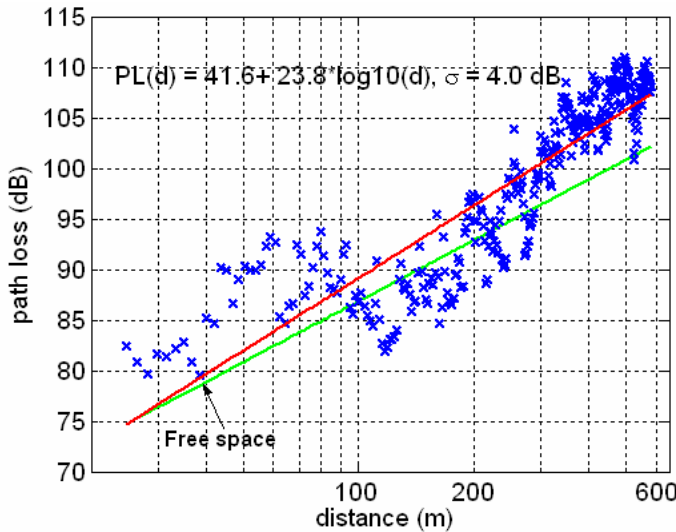


Figure 3-121: Path-loss in a suburban environment and LOS propagation conditions.

3.8.3.1.2 NLOS case

Propagation studies at 5 GHz frequency band in indoor domestic, office and commercial environments have been frequently reported, but wideband outdoor studies at 5 GHz are not as numerous. In [ZKV+02] results for urban, suburban and rural environments have been reported. In this case the maximum mobile (MS) to base station (BS) distances were limited up to 300 meters, which for outdoor cellular channel modelling is not fully representative. Path loss models around 5 GHz in residential areas and with BS heights less than 10 meters are reported in [SG00] and [DRX98].

More studies around 2 GHz frequency have been made. In [EGT+99] results for extensive macrocellular suburban measurements in US have been reported with BS antenna heights 12...79 meters. Maximum MS-BS distances up to 8 km were measured in variety of environments containing both hilly and flat terrains as well as light and moderate-to-heavy tree densities. Shadow fading standard deviation was found to be in range 5-16 dB, and path loss exponent was always found to be greater than two. Path loss exponent was found to have a strong dependency on the BS antenna height and the terrain type: the higher the BS antenna height the smaller the path loss exponent.

In [MRA93] and [MEJ91] radio propagation differences between 900 and 1800 MHz carrier frequencies have been compared in different environments. In both the studies it was found that path loss values at 900 and 1800 MHz were highly correlated, and there was no significant difference in distance dependent behaviour. Theoretical free space path loss difference between 900 and 1800 MHz is 6 dB, and in flat open areas a value very close to it, 5.7 dB, was obtained [MRA93]. In suburban areas, however, this difference was increased to 9.3 dB [MRA93], which was explained to be due to higher vegetation in suburban environments, which attenuate 1800 MHz signals more than 900 MHz signals. In [MRA93] PL differences between 900 and 1800 MHz frequencies were found to be 9...11 dB, i.e. higher than theoretical free space loss. In [MEJ91] shadow fading standard deviation was found to be approximately 1 dB higher at 1800 MHz, which agrees with results from Okumura [OOK+68].

Ref. [BBK+02] presents wideband channel measurements at 3.7 GHz and 20 MHz bandwidth in moderate density macrocellular suburban setting outside Illinois. Reported path loss exponents are between 2.9 and 3.4, and shadow fading standard deviations vary between 5-10 dB. Maximum measured MS-BS distances were ~ 6 km.

Effect of vegetation at 3.7 GHz has been studied in [BBK04], and it was shown that tree foliage creates an excess path loss of between 3 and 7 dB.

In Figure 3-122 suburban macrocellular path loss model and shadow fading distribution obtained from Helsinki 5.3 GHz measurements is shown. Two different BS sites, one of them with two sectors, were

chosen, so altogether data from three different BS sectors were collected for data analysis during different measurement runs. More detailed descriptions on measurements can be found in [RJK05]. The path loss model for suburban macrocellular environment obtained from WINNER measurements reads as

$$PL = 27.7 + 40.2 \log_{10}(d[m]) \quad (3.60)$$

The path loss exponent $n=4$ was obtained. Similar PL exponent values for flat macrocellular suburban environment with moderate or high tree density have reported in [EGT+99] around 2 GHz carrier frequency, and PL exponent values around 2.0-3.3 for LOS and 3.5-5.9 for NLOS can be found in [SG00], and [DRX98]. However, in some of these cases the BS height, which is known to have effect on the PL behaviour, is lower than in our measurements. In our WINNER measurement we found the shadow fading component is log-normally distributed with standard deviation of 6.1 dB.

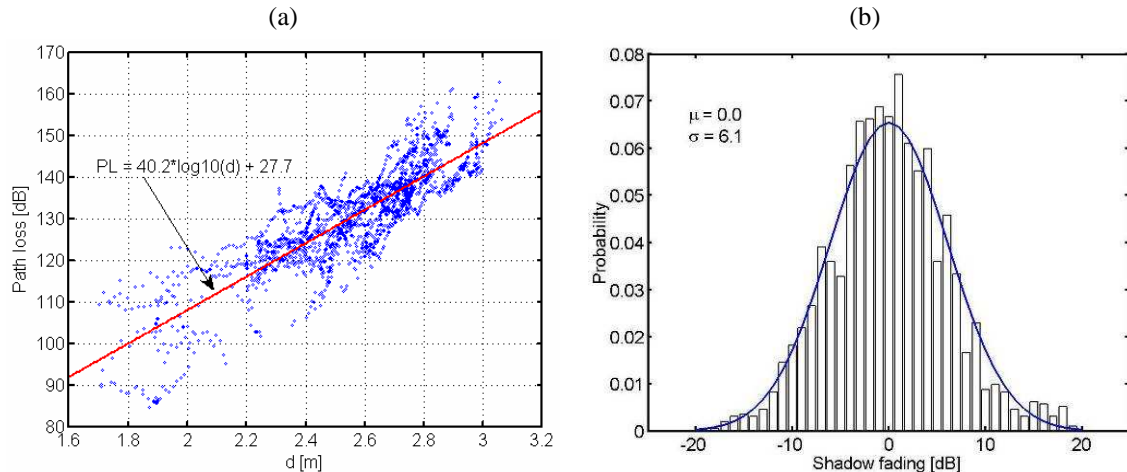


Figure 3-122: (a) Path loss model and (b) shadow fading distribution obtained from Helsinki 5.3 GHz suburban measurements.

COST231-Hata path loss model [COST231] for suburban macrocells is written as

$$PL = [44.9 - 6.55 \log_{10}(h_{BS})] \log_{10}(d / 1000) + 45.5 + (35.46 - 1.1h_{MS}) \log_{10}(f_c) - 13.82 \log_{10}(h_{BS}) + 0.7h_{MS} \quad (3.61)$$

In above all the distances and heights are given in meters, and carrier frequency f_c is given in MHz. With $h_{BS} = 20$ m, $h_{MS} = 2$ m (same as values used in Nokia suburban measurements), and $f_c = 2000$ MHz the model becomes

$$PL = 29.6 + 36.4 \log_{10}(d) \quad (3.62)$$

Path loss difference due to theoretical free space propagation is $20 * \log_{10}(5.3/2) = 8.5$ dB. If this is taken into account, the PL equation from Helsinki measurements shows a reasonable good match with COST231-Hata approach. If we assume the MS height fixed, $h_{MS} = 1.5$ m, we therefore propose the following frequency scaled COST231-Hata model for NLOS suburban macrocells

$$PL = [44.9 - 6.55 \log_{10}(h_{BS})] \log_{10}(d) + 23.46 + 5.83 \log_{10}(h_{BS}) + 20 \log_{10}(f[\text{GHz}]/2) \quad (3.63)$$

with $50m < d < 5km$ $h_{BS} > 15m$ $f_c = 2...6\text{GHz}$

3.8.4 C1 Delay Spread and Maximum Excess Delay Distribution

3.8.4.1 C1 Rms delay spread and maximum excess delay distributions (D1.1.1)

Delay spreads around 2 GHz carrier frequency and 5 MHz bandwidth have been reported in [APM02]. For suburban environment with BS height of 12 meters and no direct LOS between MS and BS reported delay spread values typically vary between 200...800 ns, the median being around 350 ns. Log-normal distribution was found to give a good fit to the measured delay spread distribution. In typical urban environments delay spreads were found to decrease with increasing BS antenna height.

In [WHL+93] rms delay spread distributions were compared in different environments at 900 MHz and 1900 MHz carrier frequencies. With both frequencies the used chip rate was 10 MHz, and data was recorded simultaneously with both the frequencies. It was seen that propagation behaviour in terms of

rms delay spread was very similar with both the carrier frequencies in semi rural, suburban and urban cells.

Delay spread characteristics for 3.7 GHz carrier frequency with 20 MHz bandwidth are given [KKM02]. Measurements were made in suburban areas outside Chicago, where also some distant high-rise buildings were in the environment. BS height was 49 meters, and MS was installed at 2.7 meters above the ground. 15 dB dynamics criterion from the max peak power was used in calculating delay spreads. Median delay spread values for LOS and NLOS propagation conditions were 240 and 360 ns, respectively. The combined delay spread was found to be 300 ns. As for number of rays, defined as local maxima of (instantaneous) power delay profiles, 90 percentile value of the cdf for LOS, NLOS and combined data were 3, 8 and 7 rays, respectively.

In our WINNER measurements typical delay spreads were of the order of 13...125 ns, which are considerably smaller values than reported by [APM02]. One reason for the difference is the higher BS antenna position. Rms delay spreads have often been reported to show log-normal distribution, as summarized for example in [GEY97]. Delay spread also depends on used bandwidth due to finite system impulse size. This is discussed in more detail in section 3.9.4.

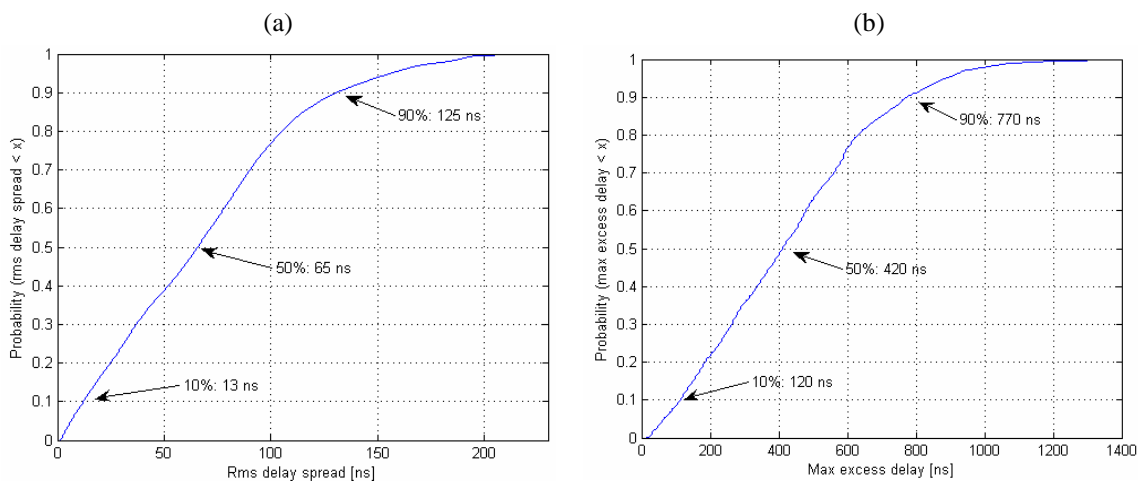


Figure 3-123: (a) Rms delay spread, and (b) maximum excess delay cdfs for Helsinki suburban macrocellular measurements at 5.3 GHz.

3.8.4.2 C1 rms delay spread and maximum excess-delay distribution (D5.4)

3.8.4.2.1 Measurements in LOS conditions

The distribution of the RMS-delay spread in C1 suburban scenario was investigated. The 10, 50 and 90 % values for the Cumulative Distribution Functions of the distribution of the RMS-delay spread are given below for the 5.25 GHz centre-frequency and LOS propagation conditions.

RDS (ns)	10%	50%	90%	mean
Suburban environment	9	59	175	84

Table 3.44: Percentiles of the RMS-delay spread in suburban environment.

3.8.5 C1 Azimuth AS at BS and MS (D1.1.1)

Azimuth spreads at BS have been given in [Paj03] for rural and suburban environments at 2 GHz carrier and 10 MHz bandwidth. The mean angular spread of 2 degrees was found, with standard deviation of 2 degrees. In urban areas they have been reported to be 14 degrees and 5 degrees, respectively. The difference between the geometrical direction of the mobile and the direction of maximum received power was modelled as Gaussian. The standard deviation is about 16 degrees near the base station and decreased to 8 degrees far away in urban environment. In rural and suburban is much smaller, 2.7 degrees when

distance is below 2 km and above this decrease to 1.7 degrees. Mobile azimuth spreads were reported as 35 degrees in suburban, and 20 degrees in rural environment.

3.8.6 C1 Modelling of PDP (D5.4)

Power delay profile at 100 MHz bandwidth and 5.25 GHz centre-frequency in a suburban environment is shown in the Figure 3-124 for LOS propagation conditions. The profile has been fitted to the exponential function

$$P(\tau) = e^{-b\tau} \quad (3.64)$$

where τ is the excess delay and b is a time constant. For the suburban LOS environment the constant b is 40 MHz.

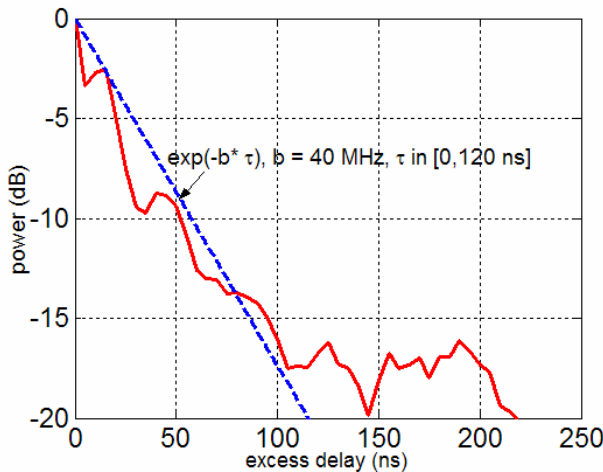


Figure 3-124: Power delay profile in the C1 (suburban) LOS environment with fitting to exponential model.

3.8.7 C1 Number of ZDSC (D5.4)

This sub-section presents number of clusters that has been extracted from measurements. The extracted clusters are based on definition that used in the channel model as clusters with zero delay spread. In other words, the considered clustering is in angle domain. These clusters are called zero-delay-spread clusters (ZDSC). Detailed discussion about ZDSC is given in Chapter 4.

The distribution of the number of clusters was investigated in a suburban C1 LOS environment. The results are shown in the Table 3.45 below as the 10, 50 and 90 % percentiles of the distribution.

Table 3.45: Percentiles of the CDF of the distribution of the number of clusters in a suburban (C1) LOS environment.

No. ZDSC	10%	50%	90%	mean
Suburban macro	3	8	22	8

3.8.8 C1 Distribution of ZDSC delays (D5.4)

The percentiles of the distribution of the path delays are shown in the Table 3.46.

Table 3.46: Percentiles of the distribution of the path delays in a suburban C1 LOS scenario.

Path delay (ns)	10%	50%	90%	mean
Suburban macro	9.0	175	1525	528

Also now the distribution of the path delays fits well with the exponential distribution.

3.8.9 C1 Delay proportionality factor (D5.4)

The delay proportionality factor (r_{DS}) is defined as the ratio between the standard deviation of the delays of the multipath components and RMS delay spread. The percentiles for the CDF of the delay proportionality factor are shown in the Table 3.47 below.

Table 3.47: The 10, 50 and 90 % percentiles for the cumulative distribution function of the delay proportionality factor in a rural environment.

Delay proportionality factor: r_τ		LOS	NLOS
Percentile	10%	2.0	1.2
	50%	3.8	1.7
	90%	8.5	2.9
	mean	4.7	1.9

3.8.10 C1 K-factor

3.8.10.1 C1 K-factor (New)

In [WIN1D54] and [WIN2D111] K-factor was given as a function of distance. Now we have increased the level of randomness in the model and will draw the K-factor randomly from the Lognormal distribution: see the following figure.

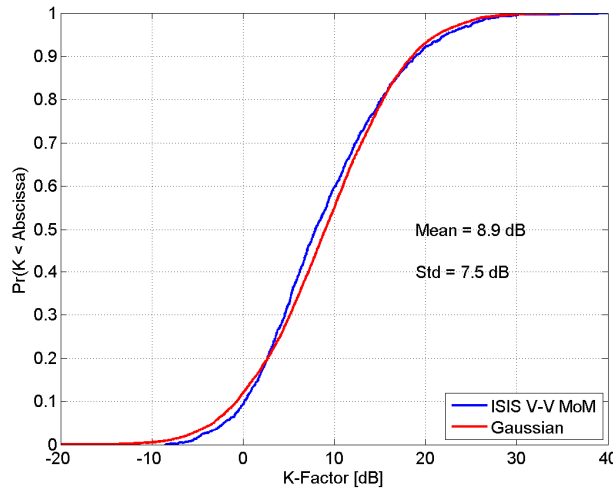


Figure 3-125 K-factor in dB. ISIS V-V MoM means the data is the super-resolution data from vertical polarisation and the method of K-factor calculation is the Greenstein's Moments Method.

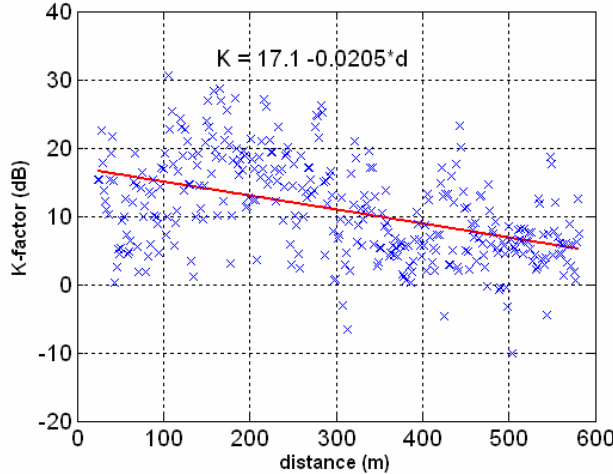
3.8.10.2 C1 K-factor (D5.4)

Narrowband Ricean K factor in the LOS regions has been analysed. Ricean K-factor is the ratio of power of the direct LOS component to the total power of the diffused non-line-of-sight components. The CDF percentiles of the K-factor in a suburban LOS environment are given in the Table 3.48.

Table 3.48: Percentiles of the CDF of the Ricean K-factor in a C1 LOS environment.

Percentile	10%	50%	90%	mean
K-factor (dB)	2.6	10.0	20.7	10.9

The Ricean K-factor as a function of distance in a suburban LOS environment is shown in the Figure 3-126.

**Figure 3-126: Ricean K-factor as function of distance in a suburban environment.**

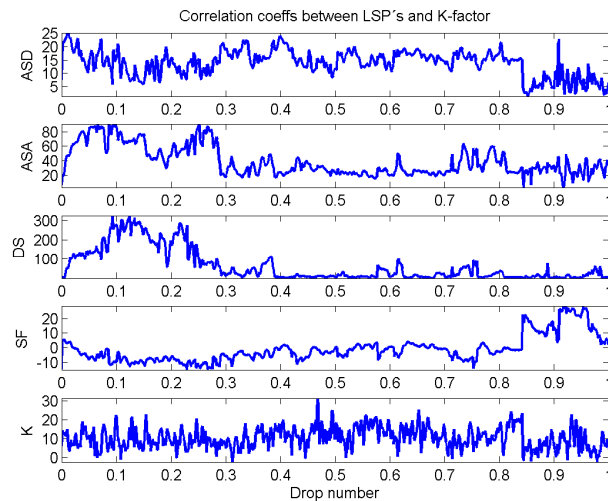
The equation for the K-factor can be expressed as

$$K = 17.1 - 0.0205 d, \quad (3.65)$$

where d is the distance between the BS and the MS.

3.8.11 C1 Cross Correlations

In [WIN1D54] and [WIN2D111] cross-correlation was analysed between the large scale parameters except the K-factor. However, since we have one K-factor value for each stationarity interval we can calculate the cross-correlation between the K-factor and e.g. delay spread also. Figure 3-127 depicts the correlation as a function of drop number.

**Figure 3-127 Correlation between the LSP's and K-factor.**

3.8.12 C1 Cross-polarization ratio (D5.4)

The cross-polarization ratio XPR_V is defined as the ratio of power received from vertical to vertical polarization to the power received from vertical to horizontal polarization as

$$XPR_V = \frac{P_{VV}}{P_{VH}} \quad XPR_H = \frac{P_{HH}}{P_{HV}} \quad \text{and} \quad (3.66)$$

Respectively, XPR_H is defined as the power ratio between HH and HV components. The XPR values are extracted from the estimated propagation paths using the strongest path (LOS) and the reflected paths (scattering).

3.8.12.1 LOS propagation conditions

The CDF of the XPR values at 100 MHz bandwidth and 5.25 GHz centre-frequency in a suburban environment is shown in the Figure 3-128.

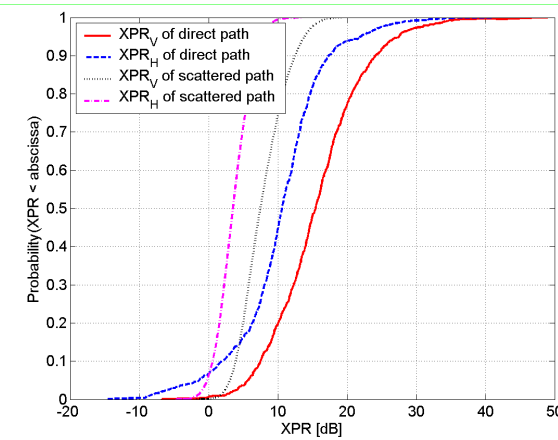


Figure 3-128: CDF's of the XPR_V and XPR_H for 5.25 GHz in suburban environment.

3.9 C2 – Urban macro-cell

3.9.1 C2 – Scenario definition

In typical urban macro-cell mobile station is located outdoors at street level and fixed base station clearly above surrounding building heights. As for propagation conditions, non- or obstructed line-of-sight is a common case, since street level is often reached by a single diffraction over the rooftop. The building blocks can form either a regular Manhattan type of grid, or have more irregular locations. Typical building heights in urban environments are over four floors. Buildings height and density in typical urban macro-cell are mostly homogenous.

3.9.2 Measurements

Measurements for C2 scenario were made at 5.3 GHz carrier frequency and 100 MHz chip rate in Helsinki city center. The parameters proposed for C2 WINNER II model are not solely from those measurements, but also results from literature have been used for model parameter design.

Measurements for LoS C2 scenario have been conducted in Oulu. The measurements were relatively limited and, therefore, the model for C2 LoS is derived as a combination from literature and measurements.

The parameters, that were not found from the literature nor were there measurements done that could have been analysed to obtain the missing parameters, were derived from other measurements conducted in similar environments such as urban micro scenario B1 and suburban macro scenario C1.

3.9.3 C2 Path-loss and shadow fading

The few reported outdoor PL measurements around 5 GHz frequency range show that typical PL exponents in urban LOS areas are close to free space propagation exponent 2, and for NLOS the reported values vary between 3.5 and 5.8 [YMI+04][ZKV+02][Pap05]. In these cases the maximum MS-BS distances have been < 1000 meters.

Path losses and delay spreads between 430 and 5750 MHz frequencies have been compared in [Pap05]. Data was collected simultaneously at the same measurement points in multiple environments, and the chip rate at each carrier frequency was 100 MHz. Measurements were made in urban environment in Denver, which covered a combination of urban high-rise, urban low-rise and line-of sight propagation paths. BS was installed on top of a five floor building at 17 meters, and maximum measured distances in the case were up to 5 kilometers. It was observed that in line-of sight conditions close to the BS (100...300 meters) the path loss exponent was close to 2. In regions where radio paths become obstructed the path loss exponents were increasing, and they also showed frequency dependency: path loss exponent increased from 4.3 to 5.4 between 430 and 5750 MHz. The shadow fading was normally distributed, and ranged between 3 and 6 dB.

In [MRA93] and [MEJ91] radio propagation differences between 900 and 1800 MHz carrier frequencies have been compared in different environments. In both the studies it was found that path loss values at 900 and 1800 MHz were highly correlated, and there was no significant difference in distance dependent behaviour.

Path loss and delay spread results from Japanese urban metropolitan environment at 3 GHz, 8 GHz and 15 GHz frequencies are reported in [OTT+01]. The average building heights in were 20...30 meters, and BS height both clearly above (macrocell) and at rooftop level (microcell) were measured. In the measurements power delay profiles were recorded simultaneously for each of the three frequencies. Shadow fading standard deviations did not show considerable differences between frequencies, but values in the range 5...10 dB were obtained. Path loss frequency dependency was found to directly follow free space characteristics, i.e. $20\log_{10}(f)$. Path loss exponents were not reported.

WINNER deliverable D5.4 from phase I gives path loss models for different scenarios at 5 GHz carrier frequency for selected (fixed) base station heights. Model extensions are needed to upgrade the models for wider range of bandwidths 2-6 GHz and different BS heights. Since limited set of measurements are available in WINNER for model extensions, results found in literature has been used as a basis for the work.

In [RJK07] measurements were carried out in Helsinki city center at 5.3 GHz and 100 MHz chip rate. Three different BS sites were used, Kampintori, Dianapuisto and Bulevardi. BS height was slightly above rooftop level and most MS measurement sites were in NLOS, but some LOS cases were also included. The transmitting antenna was placed on top of a van at 2 metres. The path loss exponent for the three sites was observed to be 4.9. If the LOS and OLOS sections were excluded, the path loss exponent would be 3.7. Shadow fading was observed to be normally distributed with standard deviation of 9.3 dB.

[YMI+04] reports measurements conducted at 4.95 GHz frequency and 80 MHz bandwidth with 40 dBm transmitting power in Iwaki-city, Fukushima Prefecture, Japan. The measurement environment consisted of 2-3 floor buildings (average height 7.14 m) with some over 10-floor buildings in the measurement area also. The transmitting antenna was placed on a roof of a vehicle at 2.5 metres. The receiver was on a rooftop of a 7-floor building at 40 metres height. Propagation conditions were both LOS and NLOS. In the LOS environment, the path loss characteristics were reported to be close to those of the free-space path loss. The propagation constant was observed to be around 3.6 in a NLOS situation. Figure 3-129 shows the average path loss against the distance between the BS and MS.

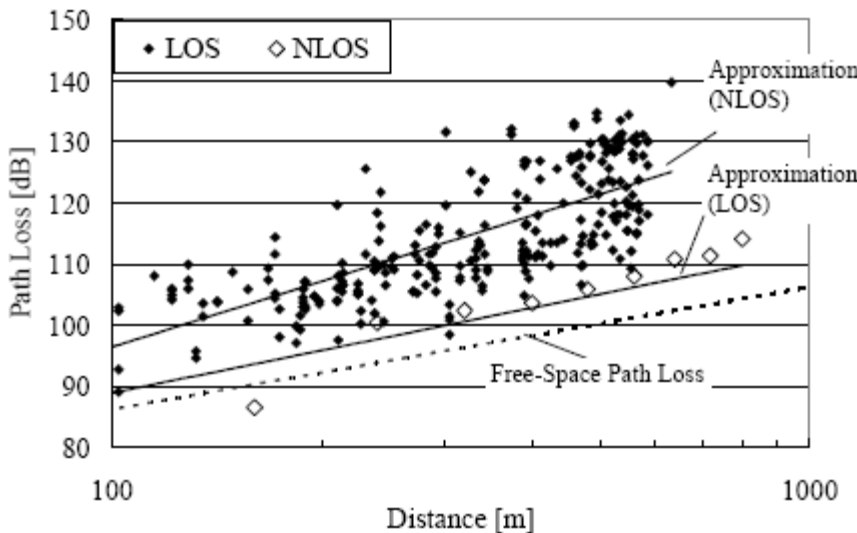


Figure 3-129: Path loss characteristics against distance. [YMI+04]

The measurement results were compared with the existing propagation models with the extension of the applicable frequency range of the original models to 5 GHz. Approximately 3.5 dB difference in terms of the median path loss was observed between the measured path loss and the estimated loss by the Walfisch model. Also the propagation constant from the measurements was mentioned to be close to that of the Walfisch model.

In [FBK+02] measurements were performed at 1.9 GHz and 2.1 GHz with 20 MHz bandwidth in Bristol, UK. Two kinds of measurement were performed, static and dynamic. The receiving antenna was at 30 metres height with down-tilt of 4°. The path loss exponent was measured to be 3.28 for the 1.9 GHz frequency and 3.21 for the 2.1 GHz frequency.

[Mar98] reports measurements performed in Frankfurt, Germany, at 1.9 GHz center frequency and 6 MHz bandwidth. The base station was located at a rooftop about 70 metres above the ground. The measurement environment was densely built-up business area with large number of skyscrapers. The transmitter was placed at different fixed positions. It was observed that the path loss slope was 37.2 dB per decade. The standard deviation of the log-normal fading was 7.2 dB. It was noted that the 38 dB per decade path loss slope of the COST 231 Walfish-Ikegami model, which is valid for urban NLOS conditions, was approximately verified by the results of the measurement campaign.

In [APM02] measurements were conducted at 1.8 GHz in Aarhus, Denmark and Stockholm, Sweden. In both measurement locations surrounding buildings were 4-6 floors high, there was NLOS between the BS and MS and the propagation scenario was classified as typical urban (TU). In Aarhus the BS antenna heights were 20 metres and 32 metres (TU20 and TU32, respectively) and in Stockholm the BS antenna height was 21 metres (TU21).

The standard deviation of the shadow fading was found to be 7.3 dB, 8.5 dB and 7.9 dB for TU32, TU21 and TU20, respectively.

In [OTT+01] the authors have conducted path loss measurements in the 457.2 MHz, 813 MHz, 2.2 GHz, 8.45 GHz and 15.45 GHz bands in both macrocell and microcell environments in different urban areas in Tokyo, Japan. The base station locations were classified into high-tier and low-tier, depending on the antenna height. High-tier locations can be considered as macrocell since the antenna height was higher than the average height of the surrounding buildings. In Table 3-49 are presented the standard deviations for slow fading for each measurement in the high-tier far- and near-areas.

Table 3-49: Standard deviations for slow fading for each measurement in the high-tier far- and near-areas [OTT+01]

High-tier far-area ($R > 1$ km)

Area	457.2 MHz	813 MHz	2.2 GHz	4.7 GHz	8.45 GHz	15.45 GHz
Nakano	7.47		7.61	7.67		7.25
Ikebukuro	5.30		5.52		6.17	6.08
Honjo	4.85	7.37	6.58		6.32	4.32
Nippori	5.36		6.35		5.95	6.58

High-tier near-area ($R < 1$ km)

Area	457.2 MHz	813 MHz	2.2 GHz	4.7 GHz	8.45 GHz	15.45 GHz
Ikebukuro	8.62		7.29		7.98	7.45
Honjo	6.34	5.10	5.59		5.48	5.20
Nippori	6.89		7.56		7.21	6.82

3.9.3.1 Extension to different BS heights and frequency range

There are studies and channel models which address the changes in path loss due to BS height variations [KI04][COST231][EGT+99]. COST231-Hata model [COST231] for urban (metropolitan) macrocells reads as

$$PL = [44.9 - 6.55 \log_{10}(h_{BS})] \log_{10}(d / 1000) + 48.5 + (35.46 - 1.1h_{MS}) \log_{10}(f_c) - 13.82 \log_{10}(h_{BS}) + 0.7h_{MS} \quad (3.67)$$

Increasing the BS height has therefore a twofold effect: the propagation exponent decreases, and there the constant intercept¹ changes due the BS height variation.

Similar dependencies are found in [KI04], which gives a PL formula for distances 100-1000 m, frequencies 0.4-8 GHz and BS antenna heights 30-120 m in urban areas in Japan (“Kitao”):

$$PL = [80.2 - 21.5 \log_{10}(h_{BS})] \log_{10}(d) - 27.9 \log_{10}(h_{BS}) + 20.4 \log_{10}(f) + 50.2 \quad (3.68)$$

In [EGT+99] the path loss model for suburban macrocells is expressed as (“Ergec”)

$$PL = A + 10\gamma \log_{10}(d / d_0) + s \quad (3.69)$$

A is a constant intercept value by a free space propagation at 100 m reference distance, and s is shadow fading component. The propagation exponent γ is a Gaussian random variable, which is written as

$$\gamma = (a - bh_{BS} + c / h_{BS}) + x\sigma_\gamma, \quad 10m \geq h_{BS} \geq 80m \quad (3.70)$$

In above the term in parenthesis is the mean of γ , x is a zero-mean Gaussian variable and σ_γ is the std of γ . Constants a, b, c and σ_γ are derived from data. For flat environment with light tree density the parameters for mean propagation exponent are $a=3.6$, $b=0.0050$ and $c = 20.0$.

Figure 3-130 shows the propagation exponent as a function of BS height from different models and publications [KI04][COST231][EGT+99]. Circles refer to unpublished 5.3 GHz measurements made by Nokia in Helsinki. In those measurements path loss was measured from one BS site in Helsinki city center with different BS heights (below, at and above rooftops, i.e. 18 m, 28 m and 38 m, respectively). Results by Kitao are from Tokyo, which probably is a considerably different environment from others (at least building heights). The other two lines and the Nokia measurements match well with each other.

¹ If PL model is written in form $PL = A + 10n \log_{10}(d)$, A is the intercept and n propagation exponent.

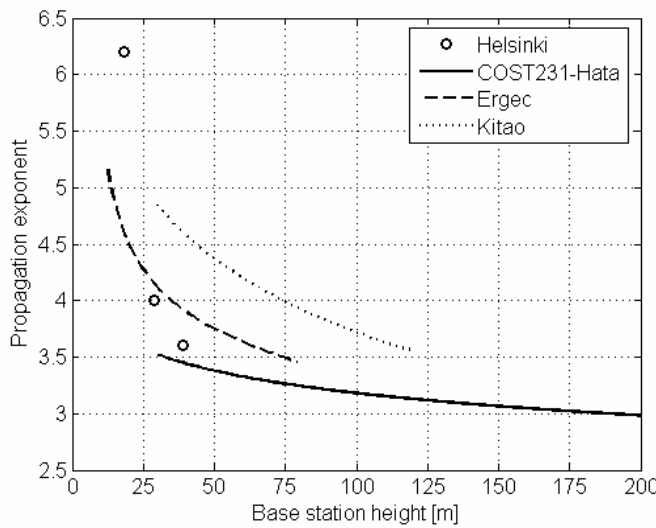


Figure 3-130: Propagation exponent as a function of BS height.

For WINNER macrocellular models we can assume that typical building heights in middle-size cities are ~30 meters, and the BS height scaling is then valid for BS heights above 30 m. For propagation exponent variation due to BS height the following scaling is proposed (directly from COST231-Hata model):

$$B = 44.9 - 6.55 \log_{10}(h_{BS}) \quad (3.71)$$

Both COST231-Hata and Kitao models propose also a constant shift in intercept due to BS height variations. With $h_{MS} = 1.5\text{m}$ and $f_c=2000\text{ MHz}$ the COST231-Hata model can be rewritten as

$$PL = [44.9 - 6.55 \log_{10}(h_{BS})] \log_{10}(d) + 26.46 + 5.83 \log_{10}(h_{BS}) \quad (3.72)$$

It is seen that the effect on intercept (last term in equation above) is fairly small, for example with BS height differences of 35 and 70 m it is only 1.7 dB.

According to results in [KI04][OTT+01][SMI+02] we adopt frequency scaling as $20\log_{10}(f)$ in range 0.5-15 GHz.

3.9.3.2 Path loss model for WINNER II

As a summary, path loss model for urban NLOS macrocells (C2) reads as

$$PL = [44.9 - 6.55 \log_{10}(h_{BS})] \log_{10}(d) + 26.46 + 5.83 \log_{10}(h_{BS}) + 20 \log_{10}(f[\text{GHz}]/2) \quad (3.73)$$

with $50\text{m} < d < 5\text{km}$ $h_{BS} > 30\text{m}$ $f_c = 2\ldots6\text{GHz}$

Path loss model for LoS scenario is determined mostly from literature and is given as

$$PL = 56.6 + 26 * \log_{10}(d[\text{km}]) + 20 * \log_{10}(f[\text{GHz}]/5), \quad (3.37)$$

which is known as the COST-Walfisch-Ikegami-Model. However, the original COST-Walfisch-Ikegami-Model has been adapted to higher frequency range.

3.9.4 C2 LOS probability

The existence of LOS/NLOS propagation conditions is selected randomly based on the following expression for LOS probability:

$$P_{LOS}(d) = \min(18/d, 1) \cdot [1 - \exp(-d/63)] + \exp(-d/63)$$

where d denotes horizontal distance between the BS and MS antennas. A plot of this expression is provided in Figure 3-240.

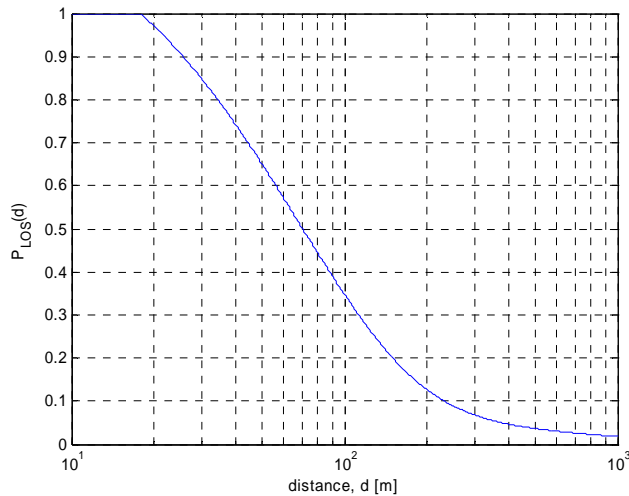


Figure 3-131: C2 LOS probability as a function of distance.

The above expression is based on the LOS probability model discussed in more detail in Section 3.4.5 based on [Jon07], with h_{BS} and h_{MS} set to 25 and 1.5 m, respectively, and the average rooftop level, h_{RT} , set to 15 m. All other parameters were chosen identical to those selected for the B1 scenario.

3.9.5 C2 Rms delay spread and maximum excess delay distributions

Papers [APM02] and [PMF00] report measurements made at 1.8 GHz carrier frequency and 4 MHz chip rate in Aarhus and Stockholm. Aarhus is a typical urban environment characterized by buildings from four to six floors and in irregular street grid. In Aarhus the measurements were done at two different BS heights, 20 and 32 m, the lower height corresponding to the average rooftop level of the surrounding buildings. In Stockholm buildings also had from four to six floors, and the BS antennas was mounted at 21 meters, which also corresponds to rooftop level. In Stockholm two sectors were measured: one classified as typical and the other as bad urban. The bad urban scenario corresponds to an area which is a mixture of densely built-up zone and an open flat area due to a river. Median reported rms delay spread values were 400 and 800 ns for Aarhus high and low antenna positions, and 1.3 μ s for Stockholm. The fairly high value for Stockholm probably also includes data from the bad urban sector over the river.

Paper [RWH02] reports measurements made in Helsinki at 2.1 GHz and 5 MHz chip rate. The environment is a typical urban macrocell with flat terrain and typical building heights between 4-6 floors. Base station is located on top of a 30 m high building at ~32 meters. This is slightly above the average surrounding rooftop height. The median reported rms delay spread values were ~500 ns.

In [Pap05] measurements were made simultaneously on four different carrier frequencies between 430 and 5750 MHz. A chip rate of 10 MHz was used. Measurements were conducted in downtown area of Denver. BS was installed on top of a five floor building at 17 m height. The site had a good view both of the urban high-rise portion of downtown Denver and mixed urban area. It was observed that median rms delay spread (with 20 dB threshold) was clearly smaller with highest measured frequency 5.7 GHz than with the lowest 430 MHz, the values being ~300 ns and ~700 ns, respectively. At 5.7GHz even lower median values, of the order of ~100 ns, were obtained in a large open boulevard with LOS areas. Values for maximum excess delays were reported as 7.7 and 6.7 μ s for 430 MHz and 5.7 GHz respectively.

In [OTT+01] measurements were carried out simultaneously in 3 GHz, 8 GHz and 15 GHz bands in Tokyo. The chip rate was 50 MHz, and three different BS sites with height 20-30 meters were measured. Power delay profile shapes and rms delay spread values were found to be very similar between all the bands. The median value for rms delay spreads was ~100 ns. Median values for maximum excess delays were ~300-400 ns.

Paper [PLB04] reports measurements at 3.7 GHz carrier and 20 MHz bandwidth in dense, urban downtown Chicago. Two BS heights were considered, 42 m and 135 m. The median rms delay spread values were ~300 ns and ~700 ns for the low and the high BS antenna position, respectively. Median maximum excess delay values (with 15 dB dynamic threshold) were ~800 ns and 2.3 μ s, respectively.

Paper [SRJ+91] reports multipath delay statistics in four German cities (Frankfurt, Hamburg, Stuttgart, Dusseldorf) at 900 MHz frequency and 4 MHz bandwidth (500 ns baseband probing pulse). The measurements were intended to emphasize the radio channel worst case characteristics. Typically rms

delay spreads (with 10 dB dynamic threshold) were limited to 2-3 μ s, but much larger delay spreads, even 10-20 μ s were observed in suburban locations where antennas have a clear view of large buildings and mountains simultaneously. One conclusion of this study was that in general measured German cities are not as time dispersive as the cities measured in the U.S. west coast [RSS90], where also worst case characteristics were emphasized in the measurements. In the U.S west coast the cities have substantially hilly and mountainous terrain within close range of receiver sites.

In [SJD94] measurements were made at 910 MHz carrier and 10 MHz chip rate in two macrocellular sites in downtown Toronto. The base station antennas were placed on buildings with 18-28 floors (~50-70 m ?). Maximum excess delay were typically below 5 μ s, but occasionally also much later echoes, > 20 μ s were observed due to high-rise buildings. Median rms delay spread values were found to be ~700 ns, and most measured values were below ~3 μ s.

In [WHL+93] measurements were taken simultaneously both in the 900 and 1800 MHz bands in macrocellular environment in Philadelphia. The used chip rate was 10 MHz. For an urban high-rise macrocellular environment the BS was installed at 167 meters from ground level, and the area consists of closely spaces buildings with heights typically exceeding 40 stories. The transmitter for an urban cell was mounted 30 m above ground. The cell is characterized by 3-4 story buildings. For the delay spread analysis a dynamic threshold of 20 dB was used. For the urban case there were no marked differences between the two frequency bands, and the median rms delay spread values were ~150 ns. For urban high-rise cells the median rms delay spread values were ~600-700 ns, and the difference between the frequencies was small but yet distinguishable (higher frequency showed slightly higher median rms delay spread).

In [TSS+05] measurements were conducted at 5.2 GHz center frequency and 120 MHz bandwidth in Munich, Germany. The height of the base station antenna was about 70 metres with 30 degrees down-tilt. The 50% fractile of the RMS delay spread was measured to be approximately 60 ns in a LOS case.

In [CP07] the authors have conducted measurements in an urban and dense urban macrocells in France at 2.2 GHz center frequency and 10 MHz bandwidth. The receiving antenna was placed on a rooftop above the mean height of surrounding buildings and the transmitting antenna on the roof of a car. In urban environment the height of the buildings was approximately 20 metres and in dense urban 30 metres. Mean value for delay spread was observed to be 250 ns.

In [RWH02] measurements were carried out at 2.125 GHz center frequency and 5 Mchips/s chip rate in Helsinki. The average building height was reported to be 20-25 metres. The MS was placed on the roof of a van at 2.5 metres. Two BS locations were used; “low” position with antenna at 5 metres below the rooftop of a 30-m high building and “high” position with antenna 1.5 metres above the same 30-m high building, clearly above the surrounding buildings. For the “high” position the median delay spread was observed to be approximately 500 ns.

Radio channel measurements at 2.1 GHz and 50 MHz bandwidth in Norway are reported in [PLN+99]. The transmitting antenna was placed on the roof of a car driven at constant speed of approximately 30 km/h. The receiver was placed at 25 metres. The measurement location was a typical quadratic city structure with five to eight storey buildings. Four routes were measured with one of them being mainly LOS. The 50 percentile from the CDF of the measured RMS delay spread varied from 20 ns to 92 ns with mean value of 56 ns. The RMS delay spread of the LOS route was 20 ns.

In [LKT+02] measurements conducted at 2.1 GHz and 100 MHz bandwidth are reported. The measurement location was Helsinki where the receiving antenna was placed below rooftop level (10 m), at rooftop level (27 m) and above rooftop level (21 m, surrounding buildings were lower). The threshold value in the impulse response was reported to vary between 15-30 dB, being mostly above 25 dB. The RMS delay spread was observed to be between 0.53-2.37 μ s for the case where the receiver was at rooftop level and 0.31-2.04 μ s for the case where the receiver was above rooftop level.

[AWK+01] reports measurements conducted at 1.9 GHz and 20 MHz bandwidth in Bristol, UK. The receiving antenna used in the measurements was placed on three different rooftop locations and down-tilts of 5°, 7.5° and 5° were applied at each BS locations, respectively. The transmitting antenna was placed on the metallic roof of a vehicle. LOS and NLOS deployments were integrated into the trials plan

For urban environment the median RMS delay spread was measured to be 0.44 μ s and the minimum and maximum values were 0.1 μ s and 2.3 μ s, respectively.

In FTB03] the authors have conducted radio channel measurements in Bristol, UK. The center frequency was 1.92 GHz and 2.12 GHz, each with 20 MHz bandwidth. The measurement environment consisted of buildings of 2-3 storeys and the measurements were performed during working day. The receiving antenna was located at the rooftop 33m above ground level. The transmitter was placed at 1.8 metres height on a roof of a electric car. The 30 dB cutoff threshold was used in the pre-processing scan of the impulse response as a 25 dB noise rejection threshold was subsequently used in the estimation step. The mean value for the RMS delay spread was measured to be 0.3 μ s

In [FBK+02] measurements were performed at 1.9 GHz and 2.1 GHz with 20 MHz bandwidth in Bristol, UK. Two kinds of measurement were performed, static and dynamic. The receiving antenna was at 30 metres height with down-tilt of 4°. A 15 dB threshold was applied in the analysis. The mean RMS delay for the 1.9 GHz frequency was 0.133 μ s and for the 2.1 GHz 0.129 μ s.

[Mar98] reports measurements performed in Frankfurt, Germany, at 1.9 GHz center frequency and 6 MHz bandwidth. The base station was located at a rooftop about 70 metres above the ground. The measurement environment was densely built-up business area with large number of skyscrapers. The transmitter was placed at different fixed positions. The mean RMS delay spread was observed to be 0.5 μ s.

[PMF00] and [AMP02] report measurement campaign performed in Aarhus, Denmark, and Stockholm, Sweden. The center frequency was 1.8 GHz and the bandwidth was 5 MHz. The measurement environments were classified to be typical and bad urban macrocell. The measurement environment in Aarhus was an area characterized by buildings ranging from four to six floors and irregular street grid. No buildings were significantly higher than the average building height. The BS antenna was placed at two different heights: 20 and 32 metres. The 20 metres corresponds to average rooftop level of the surrounding buildings and in most cases there was no LOS between the MS and BS.

The measurement environment in Stockholm consisted of buildings of 4-6 floors in a slightly rolling terrain. The receiving antenna was at 21 metres height which corresponds to the average rooftop level of the surrounding buildings. The BS antenna was pointed at two directions from which the direction 2 is classified as typical urban.

The RMS delay spread was observed to increase significantly as the antenna height was reduced in Aarhus. The 50% fractile of the RMS delay was 0.4 μ s and 0.85 μ s for low and high antenna positions, respectively. For the measurements in Stockholm, the 50% fractile of the delay spread was observed to be approximately 1.3 μ s.

In [Lar99] measurements were conducted in dense urban and suburban environments at 1.8 GHz center frequency and 150 MHz bandwidth. The receiver was located at 20 meters above the ground, approximately at the same height as the surrounding buildings, in the dense urban case. The threshold was set to 20 dB above the strongest peak in the impulse response. The average RMS spread was measured to be 115 ns.

[NLA+99] reports measurements conducted at 1.8 GHz frequency and 150 MHz bandwidth in Södertälje, Sweden. The transmitter was placed on a roof of a van and the receiver at 15 metres height. The measurement environment consisted of 15 to 20 metres high buildings. LOS was reported to be present at only few of the measurement locations. The average RMS delay spread was measured to be approximately 75 ns.

In [OTT+01] the authors have conducted wideband measurements in the 3 GHz, 8 GHz and 15 GHz bands in high-tier area in three different urban areas in Tokyo, Japan. High-tier locations can be considered as macrocell since the antenna height (30-40m) was higher than the average height of the surrounding buildings. In Table 3-50 are presented the statistical results of measured delay spread and maximum delay time.

Table 3-50: Statistical results of measured delay spread and maximum delay time in three urban locations [OTT+01]

Value (μ sec)	3 GHz	8 GHz	15 GHz
Delay spread in 50 %			
Honjo	0.08	0.1	0.1
Ikebukuro	0.05	0.07	0.05
Nippori	0.1	0.1	0.08
Delay spread in 95 %			
Honjo	0.4	0.5	0.5
Ikebukuro	0.2	0.2	0.2
Nippori	0.3	0.3	0.3
Max. delay time in 50 %			
Honjo	0.3	0.45	0.45
Ikebukuro	0.3	0.3	0.25
Nippori	0.4	0.4	0.3
Max. delay time in 95 %			
Honjo	2.3	2.5	2.5
Ikebukuro	1.4	1.4	1.4
Nippori	1.3	1.3	1.3

Summary of numbers reported above is presented in Figure 3-132.(a). There are great variations in reported results, especially at lower frequencies. The reasons behind the differences can be manifold, such as data selection and processing (especially threshold for delay spread calculation), used antennas, BS antenna height and location, environment (flat vs. mountainous terrain, open vs. regular street grid, non-uniformity of building heights, ...). One factor affecting also the rms delay spread distributions is the bandwidth used in measurements. Especially for lowest measured values this can have a significant effect. For example, we consider a single received tap without any multipath echoes (e.g. in LOS conditions). For a measurement system with 10 ns delay resolution (100 MHz chip rate) the resulting rms delay spread is only a few nanoseconds. With 500 ns delay resolution (2 MHz chip rate) it is already hundreds of nanoseconds! The effect of bandwidth on impulse response shape is illustrated in Figure 3-132.(b).

The bandwidths used at lower carrier frequencies in Figure 3-132 tend to be smaller than at higher frequencies. This might also be a reason for somewhat higher rms delay spread values at lower frequencies. Up to date the number of published macrocellular results at frequency ranges > 3 GHz are scarce, and further measurements in that range in environment would be valuable.

Results for rms delay spreads and maximum excess delays measured in Helsinki at 5.3 GHz frequency and 100 MHz chip rate are shown in Figure 3-133. For the WINNER models we propose typical rms delay spreads of the order of ~200-250 ns for C2 NLOS urban macrocellular scenario.

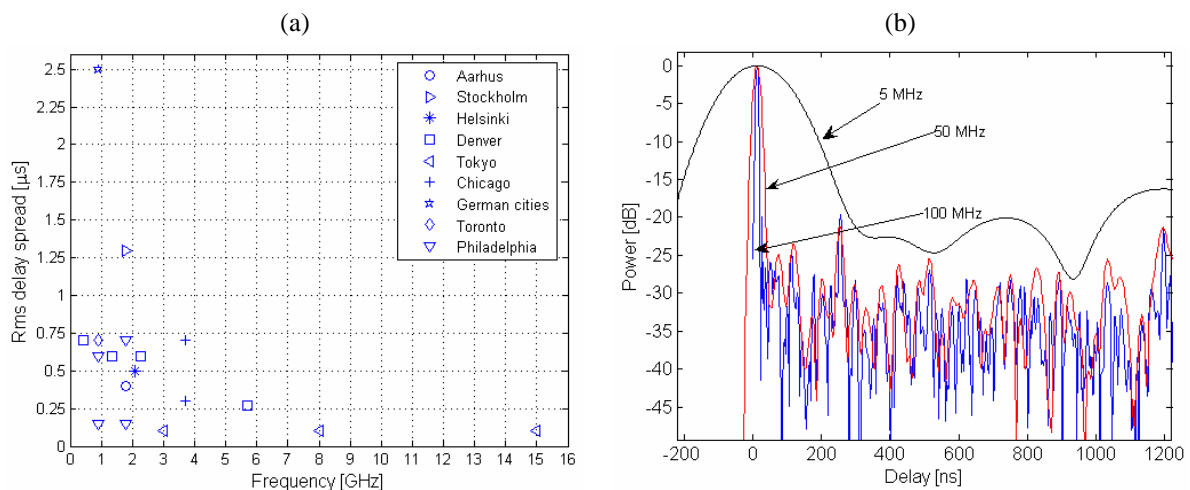


Figure 3-132: (a) Typical rms delay spreads at different carrier frequencies for urban macrocellular environment found in literature. (b) Effect of chip rate (bandwidth) on impulse response shape.

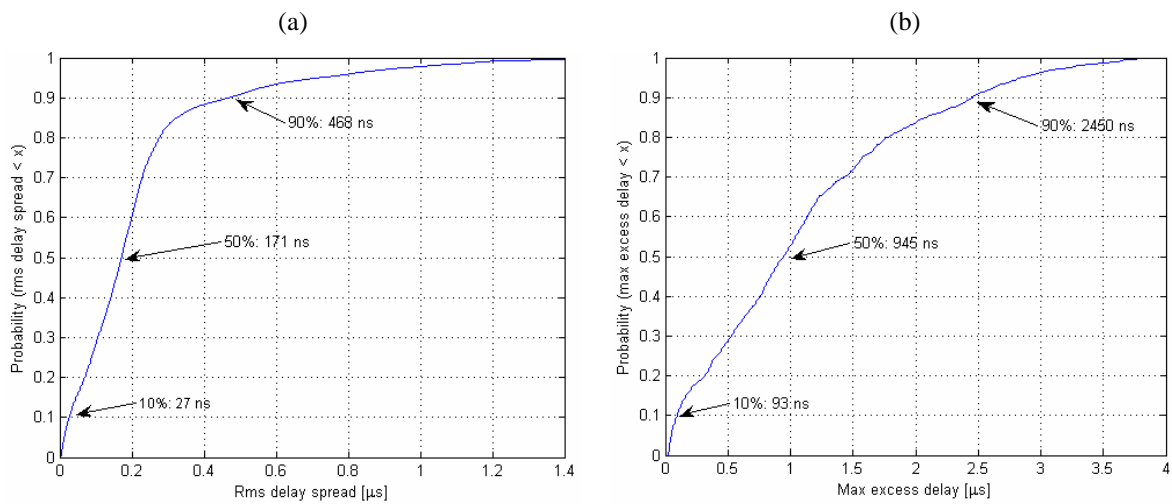


Figure 3-133: (a) Cdf for rms delay spreads and (b) maximum excess delays measured in Helsinki at 5.3 GHz carrier frequency and 100 MHz chip rate.

For the LoS C2 model, the measurement results for maximum excess and RMS delay spreads are presented in Table 3-51. CDFs for maximum excess and RMS delay spreads are presented in Figure 3-134 and Figure 3-135, respectively. Taps included in the analysis were the ones above the noise threshold level which was set to 20 dB below the power of the strongest tap in one snapshot. In order for a snapshot to be included in the analysis, the dynamic range of it had to be at least 23 dB.

Table 3-51: Measurement results for for maximum excess and RMS delay spreads

	Mean	Std	10% percentile	50% percentile	90% percentile
Maximum excess delay	333.35 ns	140.08 ns	53.37 ns	116.0 ns	389.5 ns
RMS delay	85.44 ns	286.31 ns	24.25 ns	285.88 ns	754.50 ns

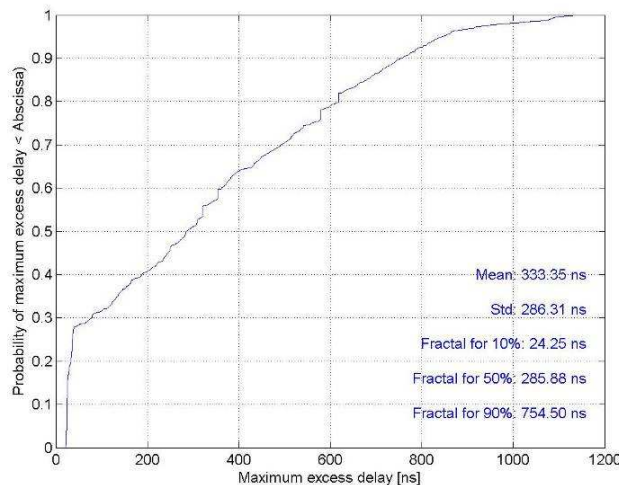


Figure 3-134: CDF of maximum excess delay spread.

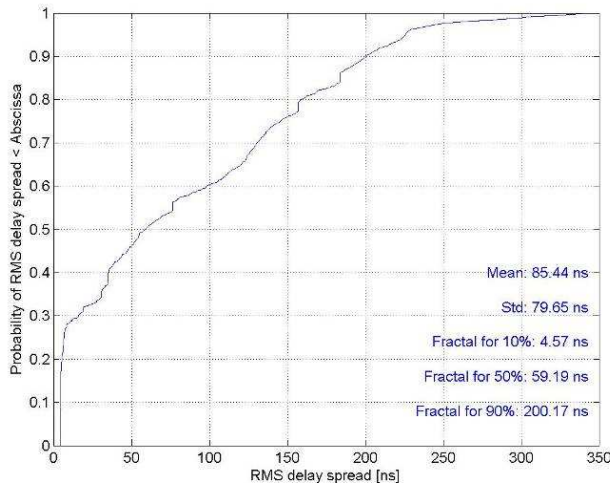


Figure 3-135: CDF of RMS delay spread

3.9.6 C2 Azimuth AS at BS and MS

Papers [APM02] and [PMF00] report measurements made at 1.8 GHz carrier frequency and 4 MHz chip rate in Aarhus and Stockholm. Base station locations were 20 and 32 m for Aarhus, and 21 m for Stockholm. Median rms azimuth spreads at BS were 5 and 10 degrees for Aarhus high and low antenna positions, and 12 degrees for Stockholm, respectively. For the bad urban sector facing over the river in Stockholm it was observed that the power delay spectrum and power azimuth spectrum are composed of two clusters. This was not observed in typical urban data. The later cluster was delayed by several microseconds compared to the first one.

In [PLN+99] directional wideband channel measurements at 2.1 GHz carrier and 50 MHz bandwidth in urban and suburban areas have been performed. It was found that in urban areas a BS antenna installed at lamppost level lead to more severe azimuth spread than a BS at rooftop level. Correlation between angular spread and delay spread was low. In urban city environment the macrocellular BS position was at 25 meters, which is slightly above surrounding rooftop levels. BS-MS distances ranges from 20 to 360 meters. In suburban environment with low residential wooden houses the BS height was 7 meters, which was above the rooftop level of most the surrounding buildings. In this scenario BS-MS distances were 50...510 meters. Typical azimuth spread values (50 percentile value in cdf) in urban macrocellular environment were 7.6...11.8 degrees, with mean value of 9.9 degrees. For the same environment typical delay delay spreads were 20...92 ns, with mean value of 56 ns. In suburban measurements azimuth spread values 12.9...18.4 degrees with mean value of 15 degrees were obtained. Corresponding delay spread values were 45...233 ns, with mean 119 ns.

In [KRB00] angular power distributions at the MS were measured in urban macrocellular environment in Paris at 890 MHz. It was found that street canyons force the long-delayed waves to come from street directions, but street crossings can cause additional signal components. For smaller delays local scatterers contribute to power spectra. Propagation over the roofs was significant: typically 65% of energy was incident with elevation angles larger than 10 degrees.

In [KSL+02] elevation angle distributions at the mobile station in different radio propagation environments have been reported at 2.15 GHz carrier frequency. Results show that in non-line-of-sight situations, the power distribution in elevation has a shape of a double-sided exponential function, with different slopes in the negative and positive sides of the peak. The slopes and the peak elevation angle depend in the environment and BS antenna height. In urban macrocells mean elevation angles of arrival are ~7...14 degrees, with standard deviations of 12...18 degrees.

Paper [VVK04] reports 5 GHz directional measurement results in Helsinki city centre. For MS mean angular spread values of 52° were obtained.

In [TSS+05] measurements were conducted at 5.2 GHz centre frequency and 120 MHz bandwidth in Munich, Germany. The height of the base station antenna was about 70 metres with 30 degrees down-tilt. The departure angular spread was observed to be approximately 70° in a LOS case and 80° in obstructed LOS case. The arrival angular spread was approximately 10° in LOS case and 5° in obstructed LOS case.

In [CP07] the authors have conducted measurements in an urban and dense urban macrocells in France at 2.2 GHz center frequency and 10 MHz bandwidth. The receiving antenna was placed on a rooftop above

the mean height of surrounding buildings and the transmitting antenna on the roof of a car. In urban environment the height of the buildings was approximately 20 metres and in dense urban 30 metres. The angular spread at the BS was measured to be 9.5°.

Radio channel measurements at 2.1 GHz and 50 MHz bandwidth in Norway are reported in [PLN+99]. The transmitting antenna was placed on the roof of a car driven at constant speed of approximately 30 km/h. The receiver was placed at 25 metres. The measurement location was a typical quadratic city structure with five to eight storey buildings. Four routes were measured with one of them being mainly LOS. The 50% fractile from the CDF of the measured angular spread at the BS varied from 7.6° to 11.8° with mean value of 9.9°. For the route, which was mainly LOS, the 50% fractile of the angular spread at the BS was 11.8°.

[AWK+01] reports measurements conducted at 1.9 GHz and 20 MHz bandwidth in Bristol, UK. The receiving antenna used in the measurements was placed on three different rooftop locations and down-tilts of 5°, 7.5° and 5° were applied at each BS locations, respectively. The transmitting antenna was placed on the metallic roof of a vehicle. LOS and NLOS deployments were integrated into the trials plan. The median of the angular spread at the BS was measured to be 10°.

In [FTB03] the authors have conducted radio channel measurements in Bristol, UK. The center frequency was 1.92 GHz and 2.12 GHz, each with 20 MHz bandwidth. The measurement environment consisted of buildings of 2-3 storeys and the measurements were performed during working day. The receiving antenna was located at the rooftop 33m above ground level. The transmitter was placed at 1.8 metres height on a roof of a electric car. The departure angular spread was measured to be approximately 75°.

In [FBK+02] measurements were performed at 1.9 GHz and 2.1 GHz with 20 MHz bandwidth in Bristol, UK. Two kinds of measurement were performed, static and dynamic. The receiving antenna was at 30 metres height with down-tilt of 4°. The arrival angular spread was measured to be 8.4° for 1.9 GHz and 9.6° for 2.1 GHz center frequency.

[Mar98] reports measurements performed in Frankfurt, Germany, at 1.9 GHz center frequency and 6 MHz bandwidth. The base station was located at a rooftop about 70 metres above the ground. The measurement environment was densely built-up business area with large number of skyscrapers. The transmitter was placed at different fixed positions. The mean angular spread at the BS was observed to be 8°.

In [PMF00] and [APM02] measurement campaign was performed in Aarhus, Denmark, and Stockholm, Sweden. The center frequency was 1.8 GHz and the bandwidth was 5 MHz. The measurement environments were classified to be typical and bad urban macrocell. The measurement environment in Aarhus was an area characterized by buildings ranging from four to six floors and irregular street grid. No buildings were significantly higher than the average building height. The BS antenna was placed at two different heights: 20 and 32 metres. The 20 metres corresponds to average rooftop level of the surrounding buildings and in most cases there was no LOS between the MS and BS.

The measurement environment in Stockholm consisted of buildings of 4-6 floors in a slightly rolling terrain. The receiving antenna was at 21 metres height which corresponds to the average rooftop level of the surrounding buildings. The BS antenna was pointed at two directions from which the direction 2 is classified as typical urban. It was observed that the angular spread increases significantly as the antenna height is reduced. The 50% quantile of the angular spread at the BS was measured to be 5° and 10° for the high and low antenna positions, respectively. Angular spread at the BS in Stockholm measurement location was approximately 12°.

In [Lar99] measurements were conducted in dense urban and suburban environments at 1.8 GHz center frequency and 150 MHz bandwidth. The receiver was located at 20 meters above the ground, approximately at the same height as the surrounding buildings, in the dense urban case. The average angular spread at the BS was observed to be 8° in the dense urban environment.

[NLA+99] reports measurement conducted at 1.8 GHz frequency and 150 MHz bandwidth in Södertälje, Sweden. The transmitter was placed on a roof of a van and the receiver at 15 metres height. The measurement environment consisted of 15 to 20 metres high buildings. LOS was reported to be present at only few of the measurement locations. The median angular spread was found to be approximately 10° in the urban environment. From the CDF the 50% fractile was observed to be 7-8°.

In [CP07] there is a reference to measurements conducted in Helsinki at 5.3 GHz frequency and 60 MHz bandwidth, where the angular spread at the MS was observed to be 52.3° and at the BS 7.6°. [VKV04]

Based on values presented above we choose for WINNER II C2 scenario typical azimuth spread of 10 degrees for BS, and 52 degrees for MS end of the link.

Regarding the LoS model, there are no results available from our measurements. Hence, angular spreads have to be derived from the literature. It was seen that the values reported in the literature indicated

angular spread at the BS to be in the range of 7° - 27° with most of the values reported being less than 10° . Arrival angular spread varied from 50° to 80° .

Most of the references did not report results separately for LOS conditions. In [PLN+99] the authors presented 11.8° angular spread at the BS for a route that was mainly LOS. Also in [TSS+05] there were angular spread results reported for a LOS case. The spread for BS was 10° and 70° for MS. These results did not deviate much from the results reported in other sources for routes that have both LOS and NLOS conditions.

3.9.7 C2 Ricean K-factor

The measurement results for K-factor are presented in Table 3-52.

Table 3-52: Measurement results for K-factor

	Mean	Std	10% percentile	50% percentile	90% percentile
K-factor	7.2 dB	3.4 dB	2.2 dB	7.3 dB	12.7 dB

[AWK+01] reports measurements conducted at 1.9 GHz center frequency and 20 MHz bandwidth in Bristol, UK. The receiving antenna used in the measurements was placed on three different rooftop locations and down-tilts of 5° , 7.5° and 5° were applied at each BS locations, respectively. The transmitting antenna was placed on the metallic roof of a vehicle. LOS and NLOS deployments were integrated into the trials plan. The median of the Ricean K-factor was found to be -3, with minimum of -5.5 and maximum of 1.

In [TPJ06] the authors have conducted measurements at 5.2 GHz frequency and 120 MHz bandwidth. The transmitter was mounted on a trailer driving 21 km/h and 9 km/h for SIMO and MIMO measurements, respectively. The receiving antenna was located on the roof top of a 52 m building. The authors focus on small-scale fading caused by the presence of several Doppler shifts. In the paper they describe a new approach for the estimation of the Ricean k-factor and present results from the measurements. In Figure 3-136 is presented the CDF of the measured Ricean k-factor within selected distance ranges. In Table 3-53 are presented the mean and standard deviation of the measured Ricean k-factor values within selected distance ranges.

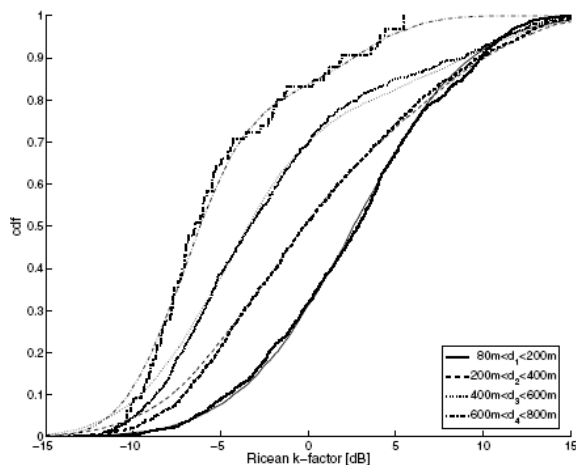


Figure 3-136: CDF of the Ricean k-factor within selected distance ranges. [TPJ06]

Table 3-53: Mean and standard deviation of the measured Ricean k-factor within selected distance ranges [TPJ06]

Distance	80m< d1 <200m	200m< d2 <400m	400m< d3 <600m	600m< d4 <800m
Mean [dB]	2.75	0.54	-1.91	-5.0
Std [dB]	5.3	6.28	6.29	4.42

3.9.8 C2 Number of Taps

In Figure 3-137 is presented the PDF of the number of taps. The mean value is 8.

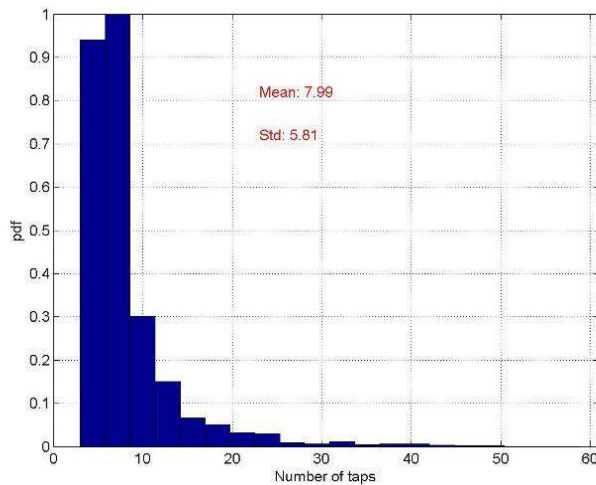


Figure 3-137: PDF of number of taps.

In [RJK07] measurements were carried out in Helsinki city center at 5.3 GHz and 100 MHz chip rate. For the DoA analysis a separate set of measurements were conducted in Kallio BS site. The BS antenna was at 34 metres, above the surrounding rooftop level. Spatial processing was done using the SAGE algorithm with 20 path and maximum dynamic range of 25 dB. Propagation conditions were reported to be mainly NLOS but also some LOS street sections were included. 50% percentile of the number of taps was observed to be in the range of 13-19.

In [TSS+05] measurements were conducted at 5.2 GHz center frequency and 120 MHz bandwidth in Munich, Germany. The height of the base station antenna was about 70 metres with 30 degrees down-tilt. The number of propagation paths was observed to be in a LOS case was approximately 42.

3.9.9 C2 Cross Correlation

In Figure 3-138 is presented the correlation between logarithmic delay spread and the shadow fading. The correlation coefficient between logarithmic DS and the SF was found to be 0.62.

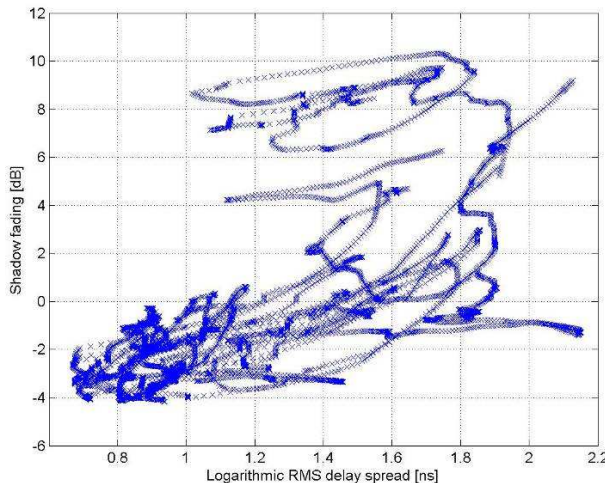


Figure 3-138: Cross-correlation between logarithmic RMS delay spread and shadow fading.

In [RJK07] measurements were carried out in Helsinki city center at 5.3 GHz and 100 MHz chip rate. For the DoA analysis a separate set of measurements were conducted in Kallio BS site. The BS antenna was at 34 metres, above the surrounding rooftop level. Spatial processing was done using the SAGE algorithm with 20 path and maximum dynamic range of 25 dB. Propagation conditions were reported to be mainly NLOS but also some LOS street sections were included. Correlation between shadow fading and logarithm of delay spread was observed to be in the range of -0.62 ... -0.35. The negative correlation implies that increase in shadow fading decreases the delay spread.

In [APM02] measurements were conducted at 1.8 GHz in Aarhus, Denmark and Stockholm, Sweden. In both measurement locations surrounding buildings were 4-6 floors high, there was NLOS between the BS and MS and the propagation scenario was classified as typical urban (TU). In Aarhus the BS antenna heights were 20 metres and 32 metres (TU20 and TU32, respectively) and in Stockholm the BS antenna height was 21 metres (TU21). The cross-correlation coefficients for angular spread at the BS (AS), delay spread (DS) and shadow fading (SF) are presented in Table 3-54.

Table 3-54: Cross-correlation coefficients for the different antenna heights [APM02]

	AS & DS	AS & SF	DS & SF
TU32	0.39	-0.51	-0.4
TU21	0.34	-0.47	-0.5
TU20	0.6	-0.65	-0.48

In [CP07] the authors have conducted measurements in an urban and dense urban macrocells in France at 2.2 GHz center frequency and 10 MHz bandwidth. The receiving antenna was placed on a rooftop above the mean height of surrounding buildings and the transmitting antenna on the roof of a car. In urban environment the height of the buildings was approximately 20 metres and in dense urban 30 metres. Correlation between the delay spread and the angular spread at the BS was observed to be 0.60.

Radio channel measurements at 2.1 GHz and 50 MHz bandwidth in Norway are reported in [PLN+99]. The transmitting antenna was placed on the roof of a car driven at constant speed of approximately 30 km/h. The receiver was placed at 25 metres. The measurement location was a typical quadratic city structure with five to eight storey buildings. Four routes were measured with one of them being mainly LOS. The correlation coefficients between angular spread at the BS and the delay spread varied from -0.20 to 0.23 with the mean value of 0.05. For the route that was mainly LOS the correlation between the angular spread and the delay spread was 0.23.

[NLA+99] reports measurement conducted at 1.8 GHz frequency and 150 MHz bandwidth in Södertälje, Sweden. The transmitter was placed on a roof of a van and the receiver at 15 metres height. The measurement environment consisted of 15 to 20 metres high buildings. LOS was reported to be present at only few of the measurement locations. The correlation between RMS delay spread and angular spread at the BS was measured to be 0.40.

References [APM02], [CP07], [PLN+99] and [NLA+99] report the correlation between delay spread and angular spread at the BS to be positive and in the range of 0.23-0.6. In [PLN+99] it was observed to be 0.23 for a LOS path. In other references the propagation conditions were mentioned to be mostly NLOS with only few LOS paths.

The correlation coefficient between delay spread and shadow fading was reported to be negative in [RJK07] and [APM02]. In [APM02] the authors have also reported the correlation between angular spread and shadow fading to be negative.

3.10 C3 – Bad urban macro-cell

3.10.1 C3 – Scenario definition

Bad urban environment describes cities with buildings with distinctly inhomogeneous building heights or densities, and results to a clearly dispersive propagation environment in delay and angular domain. The inhomogeneities in city structure can be e.g. due to large water areas separating the built-up areas, or the high-rise skyscrapers in otherwise typical urban environment. Increased delay and angular dispersion can also be caused by mountainous surrounding the city. Base station is typically located above the average rooftop level, but within its coverage range there can also be several high-rise buildings exceeding the base station height. From modelling point of view this differs from typical urban macro-cell by an additional far scatterer cluster.

3.10.2 C3 – Measurements

In [RJK07] macrocellular measurements were taken in Helsinki at 5.3 GHz carrier frequency and 100 MHz bandwidth over a bay area surrounded by densely built urban environment. Bad urban channel characteristics with exceptionally long echoes were observed in about 5% of the measured locations. Maximum excess delays were $\sim 7 \mu\text{s}$ long. Occasionally the power of these very late echoes could be comparable to that of the first taps in the power delay profile. Example of this is given in Figure 3-139. Paper [SG02] reports measurements taken in Manchester at 2 GHz carrier and 60 MHz bandwidth. In this environment the maximum observed excess delays were of the order of $\sim 10 \mu\text{s}$.

We do not expect bad urban channels with very late multipath echoes to be very common in urban environments at 5 GHz. The increased path loss reduces the effective operation range, and especially with high bandwidths the power is insufficient to capture reflections from very far scatterers. Therefore we propose bad urban channel model as a specific feature, which can be switched on for certain proportion of urban micro- and macrocellular users. The procedure is described in detail in section 4 of Part I.

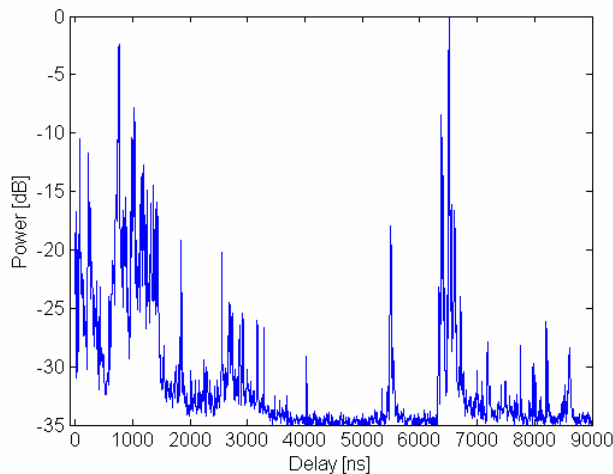


Figure 3-139: Example of a bad urban power delay profile with rms delay spread of 2.8 μ s, maximum excess delay of 6.6 μ s [RJK07].

3.11 C4 – Urban macro outdoor to indoor

3.11.1 C4 – Scenario definition

The Outdoor-to-Indoor in urban macrocellular scenario is modelled in the same way as the corresponding microcellular scenario. However, there are the following differences:

- As a rule there is no LOS path from the BS to the nearest wall.
- Normally there is no grid where the indoor MS can be located (if not artificially generated).

The Outdoor-to-Indoor scenario is specified here as follows:

- The outdoor environment is the same as in urban macrocellular case, C2.
- The indoor environment is the same as in indoor case, A1.
- The perpendicular distance of the MS from the outer wall between the BS and MS, the through-wall penetration point, is d_{in} .
- The Base Station is located at distance d_{out} from the through-wall penetration point in the outer wall between the BS and indoor MS.
- The Base Station antenna height is h_{BS} .
- The direction of the BS from the outer wall in the signal path is given as θ .
- The height of the MS measured from the surroundings of the building is h_{MS} .

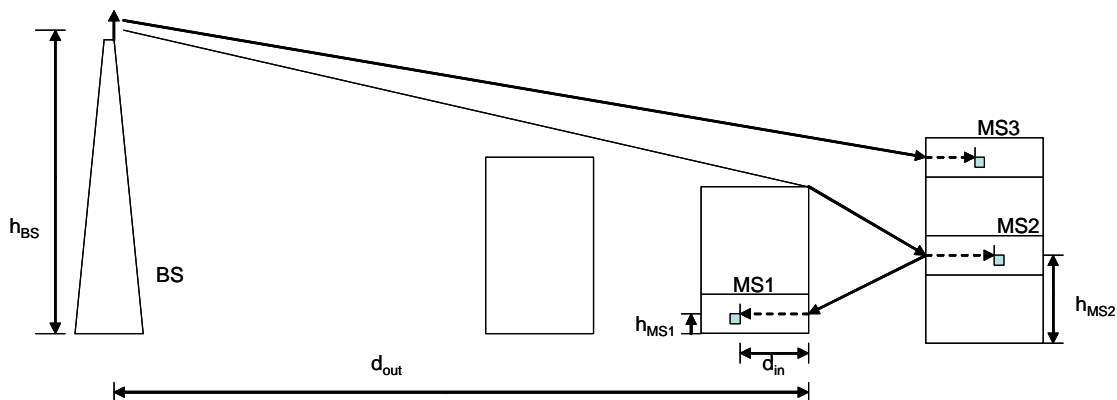


Figure 3-140 C4 scenario.

3.11.2 C4 Path-loss model

The path-loss is modelled with three parts with the same approach as in B4 [COST231]:

Basic path-loss from the BS to the MS.

Path-loss through the outer wall.

Path-loss in the interior of the building, from the outer wall to the MS.

Basic path-loss from the BS to the MS is modelled as the path-loss in C2. In addition, the fact that the MS can be located in different floors has to be taken into account by introducing a floor height gain factor, see the formula below.

Combining the losses discussed above, we get

$$PL = PL_b + PL_{tw} + PL_{in} - G_{FH}$$

where

$$PL_b = PL_{C2}(d_{out} + d_{in}) \quad (3.74)$$

$$PL_{tw} = We + WG_e (1 - \cos(\theta))^2$$

$$PL_{in} = \alpha d_{in}$$

$$G_{FH} = G_h h_{MS}$$

PL_b above is the basic loss between the BS and MS along the route $d_{out} - d_{in}$ without wall effects, PL_{in} is the loss inside the building, PL_{tw} is the loss through the outer wall and G_{FH} is the Floor Height Gain. The parameters in the equation are:

d_{out} = outside distance,

d_{in} = inside distance,

α = loss coefficient for the indoor propagation,

W_e = loss through wall for the perpendicular penetration,

WG_e = loss through wall for the parallel penetration and

θ = angle between the normal of the wall and outgoing (incoming) ray

G_h = height gain factor

h_{MS} = MS height from the building surroundings

From our earlier measurements the most appropriate values for the model constants have been found (See scenarios A2/B4) and they are:

W_e : 14 dB,

WG_e : 15 dB

α : 0.5 dB/m.

For cases, where the angle θ is not used, replace the second term in the penetration loss with an average:

$$PL_{tw} = We + WG_e \left(1.5 - \frac{4}{\pi} \right)$$

Using the average and inserting the given value for WG_e we get

$$PL_{tw} = 14 + 3.4 \text{ dB} = 17.4 \text{ dB}$$

For the height gain factor we base our value mostly on results from literature. In [COST231] height gain factor has been discussed. The values are for 1800 MHz and there are two sets of values. In the set, where floor height is about 2.5 m, the values are in the range 0.5 – 0.67 dB/m. In the other set with higher room

heights, the values are in the range 1.1 – 1.6 dB. The frequency dependence is given for frequencies 900 MHz and 1800 MHz. The trend is that the height gain increases with frequency.

WP1 made a rough estimation about height gain factor by using ray-tracing. Due to time pressure, we could simulate only a limited area, but using a realistic lay-out with high-rise buildings. The distance range of the simulations was from 30 m upto 300 m. The conclusion was that the height gain factor in these simulations was about 0.4 dB/m. This value is slightly smaller than that found in [COST231], but is reasonably close to support the values found in the literature. Due to the limited scope of the simulations, we decided to take the results from literature and put more weight to the smaller values of the two sets mentioned afore. The proposed value for the height gain factor is:

$$G_h = 0.8 \text{ dB/m.}$$

Using these values we get the formula:

$$PL = PL_{C2}(d_{out} + d_{in}) + 17.4 + \alpha d_{in} - 0.8h_{MS}$$

where

PL_{C2} is the path-loss for the scenario C2.

The standard deviation is calculated based on C2 and B4 and is 10 dB.

3.11.3 C4 Channel parameters

The channel parameters are assumed to be equal with the scenario B4, except for the delay spread and shadow fading. The rms-delay spread is calculated from the C2 and A1 results and is 240 ns.

Shadow fading was estimated earlier to be 10 dB.

3.12 D1 – Rural macro-cell

3.12.1 D1 – Scenario definition

Propagation scenario D1 represents radio propagation in large areas (radii up to 10 km) with low building density. The height of the AP antenna is typically in the range from 20 to 70 m, which is much higher than the average building height. Consequently, LOS conditions can be expected to exist in most of the coverage area. In case the UE is located inside a building or vehicle, an additional penetration loss is experienced which can possibly be modelled as a (frequency-dependent) constant value. The AP antenna location is fixed in this propagation scenario, and the UE antenna velocity is in the range from 0 to 200 km/h.

In WINNER Phase I, measurements were conducted in a flat rural environment near Oulu in Finland, at both 2.45 and 5.25 GHz, and with an AP antenna height of 18 - 25 m. A channel model derived from these measurements is available and has been reported in [WIN1D54]. The channel model from Phase I for propagation scenario D1 is generalised for the frequency range 2 – 6 GHz and different BS and MS antenna heights.

3.12.2 D1 - Measurements

3.12.2.1 EBITG campaigns

Measurements conducted during 2004 for D1 were performed at two centre-frequencies, 2.45 and 5.25 GHz in Tyrnävä, a small village near Oulu, and its surroundings. The measurement results were included in the deliverable D5.3 [WIN1D53].

In the year 2005, three new BS locations were measured at 5.25 GHz with 100 MHz bandwidth. In addition, PL measurements were conducted with a smaller band-width 10 MHz to increase the sensitivity of the receiver equipment. This arrangement allowed us to obtain path losses up to 10 km distance.

At the same locations some measurements at 2.45 GHz were performed to investigate the effect of centre-frequency on the path loss and other channel parameters. For practical reasons the measurements at 2.45 GHz were conducted in a smaller scope with fewer routes. However, the routes used were the same as the routes used for the 5.25 GHz measurements.

Map of the measurement environment and the BS locations are shown in Figure 3-141.

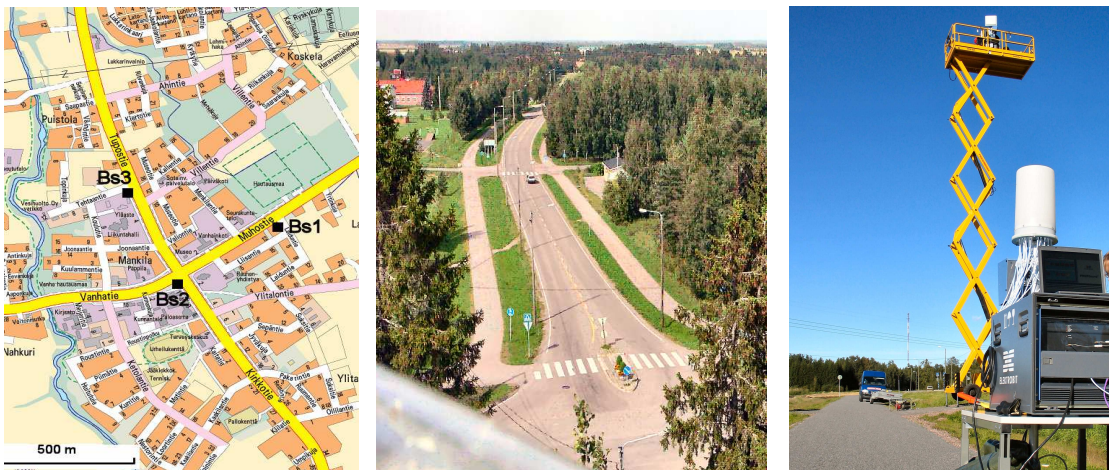


Figure 3-141. BS locations for the rural measurements in the summer 2005 (1. and 2.) and 2004 (3.).

3.12.3 D1 Path-loss and shadow fading

3.12.3.1 Measurements in LOS conditions (D5.4)

In the campaign of the year 2005, the LOS measurement was conducted in slightly different routes than in the previous year. Measurements were performed for three different BS locations, each having several measurement routes. The results are shown in the Figure 3-142.

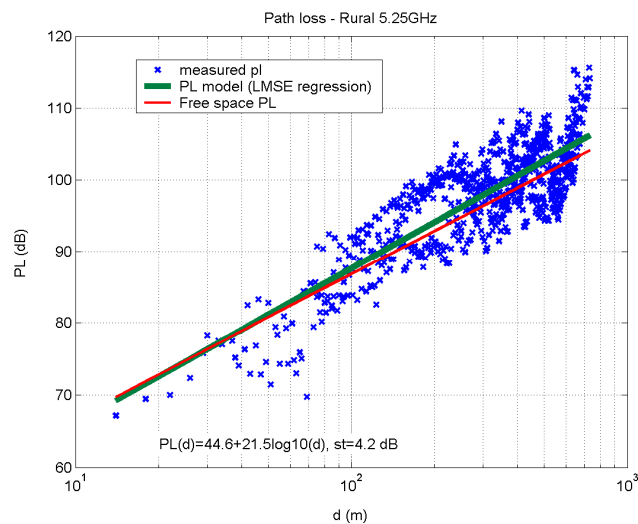


Figure 3-142: Rural LOS path loss at 5.25 GHz.

Now the equation for the rural LOS path loss was

$$PL(d) = 44.6 + 21.5 \log_{10}(d), \sigma = 4.2 \text{ dB}. \quad (3.75)$$

where d is the distance and σ is the standard deviation of the shadow fading. The equation is valid from 30 m to the break-point value. From 1 m to 30 m, the free-space loss formula should be used. This is nearly equal to the results achieved in the campaign of the previous year.

Path-loss was also investigated for longer distances in a separate measurement, where the base station antenna heights were higher, 19 – 25m, and a narrower bandwidth was used to achieve better sensitivity. At the same time path losses for rural LOS and NLOS conditions were investigated. The path-loss result for the longest route is shown in the Figure 3-143. The NLOS condition was defined so that the path loss exceeded the free-space path loss by 10 dB or more. Three long routes of this kind were measured and averaged to obtain the NLOS and over-all path-loss equations. LOS results were calculated from the short-range measurements. However, the long-distance measurements show clearly that very long LOS propagation conditions are possible in a flat environment like the one near Tyrnävä.

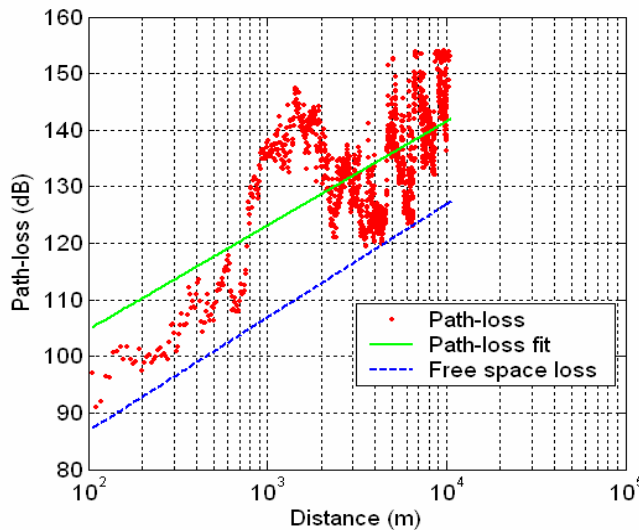


Figure 3-143: Path-loss in rural scenario on the route 3.1.

The average corrected path-loss formula for the over-all path loss in the measurements was

$$PL(d) = 50.4 + 25.8 \log_{10}(d), \sigma = 8.4 \text{ dB} \quad (3.76)$$

The average corrected path-loss formula for the NLOS path loss in the measurements was

$$PL(d) = 55.8 + 25.1 \log_{10}(d), \sigma = 6.7 \text{ dB} \quad (3.77)$$

where d is the distance and σ is the standard deviation of the shadow fading. Correction means that the cutting of the high values was estimated and compensated.

It should be noted that the definition of NLOS was performed according to the power difference of 10 dB from the free-space loss. Another note is that the noise-floor cuts the weakest signals, so that the highest path losses were cut as well. It can be assumed, however, that the effect of this limiting is relatively small.

The rural NLOS measurement results were obtained from three routes, which is quite a limited set of measurements. Therefore the model has been compared with literature and adjusted appropriately in the following sub-section.

3.12.3.2 Measurements and literature comparison (D5.4)

The path loss is shown in the figure below for the two centre-frequencies 2.45 and 5.25 GHz in LOS propagation conditions. The measurements have been conducted in a 100 MHz bandwidth. The curve for 2.45 GHz contains also a part that is measured in NLOS (or nearly NLOS) conditions around 1000 m distance.

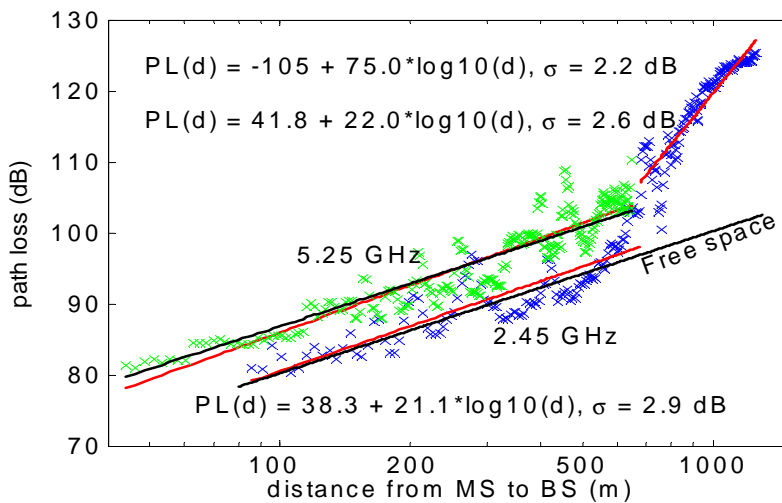


Figure 3-144: Rural path-loss at 2.45 and 5.25 GHz.

The measured model for LOS has been extended from the [WIN1D53] for longer ranges, because it has become evident that a path-loss model for LOS conditions with longer BS – MS distances is needed. The maximum distance for the model should be 10 km. Theoretically the model shown in (3.66) can be extended until so called break-point distance, which depends on the wave-length λ and base station and mobile station antenna heights h_{BS} and h_{MS} , respectively. After this break-point the loss is proportional to another, greater path-loss exponent. By flat earth theory this exponent should be 4, but in practice it can be also smaller or greater. In practice the break point distance varies around the theoretical value. The break-points or the dual-slope behaviour could not be found in our measurements. However, this depends most probably on the randomness of the practical situation: We have decided to take it as part of our rural LOS model.

For the line of sight (LOS) conditions the measurements suggest the path-loss equations:

$$PL(d) = 44.6 + 21.5 \log_{10}(d) \quad (3.78)$$

with the standard deviation $\sigma = 3.5$ dB.

The model is based partly on our measurements and partly on the literature research, where we have adopted the two ray model for distances higher than the break-point. For the LOS environment we get then:

$$\begin{aligned} PL(d) &= 44.6 + 21.5 \log_{10}(d), \sigma = 3.5 \text{ dB}, d \leq d_{BP} \\ &= 44.6 + 40 \log_{10}(d / d_{BP}) + 21.5 \log_{10}(d_{BP}), \sigma = 6.0 \text{ dB}, d > d_{BP} \end{aligned} \quad (3.79)$$

where d = distance

$$d_{BP} = 4 \cdot h_{BS} \cdot h_{MS} / \lambda = 4 \cdot h_{BS} \cdot h_{MS} \cdot f_c / c$$

h_{BS} = the height of the base station

h_{MS} = the height of the mobile station

λ = the wave length at f_c

f_c = the centre-frequency (Hz)

c = the velocity of light in vacuum

σ = standard deviation.

The path losses behave very similarly at the two frequencies. As a matter of fact the mean behaviour is very near free-space path-loss in LOS conditions. The formula above can be adapted for the frequencies between 2000 and 6000 MHz by replacing the constant 44.6 by a factor

$$C(f_c) = 36.2 + 20 \log_{10}(f_c / (2 \cdot 10^9)) \quad (3.80)$$

Note that the LOS path-loss depends on antenna heights only through the break-point distance.

3.12.3.3 D1 NLOS model (D5.4)

The NLOS model is based on our measurements which have been fitted to results found in the literature research. The measured path-loss curve for the NLOS conditions has the equation

$$PL = 55.8 + 25.1 \log_{10}(d) \quad (3.81)$$

with $\sigma = 6.7$ dB.

This path-loss equation was measured for the BS antenna height 23 m and MS antenna height 1.7 m. This equation will be compared to some theoretical path-loss curves. From the literature we found that mostly the standard deviation was a little bit higher than 6.7. Because our measurement was limited, we decided to use the value 8 dB for the standard deviation.

The formula (3.69) above can be adapted for the frequencies between 2000 and 6000 MHz by replacing the constant 55.8 by a factor

$$\begin{aligned} C(f_c) &= 46.9 + 20 \log_{10}(f_c / (2 \cdot 10^9)) \cdot 1.063 \\ &= 46.9 + 21.3 \log_{10}(f_c / (2 \cdot 10^9)) \end{aligned} \quad (3.82)$$

The constant 1.063 is based on our finding that the path loss difference in between 5.25 and 2.45 GHz for NLOS conditions was about 2.5 dB higher than for free space, see frequency comparison paragraph.

After D5.3 the following equation was proposed for the D1 rural NLOS scenario path-loss by the channel modelling WP to other work-packages. This model is called COST231-Hata model, originally for urban and suburban environments. Slightly simplified it reads as

$$PL = 20 \log_{10}\left(\frac{f_c}{2000}\right) + [44.9 - 6.55 \log_{10}(h_{BS})] \log_{10}\left(\frac{d}{1000}\right) - 13.82 \log_{10}(h_{BS}) + 153.39 \quad (3.83)$$

where h_{BS} is the height of the base station, f_c is the centre-frequency (MHz), and d is the distance between BS and MS (m).

This model and another well-known model, Erceg model 1, will be compared to the measured curve.

The modification of the BS antenna height is probably needed, because the environment of the measurements is extremely flat. This can be compensated by adding 25 m to get an effective BS antenna height that is greater in flat than in hilly environments.

Both models work equally well, if the BS antenna height is between, say, 10 and 100 m. For higher antenna heights the curves begin to differ. According to the comparison, the modified COST231-Hata model can be used from 100 m to 10 km, although originally the model has been defined for distances greater than 1 km. The modified Erceg model 1 could be applied as well.

In the figure below there are the measurement based PL curves obtained in the WINNER project compared to some well-known PL models from the literature. In addition there is the free-space loss curve. In the comparison the base station antenna height was 24.5 m; mobile antenna height was the default value 1.7 m.

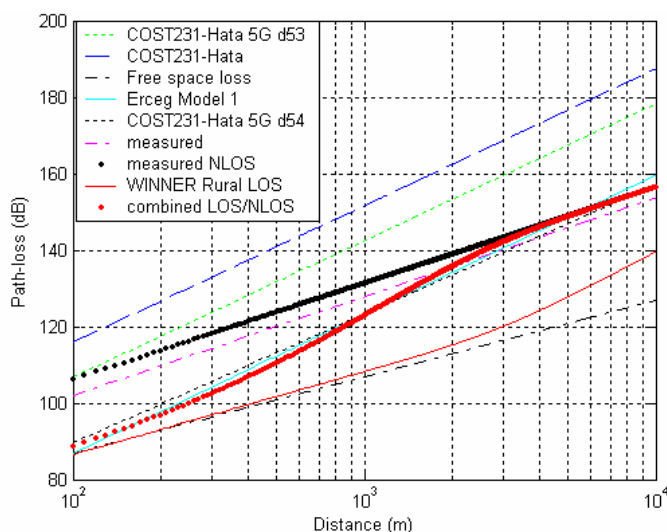


Figure 3-145: Comparison of channel models for a rural environment.

When adjusting the PL curves of the models to closely follow the measured over-all curve, the following actions were needed:

1. Cost231-Hata: Subtract 15 dB and apply $h_{BS} = 50$ m (instead of the 25 m). I.e. use an effective BS antenna height $h_{BS} + 25$ m.
2. Erceg: Apply $h_{BS} = 60$ m. I.e. use an effective BS antenna height $h_{BS} + 35$ m.

Both models could be used, after these modifications. The subtraction of 15 dB needed with the COST231-Hata model is caused by the fact that the model is not originally planned for rural environments, but for urban and suburban environments.

3.12.3.4 D1 Literature review

D1 LOS path-loss

The basic theoretical equation for LOS path-loss is

$$PL = A + B * \log_{10}(d) \quad (3.84)$$

where d is the distance between BS and MS and A and B are constants.

Normally, A and B are near the free-space values. For example, in our measurements at 5.25 GHz the values were: $A = 41.8$ and $B = 22$.

The above model can be extended until so called break-point distance, which depends on the wave-length λ and base station and mobile station antenna heights, h_{BS} and h_{MS} [Sau99]

$$d_{BP} = 4 \cdot h_{BS} \cdot h_{MS} / \lambda \quad (3.85)$$

where h_{BS} is the height of the base station, h_{MS} is the height of the mobile station, and λ is the wave length at f_c .

After this break-point, the loss is proportional to another, greater path-loss exponent. By flat earth theory, this exponent should be 4, but in practice it can be also greater. The model is based on the assumption about two rays arriving at the receiver antenna, one direct ray, the other one reflected from the flat earth. This model is also called two-ray model.

The model can be written in form [Sau99]:

$$PL = A + B \log_{10}(d), d \leq d_{BP} \quad (3.86)$$

$$PL = A + C \log_{10}(d/d_{BP}) + B \log_{10}(d_{BP}), d > d_{BP} \quad (3.87)$$

where $C = 10 n$, and n is the path-loss exponent for the distances greater than the break-point distance. Other constants are as given above.

About LOS path-loss, there is a statement in [SBA+02] about trials in a rural environment that show that the two-ray model works well there. For the urban microcellular environment it has been modified slightly to make it agree with the measurement results. Measurements for the two-ray modelling were reported at 1.9 GHz and cover the range of 0 to 1800 m with antenna heights of 6 m (BS) and 1.7 m (MS). With these values the distance of 1800 m is far beyond the break-point distance.

Also, [APM02] shows results for LOS conditions, where the path-loss exponent is near 2 with standard deviation of 6.9 dB. The behavior of the path loss is thus like in free-space. The environment is called residential. It can be classified also suburban. Measurements were conducted using 100 MHz bandwidth. For NLOS conditions, the path-loss exponent was 3.5 and the standard deviation was 9.5 dB.

In the reference [ZKV+02], based on measurements performed at 5.3 GHz with RF BW 30 MHz, and omni-directional antennas, the path-loss models, excess delay and RMS delay-spread statistical values were obtained. In the rural environments, the transmitter was placed at a hill with a mast, the total height was 55 m from ground level, the height of the mobile station was 2.5 m on top of a car. The path-loss equation is expressed as follows:

$$PL(\text{dB}) = 21.8 + 33 \log_{10}(d), \sigma = 3.7 \text{ dB} \quad (3.88)$$

D1 NLOS path-loss

The model has been based partly on measurements and partly on literature. There are numerous path-loss models for lower frequencies than 5 GHz, and especially for urban and suburban environments. For the rural environment at 5 GHz there are not many results available. One alternative is to use results of lower frequencies, e.g. 2 GHz and translate them to 5 GHz. This can be justified with results presented in the paragraph 3.12.3.4.1, which show that the path-loss properties at 2 and 6 GHz are closely related. Mean difference was found to be 8.1 dB, when the difference due to the free-space losses should be 9.7 dB. Although the results were measured in an urban environment, they suggest that the rural 2 GHz path-loss model can be converted to 5 GHz by increasing the path loss with the difference in the free-space losses.

One potential channel model for the D1 scenario is the COST-231-Hata [COST231] that is converted for 5 GHz. COST-231-Hata model for sub-urban environment is

$$PL = (44.9 - 6.55 \log_{10}(h_{BS})) \log_{10}\left(\frac{d}{1000}\right) + 45.5 + (35.46 - 1.1h_{MS}) \log_{10}(f_c) - 13.82 \log_{10}(h_{BS}) + 0.7h_{MS} \quad (3.89)$$

where h_{BS} = the height of the base station

h_{MS} = the height of the mobile station (m)

f_c = the centre-frequency (MHz)

d = distance between BS and MS (m).

The original model is applicable up to 2 GHz, and in the distance range 1 – 20 km.

It should be noted that COST-231-Hata model is not a NLOS model, but it does not make difference between the propagation conditions. However, at longer distances the propagation conditions are mostly NLOS. So it can be applied for NLOS in spite of the afore-mentioned fact.

In reference [ZKV+02] the path-loss model for NLOS was

$$PL(dB) = -27.8 + 59 \log_{10}(d), \sigma = 1.9 \text{ dB} \quad (3.90)$$

The parameters differ quite much from the values found out in this campaign. One reason is the hilly terrain, the other could be the relatively small number of routes measured.

One interesting empirical channel model for suburban environment is [Erc99]. The suburban environment is divided to three sub-environments according to the tree density and the height variation of the environment. One of these environments could well be applied to the rural environment. This model is created for 1.9 GHz. With the same reasoning as afore it can be also extended to 5 GHz. The model is

$$PL = 20 \log_{10}(4\pi 100/\lambda) + 10(a - b h_{BS} + c/h_{BS}) \log_{10}(d/100) \quad (3.91)$$

where the parameters a , b and c may get three sets of values depending on the environment (see below) and the other parameters are the same as in the previous formula. The model is applicable for distances 100 m – 20 km.

The parameter set that is closest to the rural environment in Tyrnävä is the one for low tree density and flat terrain. Then the constants are: $a = 3.6$, $b = 0.005$ and $c = 20$. The complete model defines also a distance dependent standard deviation for the path loss, but it is not discussed further in this document.

3.12.3.4.1 Frequency dependence

One reference shows that there are no remarkable differences between 1.9 GHz and 5.8 GHz propagation losses, except the frequency dependency as in the free-space-loss [SBA+02]. Another one claims that multipath-dispersion related micro-cellular channel characteristics do not differ remarkably [BHS05]. Although the results apply for micro-cellular case, they suggest that same is true for the rural environment as well. On the other hand, many references show that certain parameters like the RMS-delay spread and the angle-spreads are dependent on the centre-frequency.

3.12.3.5 D1 - Unified path loss model (D5.4)

For the overall path-loss in the D1 scenario we get from measurements the formula

$$PL(d) = 50.4 + 25.8 \log_{10}(d) \quad (3.92)$$

The drawback of this model is that it is based on relatively few measurements. In addition the LOS condition disappeared after quite a small distance from the BS. This depends e.g. on the fact that the BSs were located slightly off the roads for practical reasons. Real BSs would be located probably in more beneficial way.

The unified model can be formed also by combining the LOS model and the NLOS model using the LOS probability $p_{LOS}(d)$:

$$PL(d) = p_{LOS}(d) PL_{LOS}(d) + [1 - p_{LOS}(d)] PL_{NLOS}(d) \quad (3.93)$$

where d is the distance between MS and BS. Probability of line-of-sight condition p_{LOS} will be defined in Section 3.12.3.7.

The drawback of this model is that the p_{LOS} used here is only theoretical one. However, it gives reasonable results, and is used therefore as basis of comparison of our model and the models found in the literature.

3.12.3.6 Frequency comparison (D5.4)

In the Figure 3-146, the path losses at 5.25 GHz and 2.45 GHz are compared in a rural LOS environment in the same route. It is obvious that the path-loss functions can be modeled so that the only the difference between them is the difference between the free-space path-losses, i.e. 6.62 dB.

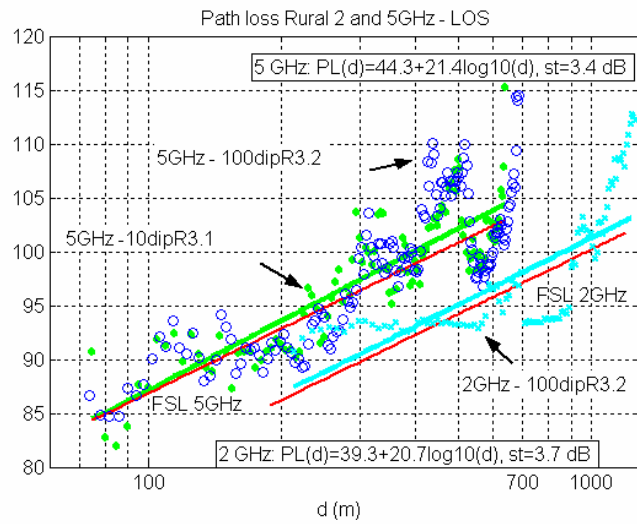


Figure 3-146: Propagation at 2.45 GHz and 5.25 GHz in rural LOS conditions.

In the figure Figure 3-147, the path losses at 2.45 GHz (a) and 5.25 GHz (b) are compared in a rural LOS/NLOS environment in the same route. The over-all behaviour of the path loss is almost identical.

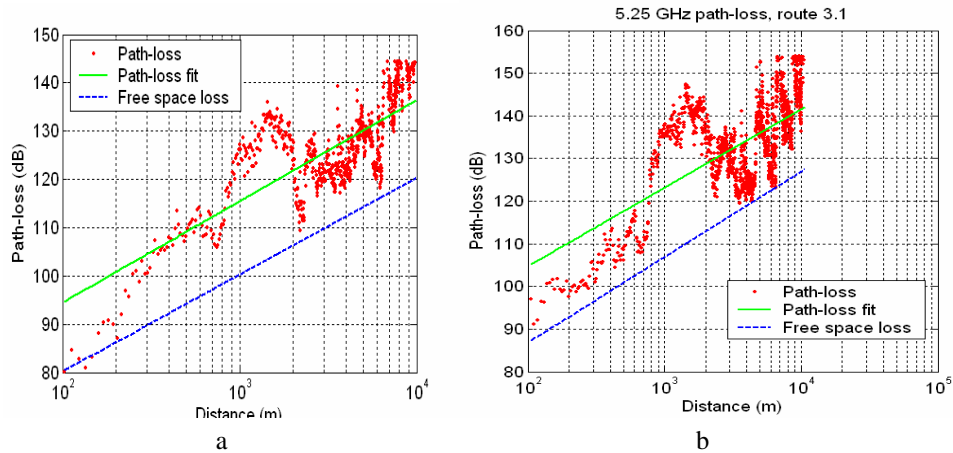


Figure 3-147: Path-loss at 2.45 GHz (a) and 5.25 GHz (b) measured in the same route.

It can be seen that the path losses are almost identical except for the difference due to the free-space losses. However, we have calculated that there is a difference of 1.7 dB in the overall standard deviation and a difference of 1 dB in the NLOS standard deviation of the path losses between the centre-frequencies 5.25 GHz and 2.45 GHz. From this we conclude that that the propagation is attenuated more in 5 GHz than in 2 GHz due to shadowing. We assume that the higher standard deviation is caused by the fact that the obstacles attenuate more at 5.25 Hz than in 2.45 GHz so that the fades caused by the shadowing are deeper for the 5.25 GHz. From the measurements we can calculate that the extra loss is about 2 - 3 dB. For the model we decided to select the value 2.5 dB. For LOS/OLOS conditions we could find a similar result, but the difference was negligible.

When comparing the shadow fading autocorrelation, we got the following results for the autocorrelations of the over-all shadowing: For 2.45 GHz the correlation distance was approximately 330 m and for the 5.25 GHz it was approximately 320 m. Note that the route used for the comparison was the one with the highest correlation distance.

3.12.3.7 D1 - WINNER2 path loss model (D1.1.1)

Channel models for the rural scenario are based on measurements conducted in Phase I in Tyrnävä, near Oulu in Finland. The models are updated for the frequency range 2 – 6 GHz and for more general antenna

heights than in Phase I. No new measurements have been performed, because several new scenarios have been deemed for higher priority level. It is pointed out that in Tyrnävä the environment is extremely flat. If another type of environment, e.g. hilly terrain, is desired to be simulated, we recommend using the model from [EGT+99].

One shortcoming of the Phase I model for D1 is the following: The long echoes were averaged off the channel model, although reported in [WIN1D54]. In this document, also long delays will be addressed.

LOS case

The WINNER D1 rural channel models were measured in Phase I at 5.25 and 2.45 GHz. The results expressed in decibels at 5.25 GHz for the LOS case are:

$$PL(d) = \begin{cases} 44.6 + 21.5 \log_{10}(d[m]), \sigma = 3.5 \text{ dB}, & 30 \text{ m} \leq d < d_{bp} \\ 44.6 + 21.5 \log_{10}(d_{bp}) + 40.0 \log_{10}(d/d_{bp}), \sigma = 6.0 \text{ dB}, & d \geq d_{bp} \end{cases} \quad (3.94)$$

where d = distance

$$d_{BP} = 4 \cdot h_{BS} \cdot h_{MS} \cdot f_c / c$$

h_{BS} = the height of the base station

h_{MS} = the height of the mobile station

f = the centre-frequency (Hz)

c = the velocity of light in vacuum

σ = standard deviation.

By using the frequency correction coefficient, the formulas are generalised for the frequency range 2 – 6 GHz. For the LOS case:

$$PL(d) = \begin{cases} 44.2 + 21.5 * \log_{10}(d[m]) + 20 * \log_{10}(f[\text{GHz}] / 5.0), \sigma = 3.5 \text{ dB}, & 30 \text{ m} \leq d < d_{bp} \\ 44.2 + 21.5 * \log_{10}(d_{bp}) + 40.0 * \log_{10}(d/d_{bp}) + 20 * \log_{10}(f[\text{GHz}] / 5.0), \sigma = 6.0 \text{ dB}, & d \geq d_{bp} \end{cases}$$

By writing d_{BP} open, we get the antenna dependencies for the LOS case:

$$\begin{aligned} PL(d,f) &= 44.2 + 21.5 \log_{10}(d) + 20 \log_{10}(f[\text{GHz}] / 5), \quad 20 \text{ m} < d \leq d_{BP} \quad (17a) \\ PL(d,f) &= 8.7 + 40.0 \log_{10}(d_1 [\text{m}]) - 19.5 \log_{10}(h_{BS} [\text{m}]) - 19.5 \log_{10}(h_{MS} [\text{m}]) + \\ &\quad 0.5 \log_{10}(f[\text{GHz}] / 5.0), \quad d > d_{BP} \\ \sigma &= 4.0 \text{ dB}, \quad 20 \text{ m} < d \leq d_{BP}; \quad \sigma = 6.0 \text{ dB}, \quad d > d_{BP} \end{aligned} \quad (3.95)$$

D1 NLOS case

For the NLOS case the measured model at 5 GHz is:

$$PL(d) = 55.8 + 25.1 * \log_{10}(d[m]), \sigma = 8 \text{ dB} \quad (3.96)$$

It has been generalised for the frequency range 1 – 6 GHz in [WIN1D54] by using the 2.45 GHz measurements together with the 5.25 GHz measurements:

$$PL(d) = 55.4 + 25.1 * \log_{10}(d[m]) + 21.3 * \log_{10}(f[\text{GHz}] / 5.0), \sigma = 8 \text{ dB} \quad (3.97)$$

For the antenna height dependence we have to rely on literature. Unfortunately very few articles appropriate to the situation exist. One of them was referred in [WIN1D54] and a similar behaviour found as in our rural measurements, namely [EGT+99]. In the reference three residential environments were defined. The one with least path-loss was called model C and was targeted for flat lightly wooded residential areas. As a matter of fact it turned out that our environment was still more flat and very lightly wooded. This could be compensated by defining an effective BS antenna height adding 25 m to the real height.

Taking this as a starting point we define the BS antenna height dependence by using Taylor series around the measurement antenna height, actually 25 m, but replaced the effective antenna height 50 m. Then the extra term needed, BS height gain factor G_{BS} , is [EGT+99]:

$$G_{BS} = 0.13 (h'_{BS} [\text{m}] - 50) \log_{10}(d/d_0) \quad (3.98)$$

where h'_{BS} is the effective BS antenna height
 d is the distance between BS and MS and
 d_0 is 100 m.

After this the actual antenna heights can be used

$$G_{BS} = 0.13 (h_{BS} [\text{m}] - 25) \log_{10}(d/d_0) \quad (3.99)$$

The formula is applicable for the actual BS antenna heights 10 ... 75 m.

For the MS there is no height gain factor in [EGT+99]. Therefore the MS height gain factor is calculated using the approach of the COST-231 Hata model [COST231]. For this model the height gain depends linearly on the MS antenna height. Let's assume that rising the MS antenna to the mean forest level gives the free-space path-loss plus 6 dB. Then the average height gain is 21 dB for the MS antenna height 25 m. From these figures we get

$$G_{MS} = 0.9(h_{MS} [\text{m}] - 1.5) \quad (3.100)$$

This height gain factor is valid from 1 to 10 m.

Subtracting the height gain factors we get:

$$PL(d) = 55.4 + 25.1 * \log_{10}(d[\text{m}]) + 21.3 * \log_{10}(f[\text{GHz}] / 5.0) - 0.13(h_{BS} [\text{m}] - 25) \log_{10}\left(\frac{d}{d_0}\right) - 0.9(h_{MS} [\text{m}] - 1.5)$$

The shadow fading standard deviation is: $\sigma = 8$ dB.

Path-loss curves for the D1 LOS and NLOS cases are shown in the Figure 3-148. In this figure: $h_{BS} = 25$ m and $h_{MS} = 2$ m.

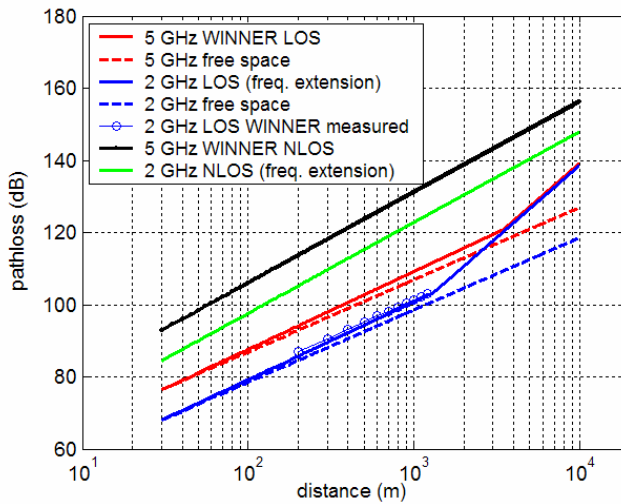


Figure 3-148. Path-loss curves for the D1 rural scenario at 2 and 5 GHz.

3.12.4 D1 - Probability of LOS model

In [3GPPSCM] there is a model given for the LOS probability. The probability formula proposed is

$$\begin{aligned} p_{LOS}(d) &= (d_0 - d) / d_0, 0 < d \leq d_0 \\ &= 0, \text{ otherwise} \end{aligned} \quad (3.101)$$

where d is the distance BS – MS and d_0 is the limit distance.

SCM has defined the cell sizes for 3GPP purposes. However, this formula could be adapted to WINNER rural scenario D1. In that case, the value d_0 remains to be defined.

In the cross WP discussions, a modification of the SCM LOS probability was proposed as an exponential function of BS – MS distance.

$$P_{LOS}(d) = \exp(-d / d_0) \quad (3.102)$$

where d is the distance BS – MS and d_0 is the distance constant.

Probability of LOS in the D1 scenario is proposed to be modelled with an exponential function

$$P_{LOS}(d) = \exp\left(-\frac{d}{d_0}\right) \quad (3.103)$$

where d is the distance between the BS and the MS and d_0 is the constant defining the steepness of the exponential decay.

Default value for d_0 is proposed to be 1000 m. The reason for proposing this model is the following: It is very near the model for LOS probability defined in [3GPPSCM] at small distances. In addition it does not go to zero at the cell boundary, so that it can be used in the system-level modelling of interference.

3.12.5 D1 Delay spread and maximum excess delay distribution (D5.4)

3.12.5.1 Ordinary delays

The 10, 50 and 90 % percentiles of the measured RMS-delay spread are shown in the Table 3-55 for 5.25 GHz in 100 MHz bandwidth in LOS and NLOS propagation conditions. In [WIN1D53] it was reported that the behaviour is very similar at 2.45 and 5.25 GHz centre-frequencies. The maximum excess delays were found to be roughly two to three times higher than the RMS-delay spreads.

Table 3-55: Percentiles of the RMS-delay spread in a rural environment.

Rms delay spread (ns)		LOS	NLOS
Percentile	10%	2.5	4.3
	50%	15.4	37.1
	90%	84.4	89.5
	mean	36.8	42.1

3.12.5.2 Exceptionally long delays

The RMS delay spread as function of distance along the measurement route was discussed in [WIN1D53]. One example is shown in Figure 3-149. It can be seen that near 740 m from the start of the measurement route, there is an abrupt rise of the RMS delay spread. The delay spread jumps there from some tens of nanoseconds up to 800 ns for a short interval, about 25 m. The reason is obviously a reflection from a nearby radio mast.

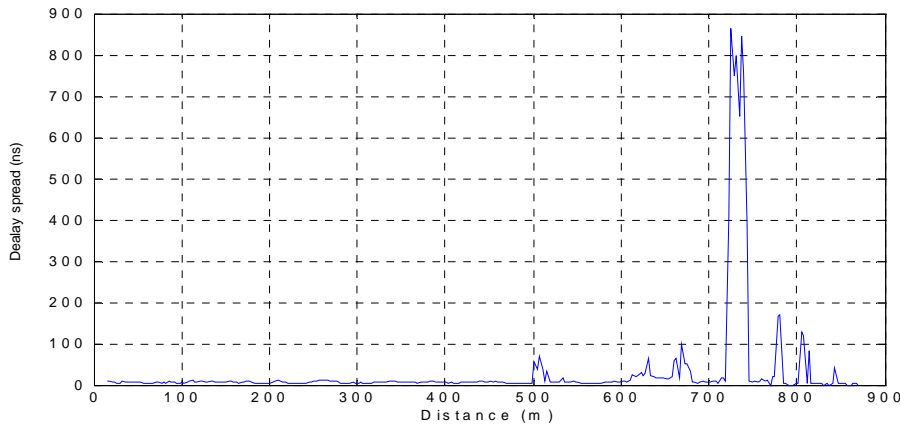


Figure 3-149: RMS delay spread as a function of distance.

It should be noted that this kind of reflectors, e.g. radio masts and supporting pillars of power lines, are quite common in our rural environments. However, the probability of reflections was not possible to be estimated in our current campaign.

This kind of exceptionally delayed paths can not be modelled with the primary model with exponentially distributed delay spreads. They have to be modelled as far clusters [3GPPSCM]. However, at the current model this kind of exceptional phenomenon has been neglected.

3.12.6 D1 Azimuth AS at BS and MS (D5.4)

Measured angle-spread cumulative distribution functions at MS and BS at 5.25 GHz are shown in Figure 3-150. The percentiles for the azimuth spreads at BS and at MS are shown in the Table 3-56.

Table 3-56: Percentiles of the RMS azimuth spread.

Rural Tyrnävä		LOS	NLOS
BS, σ_ϕ	10%	10.2	5.6
	50%	21.9	18.0
	90%	36.2	34.3
	mean	21.7	19.5
MS, σ_ϕ	10%	8.3	6.0
	50%	20.3	22.3
	90%	37.5	36.4
	mean	22.4	21.9

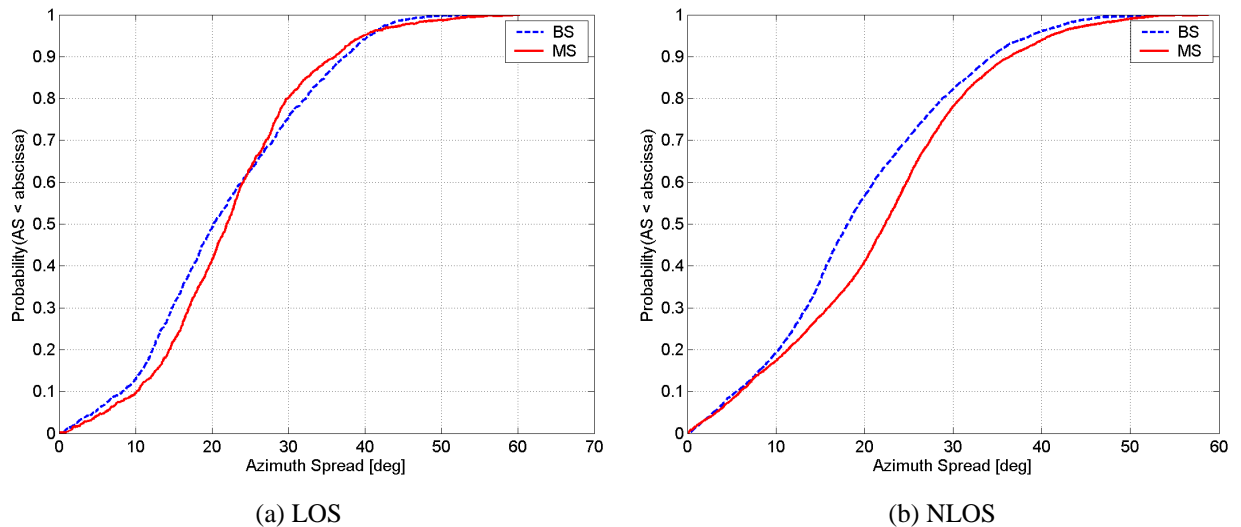


Figure 3-150: CDF of the RMS azimuth angle-spreads at BS and MS in LOS (a) and NLOS (b) conditions.

3.12.7 D1 K-factor (New)

In [WIN1D54] and [WIN2D111] K-factor was given as a function of distance. Now we have increased the level of randomness in the model and will draw the K-factor randomly from the Lognormal distribution: Figure 3-151.

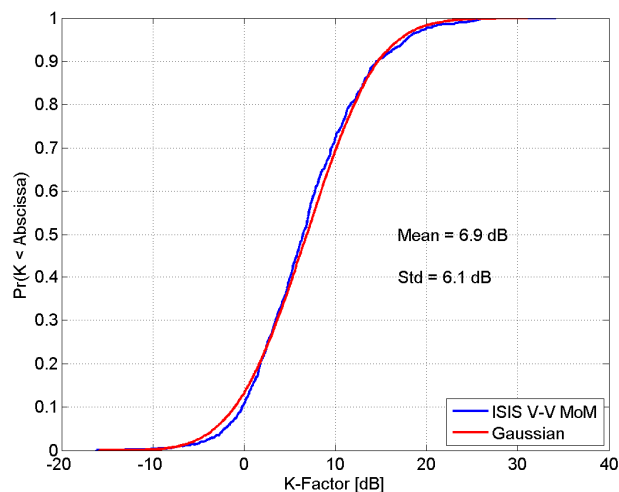
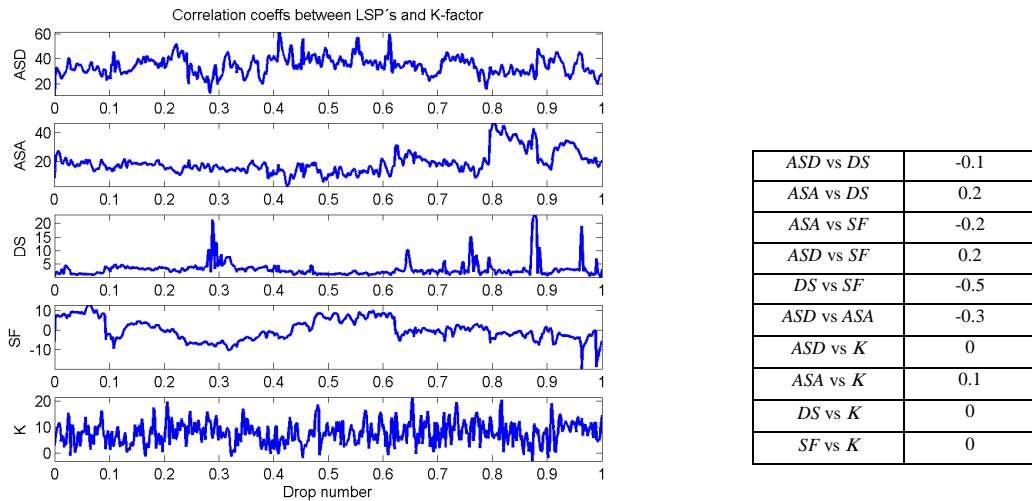


Figure 3-151 K-factor in dB. ISIS V-V MoM means the data is the superresolution data from vertical polarisation and the method of K-factor calculation is the Greenstein's Moments Method.

3.12.8 D1 Cross Correlations (New)

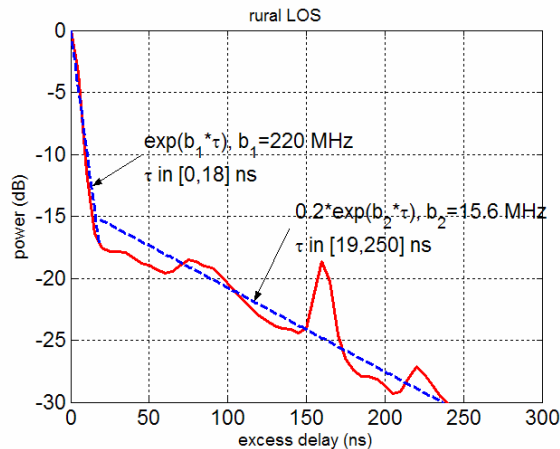
In [WIN1D54] and [WIN2D111] cross-correlation was analysed between the large scale parameters (LSP's) except the K-factor. However, since we have one K-factor value for each stationarity interval we can calculate the cross-correlation between the K-factor and e.g. delay spread also. Figure 3-152 depicts the correlation as a function of drop number.

**Figure 3-152 Correlation between the LSP's.**

3.12.9 D1 Modelling of PDP (D5.4)

Power delay profiles for the rural environment were investigated in 2004 and reported in [WIN1D53] for LOS propagation conditions. In our current campaign both LOS and NLOS conditions were investigated. The results of the current campaign are shown in the figure Figure 3-153. The results in [WIN1D53] are comparable, but less detailed.

Mean PDP profiles at 100 MHz bandwidth and 5.25 GHz centre-frequency in a rural environment are shown in the following figures.

**Figure 3-153: PDP profile in LOS propagation conditions.**

Power delay profile for LOS conditions has been fitted to two segments with an exponential function

$$P(\tau) = e^{-b\tau} \quad (3.104)$$

where τ is the excess delay and b is the time-constant. Here the constants b_1 is 220 MHz for the first segment and b_2 is 15.6 MHz for the second one.

For the D1 rural NLOS conditions the PDP has been investigated in the current measurement campaign. The measured PDP can be seen in the Figure 3-154 below with dual slope and single slope fitting.

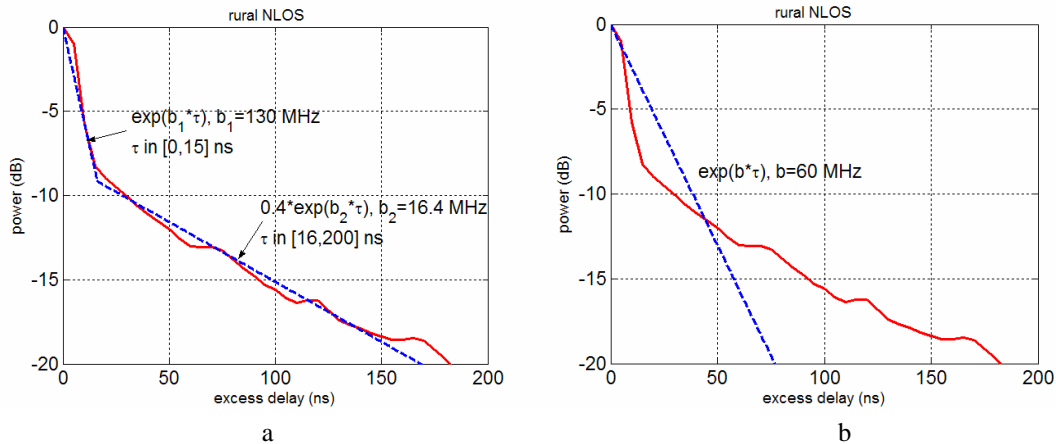


Figure 3-154: PDP profile in NLOS propagation conditions. a) dual slope model, b) single slope model.

Here the constants b_1 and b_2 for the dual slope fitting are 130 MHz and 16.4 MHz, respectively. In spite of the fact that the best fit can be obtained with the dual slope profile we will use a single slope profile in the model for simplicity. Then the line fitted to the profile will have the time-constant $b = 60$ MHz.

3.12.9.1 Literature review

In the D1 scenario the PDP is best modelled with two decaying exponentials in both LOS and NLOS propagation conditions, i.e. with a dual-slope model. However, also now we model the PDP was decided to be modelled with a single exponential in both cases. In the LOS conditions the first part is modelled with one spike and the second with an exponential.

In the NLOS conditions a single slope model is fitted to the measured PDP for simplicity. The fitting is performed to preserve the modelled RMS-delay spread equal to the measured one.

3.12.10 D1 Number of cluster (D5.4)

The distribution of the number of clusters was investigated in the measurement campaign. The results are shown in the Table 3-57 as the 10, 50 and 90 % percentiles of the distribution. The results differ from the results reported in [WIN1D53]. The reason is the larger number of routes measured in the latter campaign. Percentiles of the number of paths in rural environment are shown in the

Table 3-57: Percentiles of the number of paths in rural environment.

Number of paths		LOS	NLOS
Percentile	10%	1.0	1.0
	50%	5.0	6.0
	90%	17.0	14.0
	mean	7.4	6.7

3.12.11 D1 Distribution of cluster delays (D5.4)

The percentiles of the CDF of the path delays are shown in Table 3-58. The measured probability density functions of the path delays are shown in the Figure 3-155. The distributions can be fitted to an exponential distribution as can be seen in the figure.

Table 3-58: The 10, 50 and 90 % percentiles for the cumulative distribution function of the path delays for an outdoor LOS and NLOS environments at 5.25 GHz.

Path delay (ns)		LOS	NLOS
Percentile	10%	0	0
	50%	100	80
	90%	403	294
	mean	165	124

The time constants are 140 ns for LOS and 110 ns for NLOS conditions.

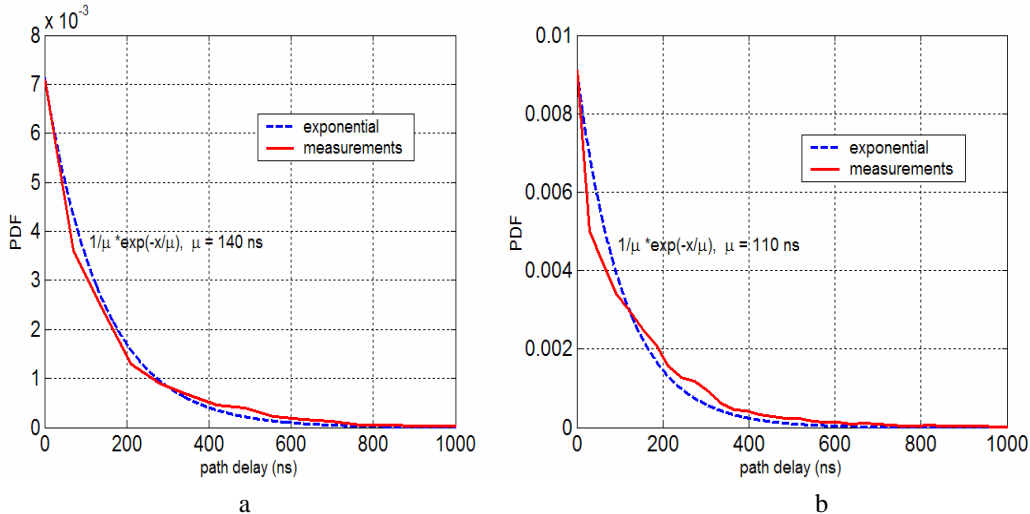


Figure 3-155: a) Distributions of the path delays for the different sub-scenarios, a) LOS, b) NLOS.

3.12.12 D1 Delay proportionality factor (D5.4)

The delay proportionality factor (r_{DS}) is defined as the ratio between the standard deviation of the delays of the multipath components and RMS delay spread.

The percentiles for the CDF of the delay proportionality factor for scenario D1 are presented in the Table 3-59.

Table 3-59: The 10, 50 and 90 % percentiles for the cumulative distribution function of the delay proportionality factor in a rural environment.

delay proportional factor: r_τ		LOS	NLOS
Percentile	10%	2.0	1.2
	50%	3.8	1.7
	90%	8.5	2.9
	mean	4.7	1.9

3.12.13 D1 Ricean K-factor (D5.4)

The percentiles of the cumulative distribution function (CDF) of the Ricean K-factor at 100 MHz bandwidth and 5.25 GHz centre-frequency in a rural LOS environment can be found in Table 3-60.

Table 3-60: The 10, 50 and 90 % percentiles for the cumulative distribution function of the narrowband K-factor (dB) for a rural LOS environment at 5.25 GHz.

K-factor (dB)

Percentile	10%	-0.6
	50%	10.9
	90%	20.0
	mean	10.1

The cumulative distribution function (CDF) of the Ricean K-factor at 100 MHz bandwidth and 5.25 GHz centre-frequency in a rural LOS environment is shown in the figure below. It can be seen that the measured results fit quite well in log-normal distribution. The parameters of the distribution are: mean 10.1 dB and standard deviation 8.0 dB.

K-factor in the D1 rural scenario and LOS propagation conditions at 5.25 GHz centre-frequency is shown in the Figure 3-156 as function of the BS – MS distance.

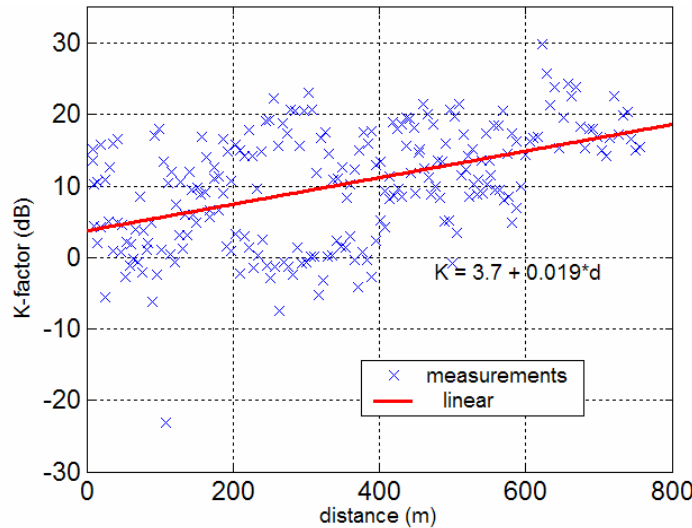


Figure 3-156: Ricean K-factor as function of distance in a D1 rural environment.

In the rural LOS, we also noticed that K increases with increasing distance for the scenario D1. The formula is

$$K = 3.7 + 0.019 d \quad (3.105)$$

where d is the distance between the BS and the MS.

3.12.14 D1 Cross-polarisation ratio (D5.4)

The CDF of the cross-polarization ratio (XPR) at 100 MHz bandwidth and 5.25 GHz centre-frequency in a rural environment is shown in the Figure 3-157. The corresponding percentiles are listed in the Table 3-61.

Table 3-61: Percentiles of the cross-polarization ratios in a D1 rural environment.

D1 rural		direct path (LOS)	scattered paths (NLOS)
XPR _V	10%	1.7	3.7
	50%	12.2	6.3
	90%	20.7	9.2
	mean / std	11.7 / 7.8	6.4 / 2.2
XPR _H	10%	3.2	3.2
	50%	13.5	6.1
	90%	23.3	9.1

	mean / std	13.2	6.1 / 2.3
--	------------	------	-----------

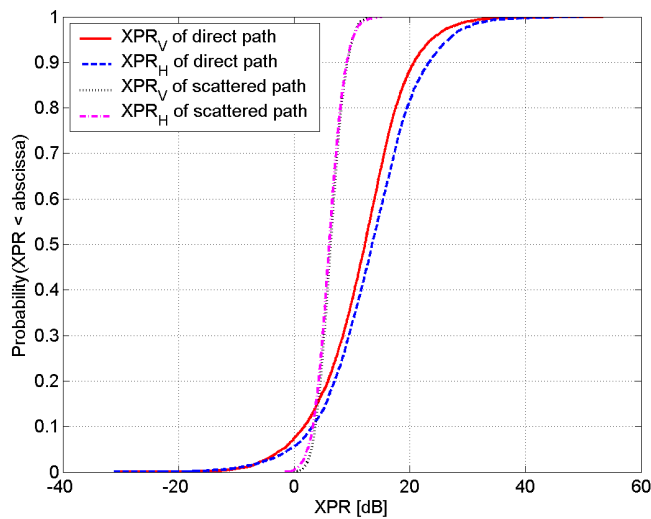


Figure 3-157: CDFs for the XPR_V and XPR_H for 5.25 GHz.

3.13 D2 – Moving networks

3.13.1 D2 - Scenario definition

Propagation scenario D2 (“Rural Moving Network”) represents radio propagation in environments where both the AP and the UE are moving, possibly at very high speed, in a rural area. A typical example of this scenario occurs in carriages of high-speed trains where wireless coverage is provided by so-called moving relay stations (MRSs) which can be mounted, for example, to the ceiling. Note that the link between the fixed network and the moving network (train) is typically a LOS wireless link whose propagation characteristics are represented by propagation scenario D1.

Moving networks scenario D2 means primarily the environment of fast trains with the maximum speed of 350 km/h, Figure 3-158. The connection to the trains is arranged by using a moving relay station (MRS) mounted on the roof of the carriage. The link from the MRS to the interior of the train is assumed to be arranged by an interior part of the MRS with the antennas mounted on the ceiling of the carriage. In this deliverable we consider the connection from the AP to the MRS and call this sub-scenario as D2a. The other link, from the MRS to the UT, will be covered with the model for A1 NLOS. For convenience we will call it D2b, when applicable.

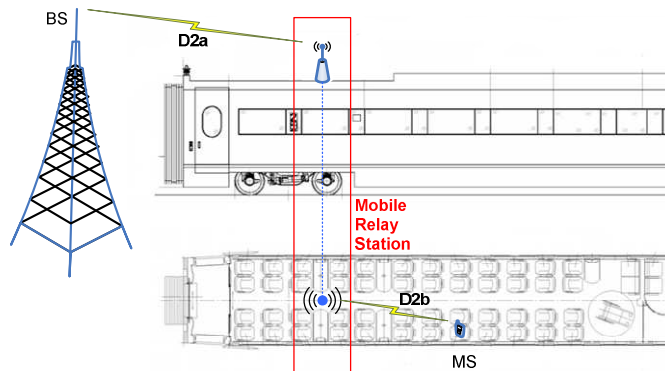


Figure 3-158: Moving network reference scenario.

In the literature the case of railway tunnels has received quite much attention. This would suggest to include tunnels in the moving network scenario. However, we have not performed our own measurements in tunnel environment. In addition it turned out in several of the references, e.g. [AGV98] and [AI00] that the tunnel environment of the fast trains is quite a favourable one. Therefore we assumed that simulations in tunnel environment are not performed in WINNER II and consequently we have not created a channel model for it.

There are also other phenomena that could be important for a precise fast train model, like some regular constructions at regular intervals like pylons. In addition, oncoming train on an adjacent track would certainly cause noticeable effect in the propagation. However, for simplicity, we do not model such details in this model.

One crucial matter for the fast train scenario is the Doppler behaviour: This is the most characteristic and potentially the most harmful effect encountered in the fast moving (train) environment. The effect is emphasized in tunnels, where the Base Stations are situated on quite a low height, say 5 m. In addition the Base Stations are very near the tracks in a tunnel. To be able to model such extreme cases, we propose to use two types of Base Stations. High ones are about 50 m far from the track and low ones are very near the track, slightly above the carriage roof.

3.13.1.1 D2a – Reference setup

The scenario for D2a is specified so that:

- There is track accompanied with Base Stations in the intervals of 1000 - 2000 m.
- The Base Stations are
 - 50 m away from the tracks and the antenna heights are 30 m, or
 - 2 m away from the tracks and the antenna heights are 5 m.
- Height of the train (and MRS) is 2.5 m
- Speed of the train is 350 km/h.

3.13.1.2 D2b - Model from MRS to UE

The connection from the MRS to UE is modelled with the model D2b. D2b is the same as the model A1 NLOS.

3.13.2 D2a - Measurements

The D2a model is based on the TUI fast-train measurements with SIMO setup [WIN2D111], “high mobility short range” (HMSR) setup (section 9.3.2 in [WIN1D54]) and measurements used for D1 (rural) scenario parameterization.,.

3.13.2.1 D2a – “High mobility short range hot spot”

In TUI measurements “high mobility short range hot spot” is represented by bridge-to-car scenario, Figure 3-159. The measurement data were gathered at a highway bridge close to Ulm (Germany). The BS (Rx) was mounted at the bridge (height of ~5.5m with a down tilt of 45°) whereby the transmit antennas were fixed on the roof of a car (~2m height). During the measurements car with Tx was approaching the bridge on the right and left side lane of a two lane highway road (2 lanes per direction). The maximum distance between Tx and Rx antenna position was 250m, which defines the short range area for the hot spot application. In this measurement LoS was dominate propagation condition; NLoS is exhibited after the car had been coming under the bridge.



Figure 3-159: Bridge-to-car hot spot scenario.

These measurements were performed with RUSK ATM MIMO sounder [Medav]. The carrier frequency of 5.2 GHz and 120 MHz bandwidth are used in the measurement.

3.13.2.2 D2a – Fast train measurement²

The characteristics of the radio-link between moving fast-train and fixed base station, being located next to the railroad track, were measured. This measurement was conducted on the railway line between Siegburg und Frankfurt (Germany, 2006). During the campaign the fast train was used exclusively for measurement purposes. In that way it was possible to take measurements on different speeds: 20, 100 and 240 km/h.

It should be also noted that measurement setup does not fully match D2a reference setup since the BS height (6m) was similar to the MRS antenna height (approx 5m). In this campaign, existing monopole antenna mounted at roof-top of the carriage was used as transmitter and because of that limitation only SIMO setup is supported. Additionally, it was not feasible to measure 3D radiation pattern of the train roof-top antenna (Figure 3-160 b), nor to properly estimate influence of the metallic rooftop to the effective radiation pattern.

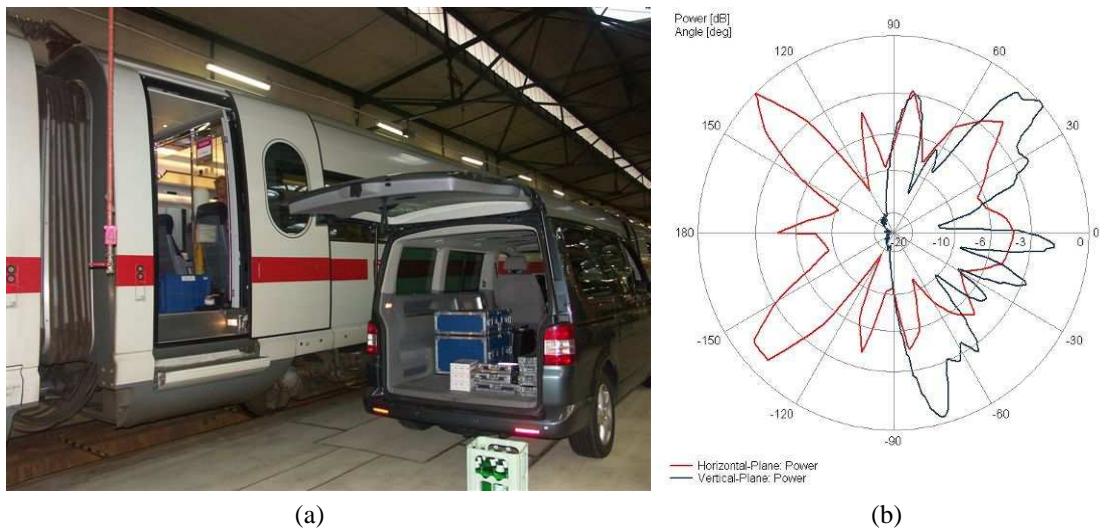


Figure 3-160. Inter-City-Express (ICE) measurement: (a) equipment, (b) radiation pattern of Huber+Suhner rooftop antenna SWA 0859 – 360/4/0/DFRX30 @ 5.25 GHz.

² The measurement campaign was mainly financed from WIGWAM project. It was conducted jointly by Medav, TU-Karlsruhe and TU-Ilmenau.

Measurements were performed by RUSK TUI-FAU channel sounder, and UCA 16 antenna array with vertically polarized disc-cone elements (Part I, section 2.4.2). The data post-processing is performed according to procedures defined in section 4. Analysis items.

3.13.3 D2a - Model parameters

In this document we will update the model in some respects although mostly the model will be as earlier. The updates are the following:

- Path-loss is updated for the path-loss exponent.
- Path-loss is updated to include an environment-based antenna gain (mostly negative)
- Outdoor-to-indoor term is introduced to the path-loss for cases where the MSR is bypassed.
- Since [WIN2D111] the following parameters have been updated in the Table 4-5 in D.1.1.2, Part I.:

Shadow fading σ_{SF} [dB]	σ	4/6 ⁺
Delay scaling parameter r_τ		3.8
XPR _V [dB]	μ	12
	σ	8
XPR _H [dB]	μ	12
	σ	8
XPR _U [dB]	μ	12
	σ	8
K-factor	μ	6
	σ	4
Number of clusters		8

3.13.3.1 D2a - Path-loss and shadow fading

Path loss result obtained from fast-train measurements (Figure 3-161 a), deviates from the expected free-space propagation: the path-loss exponent of the curve was too high. It was concluded that the extraordinary behaviour of the propagation curve depends on the special circumstances in the measurement: The antenna used in the carriage roof of the train was a monopole that was mounted very near the roof that now acts as a ground plane. This makes that the roof will affect the antenna radiation pattern. It is typical that there appears a null in the radiation pattern in the surface containing the ground plane (roof). At the same time the BS antenna of the measurement equipment was quite low, which emphasizes the effect.

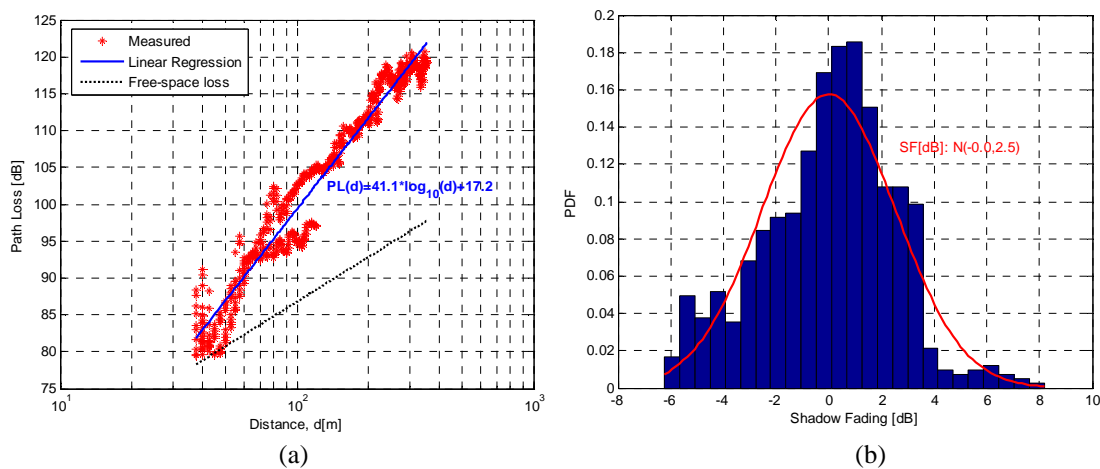


Figure 3-161: (a) Path-loss and (b) shadow fading @ 5.2 GHz for fast train measurement.

The model matching measured data would most probably over-estimate the path-loss for D2a reference setup, and therefore the path-loss model is modified as follows:

- the path-loss of the D1 scenario is used as a basis in over ground propagation,
- an environment-based radiation pattern term is added,
- an optional term for describing the outdoor-to-indoor penetration is provided.

Now the basic path-loss model for D2a LOS can be expressed as:

$$PL_{D1} = \begin{cases} 44.2 + 21.5 * \log_{10}(d[m]) + 20 * \log_{10}(f[\text{GHz}]/5.0), \sigma = 3.5 \text{ dB}, & 30 \text{ m} \leq d < d_{bp} \\ 44.2 + 21.5 * \log_{10}(d_{bp}) + 40.0 * \log_{10}(d/d_{bp}) + 20 * \log_{10}(f[\text{GHz}]/5.0), \sigma = 6.0 \text{ dB}, & d \geq d_{bp} \end{cases}$$

where d = distance

$$d_{BP} = 4 \cdot h_{BS} \cdot h_{MS} \cdot f_c / c$$

h_{BS} = the height of the base station

h_{MS} = the height of the mobile station

f = the centre-frequency (Hz)

c = the velocity of light in vacuum

σ = standard deviation.

The complete path-loss model for the moving relay connection is

$$PL = PL_{D1} + PL_{env}, \text{ where } PL_{env} = \begin{cases} 0, & d \leq d'_{BP} \\ 18.5 \log_{10}\left(\frac{d}{d'_{BP}}\right), & d > d'_{BP} \end{cases} \quad (3.106)$$

The parameter d'_{BP} is the environmental break-point length, value here 120 m, different from d_{bp} , PL_{env} means the extra attenuation caused by the train environment. Here it is assumed that the extra path-loss is due to the placement of the MRS antenna very near the carriage roof, and the extra path-loss is considered as caused by an attenuation after the break-point, now caused by the carriage roof. Actually there must be better antenna placements than found so far. Therefore the PL_{env} presented here is probably over-pessimistic. A pragmatic way around this could be to use half of this extra loss in simulations.

The proposed path-loss model shows good matching to measured path-loss exponent for HMSC bridge-to-car scenario (Figure 3-162 a):

$$PL = 60.6 + 19.3 \log_{10}(d), \text{ with } \sigma = 3.1 \text{ dB}, \quad (3.107)$$

however covered distances are not long enough to validate all proposed path-loss terms.

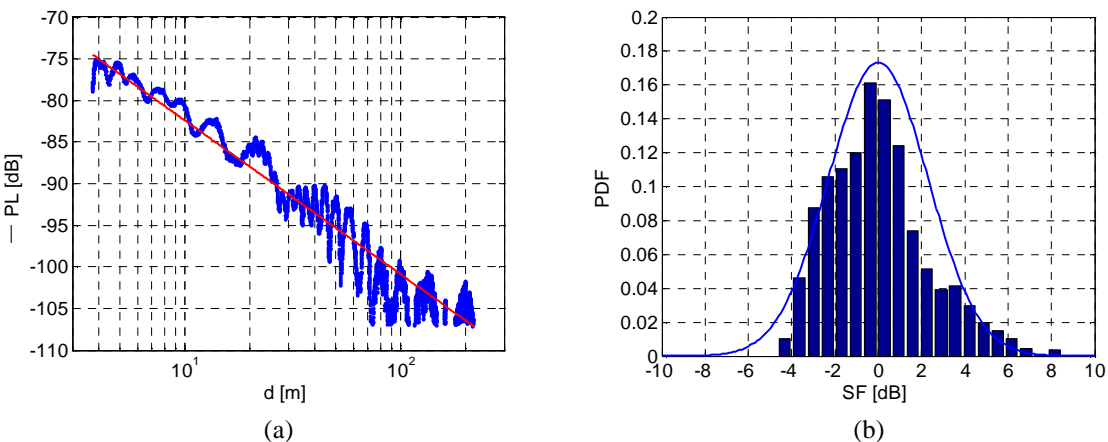


Figure 3-162: (a) Path-loss and (b) shadow fading for HMSC measurement.

3.13.3.2 Path-loss between outdoor BS and indoor UE

The complete path-loss model for the propagation from the BS to the UE in the train carriage is

$$PL = PL_{D1} + PL_{tw}$$

where

$$PL_{tw} = We + WG_e (1 - \cos(\theta))^2$$

The parameters are:

W_e = Loss through wall for the perpendicular penetration,

WG_e = Loss through wall for the parallel penetration, and

θ = angle between the normal of the wall and outgoing (incoming) ray

PL_{tw} means the penetration through the carriage windows and walls. It is calculated by the same formula as used in the Outdoor-to-Indoor case. Just the parameters have to be re-specified. This term is zero, if the MRS antenna is used outside the carriage.

From the literature [AI00] the most appropriate values for the PL_{tw} model constants have been found and they are:

$$\begin{aligned} W_e &: 20 \text{ dB}, \\ WG_e &: 12 \text{ dB}. \end{aligned}$$

Although we present the path-loss formula for BS – MRS, where the model has an extra loss term for signal interactions with the environment, we assume that using appropriate antenna placing and radiation patterns it is possible to make this extra term zero. Therefore we propose to use only the path-loss term P_{D1} in the simulations.

The formula for propagation from the BS to the UE is given for reference. Actually it is assumed not to be used in WINNER simulations.

3.13.3.3 D2a - Ricean K-factor

The Ricean K-factor has been taken from the HMSR measurement: its distance dependence and cdf are shown in Figure 3-163. The Ricean K-factor was nearly constant over the measured distance and its median value was approx. 6 dB.

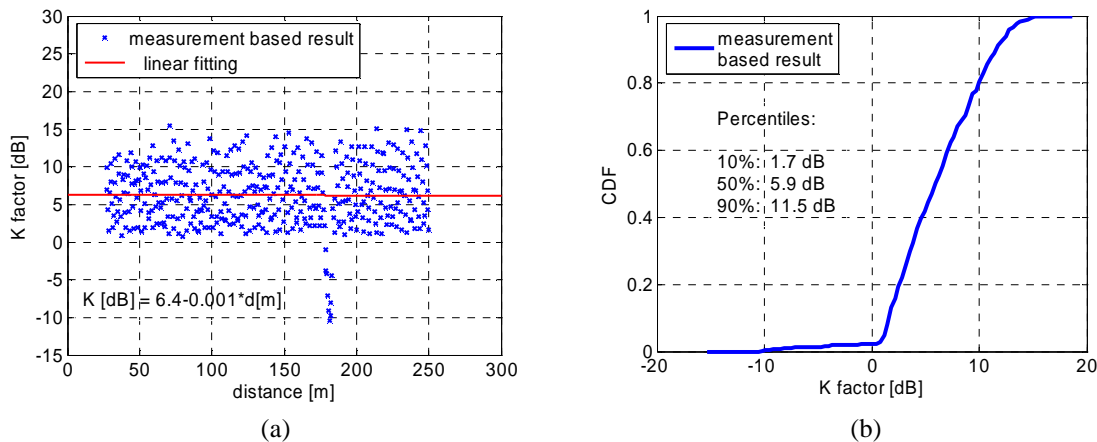


Figure 3-163: D2a LOS Scenario: (a) Ricean K factor as a function of distance, (b) CDF of the Ricean K factor.

3.13.3.4 D2a - RMS-delay spread and maximum excess delay distributions

The RMS-delay distributions for LOS case are determined from fast-train measurements (Figure 3-164).

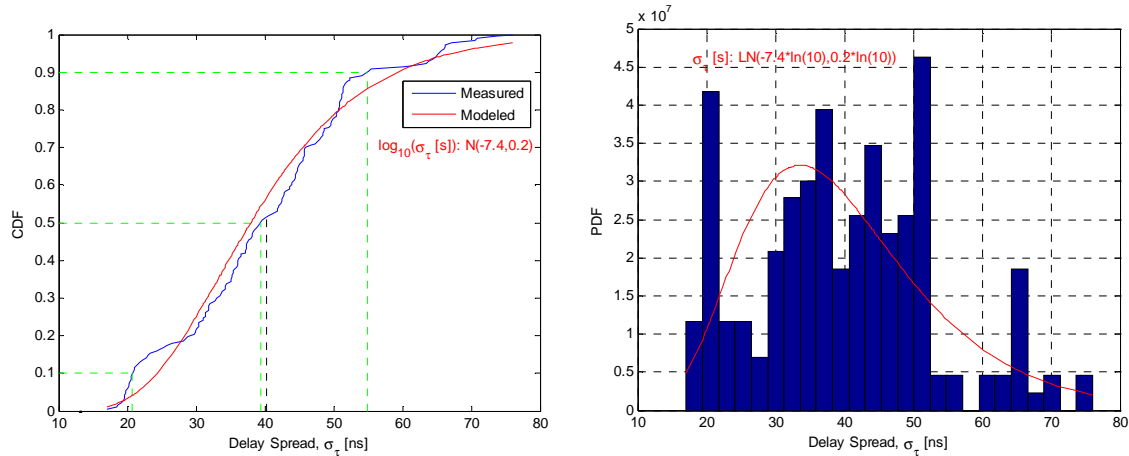


Figure 3-164: Probability functions of RMS-delay spread for D2a LOS scenario.

The RMS-delay distribution for NLOS case has been taken from the scenario D1 in [WIN1D54] by calculating mean of the values at 2.45 and 5.25 GHz. Main RMS-delay spread distributions parameters for both LOS and NLOS conditions are shown in Table below.

Table 3-62: RMS-delay spread percentiles.

RMS delay spread [ns]	LOS	NLOS
10%	21	8
50%	39	50
90%	55	110
mean	40	55

Probability distributions of max. excess delay obtained from fast-train measurements are given in Figure 3-165.

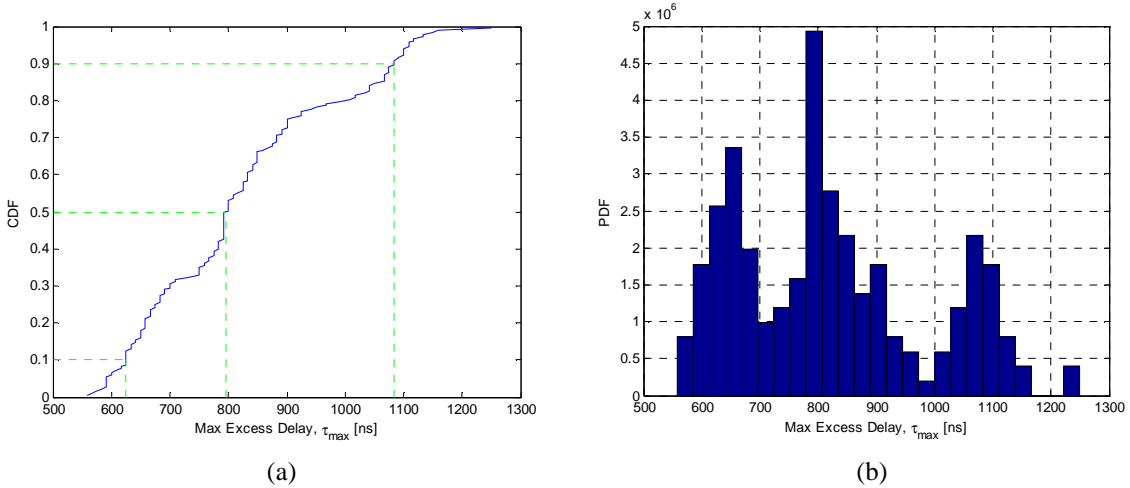


Figure 3-165: (a) Cumulative and (b) probability distribution functions of max. excess delay for D2a LOS scenario.

3.13.3.5 D2a - Azimuth AS at BS and MS

Azimuth AS for D2a LoS is determined from the HMSR (@BS) and fast-train (@MS) measurements. . For the NLOS propagation conditions D1 (rural) parameters from [WIN1D54] are used.

The placement of the Rx (on the bridge) in HMSR measurement corresponds to D2a reference setup with dominant Base-Station (BS). The cdf of circular azimuth angle spread obtained from this measurement is shown in Figure 3-166.

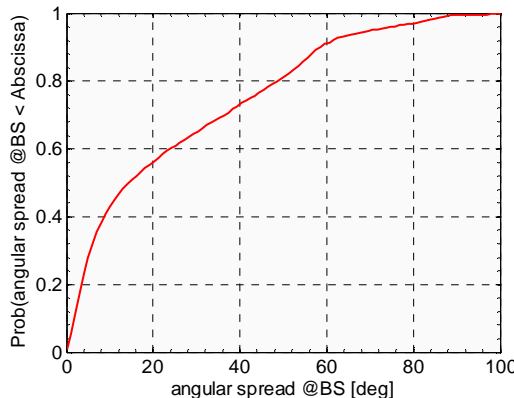


Figure 3-166: RMS angle-spreads at BS for the Bridge-2-Car scenario under LOS propagation condition.

In the fast-train (FT) measurement, height of the base station receiver antenna array is not dominant if compared to train-mounted antenna. From that reason it can be assumed that similar angular distribution will be measured at moving station. Probability distributions for azimuth angular spread at receiver side in TUI FT measurements (SIMO) are shown in Figure 3-167.

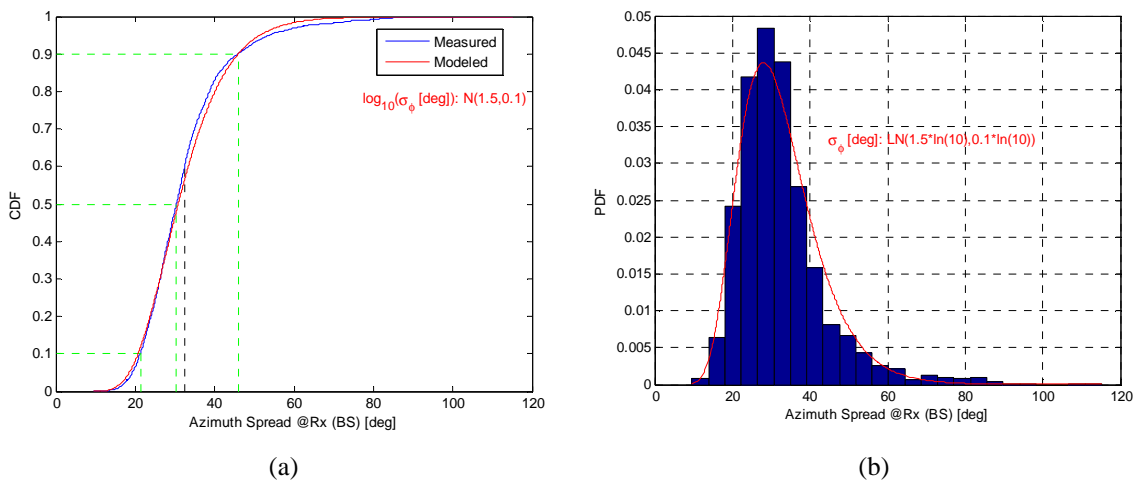


Figure 3-167: D2a LOS: a) cumulative and b) probability density functions of azimuth angular spread @ MS.

The values of the RMS azimuth spread corresponding to 10, 50 and 90 percents of the cdf are given in Table 3-63.

Table 3-63: Percentiles of the RMS azimuth spread.

D2 moving network		LOS	NLOS
BS, σ_ϕ	10%	1	5.6
	50%	5	18.0
	90%	50	34.3
	mean	21.7	19.5
MS, σ_ϕ	10%	21.3	6.0
	50%	30.4	22.3
	90%	45.9	36.4

	mean	32.5	21.9
--	------	------	------

3.13.3.6 D2a - Cross-polarisation ratio (XPR)

Cross-polarisation ratios have been taken from the scenario D1 in [WIN1D54].

Table 3-64: Percentiles of the cross-polarization ratios in a D2 environment.

D2 moving network		direct path (LOS)	scattered paths (NLOS)
XPR _V	10%	1.7	3.7
	50%	12.2	6.3
	90%	20.7	9.2
	mean / std	11.7 / 7.8	6.4 / 2.2
XPR _H	10%	3.2	3.2
	50%	13.5	6.1
	90%	23.3	9.1
	mean / std	13.2	6.1 / 2.3

3.13.3.7 D2a - Power Delay Profile

Mean PDP profiles for LOS and NLOS propagation conditions have been taken from the scenario D1 in [WIN1D54]. The LOS profile at 100 MHz bandwidth and 5.25 GHz centre-frequency are shown in the following figures.

Power delay profile for LOS conditions has been fitted to two segments with an exponential function

$$\exp(-b \cdot \tau) \quad (3.108)$$

where τ is the excess delay and b is the time-constant. Here the constant b_1 is 220 MHz for the first segment and b_2 is 15.6 MHz for the second one.

For the NLOS conditions the PDP can be fitted to the single-slope line in dB scale with the time-constant $b = 60$ MHz.

An example of PDP (averaged over QWSS interval that corresponds to 20λ) from TUI fast-train measurement is shown in Figure 3-168.

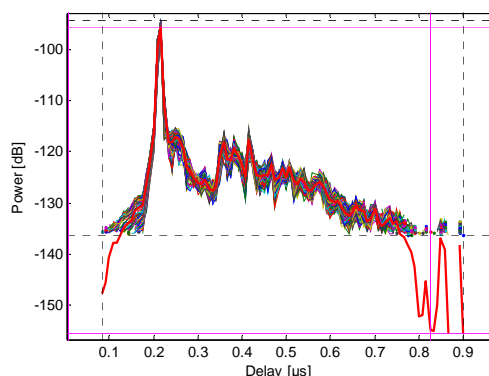


Figure 3-168: PDP example from the fast-train measurements.

3.13.3.8 D2a - Distribution of path delays

Distribution of the path delays is assumed to be exponential. The experimental pdfs determined from fast-train and HMSR measurements are shown in Figure 3-169.

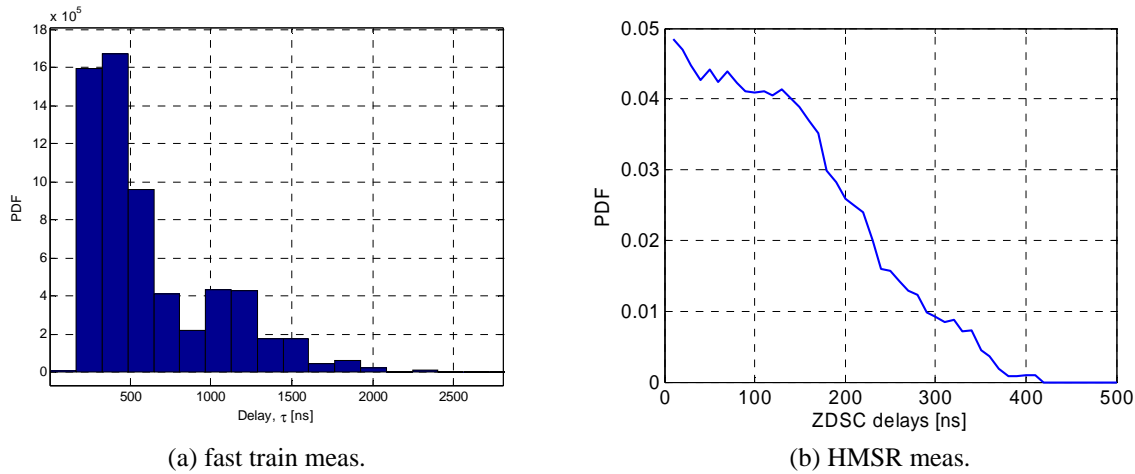


Figure 3-169: Experimental pdf of path delays for D2a LOS scenario.

3.13.3.9 D2a - Delay proportionality factor

Delay proportionality factor has been taken from the D1 model in [WIN1D54]. The percentiles for the CDF of the delay proportionality factor for scenario D2 are presented in Table 3-65.

Table 3-65: Percentiles of delay proportionality factor.

delay proportionality factor: r_τ		LOS	NLOS
Percentile	10%	2.0	1.2
	50%	3.8	1.7
	90%	8.5	2.9
	mean	4.7	1.9

3.13.3.10 D2a - Distribution of the azimuth angles

The cumulative distribution functions of the AoAs and AoDs for the multipath components at 5.20 GHz (120 MHz bandwidth) and for LOS propagation conditions is shown in Figure 3-170 for HMSR measurement. The percentiles for the CDF functions for the AoAs and AoDs are shown in Table 3-66.

Table 3-66: Percentiles of the azimuth cdf.

Link end		BS	MS
Propagation condition		LOS	LOS
Percentile (degrees)	10	-23.6	-121.8
	50	-1.8	-1.8
	90	16.4	107.3
	mean	-0.2	-1.8

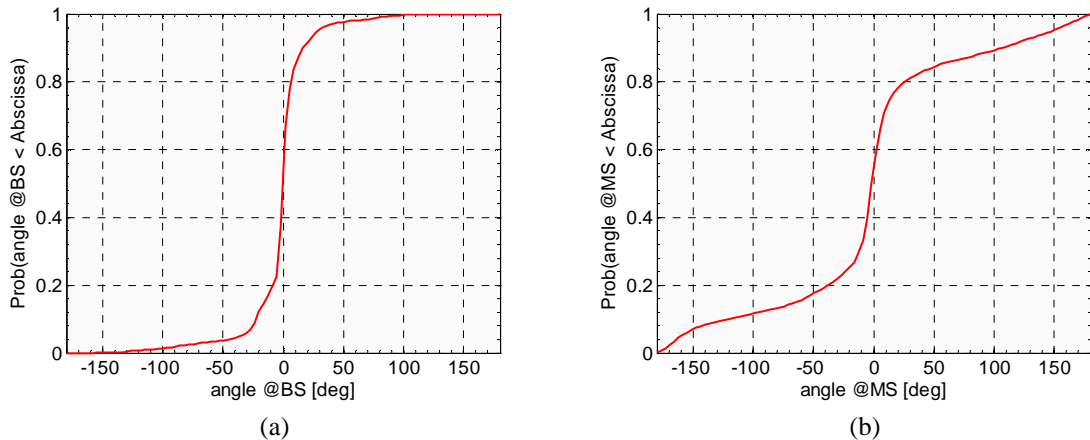


Figure 3-170: CDFs of azimuth angles at (a) BS (AoA) and (b) MS (AoD) for the High Mobility Short Range Hot Spot – (Bridge-2-Car) scenario under LOS propagation condition.

3.13.3.11 D2a - Number of clusters

The distribution of the number of clusters has been taken from the HMSR measurement and D1 model [WIN1D54]. The percentiles for the CDF of the delay proportionality factor for scenario D2 are presented in the Table 3-67.

Table 3-67: CDF values for number of clusters

Number of clusters		LOS	N LOS
Percentile	10%	1	1.0
	50%	5	6.0
	90%	17	14.0
	mean	7.4	6.7

3.13.3.12 D2a - Per-cluster shadowing

Per-cluster shadowing standard deviation is assumed to be 3 dB.

3.13.4 D2 - Literature research

[CBW95] introduces a Ray-Tracing tool IHE-TUNNEL for the calculation of signal behaviour in rail-way tunnels. Typical electrical constants for trains and rail-way environment are introduced. Typical lay-out of a High-speed train tunnel is introduced. Doppler-shift in the case of two encountering trains can be very high.

In [KMV+05] two scenarios are considered: Vegetation scenario with a tracks leading through rural environment covered with trees, and noise barrier scenario, where concrete walls are placed along the two sides of the tracks. APs are placed near the tracks and the routes are straight so that LOS conditions exist in the simulations. The train antennas are situated on the roof in the middle of the train. All antennas are omni-directional. These cases are simulated by ray-tracing assuming 5 GHz carrier frequency. In both cases a different power delay profile (PDP) is obtained as well as a different Doppler shift and Doppler delay spread. The effect of the train passing by an AP quite near the rail-way can be clearly seen in the simulations. The Doppler shift is then changed from 2 kHz to -2 kHz within one second. These figures are, of course, dependent on the train speed and the distance from the AP to the rail-way as well as the carrier frequency. In this simulation the train speed is 400 km/h, carrier frequency 5 GHz and the distance of AP to the train is only few meters. Consequences for an OFDM based system are considered. 2 kHz Doppler shift is seen problematic for systems with the sub-carrier spacing of same size.

[OKT+04] describes a Japanese WLAN trial system with connections also to trains. Actually there were several frequency bands investigated in the trial, but we concentrate here on the one most similar to the WINNER definitions. There the operating frequency is about 5 GHz and the band-width is 16.5 MHz according to the Japanese version of the ETSI BRAN HiperLAN2. OFDM is used.

In the trial relays were used for the connections, like in the current WINNER concept: The link between the Access Point and Train (AP – MR) was a Moving Feeder Link at 5 GHz frequency. The links from the MR to the Users operated at 2.4 GHz. The MR antenna towards the AP was a directive horn antenna, as the AP antenna. Actually there were two antennas for the diversity effect in the APs and MR. The placement in the train, deduced from a picture, was at the end of the carriage roof. For a High-Speed train possibly a questionable positioning, but the reported speed was not actually High-Speed level, but it was 120 km/h in this trial. The MR antennas towards the UEs were dipole antennas, two per MR for the diversity. The placement of the AP was near the rails (about 3 m) and the height was about 2 m, deduced by a figure. Obviously the strategy was to illuminate the train from the direction of the rails. This is consistent with the placing of the MR antennas.

The trial showed that OFDM signal could be transmitted up to 800 m, although the obtained throughput decreased to 14 per cent from the maximum with the increasing distance and train speed. Doppler did not cause any problem in the trials and hand over was operated with success.

[AGV98] discusses propagation in High Speed Train tunnels at 2.154 GHz carrier frequency in 53.85 MHz RF bandwidth (chip rate). Vertical polarisation was transmitted. Path-loss was found to change about 30 dB in 200 m distance from the BS location. The BS height 3.7 m inside the tunnel gave good results for path-loss. RMS delay spread ranged from about 10 to 250 ns. Cross-polarisation value of 18 dB was obtained. Doppler frequency corresponding the speed 350 km/h was measured to be about 800 Hz and Doppler spread of 200 Hz was reported. The values have to be calculated from normalised values, because 350 km/h is not a realistic measuring velocity.

In [KBM+06] the authors investigate the effect of using directive antennas at the moving High Speed Train in similar scenarios as in [KMV+05]. The results show that by using directive antennas the RMS delay spread can be reduced near 25 % of the corresponding values of the omni-directional case. The Doppler spreads behave in a similar manner. This reference clearly shows the benefit of using directive antennas in the train.

[AI00] discusses the provision of voice services to high-speed trains based on literature. The authors consider fast fading, Doppler, slow fading, penetration loss and propagation in tunnels. The aim is to find good channel models for the train scenario. The discussion is mostly based on GSM due to the age of the references used. Many references are from the European project MOSTRAIN. However, some results are relevant for WINNER, at least with some updating. The authors discuss the slow fading experienced in deep cuttings, if off-track-side Base Stations are used. On the other hand they claim that track-side Base Stations suffer from high penetration loss from the BS to the interior of the train. However, this effect has been removed in WINNER, where Moving Relays are used with the antennas on top of the train. Another problem of the track-side Base Stations remain, i.e. the fast change of the mean Doppler shift near the BS. Propagation in tunnels is discussed in several articles, like in [AGV98]. In [AI00] the authors conclude that the tunnels provide a good propagation medium. Although the measurements have been performed at 2 GHz, the result should remain valid also for the range 2 – 6 GHz as well.

3.13.5 D2 - Interpretation of the results

As discussed above, the model is not complete yet. It does cope for only the LOS connections between the BS and MRS. The tunnels and other NLOS environments have not been coped for. In addition, the systematic inclusion of the Doppler shift and its evolution is still missing. In spite of this the model is a good start for specifying the D2a link BS to MRS. According to literature, the tunnel environment was claimed to be a rather favourable one for the fast trains.

Our model provides the other relevant parameters for the simulations and the scenario definition is compliant with many of the current trials.

3.14 Path Loss frequency dependency

In [WIN2D111], the frequency dependency of all the pathloss models is $20 * \log_{10}(f/5\text{GHz})$. Some open literature is available to discuss the path loss frequency dependencies, e.g. [RMB+06], [CG99], [ITU-R], [JHH+05] and their related references. In [ITU-R], some explicit intra- or inter-polation were given when using the measured path losses at two different frequencies to predict the PL within or without the

measured frequency bands. However, for WINNER path loss models, they were mainly developed by measurements at 5 GHz. In order to get the accurate frequency dependence of the path loss, elaborate calibration is needed, and more over, the selected antenna types are also very important. In [RMB+06] is mentioned that it is better to use dipole antennas and then the antenna radiation pattern in the elevation plane can be kept the same. The conclusions of [RMB+06] is that when carrier frequency is increased, the additional loss is quite large when going from 450 MHz to 900 MHz which results in $30*\log_{10}(f)$ dependency on average. When going from 900 MHz to 1800 MHz or from 1800 MHz to 5100 MHz the additional loss is smaller and a $23*\log_{10}(f)$ dependency is seen on average, which is a bit close to WINNER model ($20*\log_{10}(f)$). In [RMB+06], the measurements were for macrocells. The measurement scenarios include urban and suburban environments. In [CG99], by summarizing some published measurement results and performing the linear regression of the measured data, it was concluded that for NLOS urban and suburban macrocells, the frequency dependency was $26*\log_{10}(f)$; In urban microcells when the base station antenna height is at or below the surroundings, frequency dependency could be $31*\log_{10}(f)$ due to diffractions.

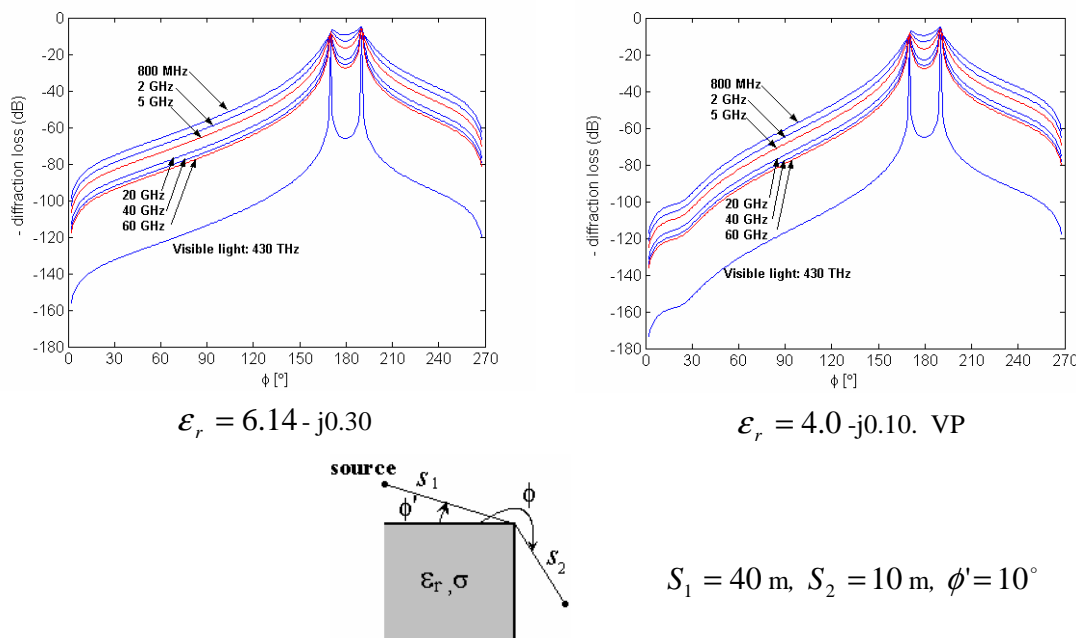


Figure 3-171: Diffraction frequency responses for a lossy wedge.

However, frequency dependencies of the diffraction by a building or indoor corner in the above figures (calculated by theory) show that in NLOS the $20*\log_{10}(f)$ still holds.

In contrast to urban and suburban environments, signals propagating over rural environments are subjected to very little diffraction. The frequency dependency can be again $20*\log_{10}(f)$ which is supported by Hata's model. However, if there is heavy tree obstruction, then the frequency dependency can also be: $30*\log_{10}(f)$ [CG99].

In [JHH+05], UWB measurements were performed in indoor environments, the frequency dependencies of path loss were found to be $20*\log_{10}(f)$.

One available paper for the measured penetration loss of the buildings using a balloon is [Rudd03]. The following figure shows that the penetration loss has a slight frequency dependency in the results. Mean values of the loss are 9.2 dB at 1.3 GHz, 11.2 dB at 2.4 GHz, and 12.7 dB at 5.7 GHz. Based on [Rudd03], the frequency dependency of the penetration loss can be less than $20*\log_{10}(f)$. However, so far no theoretical results can be found.

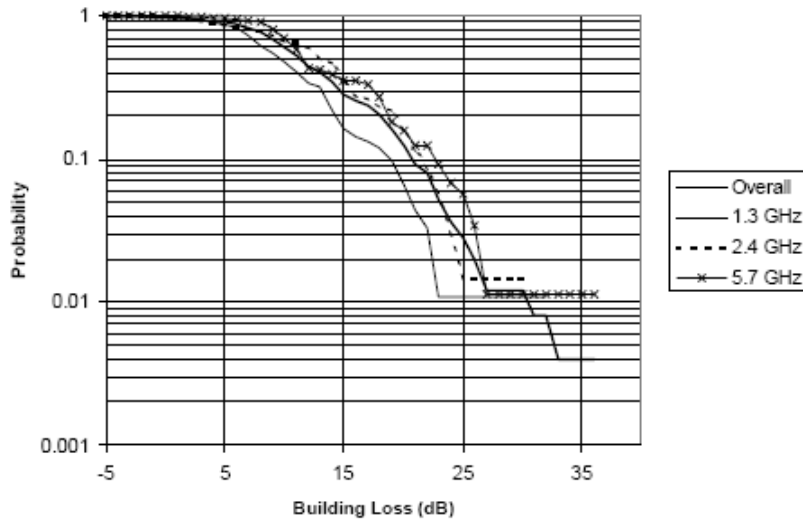


Figure 3-172: Frequency dependence of building penetration loss

In [BSK+07], measurements were performed at 1.9 and 5.8 GHz, the mean pathloss difference is 8.1, it supports $20 \cdot \log_{10}(f)$ frequency dependence.

In [SMI+02] which were for measured path loss for urban macrocells, the frequency bands: 3.35 GHz, 8.45 GHz and 15.75 GHz. It's seen that the frequency dependencies of path loss can be $22.8 \cdot \log_{10}(f)$ and also $26.3 \cdot \log_{10}(f)$ for base station heights of 55 m and 10 m, respectively. For macrocells, 10 m BS is too low, so that in urban macrocells the frequency dependency still could be $23 \cdot \log_{10}(f)$.

In [OTT+01], pathloss measurements were carried out in the 457.2 MHz, 813 MHz, 2.2. GHz, 4.7 GHz, 8.45 GHz and 15.45 GHz in both macrocell and microcell environments for comparisons at different frequencies under similar conditions for all frequency bands. All the results were show $20 \cdot \log_{10}(f)$ frequency dependencies of the path loss. The trends are similar to the Walfisch-Bertoni model [reference [3] in OTT+01], but differ from the Hata and COST-Walfisch-Ikegami models [references [2] and [4] in OTT+01], where the coefficients of the frequency term in the Hata, Walfisch-Bertoni, and COST-Walfisch-Ikegami models are approximately 26, 21, and 26 to 29, respectively. The measurements were performed, however, below 2 GHz.

In [KI04], measurements were performed at 0.457/0.813/2.2/3.35/4.7/5.2/8.45 GHz for urban macrocells in three cities. The final frequency coefficient was 20.7. However, we can also find the coefficient can be 22, 24, 23 as well as 20.

In [YIT06], the measured were performed at 0.8/5/8 GHz for urban macrocells, the measured medians of the differences in frequency domain in path loss are: 18.3 dB between 0.8 and 5 GHz, 23.3 dB between 0.8 and 8 GHz, 5.4 dB between 5 and 8 GHz. The median frequency dependency of path loss is $23.2 \cdot \log_{10}(f)$.

In [Fuj03], the measurements were for urban and suburban macrocells, it offers one general path loss formula, and the frequency dependence is: $20 \cdot \log_{10}(f)$.

It can be seen that most of the measurements introduced above were mainly for urban and suburban macrocells, there are not enough measurements for indoor-to-outdoor, and outdoor-to-indoor scenarios.

Suggestions for WINNER path loss frequency dependencies

- (1) All the LOS scenarios, and for rural NLOS , keep $20 \cdot \log_{10}(f_c/5\text{GHz})$ as in the present models.

- (2) For NLOS urban and suburban macrocells, the frequency dependency can be $23 \cdot \log_{10}(f_c/5\text{GHz})$
- (3) For urban microcells: $23 \cdot \log_{10}(f_c/5\text{GHz})$.
- (4) For indoor environments: $20 \cdot \log_{10}(f_c/5\text{GHz})$.
- (5) Outdoor-to-indoor environments: $20 \cdot \log_{10}(f_c/5\text{GHz})$, where the frequency dependence of the penetration loss should be key factor to decide the frequency dependence of the path loss.
- (6) Indoor-to-outdoor: can also be $20 \cdot \log_{10}(f_c)$.
- (7) For feeder scenarios, in urban and suburban environments: $23 \cdot \log_{10}(f_c/5\text{GHz})$, otherwise keep $20 \cdot \log_{10}(f_c/5\text{GHz})$.

4. Analysis items

Purpose of this section is to give unambiguous definition of parameters like e.g. XPR and Delay scaling parameter r_v . Originally the analysis items are described in WINNER II internal report [WIN2IR112].

All analysis items could be sorted into 5 groups, related to domain that are calculated from (Delay, Angular), to joint processing of both domains (Cluster), or to the property that they describe (Polarization, Correlation), as shown in Figure 4-1:

- Delay
- Angular
- Cluster
- Polarization
- Correlation

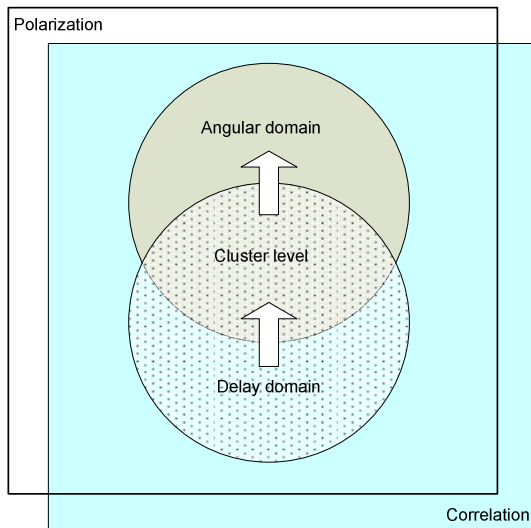


Figure 4-1. Analysis items grouping.

Described grouping of analysis items would be used to organize content of this document. However, more important relations are coming from the computation sequence that shows which analysis items have been used as required input when other items are calculated.

4.1.1 Delay domain

4.1.1.1 Channel Impulse Response (Per Polarization)

D1 - Channel Impulse Response (Per Polarization)		
Short Parameter Name		WIM parameter
CIR(PerPolarization)		WIM validation
		priority 1
<ul style="list-style-type: none"> - Channel impulse response is a function of time, delay, position of transmitting and receiving antennas, and their position: $h(t, \tau, s, u, p)$. Single realization of $h(\tau)$ is provided for every sub-channel (s, u, p) inside every snapshot (t-dim). - If $h(\tau)$ for (t, s, u, p) dim does not satisfy SNR criterion it would not be used for further processing 		
Extraction procedure		
#	verbal	math
	for each (t, s, u, p)	
1	Estimate noise threshold	
2	If the difference between the level of the highest peak and the noise level exceeds predefined value, CIR is valid	
3	For valid CIR set all values below noise level to zero	
4	Valid snapshot contains at least one valid CIR	
5	Form snapshots set as collection of n_t consecutive valid snapshots, where n_t represents number of snapshots inside stationarity interval.	
Results reported as		
Figure	CIR magnitude	<p> CIR [dB]=func(Delay [ns])</p> <p>Magnitude of CIR can be shown as a function of, at most, 3 dimensions: e.g. time, delay and polarization. But even if 2 dimensions (1. time, 2. delay, and in 3. dim. CIR is showed) are used, 3D picture is not of practical usage (such graph is usually used only for overview). Contour 2D plot, having 3rd dimension represented by the colour usually offers more insight.</p> <p>Most natural approach would be to show dependence only over 1 dim, $h(\tau)$, while another dimensions are used for parameterization. It would be best if only one dimension-parameter is changed per figure: e.g. $h(\tau t_i)$, $t_i = 1, \dots, n_t$, while (s, u, p) dimensions are kept constant.</p>
	Noise level	Show estimated noise level together with CIR, or use noise level as starting point for ordinate axis (the latter is preferred).

<i>Table</i>	If percent of valid values per sub-channel is calculated it is possible to compare quality of measurements (as whole, per sub-channel (s, u, p), or per polarization).
--------------	--

4.1.1.2 Time Variant Power Delay Profile (Per Polarization)

D2 – Time Variant Power Delay Profile (Per Polarization)

Short Parameter Name TimeVariantPowerDelayProfile(PerPolarization)	<i>WIM parameter</i>
	<i>WIM validation</i>
	priority 1

- Averaged power of CIR over (s, u) dimensions.
- If comparison of parameters (AI) for different (s, u) dimensions is to be done, averaging step can be skipped

Extraction procedure

#	verbal	math
	for each snapshot (t -dim)	
1	Calculate instant powers	$P(t, \tau, s, u, p) = h(t, \tau, s, u, p) ^2$
2	Detect delay corresponding to highest peak.	$\tau_m(p) = \arg \max_{\tau} (P(\tau, p))$
3	Introduce delay-shift in order to align highest peaks of all CIR components.	$P(t, \tau', s, u, p) = P(t, \tau - \tau_m, s, u, p)$
4	Average the instant powers over (Tx,Rx) dimensions	$P(t, \tau', p) = \frac{1}{N_s N_u} \sum_{s=1}^{N_s} \sum_{u=1}^{N_u} P(t, \tau', s, u, p)$

Results reported as

<i>Figure</i>	$PDP(t)$	Power [dB]=func(Excess delay [ns]) with time (or snapshot number) as a parameter. Show variation of PDP over time $P(\tau' t_i,)$, $t_i = 1, \dots, n_t$, while (s, u, p) dimensions are kept constant. Measured data can be represented by different lines.
<i>Table</i>	If averaging of TimeVatiantPowerDelayProfile over (s, u) -dim is skipped, table reporting percent of total received power for each (s, u, p) -dim can be used.	

Additional Processing instructions

Comments
Averaging over t -dim is performed in separate step, to allow use of non-averaged data in detection of number of clusters.

4.1.1.3 Power Delay Profile (Per Polarization)

D3 - Power Delay Profile (Per Polarization)		
<i>Short Parameter Name</i>		<i>WIM parameter</i> x
PowerDelayProfile(PerPolarization)		<i>WIM validation</i> x
		<i>priority</i> 1
<ul style="list-style-type: none"> - Averaged TimeVariantPowerDelayProfile over n_t snapshots, where n_t represents number of snapshots contained inside Stationarity Interval (SI). 		
Extraction procedure		
#	<i>verbal</i>	<i>math</i>
	for each snapshot set (collection of n_t consecutive valid snapshots)	
1	Average TimeVariantPowerDelayProfile $P(t, \tau^*, p)$ over t dimension	$P(\tau^*, p) = \frac{1}{n_t} \sum_{i=1}^{n_t} P(t_i, \tau^*, p)$
Results reported as		
<i>Figure</i>	<i>PDP</i>	Power [dB]=func(Excess delay [ns]). Per (s, u, p) dimension dependence $P(\tau^* s, u, p)$ can be showed. Measured data can be represented by line.
<i>Table</i>	If averaging of TimeVariantPowerDelayProfile over (s, u) -dim. is skipped in previous processing step, table reporting percent of total received power for each (s, u, p) -dim. could be reported.	

4.1.1.4 Max. Excess Delay

D4 - Max. Excess Delay

<i>Short Parameter Name</i>		<i>WIM parameter</i>		
MaxExcessDelay		<i>WIM validation</i>		
		<i>priority 1</i>		
<ul style="list-style-type: none"> - Maximum delay bin with non-zero power in . 				
Extraction procedure				
#	<i>verbal</i>	<i>math</i>		
for each snapshot set (collection of n_t consecutive valid snapshots)				
1	Find maximum excess delay bin with non-zero Power in PowerDelayProfile	$\tau'_{\max}(p) = \max_{\tau'} \arg(P(\tau', p) > 0)$		
2	Collect values (calculated at SS level) for the duration of the whole measurement, in order to estimate pdf, cdf, correlation coefficient or distance.	$\text{pdf}(\tau'_{\max}, p)$		
Results reported as				
<i>Figure</i>	<i>pdf</i>	<code>pdf=func(Max. excess delay [ns]).</code>		
	<i>cdf</i>	<code>cdf=func(Max. excess delay [ns]).</code>		
<i>Table</i>	Use default table for certain plot type (see 6.Common processing methods).			
Additional Processing instructions				
Comments				
This parameter is strongly influenced by the measured CIR quality, since τ'_{\max} represents crossing of PDP and the noise level. This means that some percent of total power, that is below noise level stays undetected.				

4.1.1.5 Delay Spread

D5- Delay Spread

Short Parameter Name DelaySpread	<i>WIM parameter</i>	x
	<i>WIM validation</i>	x
	<i>priority</i>	1
– Statistical second order central moment, where pdf is estimated from PDP (PAS)		
Extraction procedure		
#	<i>verbal</i>	<i>math</i>
for each snapshot set (collection of n_t consecutive valid snapshots)		
1	Use only upper 20dB of PowerDelayProfile. Skip snapshots that do not provide 20 dB dynamics.	$P^*(\tau_i, p) = \begin{cases} P(\tau_i, p) & P(\tau_i, p) \geq \max\{P(\tau_i, p)\}/100 \\ 0 & \text{otherwise} \end{cases}$
2	Estimate power-distribution-function (pdp) from PDP.	$p(\tau_i, p) = \frac{P^*(\tau_i, p)}{\sum_{i=1}^{N_x} P^*(\tau_i, p)}$
3	Calculate the first and the second order moment	$\bar{\tau}(p) = \sum_{i=1}^{N_x} \tau_i p(\tau_i, p)$ $\bar{\tau^2}(p) = \sum_{i=1}^{N_x} \tau_i^2 p(\tau_i, p)$
4	Calculate the standard deviation (spread)	$\sigma(p) = \sqrt{\bar{\tau^2} - \bar{\tau}^2}$
5	Collect values (calculated at SS level) for the duration of the whole measurement, in order to estimate pdf, cdf, correlation coefficient or distance. See common processing method named Correlation/Covariance.	$\text{pdf}(\sigma, p), \text{cdf}(\sigma, p), \text{CorrC}(\sigma, p), \text{CorrD}(\sigma, p)$
Results reported as		
Figure	<i>cdf</i>	<code>cdf=func(Spread [<spread_unit>])</code>
	<i>CorrC</i>	<code>CrossC=func(Spread [<spread_unit>])</code>
Table	Use default table for certain plot type (see 6.Common processing methods).	
Value	<i>CoorD</i>	Correlation distance.

Additional Processing instructions
Comments

Usage of upper 20 dB of PDP gives biased estimate being independent from SNP per snapshot.

4.1.1.6 Total Power (Per Polarization)

D6 – Total Power (Per Polarization)		
<i>Short Parameter Name</i>		<i>WIM parameter</i>
TotalPower(PerPolarization)		<i>WIM validation</i>
		<i>priority</i> 1
<ul style="list-style-type: none"> – Sum of PowerDelayProfile over N_τ delays, where N_τ represents number of samples of CIR in delay domain (τ-dim). 		
Extraction procedure		
#	<i>verbal</i>	<i>math</i>
	for each snapshot set (collection of n_t consecutive valid snapshots)	
1	Sum PowerDelayProfile $P(\tau', p)$ over τ' dimension	$P(p) = \sum_{i=1}^{N_\tau} P(\tau'_i, p)$
Results reported as		
<i>Figure</i>		
<i>Table</i>		

4.1.1.7 Path Loss

D7 - Path Loss		
<i>Short Parameter Name</i>		<i>WIM parameter</i> x
PathLoss		<i>WIM validation</i> x
		<i>priority</i> 1
<ul style="list-style-type: none"> – Dependence of the power loss from distance 		
Extraction procedure		

#	verbal	math
	It is calculated for each snapshot set (collection of n_t consecutive valid snapshots) from Power(PerPolarization).	
1	For each SS distance between Tx and Rx has to be known.	$P(p) \xrightarrow{d} P(d, p)$
2	Additional input parameters are also required: Transmitter power (P_{Tx}), total (Tx and Rx) antenna gain $\left(\sum_i G_i\right)$ and total cable attenuation $(\sum_i A_i)$	$PL(d, p) = P_{Tx}(p) + \sum_i G_i - \sum_i A_i - P(d, p)$
3	For $PL(d, p)$ data collected at measurement level, perform linear regression. It is assumed that the least squares criterion is used, as in the MATLAB function regress().	$\begin{bmatrix} PL(d_1, p) \\ \vdots \\ PL(d_n, p) \end{bmatrix} = \begin{bmatrix} 1 & d_1 \\ \vdots & \vdots \\ 1 & d_n \end{bmatrix} \begin{bmatrix} B(p) \\ A(p) \end{bmatrix}$
4	Use linear expression to describe expected path loss. Provide second expression if double slope model is used.	$\overline{PL}(d, p) = A(p) \log_{10}(d) + B(p)$
Results reported as		
Figure	PL	PL [dB]=func(distance [m]) Show 3 data sets 1)measured data, 2)linear regresion, 3) Free-space PL. Expected and free-space PL are shown as straight lines, while measured data points are represented with marks. Add expression to Figure.
Table	Use default table for certain plot type (see 6.Common processing methods).	
Expression1	$\overline{PL}(d, p) = A(p) \log_{10}(d) + B(p)$ as well as all calculated values of A and B should be provided.	

4.1.1.8 Standard Deviation of Shadow Fading

D8 - Standard Deviation of Shadow Fading

Short Parameter Name	WIM parameter	x
ShadowFadingStd.	WIM validation	x
	priority	1
– Deviation of measured data from expected PathLoss.		
Extraction procedure		
#	verbal	math

	for each snapshot set (collection of n_t consecutive valid snapshots)
1	For data points $PL(d_n, p), n = 1..N_{SE}$ calculate the deviation from expected path loss $\overline{PL}(d_n, p)$. Both PL and \overline{PL} are dimensionless.
2	Collect values (calculated at SS level) for the duration of the whole measurement, in order to estimate pdf, cdf, correlation coefficient or distance. See common processing method named Correlation/Covariance.
3	Estimate the mean value of standard deviation for complete measurement set (over all SS) $\sigma_{SF}(p) = \sqrt{\frac{1}{N_{SE}-1} \sum_{n=1}^{N_{SE}} [SF_n(p)]^2}$
Results reported as	
Figure	pdf <code>pdf=func(SF[dB])</code>
	CorrC <code>CrossC=func(SF[dB])</code>
Table	Use default table for certain plot type (see 6.Common processing methods).
Value	Std. SF Standard deviation of shadowing fading, $\sigma_{SF}(p)$
	CoorD Correlation distance.

4.1.1.9 Narrowband K-factor (by Moment Method)

D9 – Narrowband K-factor (by Moment Method)

Short Parameter Name	WIM parameter	x
NarrowbandK-factor(MoM)	WIM validation	x
	priority	1
– Narrowband Ricean K-factor is equal to the ratio of powers between dominant (both LOS and NLOS condition) and all other multi-path components.		
Extraction procedure		
#	verbal	math
	for each snapshot set (collection of n_t consecutive valid snapshots)	
1	Perform analysis of wideband CIR in N narrowband frequency bins (see Comments). Narrowband (partial) CIR from i-th bin is	

labelled as $h_i(t)$.	
2	Calculate instant power of narrowband (partial) CIR. $P_i = h_i(t) ^2$
3	Calculate mean value and variance of instant power. $E\{P_i\} = \frac{1}{n_t} \sum_{i=1}^{n_t} P_i$ $Var\{P_i\} = \frac{1}{n_t - 1} \sum_{i=1}^{n_t} (P_i - E\{P_i\})^2$
4	Calculate narrowband using Moment Method (MoM) proposed in [1]. $m_i = \sqrt{(E\{P_i\})^2 - Var\{P_i\}}$ $K_i = \frac{1}{\frac{E\{P_i\}}{m_i} - 1}$
5	If distance information is available for all measurement set, approximate dependence of K-factor over distance by linear regression. $K_i [dB] = C_i + D_i \cdot d [m]$
Results reported as	
<i>Figure</i>	$K(\Delta f_i)$
	$K_i [dB] = \text{func}(\text{frequency bins [MHz]})$ $K_i(d), i = 1..N$ If linear approximation is available use 2 data sets: 1)original data (marker), 2)linear regression
<i>Table</i>	
Additional Processing instructions	
Comments	
Proposed method is valid only for narrowband K-factor: calculated values are appropriate for frequency segments narrower than the correlation bandwidth (B_c) of the channel, when averaging period is longer than correlation time of the short-term fluctuations [1]. If this property is to be analyzed for selective fading channels, separate analysis is to be performed per frequency bins narrower than B_c . Value of K-factor can be used to estimate probability of Line-Of-Site condition.	
See also	
[1] Greenstein et al: "Moment method estimation of the Ricean K-factor", IEEE Comm. Lett. Vol 3, Issue 6, p.175, 1999.	

4.1.2 Both domains (Delay-Angular)

4.1.2.1 Proportionality Factor (Delay, Angular)

DA1 - Proportionality Factor (Delay, Angular)

Short Parameter Name	WIM parameter	x
ProportionalityFactor (Delay, Angular)	WIM validation	x
	priority	1
<ul style="list-style-type: none"> - Ratio of standard deviation calculated from pdf and spread calculated from power distribution function (pdp or pas) - Shows relation between parameters (2nd central moments) of probability and power distribution functions. - For current modelling purposes, where both probability and power distribution have same analytical form, and both distributions use only one control parameter, proportionality factor completely describes their interdependence. 		
Extraction procedure		
#	verbal	math
for each snapshot set (collection of n_t consecutive valid snapshots)		
1	Proportionality factor is calculated as a ratio of parameters used by pdf and power distribution function (pdp)	If, in delay domain, $\text{pdf}(\tau) \propto e^{-\frac{\tau}{\sigma_{\text{pdf}}}}$ and $\text{PDP}(\tau) \propto e^{-\frac{\tau}{\sigma_{\text{pdp}}}}$ than $r_\tau = \frac{\sigma_{\text{pdf}}}{\sigma_{\text{pdp}}}$
2	Since wrapping is introduced in angular domain σ_{pdf} and σ_{pas} DO NOT represent true standard deviation!	If, in angular domain, $\text{pdf}(\varphi) \propto e^{-\frac{1}{2}\left(\frac{\varphi}{\sigma_{\text{pdf}}}\right)^2}$ and $\text{PAS}(\varphi) \propto e^{-\frac{1}{2}\left(\frac{\varphi}{\sigma_{\text{pas}}}\right)^2}$ than $r_\varphi = \frac{\sigma_{\text{pdf}}}{\sigma_{\text{pas}}}$
3	Collect values (calculated at SS level) for the duration of the whole measurement, in order to estimate pdf and cdf	
Results reported as		
Figure	cdf	cdf=func(Proportionality factor [<PF unit>])
Table	Use default table for certain plot type (see 6.Common processing methods).	

4.1.2.2 MPC Parameters

DA2 - MPC Parameters

<i>Short Parameter Name</i>	<i>WIM parameter</i>
<i>MPCParameters</i>	<i>WIM validation</i>
	<i>priority 1</i>
<ul style="list-style-type: none"> - Pair $[(\tau_i, \phi_i, \varphi_i), P_i]$ uniquely identifies one multi-path component: triplet $(\tau_i, \phi_i, \varphi_i)$ defines coordinates in delay-angular domain, while P_i is power associated with MPC. If elevation information is to be used multi-path component is described by two additional components (θ_i, ϑ_i). 	
Extraction procedure	
#	<i>verbal</i>
for each snapshot	
Apply high-resolution procedure for extraction of $[(\tau_i, \phi_i, \varphi_i), P_i]$ for all resolvable MPCs.	
1	If necessary, from previous procedure elevation angles (θ_i, ϑ_i) could be also obtained.
Results reported as	
<i>Figure</i>	MPCPower $\text{Power}[\text{dB}] = \text{func}(\text{Delay} [\text{ns}], \text{AoD} [\text{deg}], \text{AoA} [\text{deg}])$ 4D representation (Power dependence over 3 dimensions) can be used for illustrative purposes.
<i>Table</i>	MPC Parameters could be reported inside table: one row per MPC, with 4 columns: Delay [ns], AoD [deg], ,AoA [deg] (for azimuth and/or elevation) and Power[dB]. MPC could be sorted with increasing delay.

4.1.3 Angular domain

4.1.3.1 Power Angular Spectrum

A1 - Power Angular Spectrum		
<i>Short Parameter Name</i>		<i>WIM parameter</i>
<i>PowerAngularSpectrum</i>		<i>WIM validation</i>
		<i>priority 1</i>
<ul style="list-style-type: none"> - Distribution of power over departure/arrival angle 		
Extraction procedure		
#	<i>verbal</i>	<i>math</i>
for each snapshot		

	Reconstruct dependence $P_i(\phi_i)$ or $P_i(\varphi_i)$ from MPCParameters. Same applies to $P_i(\theta_i)$ or $P_i(\vartheta_i)$ if information about elevation angles is available.
1	Average the PAS for all snapshots belonging to the same snapshot set (collection of n_t consecutive valid snapshots)
Results reported as	
<i>Figure</i>	PAS Power [dB]=func(Departure/Arrival angle [deg]) It is possible to use 3D figure to show joint distribution or 2D for two marginal distributions.
<i>Table</i>	

4.1.3.2 Main DoA Offset From Line-Of-Site direction

A2 - Main DoA Offset From Line-Of-Site direction		
	<i>Short Parameter Name</i>	<i>WIM parameter</i>
	MainDoAOFFsetFromLOS	<i>WIM validation</i>
		<i>priority</i> 1
<ul style="list-style-type: none"> - Expected difference between DoA and LOS direction, calculated for each stationarity interval (snapshot set) 		
Extraction procedure		
#	<i>verbal</i>	<i>math</i>
	for each snapshot set (collection of n_t consecutive valid snapshots)	
1	Angular distribution is estimated from MPCParameters. DoA offset is equal to difference between mean angular value and LOS direction. Additional information expressing LOS direction in respect to antenna broadside is necessary.	$\phi_0 = E\{\phi\} - \phi_{LOS}$
2	Collect values (calculated at SS level) for the duration of the whole measurement, in order to estimate pdf or cdf.	
Results reported as		
<i>Figure</i>	<i>pdf</i>	

Table	

4.1.3.3 Angular Spread (Azimuth, Elevation)

A3 – Angular Spread

Short Parameter Name	WIM parameter	x
AngularSpread	WIM validation	x
	priority	1
– Statistical second order central moment (standard deviation), estimated from PAS		
Extraction procedure		
#	verbal	math
	for each snapshot set (collection of n_t consecutive valid snapshots)	
1	Introduce shift Δ to all angles. Mean and standard deviation are shift dependant since wrapping of angles to certain range represents nonlinear operation.	$x_i(\Delta) = x_i + \Delta, x_i \in \{\phi_i, \varphi_i\}$
2	Wrap angles: azimuth range $[-\pi, \pi]$, elevation range $[-\pi/2, \pi/2]$.	$x'_i(\Delta) = \text{mod}(x_i(\Delta), WR), WR = \begin{cases} 2\pi & \text{azimuth} \\ \pi & \text{elevation} \end{cases}$ $\text{if } x'_i(\Delta) > \frac{WR}{2} \Rightarrow x'_i(\Delta) = x'_i(\Delta) - WR$
3	Estimate power-distribution-function (pas) from PAS	$\text{pas}(x'_i(\Delta), p) = \frac{P(x'_i(\Delta), p)}{\sum_{i=1}^{N_x} P(x'_i(\Delta), p)}$
4	Calculate the first order moment (mean value)	$\bar{x}'(\Delta, p) = \sum_{i=1}^{N_x} x'_i(\Delta) \text{pas}(x'_i(\Delta), p)$
5	Subtract mean value from angles	$x''_i(\Delta) = x'_i(\Delta) - \bar{x}'(\Delta, p)$
6	Wrap angles differences: azimuth range $[-\pi, \pi]$, elevation range $[-\pi/2, \pi/2]$.	$x'''_i(\Delta) = \text{mod}(x''_i(\Delta), WR), WR = \begin{cases} 2\pi & \text{azimuth} \\ \pi & \text{elevation} \end{cases}$ $\text{if } x'''_i(\Delta) > \frac{WR}{2} \Rightarrow x'''_i(\Delta) = x'''_i(\Delta) - WR$

7 Calculate the second moment for differences (standard deviation (spread) for angles) for given shift Δ .	$\sigma(\Delta, p) = \sqrt{\sum_{i=1}^{N_x} [x_i''(\Delta)]^2 \text{pas}(x_i'(\Delta), p)}$
8 Angle spread represents minimum std. deviation over Δ (Repeat steps 1-7 until minimum is found.)	$\sigma_{AS}(p) = \min_{\Delta} \sigma(\Delta, p)$
9 Collect values (calculated at SS level) for the duration of the whole measurement, in order to estimate pdf, cdf, correlation coefficient or distance. See common processing method named Correlation/Covariance.	$\text{pdf}(\sigma_{AS}, p), \text{cdf}(\sigma_{AS}, p), \quad \text{CorrC}(\sigma_{AS}, p), \\ \text{CorrD}(\sigma_{AS}, p)$
Results reported as	
Figure	<i>cdf</i> <code>cdf=func(Spread [<spread_unit>])</code>
	<i>CorrC</i> <code>CrossC=func(Spread [<spread_unit>])</code>
Table	Use default table for certain plot type (see 6.Common processing methods).
Value	<i>CoorD</i> Correlation distance.

4.1.4 Cluster level

4.1.4.1 Clusters (Number Of Clusters)

C1 - Clusters (Number Of Clusters)		
<i>Short Parameter Name</i>		<i>WIM parameter</i>
Clusters (NumberOfClusters)		<i>WIM validation</i>
		priority 1
Cluster represents collection of MPCs that are collocated in delay-angular domain.		
Extraction procedure		
#	<i>verbal</i>	<i>math</i>
	for each snapshot	
1	Each cluster is represented by centroid. When centroids are calculated, power weighting is used [1].	$(\hat{\tau}, \hat{\phi}, \hat{\varphi})_n \quad n = 1..N$
2	Apply clustering algorithm to MPCParameters , that will sort MPCs into N groups – clusters. Adaptive algorithm that does not use predefined number of clusters should be used. New clusters should be introduced when distance measure to the existing clusters exceeds predefined value and maximum allowed number of cluster is not reached. TimeVariantPowerDelayProfile can also be	$(\tau, \phi, \varphi)_i \in C_n, \quad n = 1..N$

	used to detect resolvable peaks in delay domain.			
3	When clustering procedure has finished NumberOfClusters for current snapshot is also known.	N		
4	Collect values (calculated at S level) for the duration of the whole measurement, in order to estimate pdf, cdf, correlation coefficient or distance.	$\text{pdf}(N, p), \text{cdf}(N, p), \text{CorrC}(N, p), \text{CorrD}(N, p)$		
5	Estimating of (Joint) Distributions, Power Angular Spectrum, Angle Spread per cluster is the same as for whole set of MPCs. (Only difference is that only subset of MPC is considered). All these items are estimated once per stationarity interval.			
Results reported as				
<i>Figure</i>	<i>CPower</i>	CPower=func(CDelay [ns], CAoD [deg], CAoA [deg]) 4D representations of total cluster power associated to cluster centroids (Power showed over 3 dimensions) can be used for illustrative purposes. Better way would be to separate angular (power over 2D: AoD,AoA) and delay (power over 1D: delay) domains. Animation over consecutive snapshots can be used.		
	<i>cdf</i>	cdf=func(Number of clusters)		
<i>Table</i>	Positions of cluster centroids could be reported inside table: one row per centroid, with 4 columns: Delay [ns], AoD [deg], ,AoA [deg] and PerClusterPower[dB]. For pdf, cdf, CorrC plots use default table (see 6.Common processing methods).			
Additional Processing instructions				
Clusters having large excess delay values are regarded as far clusters (FCL). Since these clusters occur only occasionally, they are not used in analysis of delay and angular distributions. Instead they are analyzed separately. For FCL similar properties could be calculated as for “close” clusters: delay and angular spreads, mean angle of departure and arrival, etc. and they could be characterized additionally by relative power and frequency of occurrence.				

4.1.4.2 Tracking Of Clusters

C2 - Tracking Of Clusters		
Short Parameter Name		WIM parameter
ClusterLifeTime, ClusterBirthRate, DriftingOfDelaysAndAngles		WIM validation
		priority 1
<ul style="list-style-type: none"> - Cluster Life Time should represent average existence of cluster over time dimension. - Cluster Birth Rate defines how often new clusters arise. - Drifting of Delays and Angles describes changes in centroid positions in consecutive snapshots - From tracking of clusters over consecutive snapshots following properties could be estimated: 		
Extraction procedure		
#	verbal	math

<p>From tracking of clusters over consecutive snapshots following properties could be estimated:</p>	
1	If life time is noted for each cluster, at measurement level pdf could be estimated. Parameter ClusterLifeTime can represent average value. Other possibility is to use parameter from analytical pdf approximation.
2	From information in which snapshot new clusters occur it is possible to express probability that new cluster(s) would occur in given time. This distribution can be parameterized or just mean value ClusterBirthRate can be used.
3	Drifting of Delays and Angles describes changes in centroid positions in consecutive snapshots. Cumulative sum of offsets over SS will show total change inside stationarity interval (drop). Offset data (per drop) can be used to get pdf, that can later be used for time evolution.
<p>Results reported as</p>	
<i>Figure</i>	<i>pdf</i>
	<i>cdf</i>
<i>Table</i>	
<p>Additional Processing instructions</p>	
<p>Comments</p>	
<p>See also</p>	
<p>[1] N. Czink et al: "Cluster-Based MIMO Channel Model Parameters Extracted from Indoor Time-Variant Measurements", Submitted to GlobeCom 2006</p>	

4.1.4.3 Per-Cluster Shadowing Standard Deviation

C3 – Per-Cluster Shadowing Standard Deviation

Short Parameter Name PerClusterShadowingStd.	<i>WIM parameter</i>	x
	<i>WIM validation</i>	x
	<i>priority</i>	1
<ul style="list-style-type: none"> - Total power of different clusters is, in general, also different. Shadowing standard deviation describes deviation of powers between clusters, depending on cluster delay and angular dimensions. 		

Extraction procedure		
#	<i>verbal</i>	<i>math</i>
	for all (n_t) snapshots belonging to snapshot set (SS)	
1	<p>Calculate total power contained in each cluster c in every snapshot t_i. c-th cluster of snapshot t_i consists of $N_j(c, t_i)$ MPCs.</p> <p>Assign calculated power to cluster centroid.</p>	$\bar{P}_c^{t_i}(\hat{\tau}, \hat{\phi}, \hat{\phi}, p) = \sum_{j=1}^{N_j(c, t_i)} P_{c,j}^{t_i}(\tau_j, \phi_j, \varphi_j, p)$
2	<p>Depending on available number of clusters define multidimensional bins $(\Delta\tau_b, \Delta\phi_b, \Delta\varphi_b), b = 1..B$.</p> <p>Each cluster belongs to exactly one bin.</p> <p>Exactly same approach is used if one-dimensional (marginal) analysis is performed in delay or angular domain. Summing of powers from others domains is required.</p>	$\bar{P}_{b,c}^{t_i}(p) = \begin{cases} \bar{P}_c^{t_i}(\hat{\tau}, \hat{\phi}, \hat{\phi}, p) & (\hat{\tau}, \hat{\phi}, \hat{\phi}) \in (\Delta\tau_b, \Delta\phi_b, \Delta\varphi_b) \\ 0 & otherwise \end{cases}$
3	Calculate the mean powers per bin inside SS. In snapshot t_i there are $N_c(t_i)$ clusters.	$\bar{P}_b(p) = \frac{1}{\sum_{i=1}^{n_t} N_c(t_i)} \sum_{i=1}^{n_t} \sum_{c=1}^{N_c(t_i)} \bar{P}_{b,c}^{t_i}(p)$
4	Calculate average standard deviation for all clusters inside SS.	$\zeta(p) = \sqrt{\frac{1}{\sum_{i=1}^{n_t} N_c(t_i)} \sum_{i=1}^{n_t} \sum_{c=1}^{N_c(t_i)} [\bar{P}_{b,c}^{t_i}(p) - \bar{P}_b(p)]^2}$
5	<p>Alternatively, if power distribution model $P_m(\tau, \phi, \varphi, p)$ is available we can use cluster centroids to calculate deviation.</p> <p>(E.g. in one-dimensional case exponential function can be fitted to experimental PowerDelayProfile, and whole analysis conducted in delay domain only)</p>	$\zeta(p) = \sqrt{\frac{1}{\sum_{i=1}^{n_t} N_c(t_i)} \cdot \sum_{i=1}^{n_t} \sum_{c=1}^{N_c(t_i)} [\bar{P}_c^{t_i}(\hat{\tau}, \hat{\phi}, \hat{\phi}, p) - P_m(\hat{\tau}, \hat{\phi}, \hat{\phi}, p)]^2}$
6	Express result in [dB-W]	$\zeta(p) [\text{dB} - \text{W}] = 10 \log_{10} \left(\frac{\zeta(p)}{1 \text{ W}} \right)$
Results reported as		
<i>Figure</i>	<i>cdf</i>	cdf=func(Per-Cluster Shadowing [dB])
<i>Table</i>	For pdf, cdf, CorrC plots use default table (see 6.Common processing methods).	
Additional Processing instructions		

If processing is performed in delay domain only (one-dimensional analysis) clusters are detected from TimeVariantPowerDelayProfile, and deviations are calculated in respect to PowerDelayProfile (or its model).

4.1.4.4 K-factor

C4 - K-factor

<i>Short Parameter Name</i>		<i>WIM parameter</i> <input checked="" type="checkbox"/>
<i>K-factor</i>		<i>WIM validation</i> <input checked="" type="checkbox"/>
		<i>priority</i> 1
K-factor is equal to the ratio of powers between LOS component and all other multi-path components.		
Extraction procedure		
#	<i>verbal</i>	<i>math</i>
	for each snapshot set (collection of n_t consecutive valid snapshots)	
1	Estimate K factor for each cluster separately. Meaning of K factor is different on cluster level: It is ratio of the powers between strongest and the rest of components. (Due to clustering approach it can happen that strongest component is not the first one)	$K_n = \frac{P_{n,\max}}{\sum_{i \neq \max} P_{n,i}}$
2	If cluster with lowest delay MPCs shows significant value of K-factor (per cluster), much greater than other clusters, high probability exist that cluster contains LOS component. Power ratio between LOS candidate and all others MPCs could be calculated. If predefined threshold is exceeded LOS condition is assumed.	
3	Problem with previous approach is that, due to time reference lack, first strong reflection can be regarded as LOS component. Additional information: distance between Tx and Rx is necessary for reliable estimation.	
4	Use linear expression to describe dependence of K-factor over distance.	$K [dB] = C + D \cdot d [m]$
Results reported as		
<i>Figure</i>	<i>K</i>	K [dB]=func(distance [m]) If linear approximation is available use 2 data sets: 1)original data (marker), 2)linear regression
<i>Table</i>		
Additional Processing instructions		

Comments	
Value of K-factor can be used to estimate probability of Line-Of-Site condition.	

4.1.5 Polarization analysis

4.1.5.1 Cross-polarization ratio

P1 - Cross-polarization ratio

		WIM parameter x
		WIM validation x
		priority 1
Find ratios of Powers that are calculated for different polarizations.		
Extraction procedure		
#	verbal	math
1	for each snapshot set (collection of n_t consecutive valid snapshots)	
1	Find ratios of Powers for different polarizations. Rows of the XPR matrix (first index of XPR elements) correspond to Tx polarization, while columns (second index) correspond to Rx polarization.	$XPR = \begin{bmatrix} 1 & \frac{P_{vv}}{P_{vh}} \\ \frac{P_{hh}}{P_{hv}} & 1 \end{bmatrix}$
2	If normalization of power is required at receiver side, sum of row elements should be equal to 1	$\frac{1}{XPR} = \begin{bmatrix} \frac{P_{vv}}{P_{vv} + P_{vh}} & \frac{P_{vh}}{P_{vv} + P_{vh}} \\ \frac{P_{hv}}{P_{hv} + P_{hh}} & \frac{P_{hh}}{P_{hv} + P_{hh}} \end{bmatrix}$
Results reported as		
Figure	cdf	cdf=func(XPR _{V/H} [dB]) Two distributions are used: one for each off-diagonal element of XPR matrix
Table	Use default table for certain plot type (see 6.Common processing methods).	

4.1.5.2 Cluster-wise polarisation cross-correlation

P2 – Cluster-wise polarization cross-correlation

Short Parameter Name	WIM parameter
----------------------	---------------

PolarizationXCorrelation	<i>WIM validation</i>	
	<i>priority</i>	
If measurement data contain different polarization sub-channels measured between orthogonal Tx and Rx antennas (vv, vh, hv, hh or slanted ones, e.g. as in figure below), it is possible to analyze correlation between co and cross polarized components.		
Extraction procedure		
#	<i>verbal</i>	<i>math</i>
During cluster life-time, for all MPC belonging to the same cluster c		
1	Identify same multi-path components $m = 1..M(c)$ existing for different polarization sub-channels designated by 11, 12, 21 and 22.	
2	Calculate cross-correlation coefficient of MPCs complex gains h_{ij}^m averaging over space-time. For each MPC in cluster we get 4x4 correlation matrix.	$\rho_c^m(h_{ij}^m, h_{i'j'}^m) = \frac{\mathbb{E}\{h_{ij}^m (h_{i'j'}^m)^*\}}{\sqrt{\mathbb{E}\{h_{ij}^m (h_{ij}^m)^*\} \mathbb{E}\{h_{i'j'}^m (h_{i'j'}^m)^*\}}}$
3	Average the result over different MPCs in cluster and over different clusters.	$\rho_{[4x4]} = \frac{1}{\sum_{c=1}^{N_c} M(c)} \sum_{c=1}^{N_c} \sum_{m=1}^{M(c)} \rho_c^m(h_{ij}^m, h_{i'j'}^m)$
Results reported as		
<i>Figure</i>		
<i>Table</i>		

4.2 Common processing methods

4.2.1 Probability density Function (experimental)

M1 - Probability density function (experimental)

Short Parameter Name pdf	<i>WIM parameter</i>	x
	<i>WIM validation</i>	x
	<i>priority</i>	1
- Approximation of probability density function from input data samples.		

Extraction procedure																										
#	<i>verbal</i>	<i>math</i>																								
for collection of N input values of RV x.																										
1		<p>Calculate histogram (number of input data contained inside separate bins). Required parameters are number of bins, and their borders (edges). MATLAB function <code>histc(x,edges)</code>, with <code>edges = [e0,e1, e2 ...eN]</code>, can be used to count data in N bins. MATLAB function <code>hist()</code> offers simpler interface: to define only number of equally wide beans.</p> <table border="1"> <caption>Data for Histogram (Figure 1)</caption> <thead> <tr> <th>Bin Range (x)</th> <th>Frequency (y)</th> </tr> </thead> <tbody> <tr><td>[0.0, 0.25)</td><td>2</td></tr> <tr><td>[0.25, 0.50)</td><td>3</td></tr> <tr><td>[0.50, 0.75)</td><td>2</td></tr> <tr><td>[0.75, 1.00)</td><td>3</td></tr> <tr><td>[1.00, 1.25)</td><td>7</td></tr> <tr><td>[1.25, 1.50)</td><td>7</td></tr> <tr><td>[1.50, 1.75)</td><td>5</td></tr> <tr><td>[1.75, 2.00)</td><td>3</td></tr> <tr><td>[2.00, 2.25)</td><td>2</td></tr> <tr><td>[2.25, 2.50)</td><td>1</td></tr> <tr><td>[2.50, 2.75)</td><td>1</td></tr> </tbody> </table>	Bin Range (x)	Frequency (y)	[0.0, 0.25)	2	[0.25, 0.50)	3	[0.50, 0.75)	2	[0.75, 1.00)	3	[1.00, 1.25)	7	[1.25, 1.50)	7	[1.50, 1.75)	5	[1.75, 2.00)	3	[2.00, 2.25)	2	[2.25, 2.50)	1	[2.50, 2.75)	1
Bin Range (x)	Frequency (y)																									
[0.0, 0.25)	2																									
[0.25, 0.50)	3																									
[0.50, 0.75)	2																									
[0.75, 1.00)	3																									
[1.00, 1.25)	7																									
[1.25, 1.50)	7																									
[1.50, 1.75)	5																									
[1.75, 2.00)	3																									
[2.00, 2.25)	2																									
[2.25, 2.50)	1																									
[2.50, 2.75)	1																									
2		<p>To estimate pdf from histogram devide number of data per bin with bin width and with total number of data samples.</p> <table border="1"> <caption>Data for Estimated PDF (Figure 2)</caption> <thead> <tr> <th>Bin Range (x)</th> <th>Estimated PDF (y)</th> </tr> </thead> <tbody> <tr><td>[0.0, 0.25)</td><td>0.3</td></tr> <tr><td>[0.25, 0.50)</td><td>0.4</td></tr> <tr><td>[0.50, 0.75)</td><td>0.3</td></tr> <tr><td>[0.75, 1.00)</td><td>0.4</td></tr> <tr><td>[1.00, 1.25)</td><td>1.0</td></tr> <tr><td>[1.25, 1.50)</td><td>1.0</td></tr> <tr><td>[1.50, 1.75)</td><td>0.7</td></tr> <tr><td>[1.75, 2.00)</td><td>0.4</td></tr> <tr><td>[2.00, 2.25)</td><td>0.3</td></tr> <tr><td>[2.25, 2.50)</td><td>0.15</td></tr> <tr><td>[2.50, 2.75)</td><td>0.1</td></tr> </tbody> </table>	Bin Range (x)	Estimated PDF (y)	[0.0, 0.25)	0.3	[0.25, 0.50)	0.4	[0.50, 0.75)	0.3	[0.75, 1.00)	0.4	[1.00, 1.25)	1.0	[1.25, 1.50)	1.0	[1.50, 1.75)	0.7	[1.75, 2.00)	0.4	[2.00, 2.25)	0.3	[2.25, 2.50)	0.15	[2.50, 2.75)	0.1
Bin Range (x)	Estimated PDF (y)																									
[0.0, 0.25)	0.3																									
[0.25, 0.50)	0.4																									
[0.50, 0.75)	0.3																									
[0.75, 1.00)	0.4																									
[1.00, 1.25)	1.0																									
[1.25, 1.50)	1.0																									
[1.50, 1.75)	0.7																									
[1.75, 2.00)	0.4																									
[2.00, 2.25)	0.3																									
[2.25, 2.50)	0.15																									
[2.50, 2.75)	0.1																									
Results reported as																										
<i>Figure</i>	<i>pdf</i>	<p> xlabel: <item_name> [<item_unit>] ylabel: pdf MATLAB function <code>bar()</code> can be used to display experimental pdf</p>																								
<i>Table</i>	Default values to accompany pdf plot: [<code>mean()</code> , <code>std()</code>]																									

4.2.2 Cumulative probability density function (experimental)

M2 - Cumulative probability density function (experimental)

Short Parameter Name cdf	<i>WIM parameter</i>	x
	<i>WIM validation</i>	x
	<i>priority</i>	1
- Approximation of cumulative probability density function from input data samples.		
Extraction procedure		
#	<i>verbal</i>	<i>math</i>
for collection of N input values of RV x.		
1	Order the values (x_{sorted}). Approximate the cdf by using ordering position. The same result would be obtained by MATLAB function <code>ecdf()</code> when additional parameter are not used. Note that MATLAB function use different expression: cdf is calculated from product-limit (Kaplan-Meier) estimate of the survivor function.	$cdf(x_{sorted}(i)) = \frac{i}{\#x_{sorted}}$
2	Plot cdf using MATLAB function <code>stairs()</code> . When more data is available cdf curve would be smoother.	
Results reported as		
Figure	<code>cdf</code>	xlabel: <item_name> [<item_unit>] ylabel: cdf
Table	Default values to accompany cdf plot: cdf arguments for cdf equal to (10%, 50%, 90%), <code>mean()</code> , <code>std()</code>	

4.2.3 Distribution Modelling

M3 - Distribution Modelling

<i>Short Parameter Name</i> DistributionModelling	<i>WIM parameter</i>	x
	<i>WIM validation</i>	x
	<i>priority</i>	1
Find best matched function (having simple analytical expression) and optimize their parameters.		
Extraction procedure		
#	<i>verbal</i>	<i>math</i>
for collection of N input values of RV x.		
1	If probability distribution function is to be modelled perform Kolmogorov-Smirnov test on available data. Repeat testing for different parameters and different distributions until best match is found.	
2	Modelling distribution consist of analytical expression for pdf or cdf and numerical values for its parameters.	
Results reported as		
<i>Figure</i>	<i>DM</i>	Show best matched analytical distribution and original data samples (experimental function), at the same figure. Add analytical expression for modelling pdf/cdf (with numeric parameter values)
<i>Table</i>	Numeric parameter values of modelling pdf/cdf could be reported inside table. If only one parameter exist it is not necessary to use table.	

4.2.4 Function Modelling

M4 - Function Modelling		
Short Parameter Name	<i>WIM parameter</i>	x
FunctionModelling	<i>WIM validation</i>	x
	<i>priority</i>	1
Find best matched function (having simple analytical expression) and optimize their parameters.		
Extraction procedure		
#	<i>verbal</i>	<i>math</i>
for collection of N data values at known positions x.		
1	If e.g. power distribution is modelled, calculate RMS error for available data. Repeat testing for different parameters and different analytical functions until the best match is found.	
2	Modelling function consist of analytical expression and numerical values for its parameters.	
Results reported as		
<i>Figure</i>	<i>FM</i>	Show best matched analytical function and original data values at the same figure. Add analytical expression for modelling pdf/cdf (with numeric parameter values)
<i>Table</i>	Numeric parameter values of modelling pdf/cdf could be reported inside table. If only one parameter exist it is not necessary to use table.	

4.2.5 Correlation/Covariance

M5 - Correlation/Covariance

Short Parameter Name Corr/Cov	<i>WIM parameter</i>	x															
	<i>WIM validation</i>	x															
	<i>priority</i>	1															
<ul style="list-style-type: none"> - Correlation function shows parameter (signal) resemblance, over one (or more) dimensions. - Covariance is obtained when product of mean values is subtracted from correlation - Correlation coefficient represent normalized covariance - Correlation distance is symmetrical around maximum covariance value and it is proportional to the surface below covariance function. 																	
Extraction procedure <table border="1" style="width: 100%; border-collapse: collapse;"> <thead> <tr> <th>#</th> <th><i>verbal</i></th> <th><i>math</i></th> </tr> </thead> <tbody> <tr> <td>1</td> <td>for collection of N_x values of $x(n)$, and N_y values of $y(n)$.</td> <td></td> </tr> <tr> <td>2</td> <td>If uniform sampling is assumed, product $x(n)y^*(n+k)$ is available for $n \in [N_1, N_2]$ where $N_1 = \max(-k, 0)$ and $N_2 = \min(N_y, N_x - k)$. For $N_x = N_y$ this is equivalent to MATLAB function <code>xcorr(x,y,'unbiased')</code> since function <code>xcorr(x,y)</code> without any option does not perform normalization.</td> <td> $R_{xy}(k) = \frac{1}{N_2 - N_1} \sum_{n=N_1+1}^{N_2} x(n+k)y^*(n),$ $k = [-N_y + 1, N_x - 1]$ </td> </tr> <tr> <td>3</td> <td>Obtained estimate is unbiased but its variance increases with k. Other possibility is to use biased estimate with lower variance: (MATLAB function <code>xcorr(x,y,'biased')</code>) requires that $N_x = N_y$</td> <td> $R_B(k) = \left(\frac{N_2 - N_1}{\min(N_x, N_y)} \right) R_{xy}(k)$ </td> </tr> <tr> <td>4</td> <td>Cross-covariance. Is calculated in the same way as correlation, only mean values are subtracted prior to averaging. (MATLAB function <code>xcov(x,y,'unbiased')</code>) requires that $N_x = N_y$</td> <td> $C_{xy}(k) = \frac{1}{N_2 - N_1} \sum_{n=N_1+1}^{N_2} (x(n+k) - \mu_x)(y^*(n) - \mu_y),$ $k = [-N_y + 1, N_x - 1]$ </td> </tr> </tbody> </table>			#	<i>verbal</i>	<i>math</i>	1	for collection of N_x values of $x(n)$, and N_y values of $y(n)$.		2	If uniform sampling is assumed, product $x(n)y^*(n+k)$ is available for $n \in [N_1, N_2]$ where $N_1 = \max(-k, 0)$ and $N_2 = \min(N_y, N_x - k)$. For $N_x = N_y$ this is equivalent to MATLAB function <code>xcorr(x,y,'unbiased')</code> since function <code>xcorr(x,y)</code> without any option does not perform normalization.	$R_{xy}(k) = \frac{1}{N_2 - N_1} \sum_{n=N_1+1}^{N_2} x(n+k)y^*(n),$ $k = [-N_y + 1, N_x - 1]$	3	Obtained estimate is unbiased but its variance increases with k. Other possibility is to use biased estimate with lower variance: (MATLAB function <code>xcorr(x,y,'biased')</code>) requires that $N_x = N_y$	$R_B(k) = \left(\frac{N_2 - N_1}{\min(N_x, N_y)} \right) R_{xy}(k)$	4	Cross-covariance. Is calculated in the same way as correlation, only mean values are subtracted prior to averaging. (MATLAB function <code>xcov(x,y,'unbiased')</code>) requires that $N_x = N_y$	$C_{xy}(k) = \frac{1}{N_2 - N_1} \sum_{n=N_1+1}^{N_2} (x(n+k) - \mu_x)(y^*(n) - \mu_y),$ $k = [-N_y + 1, N_x - 1]$
#	<i>verbal</i>	<i>math</i>															
1	for collection of N_x values of $x(n)$, and N_y values of $y(n)$.																
2	If uniform sampling is assumed, product $x(n)y^*(n+k)$ is available for $n \in [N_1, N_2]$ where $N_1 = \max(-k, 0)$ and $N_2 = \min(N_y, N_x - k)$. For $N_x = N_y$ this is equivalent to MATLAB function <code>xcorr(x,y,'unbiased')</code> since function <code>xcorr(x,y)</code> without any option does not perform normalization.	$R_{xy}(k) = \frac{1}{N_2 - N_1} \sum_{n=N_1+1}^{N_2} x(n+k)y^*(n),$ $k = [-N_y + 1, N_x - 1]$															
3	Obtained estimate is unbiased but its variance increases with k. Other possibility is to use biased estimate with lower variance: (MATLAB function <code>xcorr(x,y,'biased')</code>) requires that $N_x = N_y$	$R_B(k) = \left(\frac{N_2 - N_1}{\min(N_x, N_y)} \right) R_{xy}(k)$															
4	Cross-covariance. Is calculated in the same way as correlation, only mean values are subtracted prior to averaging. (MATLAB function <code>xcov(x,y,'unbiased')</code>) requires that $N_x = N_y$	$C_{xy}(k) = \frac{1}{N_2 - N_1} \sum_{n=N_1+1}^{N_2} (x(n+k) - \mu_x)(y^*(n) - \mu_y),$ $k = [-N_y + 1, N_x - 1]$															

	$\mu_x = \frac{1}{N_x} \sum_{n=1}^{N_x} x(n), \mu_y = \frac{1}{N_y} \sum_{n=1}^{N_y} y^*(n)$
	Correlation coefficient ($CorrC()$). There is no appropriate matlab function. From MATLAB function <code>xcov(x,y, 'coeff')</code> it is possible to calculate correlation coefficient only with convolution that is not normalized, because function does not accept two different options (second should be 'unbiased').
5	$\rho_{xy}(k) = \frac{C_{xy}(k)}{\sqrt{C_{xx}(0)C_{yy}(0)}}$
Results reported as	
Figure	ACF <code>ACF=func(<dimension_name> [<dimension_unit>])</code>
	CorrC <code>CorrC=func(<dimension_name> [<dimension_unit>])</code>
Table	
Value	Correlations distance
Additional Processing instructions	
When correlation/covariance items are calculated over space, difference in snapshot index k is not constant between all snapshots being at shortest spatial (geometrical) distance Δ . This comes from the fact that measured routes in practice are not always straight, but often having turns. As a consequence, in preprocessing phase it is necessary to detect groups of snapshots being at different distances Δ . Averaging is then performed over formed grups e.g. $R(\Delta) = E\{x(n)y^*(n+k(\Delta,n))\} = \frac{1}{N(\Delta)} \sum_n \sum_{k(\Delta,n)} x(n)y^*(n+k(\Delta,n)), \text{ where } N(\Delta) \text{ is total number of pairs } [x(n), y^*(n+k(\Delta,n))] \text{ being at distance } \Delta.$	
Comments	
See also	
[1] A. Papoulis: "Probability, Random Variables and Stochastic Processes", McGraw-Hill, Inc. 1991.	

5. References

- [3GPPSCM] 3GPP TR 25.996, “3rd Generation Partnership Project; technical specification group radio access networks; spatial channel model for MIMO simulations (release 6)”, V6.1.0.
- [AGV98] Pauli Aikio, Ralf Gruber and Pertti Vainikainen, Wideband radio channel measurements for train tunnels. VTC 1998.
- [AHHM07] M. Alatossava, L. Hentilä, V-M. Holappa and J. Meinilä; “Comparison of Outdoor-to-Indoor and Indoor-to-Outdoor MIMO Propagation Characteristics at 5.25 GHz”, hyväksytty, IEEE VTC’07 Spring, April, 2007, Dublin, Ireland
- [AHY06] M. Alatossava, V-M. Holappa, J. Ylitalo, “Outdoor to indoor MIMO radio channel measurements at 5.25 GHz – characterization of propagation parameters”, to be published in EUCAP, November 2006, Nice, France.
- [AI00] Farrokh Abrishamkar , James Irvine, Comparison of Current Solutions for the Provision of Voice Services to Passengers on High Speed Trains. IEEE VTC-Fall, VTC 2000. 24 - 28 Sept. 2000.
- [APM02] A. Algans, K. I. Pedersen, P.E. Mogensen,”Experimental analysis of the joint statistical properties of azimuth spread, delay spread and shadow fading”, IEEE J. Selected Areas in Comm., Vol. 20, pp.523-531, 2002.
- [AP02] J. B. Andersen and K. I. Pedersen, “Angle-of-arrival statistics for low resolution antennas,” IEEE Trans. Antennas Propagat., vol. 50, pp. 391–395, Mar. 2002.
- [AWK+01] Allen B., Webber J., Karlsson P. and Beach M., “UMTS Spatio-Temporal Propagation Trial Results”, IEE 11th International Conference on Antennas and Propagation, Vol.2, pp. 497-501, Manchester, UK, 2001.
- [BSK+07] Bultitude, R.J.C. Schenk, T.C.W. den Kamp, N.A.A.O. Adnani, N., “A propagation-measurement-based evaluation of channel characteristics and models pertinent to the expansion of mobile radio systems to frequencies beyond 2 GHz, ” IEEE Trans. VT, vol. 56, no. 2, pp. 382-388, Mar. 2007
- [Bul02] Bultitude, R.J.C., “A Comparison of Multipath-Dispersion-Related Micro-Cellular Mobile Radio Channel Characteristics at 1.9 GHz and 5.8 GHz”, in Proc. ANTEM’02, Montreal, Jul. 31 – Aug. 2, 2002, pp. 623-626.
- [BBK04] M.D. Batiere, T.K. Blankenship, J.F. Kepler, T.P. Krauss, ”Seasonal variations in path loss in the 3.7 GHz band”, IEEE RAWCON, pp. 399-402, 2004.
- [BBK+02] M.D. Batiere, T.K. Blankenship, J.F. Kepler, T.P. Krauss, I. Lisica, S. Mukthvaram, J.W. Porter, T.A. Thomas, F.W. Vook: “Wideband MIMO mobile impulse response measurements at 3.7 GHz”, IEEE 55th VTC, pp. 26-30, 2002.
- [BHS05] D. Baum, J. Hansen, J. Salo, G. Del Galdo, M. Milojvic, P. Kyösti: An Interim Channel Model for Beyond-3G Systems, IEEE VTC’05, April 2005.
- [CBW95] D. J. Cichon, T. C. Becker, W. Wiesbeck, Determination of Time-Variant Radio Links in High-Speed Train Tunnels by Ray Optical Modeling. AP-S 1995.
- [CBH+06] N. Czink, E. Bonek, L. Hentilä, J.-P. Nuutinen, and J. Ylitalo, “Cluster-based MIMO channel model parameters extracted from indoor time-variant measurements,” in IEEE GlobeCom 2006, San Francisco, USA, Nov. 2006.
- [Cha03] Ashok Chandra, Propagation of 2000 MHz Radio Signal into A Multi-Storeyed building Through Outdoor-Indoor Interface. The 14th IEEE 2003 International Symposium on Personal, Indoor and Mobile Radio Communication Proceedings. 2003.
- [CG99] T.-S. Chu, L.J. Greenstein, “A quantification of link budget differences between the cellular and PCS bands“, IEEE Trans. Veh. Tech., Vol 48, pp. 60-65, 1999.
- [C02] M. Celidonio, “Outdoor-indoor propagation measurements in the 3.6-4.2 GHz band”, IEEE 13th PIMRC, Vol. 2, pp. 644-648, 2002.

- [CC05] N. Czink, P. Cera, "A Novel Framework for Clustering Parametric MIMO Channel Data Including MPC Powers," presented at COST 273 Meeting, Lisbon, Portugal, November, 2005.
- [CKC03] A. Chandra, A. Kumar, P. Chandra, "Propagation of 2000 MHz radio signal into a multi-storeyed building through outdoor-indoor interface", Proceedings on 14th PIMRC, Vol. 3, pp. 2983-2987, 2003.
- [COST231] European Commission: European cooperation on the field of scientific and technical research (EURO-COST 231): "Digital mobile radio towards future generation systems", Final report, <http://www.lx.it.pt/cost231/>, Bruxelles, 1999.
- [COST259] Luis M. Correia: "Wireless Flexible Personalised Communications, COST 259: European Co-operation in Mobile Radio Research", John Wiley & Sons Ltd, England, 2001.
- [CP07] Contrat J-M. and Pajusco P., "Typical MIMO Propagation Channels in Urban Macrocells at 2 GHz", Proceedings of the 13th European Wireless Conference, Paris, France, April 2007.
- [DDA00] Michael Doebler, Monica Dell' Anna, A. H. Aghvami, Pdf - Transformation for the Outdoor-Indoor Propagation Model. VTC 2000-Spring. 2000, 15 – 18 May 2000 Pages 1646-1650 Vol. 3.
- [deJKH02] Y.L.C.deJong. M.H.J.L Koelen, and M.H.J.Herben, "A building transmission model for improved propagation prediction in urban microcells," IEEE Trans., Veh. Technol., vol. 53, no. 2, 2002.
- [DGM+03] A. Domazetovic, L. J. Greenstein, N. B. Mandayam, and I. Seskar. "Estimating the Doppler Spectrum of a Short-Range Fixed Wireless Channel", *IEEE Comm. Lett.*, 7(5):227-229, May 2003.
- [DRX98] G. Durkin, T.S Rappaport, H. Xu: "Measurements and models for radio path loss and penetration in and around homes and trees at 5.85 GHz, IEEE Trans. Comm., Vol. 46, pp.1484-1496, 1998.
- [Dug99] A. Dugas, "5 GHz MILTON Propagation Study", slide-set downloadable from <http://www.crc.ca/en/html/milton/home/documents>.
- [EGT+99] V. Erceg , L.J. Greenstein, S. Tjandra, S. Parkoff, A. Gupta, B. kulin, A. Julius, R. Bianci., "An empirically based path loss model for wireless channels in suburban environments", IEEE J. Sel. Areas Comm., Vol. 17, pp. 1205-1211, 1999.
- [Erc01] V. Erceg et al., "Channel Models for Fixed Applications", Technical report, IEEE 802.16 Broadband Wireless Working Group, Jul. 2001.
- [FBK+02] Foo S.E., Beach M.A., Karlsson P., Eneroth P., Lindmark B. and Johansson J., "Spatio-Temporal Investigation of UTRA FDD Channels", 3rd International Conference on 3G Mobile Communication Technologies, pp. 175-179, May 2002.
- [FBR+94] Feuerstein, M.J.; Blackard, K.L.; Rappaport, T.S.; Seidel, S.Y.; Xia, H.H., "Path-loss, delay spread, and outage models as functions of antenna height for microcellular system design", in *Proc. IEEE VTC'94*, Vol. 43, Iss. 3, Aug. 1994, pp. 487 – 498.
- [FDS+94] Foster, H.M.; Dehghan, S.F.; Steele, R.; Stefanov, J.J.; Strelouhov, H.K., "Microcellular measurements and their prediction", IEE Colloquium on "Role of Site Shielding in Prediction Models for Urban Radiowave Propagation" (Digest No. 1994/231), Nov. 1994, pp. 2/1 - 2/6.
- [FTB03] Foo S.E., Tan C.M and Beach M.A., "Spatial Temporal Characterization of UTRA FDD Channels at the User Equipment", IEEE 57th Vehicular Technology Conference, Vol. 2, pp. 793-797, April 2003.
- [Fuj03] T. Fujii, "Path loss prediction formula in mobile communication -an expansion of "SAKAGAMI" path loss prediction formula-", Trans. IEICE, Japan, J86-B, 10, pp. 2264-2267, 2003.
- [GEA03] S. Geng et al., " Measurements and Analysis of Wideband Indoor Radio Channels at 60 GHz," Proc. of 3rd ESA Workshop on Millimeter Wave Technology and Applications, Espoo, Finland, May 21-23, 2003.

- [GEY97] L.J. Greenstein, V. Erceg, Y.S. Yeh, M.V. Clark,"A new path-gain/delay spread model for digital cellular channels", IEEE Trans. Veh. Tech., Vol. 46, pp. 477-485, 1997.
- [GME99] Greenstein L.J. et al. "Moment-method estimation of the Ricean K-factor, Communications Letters, IEEE, vol. 3, issue 6, Jun. 1999, pp. 175-176.
- [GRZ07] Guo Rui Zhang, "Measurement and Characterisation of Delay, Angular and Frequency Dispersion and their Evolution at Mobile Receivers in 2.25 GHz Microcells," M.Sc. Thesis. Report, Dept. of Systems and Computer Engineering, Carleton University, Ottawa, to be submitted, spring 2007.
- [HACK07] L. Hentilä, M. Alatossava, N. Czink and P. Kyösti; "Cluster-level parameters at 5.25 GHz indoor-to-outdoor and outdoor-to-indoor MIMO radio channels", lähetetty, IST-SUMMIT'07, July, 2007, Budapest, Hungary
- [ITU] ITU Rec. ITU-R P.1238-4.
- [ITU-R] Rec. ITU-R P.1546-2, "Method for point-to-area predictions for terrestrial services in the frequency range 30 MHz to 3000 MHz"
- [JHH+05] T. Jämsä, V. Hovinen, L. Hentilä, and J. Iinatti, "Comparisons of Wideband and Ultra-wideband channel measurements " IEEE IWS2005/WPMC2005, Aalborg, Denmark.
- [Jon07] Y. L. C. de Jong, "Line-of-sight probability model for land-mobile radio in urban environments", in preparation.
- [KeM90] J.M Keenan, A.J. Motley, "Radio coverage in buildings", British Telecom Tech. Journal, vol.8, no.1, Jan. 1990, pp.19-24.
- [KI04] K. Kitao, S. Ichitsubo,"Path loss prediction formula for microcell in 400 MHz to 8 GHz band", Electronics Letters, Vol. 40, No. 11, 2004.
- [KKM02] J. F. Kepler, T.P. Krauss, S. Mukthvaram;"Delay spread measurements on a wideband MIMO channel at 3.7 GHz", IEEE 56th VTC, pp. 2498-2502, 2002.
- [KBM+06] Sandra Knoerzer, Michael A. Baldauf, Juergen Maurer, Werner Wiesbeck, "OFDM for Multimedia Applications in High-Speed Trains: Channel Model Including Different Antenna Types.", 2006.
- [KMV+05] Sandra Knoerzer, Juergen Maurer, Sven Vogeler, Karl-Dirk Kammeyer and Werner Wiesbeck, "Channel Modeling for a High-Speed Train OFDM Communication Link Supporting High Data Rates". ITST 2005.
- [KP02] M. B. Knudsen, Member, IEEE, and G. F. Pedersen, "Spherical Outdoor to Indoor Power Spectrum Model at the Mobile Terminal". IEEE Journal on Selected Areas in Communications, vol. 20, no. 6, August 2002.
- [KRB00] A. Kuchar, J-P. Rossi, E. Bonek:"Directional macro-cell channel characterization from urban measurements", IEEE Trans. Antennas and Propagation, Vol. 48, pp.137-145, 2000.
- [KSL+02] K. Kalliola, K. Sulonen, H. Laitinen, O. Kivekäs, J. Krogerus, P. Vainikainen;"Angular power distribution and mean effective gain of mobile antenna in different propagation environments", IEEE Trans. Veh. Techn., Vol. 51, pp.823-838, 2002.
- [KVV05] A. Kainulainen, L. Vuokko, and P. Vainikainen, "Polarization Behavior in Different Urban Radio Environments at 5.3 GHz," COST273 TD(05)18, Bologna, Jan. 19-21.
- [KZV01] J. Kivinen, X. Zhao, P. Vainikainen: Empirical characterization of wideband indoor radio channel at 5.3 GHz, IEEE Trans. on Antenna and Propagation, Vol. 49, No. 8, 2001, pp. 1192-1203.
- [Lar99] Larsson M., "Spatio-Temporal Channel Measurements at 1800 MHz for Adaptive Antennas", IEEE 49th Vehicular Technology Conference, Vol. 1, pp. 376-380, July 1999.
- [LKT+02] Laurila J., Kalliola K., Toeltsch M., Hugl K., Vainikainen P. and Bonek E., "Wideband 3D Characterization of Mobile Radio Channels in Urban Environment", IEEE Transactions on Antennas and Propagation, vol. 50, pp. 233, 2002.
- [Mar98] Martin U., "Spatio-Temporal Radio Channel Characteristics in Urban Macrocells", IEE Proceedings – Radar, Sonar and Navigation, vol. 145, Issue 1, pp. 42-49.
- [Medav] <http://www.channelsounder.de>

- [MEJ91] P.E. Mogensen, P. Eggers, C. Jensen."Urban area radio propagation measurements for GSM/DCS 1800 macro and micro cells", ICAP 91, pp. 500-503, 1991.
- [MHA+04] J. Medbo, F. Harryson, H. Asplund, J-E. Berg, "Measurements and analysis of a MIMO macrocell outdoor-indoor scenario at 1947 MHz", IEEE 59th VTC, Vol. 1, pp. 261-265, 2004.
- [MIS01] Masui, H.; Ishii, M.; Sakawa, K.; Shimizu, H.; Kobayashi, T.; Akaike, M., "Spatio-temporal channel characteristics at base station in microwave urban propagation," in *Proc. IEEE NRSC'01*, Vol. 2, Mar. 2001, Mansoura Univ. Egypt, pp. 609 – 615.
- [MKA02] Masui, H.; Kobayashi, T.; Akaike, M., "Microwave path-loss modeling in urban line-of-sight environments," IEEE Journal on Selected Areas in Communications, Vol. 20, Iss. 6, Aug. 2002, pp. 1151-1155.
- [MOT02] Y. Miura, Y. Oda, T. Taka, "Outdoor-to indoor propagation modelling with the identification of path passing through wall openings", IEEE 13th PIMRC, Vol. 1, pp. 130-134, 2002
- [MRA93] L. Melin, M. Rönnlund, R. Angbratt: "Radio wave propagation – a comparison between 900 and 1800 MHz", IEEE 43rd VTC conference, pp. 250-252, 1993.
- [NAH93] P. Nobles, D. Ashworth and F. Halsall: "Propagation measurements in an indoor radio environment at 2, 5 and 17 GHz," IEEE Colloquium on High Bit Rate UHS/SHF Channel Sounders – Technology and Measurement, pp. 4/1-4/6, 1993.
- [NAP05] H. T. Nguyen, J. B. Andersen, G. F. Pedersen, "Characterization of the indoor/outdoor to indoor MIMO radio channel at 2.140 GHz", Department of Communication Technology, Aalborg, Denmark, 2005.
- [NLA+99] Nilsson M., Lindmark B., Ahlberg M. and Beckman C., "Measurements of the Spatio-Temporal Polarization Characteristics of a Radio Channel at 1800 MHz", IEEE 49th VTC, Vol. 1, pp. 386-391, July 1999.
- [OBL+02] J. Ojala, R. Böhme, A. Lappeteläinen and M. Uno, "On the propagation characteristics of the 5 GHz rooftop-to-rooftop meshed network," IST Mobile & Wireless Telecommunications Summit 2002, Jun. 2002, Thessaloniki, Greece.
- [OKT+04] Ohta, G.I.; Kamada, F.; Teramura, N.; Hojo, H. 5 GHz W-LAN verification for public mobile applications - Internet newspaper on train and advanced ambulance car. Consumer Communications and Networking Conference, 2004. CCNC 2004. First IEEE. Volume , Issue , 5-8 Jan. 2004 Page(s): 569 – 574.
- [OOK+68] Y. Okumura, E. Ohmori, T. Kawano, K. Fukuda:"Field strength and its variability in VHF and UHF land-mobile radio services", Review of the Electrical Comm. Lab., Vol. 16, No 9. 1968.
- [OTH00] Oda U, Tsunekawa, K. and Hata, M., "Advanced LOS path-loss mode in microcellular mobile communications", *IEEE Trans. Vehicular Technology*, vol. 49, (6), Nov. 2000, pp. 2121-2125.
- [OTT+01] Y. Oda, R. Tsuchihashi, K. Tsunekawa, M. Hata,"Measured path loss and multipath propagation characteristics in UHF and microwave frequency band for urban mobile communications", VTC 2001 Spring, Vol.1, pp. 337-341, 2001.
- [Paj03] P. Pajusco: "Double characterisations of power angle spectrum in macrocell environment", Electronics Letters, Vol. 39, pp. 1565-1567, 2003.
- [Pap05] P. Papazian, "Basic transmission loss and delay spread measurements for frequencies between 430 and 5750 MHz", IEEE Trans. Ant. Propagation, Vol. 53, pp. 694-701, 2005.
- [PLB04] J.W. Porter, I. Lisica, G. Buchwald,"Wideband mobile propagation measurements at 3.7 GHz in an urban environment", IEEE Ant. Propagat. Intern. Symposium, Vol. 4, pp. 3645-3846, 2004.
- [PLN+99] M. Pettersen, P. H. Lehne, J. Noll, O. Rostbakken, E. Antonsen, R. Eckhoff, "Characterization of the directional wideband radio channel in urban and suburban areas", IEEE 50th VTC, pp. 1454-1459,1999.

- [PMF00] K. I. Pedersen, P.E. Mogensen, B.H. Fleury, "A stochastic model of the temporal and azimuthal dispersion seen at the base station in outdoor propagation environments", IEEE Trans. Veh. Technol., Vol. 49, pp. 437-447, 2000.
- [PT00] J. W. Porter and J. A Thweatt, "Microwave Propagation Characteristics in the MMDS Frequency Band," in Proc. IEEE ICC'00, Jun. 2000, Vol. 3, pp. 1578-1582.
- [RIMAX] R. S. Thoma, M. Landmann, and A. Richter, "RIMAX – a Maximum Likelihood framework for parameter estimation in multidimensional channel sounding," 2004 Intl. Symp. on Antennas and Propagation, Aug. 17-21, 2004, Sendai, JP.
- [RJB89] R.J.C. Bultitude, and G.K.Bedal, "Propagation characteristics on microcellular urban mobile radio channels at 910 MHz," IEEE J. Select. Areas Commun, vol.7, no. 1, 1989, pp. 31-39.
- [RJB02] R.J.C. Bultitude., "Estimating frequency correlation functions from propagation measurements on fading radio channels: A critical review," IEEE J. Select. Areas Commun. Vol. 20, no. 6, August, 2002, pp. 1133-1143.
- [RJK05] T. Rautiainen, K. Kalliola, J. Juntunen,"Wideband radio propagation characteristics at 5.3 GHz in suburban environments", PIMRC Berlin, Vol. 2, pp. 868-872, 2005.
- [RMB+06] M. Riback, J. Medbo, J.-E. Berg, F. Harrysson, and H. Asplund, "Carrier Frequency Effects on Path Loss," IEEE VTC 2006-Spring, vol. 6, pp. 2717-2721, 2006.
- [RSS90] T. Rappaport, S. Seidel, R. Singh,"900-MHz multipath propagation measurements fot U.S. digital cellular radiotelephone", IEEE Trans. Veh. Technol., Vol. 39, pp.132-139, 1990.
- [RJK07] T. Rautiainen, J. Juntunen, K. Kalliola, "Propagation analysis at 5.3 GHz in typical and bad urban macrocellular environments", IEEE 65th Veh. Technol. Conf., Dublin, April 2007.
- [RWH02] T. Rautiainen, G. Wölfle, R. Hoppe, "Verifying path loss and delay spread predictions of a 3D ray tracing model in urban environment", IEEE 56th Veh. Technol. Conf., Vol. 4, pp. 2470-2474, Sept. 2002.
- [Rudd03] R.F. Rudd, "Building penetration loss for slant-paths at L-, S- and C-band." ICAP 2003, 31.3.-1.4, 2003.
- [Sau99] S. Saunders "Antenna and propagation for communication systems concept and design", Wiley, 1999.
- [SDD00] J. Sydor, A. Dugas, and J. Duggan, "A new broadband wireless network for 5 GHz licence-exempt applications," in Proc. IEEE RAWCON'00, pp. 33-37.
- [SG02] S. Salous, H. Gokalp,"Dual-frequency sounder for UMTS frequency-division duplex channels", IEE Proc. Comm., Vol. 149, pp. 117-122, 2002.
- [SRJ+91] S. Seidel, T. Rappaport, S. Jain, K. Lord, R. Singh,"Path loss, scattering, and multipath delay statistics in four European cities for digital cellular and microcellular radiotelephone", IEEE Trans. Veh. Technol., Vol. 40, pp. 721-730, 1991.
- [SBA+02] Schenk, T.C.W., Bultitude, R.J.C., Augustin, L.M., van Poppel, R.H., and Brussaard, G., "Analysis of Propagation loss in Urban Microcells at 1.9 GHz and 5.8 GHz," in Proc. URSI Commision F Open Symposium on Radiowave Propagation and Remote Sensing, Garmisch-Patenkirchen, Germany, Feb. 2002.
- [SCK05] N. Skentos, Constantinou and A. G Kanatas, "Results from Rooftop to Rooftop MIMO Channel Measurements at 5.2 GHz," COST273 TD(05)59, Bologna, Jan. 19-21.
- [SCT03] A. Seville, S. Cirstea and J.F. Taylor. Effects of propagation between the indoor and outdoor environment. ICAP 2003. 31.3.-1.4. 2003.
- [SG00] T. Schwengler, M. Gilbert:"Propagation models at 5.8 GHz - path loss and building penetration", IEEE Radio and Wireless Conference 10-13 Sep. 2000, pp. 119-124.
- [SJD94] E. Sousa, V. Jovanovic, C. Daineault, "Delay spread measurements for the digital cellular channel in Toronto", IEEE Trans. Veh. Technol., Vol. 43, pp. 837-846, 1994.

- [SMI+00] H. Shimizu, H. Masui, M. Ishii, K. Sakawa, and T. Kobayashi, "LOS and NLOS Path-Loss and Delay Characteristics at 3.35 GHz in a Residential Environment," IEEE Antennas and Propagation Society International Symposium 2000, Vol. 2, Jul. 2000, pp. 1142 - 1145.
- [SMI+02] K. Sakawa, H. Masui, M. Ishii, H. Shimizu, T. Kobayashi, "Microwave path-loss characteristics in an urban area with base station antenna on top of a tall building", Int. Zurich Seminar on Broadband communications, pp. 31-1 -31-4, 2002.
- [SMJ+99] A. M. Street, J. G. O. Moss, A. P. Jenkins, D. J. Edwards, "Outdoor-indoor wideband study for third generation communication systems", IEE National Conference on Antennas and Propagation, pp. 128-131, 1999.
- [SS01] S. Stavrou, S. R. Saunders, "A deterministic outdoor to indoor propagation modeling approach", IEEE 54th VTC, Vol. 2, pp. 1097-1100, 2001.
- [Sva02] Svantesson, T., "A double-bounce channel model for multi-polarized MIMO systems," in Proc. IEEE VTC'02-Fall, Vol. 2, Sep. 2002, pp. 691 – 695.
- [TPE02] S. Thoen, L. Van der Perre, and M. Engels, "Modeling the Channel Time-Variance for Fixed Wireless Communication", IEEE Communication Letters, Vol. 6, No. 8, Aug. 2002.
- [TPJ06] Thiele L., Peter M. and Jungnickel V., "Statistics of the RIcean K-Factor at 5.2 GHz in an Urban Macro-cell Scenario", IEEE 17th International Symposium on Persona, Indoor and Mobile Radio Communications, pp. 1-5, September 2006.
- [TSS+05] Trautwein U., Sommerkorn G., Schneider C. and Thomä R., "Measurement and Analysis of MIMO Channels in Public Access Scenarios at 5.2 GHz", International Symposium on Wireless Personal Communications, Aalborg, Denmark, September 2005.
- [VKV04] L. Vuokko, J. Kivinen, P. Vainikainen., "Results from 5.3 GHz MIMO measurement campaign", COST273, TD(04)193, Duisburg, Germany, 20.-22.9.2004.
- [WAE+04] S. Wyne, P. Almers, G. Eriksson, J. Karedal, F. Tufvesson, A. F. Molisch, "Outdoor to indoor office MIMO measurements at 5.2 GHz", IEEE 60th VTC, pp. 101-105, 2004.
- [WHL94] J.A. Wepman, J.R. Hoffman, L.H. Loew, "Characterization of macrocellular PCS propagation channels in the 1850-1990 MHz band, 3rd Annual International Conference on Universal Personal Communications, pp. 165-170, 1994.
- [WHL+93] J.A. Wepman, J.R. Hoffman, L.H. Loew, W.J. Tanis, M.E. Hughes: "Impulse response measurements in the 902.928 and 1850.1990 MHz bands in macrocellular environments", 2nd international conference on Universal Personal Communications, Vol. 2, pp. 590-594, 1993.
- [WIN1D53] WINNER1 WP5: "Interim Channel Models" Deliverable D5.3, ver 2.4, April 2005.
- [WIN1D54] WINNER1 WP5: "Final Report on Link Level and System Level Channel Models" Deliverable D5.4, 18.11.2005.
- [WIN1D72] WINNER1 WP7, System assessment criteria specification, v1.0.
- [WIN2D111] WINNER2 WP1: "WINNER II Interim Channel Models" Deliverable D1.1.1, ver 1.2, 9.2.2007.
- [WIN2IR112] WINNER2 WP1: "Measurement results and analysis items", Internal Report IR1.1.2, 30.9.2006.
- [WAE+04] S. Wyne, P. Almers, G. Eriksson, J. Karedal, F. Tufvesson, and A. F. Molisch, Outdoor to Indoor Office MIMO Measurements at 5.2 GHz. VTC 2004-Fall. 2004 IEEE 60th Volume 1, 26-29 Sept. 2004 Pages 101-105 Vol. 1.
- [WMA+05] S. Wyne, A. F. Molisch, P. Almers, G. Eriksson, J. Karedal, F. Tufvesson, "Statistical evaluation of outdoor-to-indoor office MIMO measurements at 5.2 GHz", IEEE 61st VTC, Vol. 1, pp. 146-150, 2005.
- [WOT99] G. Woodward, I. Oppermann, J. Talvitie, "Outdoor-indoor temporal & spatial wideband channel model for ISM bands", IEEE 50th VTC, Vol. 1, pp. 136-140, 1999.
- [ZEA99] X. Zhao et al, "Diffraction over typical-shaped terrain obstacles," Journal of Electromagnetic Waves and Applications, vol. 13, pp. 1691-1707, 1999.

- [Xia96] H.H. Xia:" An analytical model for predicting path loss in urban and suburban environments", Seventh IEEE Int. Symposium PIMRC, Vol 1, pp. 19.23, 1996
- [YIT06] Yonezawa, Ishikawa, Takeuchi, "Frequency range extension of path loss prediction formula for over-rooftops propagation in microwave band", IEEE International Symp. Antennas Propagation, pp. 4747-4750, 2006.
- [YTL02] Yacoub, D.; Teich, W.; Lindner, J., „Capacity of Vehicle-Bridge MIMO Channels”, TD(02)118, COST 273, 5th Management Committee Meeting, Lisbon / Portugal, Sep. 19-20, 2002
- [YMI+04] K. Yonezawa, T. Maeyama, H. Iwai, H. Harada:" Path loss measurement in 5 GHz macro cellular systems and considerations of extending existing path loss prediction models", IEEE WCNC, Vol. 1, pp. 279-283, 2004.
- [ZKV+02] X. Zhao, J. Kivinen, P. Vainikainen, K. Skog:"Propagation characteristics for wideband outdoor mobile communications at 5.3 GHz", IEEE Sel. Areas Comm., Vol. 20, pp. 507-514, 2002.
- [ZRK+06] X. Zhao, T. Rautiainen, K. Kalliola, P. Vainikainen, "Path-loss models for urban microcells at 5.3 GHz, IEEE Antennas and Propag. Lett., Vol. 5, pp. 152-154, 2006.